DEPARTMENT OF ELECTRONIC & ELECTRICAL ENGINEERING

University of Strathclyde Engineering

NON-THERMAL PLASMA FOR WATER TREATMENT

A thesis presented in fulfilment of the requirement for the degree of

Doctor of Philosophy

Yiyi Zhao, B.Eng (Honours)

2017

Department of Electronic and Electrical Engineering

University of Strathclyde

Glasgow, UK

Declaration of Authenticity and Author's Rights

‘This thesis is the result of the author’s original research. It has been composed by the author and has not been previously submitted for examination which has led to the award of a degree.’

Signed: YIYI ZHAO

Date: 28/08/2017

ACKNOWLEDGEMENTS

I would like to thank my grandparents, Guanxin Xuen and Fengnan Wu, and my parents, Qingsong Zhao and Yuefang Xue, for the encouragement and financial support they have provided throughout the entire duration of my Ph.D. study. I am extremely lucky to have a warm, harmonious and positive family; growing up in this environment taught me how to be patient, attentive and grateful.

I would like to thank my supervisor, Dr. Tao Wang for his supervision, guidance and encouragement during my Ph.D. study. I would also like to thank Dr. Qing Chun Ren and the Strathclyde Faculty of Engineering for the financial support. I appreciate the opportunity that Tao has provided me to work on a meaningful and challenging subject.

I would also like to show thanks to Prof. Scott MacGregor for his encouragement and support. I would like to thank Dr. Mark P Wilson for his patience and encouragement, and his help on my academic papers. I would like to thank Dr. Michelle MacLean for her help and guidance during my experimental research in Lab ROLEST. I would like to thank Dr. Martin Given and Dr. Igor Timoshkin for their continuous help and advice in the research. Thanks to Mrs. Maureen Cooper for all her help in managing conference trips and ordering experimental equipment. I would like to thank all the technicians of the High-Voltage Group mechanical workshop, and the electrical workshop of the Electronic and Electrical Engineering Department: David Griffin, Sean Doak, Andy Carlin, Frank May, and James Tollan for their help.

I would like to thank my groupmates Miss Yingjia Zhou, Mr Linghe Zhou and Mr Zhongshu Zhang for their selfless help in my research. They have also made my time in Strathclyde full of happiness and laughter.

ABSTRACT

Plasma generated in contact with water has been extensively investigated in various electrode geometries and various discharge types for water treatment, of which the applications have been employed industrially on different scales. The reactive species such as OH radicals, O_3, H_2O_2 and HO_2 can be generated from the reactions that occur at the plasma-water interface. For discharges above water, the effect of positive gas ions, which lead to the formation of positive water ions, is considered the main pathway for OH radical formation; while for the discharge under water, the water dissociation by electron collisions is considered as the main pathway. However, the reaction zone for the production of reactive species (gas or liquid phase) is still controversial. This thesis presents a study of the plasma generated in the gas phase in contact with water by various discharge types for water treatment. The discharge characteristics, OH radical and H_2O_2 production, and solution conductivity and pH variation were investigated and compared under different experimental conditions. The degradation of methylene blue dye was investigated under DBD.

The transition of impulsive current discharges into impulsive-diffuse discharges was recorded by increasing the solution conductivity; a further transition of the discharge type into a spark was recorded when the solution conductivity was increased to >2.4 mS/cm. The H_2O_2 energy efficiency of 1.1 g/kWh was recorded under positive impulsive current discharges in N_2 and helium. The highest charge/H_2O_2 ratio of 1:1.26 was recorded under positive impulsive current discharges in O_2 and N_2. Under positive DC glow discharges, the H_2O_2 energy efficiency of 1.9 g/kWh was recorded in air discharges, and was slightly increased to 1.95 g/kWh when using a flow liquid electrode. Increased solution acidity and basicity from neutral solution have negative effects on H_2O_2 production. A significant amount of water vapour was observed under DC glow discharges, resulting in a negative effect on H_2O_2 production. Under negative discharges, no H_2O_2 production was detected in water after O_2, N_2, air and helium discharge treatments. In DBD, a threshold voltage is required to initiate electrical discharges between the glass plate and the water, through the micro-pores. The H_2O_2 production yield of 1.1 g/kWh was recorded in O_2 discharge treatment. The degradation yield of methylene blue dye of 310 g/kWh was achieved within the first minute of O_2 discharge treatment.

Contents

List of Abbreviations

ABS	Absorbance
AOPs	Advanced Oxidation Processes
AC	Alternating Current
CO_2	Carbon Dioxide
DBD	Dielectric Barrier Discharge
DC	Direct Current
FWHM	Full Width at Half Maximum, considered as pulse width in this study
GC-MS	Gas Chromatography-Mass Spectrometry
H_2O_2	Hydrogen Peroxide
HPLC	High-Performance Liquid Chromatography
H_3PO_4	Phosphoric Acid
H_2SO_4	Sulfuric Acid
HTA	2-Hydroxyterephthalic Acid
J	Joule
KCl	Potassium Chloride
LC-MS	Liquid Chromatography-Mass Spectrometry
$Lmol^{-1}s^{-1}$	Reaction rate constant for order two
TB	Tert-butanol
NaOH	Sodium Hydroxide

MB	Methylene Blue
M	Mole per Liter
mM	Mili-mole per Litre
mol	Mole
ns	Nanosecond
O_3	Ozone
OH	Hydroxyl
pps	Pulse per second
PTFE	Polytetrafluoroethylene
PVC	Polyvinyl Chloride
ROS	Reactive Oxygen Species
TA	Terephthalic Acid
UV	Ultraviolet
V_{app}	Applied voltage
V_{pp}	Peak-to-peak Voltage
µs	Microsecond

1 INTRODUCTION

1.1 Overview

This research focused on the investigation of electrical discharge characteristics and the production of OH radical and H_2O_2 under the effect of a water electrode. Understanding the behaviour of these chemical species under these conditions will help in the development of technologies using plasmas and discharges to treat water contaminated with microbiological organisms or organic chemicals. The electrical discharge behaviour and the reactions occurring at the plasma-water interface was investigated under different conditions, including different solution conductivity, solution pH, feed gas, discharge polarity, applied voltage, discharge type, gas flow rate, liquid flow rate and reactor structure. Locke [1] reviewed a series of studies and concluded that the reaction pathways, leading to the formation of H_2O_2 are: (i) radiation; (ii) electron attachment; (iii) excitation; and (iv) ionization of water molecules, taking place at the plasma-water interface. On the other hand, Fridman [2] introduced the ionization of gas molecules, leading to the formation of H_2O_2 by the reactions between positive gas ions and water. Locke [1] also found that the H_2O_2 production yields in electrical discharges in contact with water are mostly lower than 1 g/kWh.

1.2 Research motivation

Advanced oxidation processes (AOPs) have been widely investigated in term of water treatment, the aim of AOPs is to generate reactive species, especially OH radicals, in solutions; one of the most typical AOPs is Fenton method (R 1.1, R 1.2). However, the AOPs require large amount of chemical materials. The plasma-induced AOPs (electrical discharges) avoid the using of chemical material and lead to the direct generation of reactive species ($OH^{\cdot}$, $HO_2^{\cdot}$) *in situ*.

$$Fe^{2+} + H_2O_2 \rightarrow Fe^{3+} + OH^{\cdot} + OH^{-} \quad \text{(R 1.1)}$$

$$Fe^{3+} + H_2O_2 \rightarrow Fe^{2+} + HO_2^{\cdot} + H^{+} \quad \text{(R 1.2)}$$

Extensive research has been undertaken to generate electrical discharges in contact with water using various reactor geometries to investigate the reactive species productions. The required power consumption for the discharges in the liquid phase is at least one order of

magnitude higher than that for the discharges in the gas phase [1]. This can be due to the large amount of energy consumed to heat up the surrounding liquid; to generate gas-vapour bubbles and enable the electrical breakdown to occur in contact with water. However, the H_2O_2 production yields recorded in liquid phase discharges are mostly under 1 g/kWh, which is similar to the values recorded in gas phase discharge [1]. Therefore, in this study, the electrical discharges in gas phase with one water electrode were investigated for OH radical and H_2O_2 production. Jamro'z [3] investigated the flowing water cathode effect and found the H_2O_2 production decreased with increasing liquid flow rate. Jamro'z concluded that this result was due to the reduction of contacting time of plasma with water, when a flowing water electrode was employed. Therefore, a reactor with a flowing liquid electrode was designed in this study to investigate the effect of flowing water electrode on H_2O_2 production. Also, the solution pH has been proven to play a critical role on H_2O_2 production [1-4], which indicates that different reaction mechanisms occur in various pH value solutions. In order to investigate the mechanisms, the effect of the initial pH solution on H_2O_2 production was investigated in this study.

On the other hand, a body of research has been undertaken to clarify the discharge characteristics in the electrical breakdown generated in contact with water [4-7]. The variation of discharge current with solution conductivity was recorded [7], in which case, diffuse discharges were developed following the impulsive discharge currents; however, no clear explanation of the different current waveforms was given. In this research, the effects of solution conductivity on the variation of discharge characteristics were investigated by using a pin-to-water electrode structure.

The aim of this research can be divided into two parts: (i) to investigate the characteristics of the discharges with one water electrode; (ii) to investigate the reactions occurring at the water-plasma interface for OH radical and H_2O_2 formation. To achieve these aims, the objectives of this research are listed below.

- Analyse the variation of discharge characteristics in the pin-to-water electrode discharges with different solution conductivities.
- Investigate the discharge characteristics under different types of electrical discharge.
- Determine the OH radical and H_2O_2 production under different types of electrical discharge.
- Investigate the effect of solution pH on OH radical and H_2O_2 production.

- Investigate the effect of flowing liquid cathode on H_2O_2 production.
- Investigate the H_2O_2 production and methylene blue dye degradation (application of plasma-induced AOPs) under dielectric barrier discharge.

The significant role that OH radical and H_2O_2 play in water decontamination means that the results obtained will help in the design of practical water treatment systems.

1.3 Thesis outline

A review of the mechanisms of plasma generation is introduced in **Chapter 2**. The characteristics of liquid phase and gas phase discharges are compared. The mechanisms for reactive species production are considered differently by several research groups, and are presented and discussed in this chapter. The majority of the reactive species produced in gas phase discharges are generally considered to come from the reactions between ions (with energy) and H_2O; for liquid phase discharges, the reactive species are generated by the vibrational excitations and direct dissociation of H_2O. The generation, reaction, decomposition and termination pathways of OH radicals, H_2O_2 and O_3 are introduced. The effects of different polarity, solution pH and conductivity on reactive species production are also introduced.

Chapter 3 introduces the experimental equipment, the preparation of solutions with various solution pH and conductivity, the calculation of the charges that arrive at the water surface during electrical discharges, the calculation of the discharge energy and the OH radical and H_2O_2 production measurements that were used in this study. The preparation of a scavenger of OH radicals, tert-butanol, to investigate the H_2O_2 production pathways, is also introduced in this chapter.

Chapter 4 presents the results of an investigation into the effect of solution conductivity on discharge transition under pin-to-water electrode discharges. The effect of different applied voltage was also investigated. The discharge above ultrapure water (0.5 μS/cm) was very weak due to the accumulation of charges on the water surface; small voltage drops (several tens of volts) were recorded. Increasing the solution conductivity not only led to higher current amplitude and larger voltage drops, but also led to the development of diffuse discharges, with the presence of a tail current after the short duration (<20 ns) impulsive current; the amplitude of the tail current increased with higher solution conductivity.

Chapter 5 presents the investigation of positive impulsive current discharges above water with a DC power supply; the H_2O_2 production in 5-mM NaOH solution was much lower than that in ultrapure water, indicating the scavenging of OH radicals by OH^- ions.

Chapter 6 presents the investigation of positive and negative impulsive current discharges above water. In order to calculate the charges that arrive at the water surface during discharges in **Chapter 6**, a 1-nF high voltage capacitor was connected in parallel with the reactor.

The pin-to-water structure was also investigated in DC glow discharges under both positive and negative polarities in **chapter 7**; the reactive species production and the variation of solution properties were investigated. Also, the effect of solution pH was recorded. A large amount of water vapour was observed due to the high-power input, in which case the effect of water vapour was investigated by introducing gas flow with various flow rates during treatment. The effect of a flowing liquid cathode on the solution properties was investigated in **chapter 8**.

After the research on pin-to-water electrode discharges, a DBD structure, with one water electrode, achieved by using a porous PTFE plate, was employed in **chapter 9**. The discharge characteristics and reactive species production in various gas treatments was investigated. Also, the O_2 plasma treatment for methylene blue degradation under various solution pH values was investigated.

Chapter 10 presents the conclusion of the investigations of discharge characteristics and reactive species production in this research and its relevance to the treatment of contaminated water.

2 LITERATURE REVIEW

2.1 Introduction

Advanced oxidation processes (AOPs) have been proven to be effective for OH radical formation through a series of chemical reactions [8]. Table 2.1 lists the general oxidative species used during water treatment and the redox potential value. OH radicals with powerful oxidation strength (E^0=2.80 V) have the potential to improve the efficiency of water treatment. The reaction rate constants of OH radicals with micro-pollutants can reach 10^9 $Lmol^{-1}s^{-1}$ [8] and result in the mineralization of organic compounds into CO_2, H_2O and inorganic ions. Ozone (O_3), hydrogen peroxide (H_2O_2), oxygen (O_2) and ultraviolet (UV) radiation can be generated based on different fundamental AOPs. The most typical AOPs include the Fenton method, ozonation, catalytic peroxide oxidation, photo-catalysis, and electrochemical oxidation [8-11].

Table 2.1 Oxidative species redox potential [8-10]

Oxidative species	*Redox potential (V)*
$OH^{\cdot}$	2.8
$O^{\cdot}$	2.42
O_3	2.07
H_2O_2	1.78
$HO_2^{\cdot}$	1.7

Plasma-induced AOPs for OH radical and H_2O_2 production have been investigated in this project; this method has been widely developed and investigated for water treatment [12], and has been proven to be effective for micro-pollutant treatment in water [13].

Electrical discharges in the gas phase lead to the production of high energy electrons, and the majority of the energy is then transferred to ambient gas molecules by inelastic collisions of (i) excitation, (ii) dissociation, (iii) ionization and (iv) electron capture, leading to the formation of various radicals [14]. Table 2.2 lists the reactions between high energy electrons (e^{-*}) and various gas molecules.

When electrical discharges form in contact with water they also allow the reaction between electrons and H_2O to form highly oxidative species such as $O^{\cdot}$ and $OH^{\cdot}$ in both the gas and liquid phase, which can play important roles in the destruction of micro-pollutants. The dimerization of OH radicals leads to the formation of H_2O_2, a reactive species with lower oxidation strength (E^0=1.78 V). In addition, a large range of reactive species such as $O^{\cdot}$, O^-, O_2^-, O^+, O_2^+ (Table 2.2) can be generated in O_2 discharges, and $N^{\cdot}$, N^*, N_2^*, N^+, N_2^+ can be generated in N_2 discharges, which all can help to degrade micro-pollutants in liquids [14].

Table 2.2 Gas and water molecules reactions with electrons

Excitation		*Ionization*	
$e^{-*} + O_2 \rightarrow O_2^* + e^-$	(R 2.1)	$e^{-*} + O_2 \rightarrow O_2^+ + 2e^-$	(R 2.8)
$e^{-*} + N_2 \rightarrow N_2^* + e^-$	(R 2.2)	$e^{-*} + N_2 \rightarrow N_2^+ + 2e^-$	(R 2.9)
$e^{-*} + He \rightarrow He^* + e^-$	(R 2.3)	$e^{-*} + He \rightarrow He^+ + 2e^-$	(R 2.10)
$e^{-*} + H_2O \rightarrow H_2O^* + e^-$	(R 2.4)	$e^{-*} + H_2O \rightarrow H_2O^+ + e^-$	(R 2.11)
Dissociation		*Electron capture*	
$e^{-*} + O_2 \rightarrow O^{\cdot} + O^{\cdot} + e^-$	(R 2.5)	$e^{-*} + O_2 \rightarrow O_2^-$	(R 2.12)
$e^{-*} + N_2 \rightarrow N^{\cdot} + N^{\cdot} + e^-$	(R 2.6)	$e^{-*} + H_2O \rightarrow H^{\cdot} + OH^-$	(R 2.13)
$e^{-*} + H_2O \rightarrow OH^{\cdot} + H^{\cdot} + e^-$	(R 2.7)		

Electrical gas discharges developed above the water surface have been investigated under different discharge types such as corona, glow, gliding arc and DBD discharge [15-19]; these methods are considered as non-thermal plasma generation [1]. Discharges in the liquid phase can produce reactive species *in situ*, which is generally considered as thermal-plasma [1]. *In situ* electrical discharges can purify water by generating a wide range of reactive species. Also, the generation of ultraviolet radiation and shockwaves improves the destruction rate of micro-pollutants in water. Hybrid gas-liquid electrical discharges have been investigated due to their capability to combine the useful characteristics of both the gas and liquid phase discharge. Reactive species can be produced in both phases, thus, enhancing the degradation rate of target pollutants compared to single phase electrical discharges. The discussion of the mechanisms for different phase discharges and their efficiency for the production of oxidants are presented in the following sections.

2.2 Discharges in gas phase with water

The pin-to-water electrode structure (Figure 2.1) has been widely investigated to generate non-thermal plasma through atmospheric pressure glow discharge (APGD), plasma jets, corona discharge and streamer discharges [15, 20-22]. Under positive APGD, an anode glow, followed by the positive column, Faraday dark zone, negative glow and cathode fall on the water surface can be recorded. The formation of Taylor cones on the water surface has been observed [23] in the gas phase discharge, which are caused by a region of increased charge density that enhances the Coulombic force. The dielectric barrier discharge (DBD) has been proven to be effective for the degradation of organic pollutants in water [24], due to a homogeneous distribution of discharge filaments in the water.

OH radicals are the primary reactive species generated at the plasma-water interface; they can then diffuse into the liquid phase to directly react with organic contaminants and lead to the production of H_2O_2 through a dimerization reaction. A small amount of O_3 can be generated in electrical plasma developed above water [25], which can enhance the OH radical formation by a decomposition reaction in solution. A variety of chemically reactive species such as $O^{\cdot}$, $H^{\cdot}$, $N^{\cdot}$ radicals and NO, O=NOOH; highly oxidative reagents such as OH, HO_2, O_2^- ions and H_2O_2 are also produced during gas phase discharges [26]. In addition, energetic electrons are also produced under negative discharges and can dissociate water molecules into $H^{\cdot}$ and $OH^{\cdot}$ [1].

2.2.1 Corona discharge

The initiation of corona discharge occurs when a high electric field is applied to a sharp edge. However, complete electrical breakdown or arcing is not caused. Under positive DC corona discharge, burst corona can be observed from the beginning of the discharge [14] and the discharge frequency increases with increasing current magnitude. The burst corona starts to transit into glow discharge, streamer discharge and spark discharge with increasing applied voltage [27]. Increasing the discharge currents leads to the generation of noisy positive streamer discharges. Further increase of the discharge currents leads to the bridging of the discharge gap and the occurrence of spark discharges [28]. For positive discharges, the free electrons move towards the positive electrode and the positive charges move towards the water surface. The acceleration of positive ions at the streamer head enhances the electric field; this process is repeated and the streamer propagates towards the water surface.

In terms of negative polarity, the illuminating of corona can only be observed at the sharp edge while the remaining discharge gap is dark. Eliasson [29] investigated the energy of free electrons in negative corona discharge and found that the average electron energy is around 5 eV with an electron density of 10^{13} cm^{-3} in the plasma column. Trichel pulse corona [30] currents with amplitude of up to 140 μA and repetition rate of ranges from 1 to 100 kHz can be recorded in negative corona discharges.

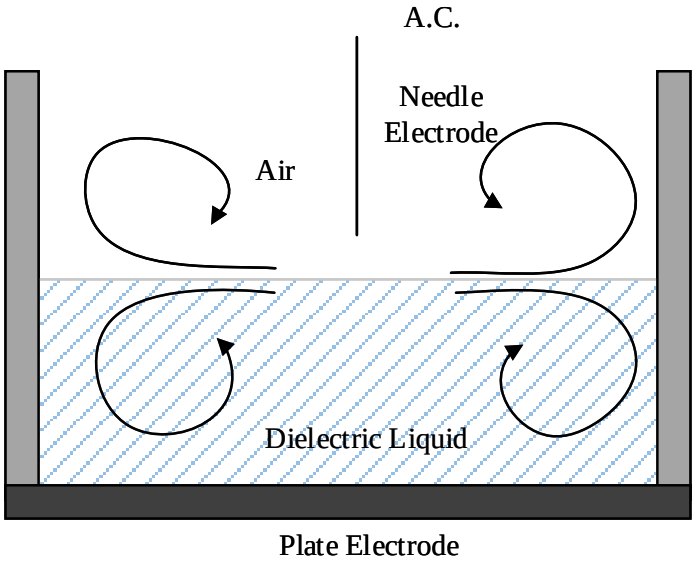

Figure 2.1 Electrohydrodynamic (EHD) flow phenomenon [31].

Ohyama [31] investigated the liquid-phase electrohydrodynamic (EHD) flow phenomena induced by AC corona discharge above the dielectric (Figure 2.1). The liquid phase EHD flow is initiated by charge injection, which enhances the heat and mass transfers in the liquid. The high electric field applied to the pin tip induces the acceleration of free electrons in the gas gap, which ionizes the ambient gas and produces more free electrons. This process is repeated until sufficient free electrons are present to initiate an electron avalanche, which results in the generation of plasma filaments.

2.2.2 Atmospheric pressure glow discharge

The APGD developed in contact with a liquid cathode is a method that has low operation cost [32, 33]. Figure 2.2 shows the discharge zone existing in an APGD when the plasma is developed on a water surface. Jamro'z [34] found that the APGD can be generated stably with a pin-to-water electrode structure with an inter-electrode gap of 0.5 to 4 mm. When the inter-electrode distance is in the range of 0.5 to 1 mm, only negative glow can be observed; increasing the inter-electrode distance to >1.5 mm results in the appearance of a positive column.

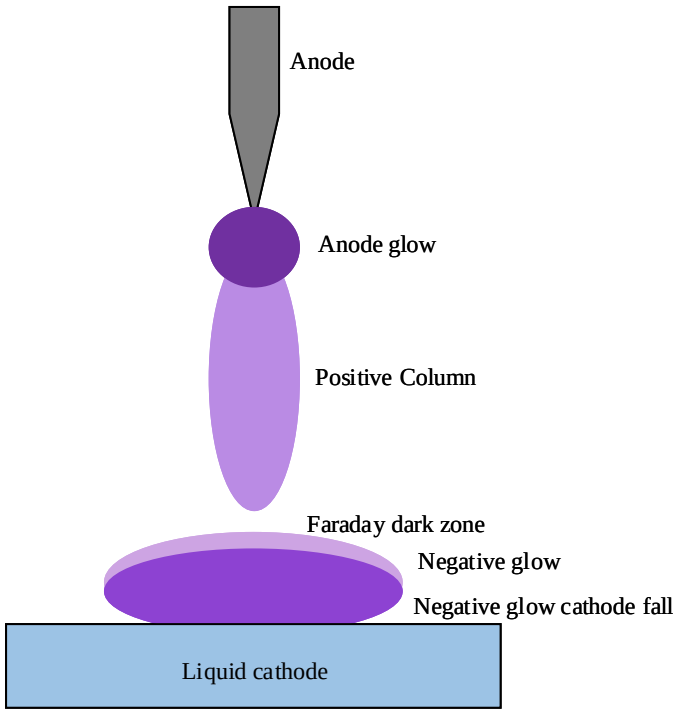

Figure 2.2 Discharge zone existing in APGD developed in contact with water. [20]

Bruggeman [35] investigated the emission characteristics under positive and negative APGD and found that under negative polarity, a bright cathode spot at the pin tip and an intense anode spot on the water surface could be observed. The light emission of the plasma column between the positive and negative spot is much less intense; however, the light intensity can be significantly increased under positive polarity. On the other hand, a ring-like structure of the anode spot can be observed under relatively low discharge current (<20 mA). Miao [36] investigated the negative DC glow discharge and found that the plasma region was a cone-like shape with a hollow anode spot on the water surface, under the discharge current of 1.5 mA and solution conductivity of >17.31 µS/cm.

2.2.3 Streamer discharge

One of the characteristics of streamer discharge is that it emits strong radio noise [37]. The generation of streamer discharges above water from corona discharges by increasing the applied voltage are more effective under positive polarity [37]. In addition, the threshold current, which indicates the discharge type transition from corona or glow to streamer, decreases with increasing radius of curvature of the pin electrode. Shimizu [38] investigated discharges above water, and recorded the plasma propagation velocity in air and the circulation of thermal liquid flow caused by the electrical breakdown. The discharge towards the water surface induced an air flow of 15 m/s and the thermal flow was initiated at the plasma-liquid contact point, and built up along the water surface; the movement of thermal flow spread throughout the liquid and resulted in the solution being well mixed.

Andre developed the discharge between metal and water films and found that the DC diffuse discharge can be generated steadily [39]. Sun [40] compared the streamer-corona and the spark discharge generated between pin-metal electrodes in water vapour for phenol degradation and found that the spark discharge resulted in higher removal efficiency.

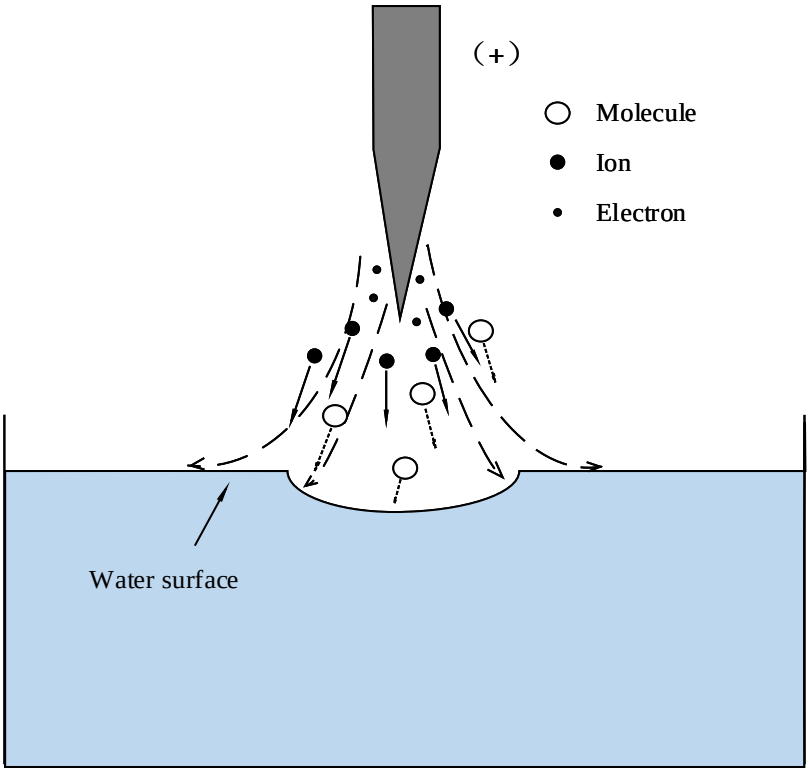

Figure 2.3 Water surface deformation by ionic wind under positive pin-to-water discharge [41].

This was explained as being due to the generation of ultraviolet radiation in the higher temperature plasma channel in the spark discharge, which can react with water vapour and form OH radicals. In addition, the ultraviolet radiation (UV) was absorbed by the surrounding plasma channel during the discharge, leading to the expansion of the plasma channel [2]. Figure 2.3 shows how the ionic flow occurs in streamer discharges [41].

2.2.4 Discharges in gas bubble

The injection of gas bubbles into a solution under a high electric field leads to the generation of plasma in the gas bubbles. This method is generally considered as a discharge in liquid [1]; however, due to the breakdown mechanism, the requirement for Joule heating of the liquid to generate water vapour bubbles is removed, significantly lowering the required input power and applied voltage compared to that in direct liquid discharge [42]. This method also benefits from the characteristics of reducing the electrode erosion rate and increasing the contact area of plasma-water, compared to that in liquid phase discharge [1].

Xiong [43] investigated discharges in gas bubbles and found that the H_2O_2 production increased linearly with time in pulsed discharges; however, it reached a saturation condition in DC discharges. Xiong explained this result was due to the thermal destruction of H_2O_2 in DC discharges. Shih [44] compared discharges in gas bubbles with discharges above a water surface, and found that, in both cases, the breakdown was initially in the gas phase. In addition, Shih also concluded that the mechanisms for discharge in gas bubbles and discharges above water surface are very similar, while the liquid was acting as grounded electrode.

2.2.5 Gliding arc discharge

Gliding arc electrical discharges have been extensively investigated for pollution control in liquid [17, 45]. These discharges combine the characteristics of thermal and non-thermal plasma, and are considered as an innovative technology [46]. Electrical breakdown can occur between two or more knife-shape electrodes; a high velocity gas flow of over 1 m/s was introduced during the discharge to prevent the transition to a spark [17]. The gliding discharges developed above the water surface or with water spray have been found to be effective for the production of reactive species at the plasma-water interface [47]. The gliding arc has been proved to be effective for H_2O_2 production, Burlica [45] investigated a water-spray gliding arc discharge and achieved an average energy yield of ~70 g/kWh.

2.2.6 Dielectric barrier discharge (DBD)

In dielectric barrier discharges, at least one dielectric barrier is placed between the high voltage electrode and the grounded electrode. Figure 2.4 shows the most commonly used DBD structures with water. The insulator layer allows no current to pass through the discharge gap, in which case, the voltage needs to be high enough to initiate the breakdown of gas molecules [48]. Both AC and pulsed power supplies can be used to operate the discharge; however, the DC power is not applicable for DBD due to the dielectric capacitive coupling effect of the barrier, in this case, the displacement current can only be driven by an alternating voltage [48]. The DBD with one water electrode leads to the accumulation of water vapour on the glass plate, resulting in the distortion of electric field and the variation of discharges.

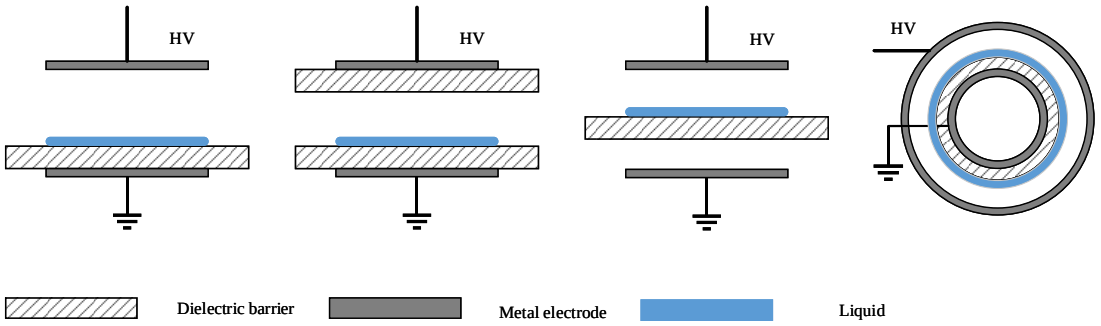

Figure 2.4 Planar and cylindrical DBD structures with water.

Under AC conditions, a large amount of discharge filaments with short current duration occur on the rising edge of the applied voltage in both positive and negative conditions, and distribute homogeneously on the barrier while photons are being emitted and filling the discharge gap. Each micro discharge acts as a source of non-thermal plasma, in which case a significant amount of reactive species can be generated in the plasma region [48]. Mark [49] proved that DBD is a self-extinguishing electrical discharge, regardless of the applied voltage. The current can be influenced by different applied frequency also.

Baroch [50] investigated discharges between a ceramic plate, which was dipped in water, and an aluminium oxide plate in the gas phase. The author recorded a transition of the discharge from a filamentary mode to a homogenous mode on the water surface. H_2O_2 production was also measured with various applied voltages and it was found that the production rate increased with increasing power input.

The Lissajous figure is frequently employed to investigate the discharge properties of DBDs [51]. If the applied voltage was lower than the threshold voltage for discharges, only a slanted straight line can be observed, indicating no discharge has occurred. The Lissajous figure opens up when the applied voltage is increased to over the threshold voltage. The parallelogram shapes that represent the voltage charge diagrams are recorded in most cases when the applied voltage is high enough to initiate the discharges in the gap.

Emile [24] introduced the application of DBD with single and double barriers, all of which have been used in environmental, industrial and human health applications. Konelschatz [51] claimed that DBDs are utilized from laboratory to industrial scales.

2.3 Discharges in liquid phase

2.3.1 Breakdown theory

Direct discharges in water can initiate a series of physical mechanisms, which require an electric field intensity of over 1 MV/cm. Since the density of liquids is much higher than that in gases (~10^6 times) [52], the breakdown mechanism is more complicated. In addition, the dissolved gases in the liquid phase can generate micro-bubbles, thus, increasing the complexity of the breakdown mechanism [53, 54]. On the other hand, the liquid purity and the dissolved substances all play important roles in the liquid breakdown process.

The discharges in liquid phase are considered as thermal plasma, in which the typical currents are over 10 A, and the temperature is over 5000 K [53-56]. Discharges in water can provide various oxidation paths and not only lead to production of reactive species such as $H^{\cdot}$, $O^{\cdot}$ and $OH^{\cdot}$ radicals and H_2O_2, but also generate ultraviolet radiation and overpressure shock waves [55-58], which all play important roles in the degradation of organic compounds and micro-pollutants in water. The pulse energy and solution characteristics, such as solution pH and conductivity, all can influence the magnitudes of the respective contributions of these paths [58-61]. Several kinds of microorganisms in solution can be destroyed by direct discharges in solution, with or without the additional action of O_3 and H_2O_2 [62].

Thermal breakdown theories and electronic breakdown theories have both been used to explain the generation of corona discharges under water; however, the detailed mechanisms involved are still not clear. In thermal breakdown theories, the currents flow through the high electric field region, heating up and vaporizing the surrounding liquid, and result in the production of large amounts of gas bubbles. Pulsed discharges then occur inside the bubbles

and heat up the liquid to produce more bubbles to repeat the process, after which the gap breakdown occurs, leading to the generation of $H^{\cdot}$, $O^{\cdot}$, $OH^{\cdot}$ and H_2O_2. The electrical breakdown theory is similar to the electron avalanche theories that take place in the gas phase discharges, the free electrons accelerate due to the electric field and then ionize ambient gas to produce more electrons, resulting in the electrical breakdown of water.

2.3.2 Liquid phase discharge types

Contact glow discharge electrolysis has been widely researched for water purification. A DC voltage supply is employed to energise a pin or wire anode, which is slightly dipped in water and isolated from the cathode [63]. Several vapour bobbles can be generated when the electric field and input energy is high enough to vaporize the local solution. In this case, the species generated in the discharge zone, which include anions, cations and neutrals, are all heated. Plasma filaments are then developed in the vapour bubbles, resulting in the production of reactive species at the vapour-water interface, aiding in the destruction of pollutants. Pulsed corona or streamer discharges can be generated by applying a pulsed voltage to the sharp-edged electrode, a method that has been proven to be effective for bacterial disinfection [62] and organic compound degradation. A large number of plasma filaments can be produced in the gaseous bubbles, which are generated around the electrode, and reactive species are mainly generated around the plasma channels. Pulsed corona or streamer discharges under water are very effective for the production of reactive species. The streamer filaments are in the shape of conical or hemispherical [64], reaching a diameter of several millimetres, and are able to propagate over 1 cm in water [65]. The length of streamer filaments decreases with increasing solution conductivity; on the other hand, the length increases with increasing pulse width. Increasing the duration of the applied voltage may lead to a full breakdown between the electrodes, as the streamer discharge becomes a spark discharge [66].

Podliński investigated the bubble flowing mechanism after breakdown in pulsed streamer discharges and found that the bubble train from the pin tip to the ground electrode is the strongest stream; increasing the capacitance of the charging capacitor or the number of pins lead to an increase in the flow velocity [67]. Gas bubble injection in under water discharges has also been investigated [67-69]. Locke [69] found that introduction of gas bubbles into the discharge area decreases the discharge voltage; this may be due to the fact that the discharge can occur in the bubbles injected into water, in which case, the heating process for vapour bubble generation is not necessary. Kurahashi [68] found a concentration of 50 ppm H_2O_2

can be produced under the input power of 42 W. Wang [70] investigated the gas bubble flowing effect and found that increasing the gas flow rate from 0 to 4 L/min enhances the H_2O_2 production yield from 0.005 to 0.014 mmol/J.

2.4 Hybrid Gas-Liquid Electrical Discharge

The hybrid electrical discharge combines the spark discharge generated above a water surface and the direct liquid phase streamer-like discharges in one system. Two structures of hybrid-series and hybrid-parallel reactors have been extensively investigated [71, 72]. The main advantage of this method is that it can produce the same physical factors and reactive species as in the independent gas and liquid phase discharges; it can treat the target pollutants in both phases. Several reactive species can be generated in the gas, at the gas-liquid interface, and in the liquid phase simultaneously [73]. However, an extremely high applied voltage of ~50 kV is needed to initiate both gas and liquid phase discharges for hybrid gas-liquid discharges [71-73].

Hybrid reactors have been employed for nitrobenzene [72] and phenol degradation, and the destruction of organic dyes [74, 75]. Appleton [72] found that the hybrid-parallel reactor improves the nitrobenzene removal efficiency compared to the treatments by hybrid-series and single-liquid phase reactors. Kusic [75] investigated the hybrid reactor for phenol and organic dye destruction and found that the hybrid-series structure provided higher removal rates. The mechanism of plasma generation and reactive species production, and the quantification need to be fully investigated for the development of hybrid reactors. Lukes [73] measured the O_3 production in different hybrid structures and found that the O_3 production rate was ~20 mg/h in a hybrid-series reactor and ~120 mg/h in a hybrid-parallel reactor, each with power input of 66 W. The difference may be due to the (i) different polarity; (ii) different reactor structures; and (iii) different relative humidity effects, in the hybrid-series reactor, the gas phase discharge gap was 10 times shorter than that in hybrid-parallel reactor, thus a part of the electronic energy, which should be used for O_3 generation, is absorbed by the water vapour.

The O_3 production was reduced by 50% in a basic solution compared to that in an acidic solution with the same solution conductivity (130 μS/cm), suggesting that the reactions occurring at the gas-basic liquid interface can lead to O_3 decomposition. The H_2O_2 production in different hybrid reactors has no obvious difference and increased linearly with input energy. Very similar production rates of H_2O_2 were obtained between hybrid reactor

and single liquid phase reactors [63, 64], which suggests that, in hybrid reactors, only a small part of the total energy is distributed in the gas phase discharge.

2.5 Reactive species production

The production of reactive species can be divided into two parts: radical products such as $OH^{\cdot}$ $O_2^{\cdot -}$, $NO^{\cdot}$, and non-radical products such as H_2O_2, O_3, O_2^{*} and O=NOOH. The radical products contain at least one unpaired electron, which leads to the characteristic of high reactivity; these products can take part in the reactions during a gas discharge, by donating the unpaired electron, or obtaining another electron from reactants to achieve stability.

2.5.1 Hydroxyl radicals

OH radicals are the most reactive oxidation species, with oxidation potential of 2.8 V, and can react with pollutants in a non-selective manner [76]. OH radicals are considered to be the major reactant during the degradation of organics, and can react with a large range of organic compounds with the reaction rate constant of 10^8-10^{10} $M^{-1}s^{-1}$ [77]. OH radicals can attack the chemical bonds in organic molecules directly by hydroxylation [1], and the initial reaction rate determines the degradation velocity.

In electrical discharges, OH radicals can be formed from the reaction of high energy electrons, excited gas molecules or ions with water molecules (Table 2.3). It has been suggested by various research that the production of OH radicals increases with a higher applied electric field and energy input [1]. The main production mechanisms of OH radicals in liquid and gas phase discharges are different.

Table 2.3 OH radical generation

Reactions	
$O_2^{+} + H_2O \rightarrow O_2 + H_2O^{+}$	(R 2.14)
$N_2^{+} + H_2O \rightarrow N_2 + H_2O^{+}$	(R 2.15)
$He^{+} + H_2O \rightarrow He + H_2O^{+}$	(R 2.16)
$H_2O^{+} + H_2O \rightarrow H_3O^{+} + OH^{\cdot}$	(R 2.17)
$O^{\cdot} + H_2O \rightarrow OH^{\cdot} + OH^{\cdot}$	(R 2.18)
$H^{\cdot} + O^{\cdot} \rightarrow OH^{\cdot}$	(R 2.19)

However, Polyakov [78] investigated the OH radical and H_2O_2 production at a plasma-water interface, and concluded that while the mechanism discussed above must take place, however, it only provides a partial contribution to OH radical generation (< 25%). The author found that the major role of reactive radical generation is from the energy that was carried by positive ions. Lukes [79] found that OH radials can also be generated in humid O_2 by the hydrogen abstraction reaction between $O^{\cdot}$ and water molecules (R 2.18). In addition to the electron and ion effects, reactive radicals such as $H^{\cdot}$ can also take part in OH radical formation (R 2.19) via the reaction with $O^{\cdot}$. Ikoma [80] investigated the OH production under pulsed discharges above a water surface, and concluded that the OH radicals were generated through the reactions between water vapour and high-energy electrons, and then diffuse into water.

In liquid phase discharges, water can be locally heated and vaporized to form water vapour columns, where the dissociation of water by its reaction with high energy electrons to produce $OH^{\cdot}$ and $H^{\cdot}$ radicals can take place directly (R 2.20). When the plasma temperature is increased to 5000 K, all the chemical bonds in water molecules can be subject to cleavage (R 2.21) [52-56]. Other than that, relatively lower average electron energy of 1 eV was measured in liquid phase discharges, this being unlikely to cause the ionization of water. In this case, vibrational excitations of water molecules with electrons are more likely to occur and further react to form $H^{\cdot}$ and $OH^{\cdot}$ (R 2.22)

$$H_2O \rightarrow H^{\cdot} + OH^{\cdot} \quad \text{(R 2.20)}$$

$$H_2O \rightarrow 2H^{\cdot} + O^{\cdot} \quad \text{(R 2.21)}$$

$$H_2O^{*} + H_2O \rightarrow H^{\cdot} + OH^{\cdot} + H_2O \quad \text{(R 2.22)}$$

H_2O_2 can be produced by discharges in water [52]; in addition, the ultraviolet light generated in electrical discharges in water can dissociate H_2O_2 into OH radicals (R 2.23) [63, 64]. The photolysis of H_2O_2 mainly takes place in liquid phase discharges and leads to the formation of two OH radicals, which can react with organic compounds or undergo the H_2O_2 regeneration reaction. Benitez [81] found that the H_2O_2 concentration during treatment was kept at a nearly constant value, proving the H_2O_2 decomposition-regeneration cycle in aqueous solutions.

$$H_2O_2 + h\nu \rightarrow OH^{\cdot} + OH^{\cdot} \quad \text{(R 2.23)}$$

The formation of OH radicals can also be terminated by a series of reactions during an electrical discharge. Listed in Table 2.4 are the ways in which radicals and electrons produced in the discharge participate in subsequent reactions, which can terminate the production of OH radicals.

Table 2.4 OH radical termination pathways [80]

Reactions	
$H^{\cdot} + OH^{\cdot} \rightarrow H_2O$	(R 2.24)
$OH^{\cdot} + OH^{\cdot} \rightarrow H_2O_2$	(R 2.25)
$H^{\cdot} + H^{\cdot} \rightarrow H_2$	(R 2.26)
$HO_2^{\cdot} + OH^{\cdot} \rightarrow H_2O + O_2$	(R 2.27)
$H_3O^+ + OH^- \rightarrow 2\ H_2O$	(R 2.28)

2.5.2 Hydrogen peroxide

Large quantities of H_2O_2 can be generated during electrical discharges, either in the gas or in the liquid phase; the measured H_2O_2 concentration can indicate the OH radical formation during electrical discharges. Ono [82] found the lifetime of OH radicals in a humid N_2/O_2 mixture was in the range of 10-100 μs. The detected H_2O_2 production also reflects the oxidation strength in the system. H_2O_2 has a lower oxidation potential of 1.78 V, comparing to the ones for OH radical and O_3. H_2O_2 is a very weak acid with a dissociation constant of pK_a=11.75 and can hydrolyse in water to generate HO_2^-, which can further hydrolyse to O_2^{2-} [83].

$$H_2O_2 \leftrightarrow H^+ + HO_2^- \quad \text{(R 2.29)}$$

$$HO_2^- \leftrightarrow H^+ + O_2^{2-} \quad \text{(R 2.30)}$$

Table 2.5 shows Henry's constant for various species. It can be seen that H_2O_2 molecules and OH radicals have higher constants, which indicate that these species can be dissolved into solution efficiently.

Table 2.5 Henry's constant for oxidative species

Species	*Henry's Constant (mol/L * atm.)*
Oxygen	1.2×10^{-3}
Ozone	1.1×10^{-2}
Hydrogen Peroxide	8.4×10^{4}

The production of H_2O_2 is affected by several factors such as applied power, gas-type, gas flow rate and solution conductivity; these factors have been investigated in this research. Several investigations have proven that the H_2O_2 yield increases with increasing electric field. One of the main pathways for H_2O_2 production is the dimerization of two OH radicals [84] (R 2.25). Moreover, a large amount of H_2O_2 can also be produced by the reaction between water molecules and the OH radicals generated by electrical discharges taking place near the surface of an aqueous solution (R 2.31). The HO_2 radicals produced during discharges also has a strong oxidative strength of 1.7 V.

Locke [1] found that the H_2O_2 production varied widely among various discharge types and different phases. Locke concluded that the energy yield was enhanced by above-water discharges compared to that in direct liquid phase discharges. However, the mechanisms and chemical products involved in gas phase discharges are more complicated to explain due to the additional chemical reactions of different gas components. The H_2O_2 production yields from liquid phase discharges ranged from 0.12 to 3.64 g/kWh, but most were lower than 1 g/kWh. The H_2O_2 can be generated by the water molecules reactions under the energy (R 2.32, Table 2.6) in liquid phase discharges. Also, the H_2O_2 can be generated by the OH radical reaction with water (R 2.31) and the radical reactions (R 2.33-R 2.35) in both liquid phase and gas phase discharges. A wider yield range of 0.04 to 5 g/kWh was observed in above-water discharges, while, in most cases, the yield values were lower than 1 g/kWh, which were similar to the cases in liquid phase discharges. The highest yield of 5 g/kWh was obtained by using positive, nanosecond, pulsed discharges with a large discharge gap of 55 mm.

Table 2.6 H_2O_2 generation pathways

Reactions	
$H_2O + OH^{\cdot} \rightarrow H_2O_2 + H^{\cdot}$	(R 2.31)
$H_2O + H_2O \rightarrow H_2O_2 + H_2$	(R 2.32)
$HO_2^{\cdot} + HO_2^{\cdot} \rightarrow H_2O_2 + O_2$	(R 2.33)
$H^{\cdot} + HO_2^{\cdot} \rightarrow H_2O_2$	(R 2.34)
$2OH^{\cdot} + HO_2^{\cdot} \rightarrow H_2O_2 + 2O_2$	(R 2.35)

The main limitations of above-liquid discharges are the mass transfer and the plasma-water interfacial area. Lower relative yields were found in hybrid discharges, ranging from 0.37 to 1 g/kWh. The highest yield of 80 g/kWh was obtained in a DBD with feed gas of $H_2 + O_2$.

H_2O_2 in basic solution has weak stability, as it can be decomposed by OH^-, and generates HO_2 radical (Table 2.7).

Table 2.7 H_2O_2 decomposition pathways

Reactions	
$H_2O_2 + OH^- \rightarrow HO_2^- + H_2O$	(R 2.36)
$H_2O_2 + OH^{\cdot} \rightarrow H_2O + HO_2^{\cdot}$	(R 2.37)
$HO_2^{\cdot} + H_2O_2 \rightarrow O_2 + H_2O + OH^-$	(R 2.38)
$H^{\cdot} + H_2O_2 \rightarrow OH^{\cdot} + H_2O$	(R 2.39)
$e^- + H_2O_2 \rightarrow OH^{\cdot} + OH^-$	(R 2.40)
$H_2O_2 + 2\ O_3 \rightarrow 2\ OH^{\cdot} + 3\ O_2$	(R 2.41)

To maximise the oxidative strength of H_2O_2 in solution, Fe^{2+} was widely added to lead to the Fenton reaction (R 1.1, R 1.2), and result in the production of $OH^{\cdot}$ and $HO_2^{\cdot}$ radicals; the oxidation potentials of these species are higher than that for H_2O_2 (Table 2.1). Reddy [85] introduced 60 mg/L of Fe^{2+} in solution during a liquid phase DBD, and found that the organic dye degradation rate was enhanced.

2.5.3 Ozone

Corona and DBD in O_2 have been employed for long-term O_3 generation [48, 51]. Ozone has a high oxidation strength, with a redox energy of 2.07 V. The solubility of O_3 in neutral water is 14-mmol/L at 20 ℃; a higher value can be recorded in solutions containing organic compounds. O_3 preferentially reacts with the functional groups and intermediate products, rather than neutral matters, with reaction rate constants of 1×10^{0}-10^{4} $M^{-1}s^{-1}$ [86, 87].

O_3 can be generated by electrical discharge through the dissociation of O_2 molecules and single O reaction with O_2 (R 2.42-2.44, Table 2.8). High-energy electrons can lead to the ionization or dissociation of O_2 molecules. On the other hand, the O_3 production yield can be significantly decreased when water vapour exists in the discharge gap [88]; therefore, O_3 is not a major oxidative product when an electric discharge is developed in contact with water.

Table 2.8 O_3 generation and decomposition in gas phase

Reactions	
$e^- + O_2 \rightarrow O^\cdot + O^\cdot + e^-$	(R 2.42)
$O^\cdot + O_2 + M \rightarrow O_3 + M$	(R 2.43)
$O_2 + O_2^* \rightarrow O_3 + O$	(R 2.44)
$O + O_3 \rightarrow 2O_2$	(R 2.45)
$O + O \rightarrow O_2$	(R 2.46)

O_3 production has been reported in multiple discharge types that are developed in contact with water, with much lower concentration being reported, compared to that recorded in dry gas discharges [22, 24, 73, 89, 90]. The O_3 production detected at the plasma-water interface is lower than that in the commercial ozone generators, due to: (i) O_3 dissolving in water and generating OH radicals; (ii) a large amount of $O^\cdot$, which is the precursor of O_3, may be consumed in reaction with water molecules (R 2.47-2.49), (iii) O_3 dissolved in water can react with radicals in solution (R 2.50-2.52) [51].

$$H_2O + O^\cdot \rightarrow OH^\cdot + OH^\cdot \quad \text{(R 2.47)}$$

$$H_2O + O^\cdot \rightarrow HO_2 + H^\cdot \quad \text{(R 2.48)}$$

$$H_2O + O^\cdot \rightarrow H_2 + O_2 \quad \text{(R 2.49)}$$

$$OH^\cdot + O_3 \rightarrow HO_2^\cdot + O_2 \quad \text{(R 2.50)}$$

$$H^{\cdot} + O_3 \rightarrow OH^{\cdot} + O_2 \quad \text{(R 2.51)}$$

$$HO_2^{\cdot} + O_3 \rightarrow OH^{\cdot} + 2O_2 \quad \text{(R 2.52)}$$

Consequently, the O_3 production in humid ambient gases is much lower than that in dry ambient gases. However, the plasma developed in contact with water improves the degradation of pollutants in liquid compared to the pure O_3 treatment, due to the production of the reactive species, OH and HO_2 radicals, and O atoms.

2.5.4 Oxy-nitride species

Oxy-nitride species can be generated during electrical discharges, when N_2 exists in the ambient gas. Table 2.9 lists the oxidation processes of N_2 to form nitride and nitrate acids during a discharge. Nitric oxide is the primary product, which can be further oxidized by various reactive oxygen species (ROS) such as $O^{\cdot}$, O_2, $OH^{\cdot}$ and $HO_2^{\cdot}$. The production of oxy-nitride species increases the acidity of plasma-treated samples, and brings the possibility for synergistic effects with ROS to occur for water treatment [90].

Table 2.9 Oxy-nitride species production in discharges

Reactions	
$N_2 + O^{\cdot} \rightarrow NO + N^{\cdot}$	(R 2.53)
$N^{\cdot} + O^{\cdot} \rightarrow NO$	(R 2.54)
$NO + O^{\cdot} \rightarrow NO_2$	(R 2.55)
$O_2 + 2\ NO \rightarrow 2\ NO_2$	(R 2.56)
$O_2 + NO \rightarrow NO_3$	(R 2.57)
$2\ NO_2 \rightarrow N_2O_4$	(R 2.58)
$NO_2 + NO_3 \rightarrow N_2O_5$	(R 2.59)
$H_2O + NO_2 \rightarrow OH + HNO_2$	(R 2.60)
$H_2O + NO_2 + NO \rightarrow 2\ HNO_2$	(R 2.61)
$HO_2 + H_2O + NO \rightarrow HNO_3 + H_2O$	(R 2.62)
$H_2O + N_2O_4 \rightarrow HNO_3 + HNO_2$	(R 2.63)
$H_2O + N_2O_5 \rightarrow 2\ HNO_3$	(R 2.64)
$H_2O_2 + NO_2^{-} \rightarrow NO_3^{-} + H_2O$	(R 2.65)
$OH^{\cdot} + NO_2^{-} \rightarrow NO_3^{-} + H^{\cdot}$	(R 2.66)

Increasing conductivity and reducing pH value can take place synchronously in both gas phase and liquid phase discharges; Ruma [91] found that the solution conductivity change in an air discharge above water was over five times higher than that in a liquid phase discharge, while the H^+ production was two orders of magnitude higher. This may be due to the fact that the conductivity changes due to liquid phase discharges were mainly caused by ions and radicals generated in the water; while the gas phase discharge leads to the production of oxy-nitride species that can dissolve in water and form nitrite and nitrate acids, thus significantly increase the solution conductivity.

Ikoma [80] found that the N_2:O_2 ratios had a critical effect on dye degradation. The degradation rate was the highest when pure O_2 was introduced during treatment, which produced no oxy-nitride species. The dye degradation rate started to decrease when 5-90% of N_2 was mixed with O_2. This proved the negative effect of oxy-nitride species for oxidative species production, which can be due to the reaction (R. 2.66).

2.5.5 Effect of polarity

For underwater discharges (direct discharges), the effect of polarity on discharge characteristics and H_2O_2 production has been investigated in a series of studies. Clements [65] investigated underwater discharge and found that positive discharges produced higher yields of active species, compared to that recorded under negative discharges. Clements also found that negative discharge generated under water produced much shorter streamer side branches. In addition, the negative underwater discharge generated much fewer gas bubbles in liquid. Lukes [79] investigated the pulsed discharges developed under water, and found that the degradation yield of phenol was approaching 1/3 less under negative polarity. Pei [104] investigated the OH production in a He-H_2O plasma jet and found that the OH density was ~30% higher under positive discharge. Lukes [105] found that the H_2O_2 production under negative polarity was less than half of that under positive polarity. Stara [106] investigated the H_2O_2 production in DC underwater discharges, and found that the H_2O_2 production under negative discharge was approaching four times lower. Summarizing these studies, the reactive species produced under liquid phase negative discharges are generally 30%-75% lower than that under liquid phase positive discharges.

For discharges above water, Polyakov [78] found neither H_2O_2 nor reactive radicals were detected during discharges under negative polarity. Thagard [4] investigated discharges in argon above water, and found that the H_2O_2 production under negative discharges was at

least 50% reduced from that recorded under positive discharges. Thagard concluded that the results can be explained by a large voltage drop being located near the high voltage electrode, rather than near the reaction zone in contact with the water surface, leading to the generation of H_2O^+ near the high voltage electrode. On the contrary, Sano [103] investigated the direct contact of gas phase corona discharges in an O_2/N_2 (O_2=20%), mixture and found that the organic compound degradation rates, which reflect the reactive species production, were much lower under positive discharges. Sano explained that the results could be due to the effect of negative oxygen ions. O^- and O_2^- ions can be formed by the electron attachment process and can move towards the water surface, initiating the reactions to produce OH and HO_2 radicals (R 2.67, 2.68). The effect of different polarity on H_2O_2 production has been investigated in this research.

$$O^- + H_2O \rightarrow OH^- + OH^\cdot \quad \text{(R 2.67)}$$

$$O_2^- + H_2O \rightarrow OH^- + HO_2^\cdot \quad \text{(R 2.68)}$$

2.5.6 Effect of pH

Sun [40, 57] investigated active species generation in underwater pulsed corona discharges, and found that the OH radical formation is pH dependent and is higher in natural and slightly basic solutions. The effect of pH has also been investigated in hybrid electrical discharges; Lukes [79] found that the energy yield for phenol degradation was around 3.5 times higher in basic solution than that in acid solution during O_2 discharges.

Thagard [4] found that the H_2O_2 production in above-water discharges is strongly dependent on the solution pH. In basic solutions of pH 10.5 to 13, the formation of H_2O_2 is almost all suppressed; this result agrees with the scavenging of OH radicals by OH^- ions in solution. Thagard also decreased the solution pH to 3-5.5 by using phosphoric acid, which cannot scavenge OH radicals, and found that the H_2O_2 production at the lower pH of 3 is almost doubled in comparison to that in the solution of pH 5.5. Thagard concluded that this result may be due to the O radical concentration being higher in lower pH solution, which can react with H_2O to form two OH radicals. As wastewater may have a range of pH values, therefore, it is worthwhile to investigate the effect of solution pH on reactive species production and pollutants degradation.

2.5.7 Effect of solution conductivity

The variation of solution conductivity has a significant effect on the reactive species production in the discharge with water. For underwater discharges, the electrical breakdown in deionized water is weak. Increasing the solution conductivity results in rapid increases of discharge current amplitudes, and significant reductions of streamer length [56]. As the ions in solution are the charge carrier, higher solution conductivity leads to faster movement of space charge. However, the ions may also consume or destroy the reactive species in solution and therefore, reduce the chemically active species production. Sato [55] found that increasing the solution conductivity results in a higher oxidation yield in underwater discharges. Sun [57] found that the reactive species production is affected by the solution conductivity due to the changing of discharge characteristics. Sunka [56] found that $H^{\cdot}$ and $O^{\cdot}$ emission spectrum lines could only be identified at low solution conductivities; in addition, the highest OH radical formation was detected in the solution with the conductivity of <100 μS/cm.

In discharges above a water surface, Lin [100] found that adding KCl into the solution increased the solution conductivity and reduced the power loss significantly, and also enhanced the dye degradation initially; however, this effect disappeared after a few minutes and no explanation was given. Thagard [4] compared H_2O_2 production in solution with 200 μS/cm and 2000 μS/cm conductivity, and found that increasing the solution conductivity inhibited the H_2O_2 generation significantly in both acidic and basic conditions. Therefore conductivity of the water and its influence of H_2O_2 production will be investigated in this research.

2.6 Pollutants degradation mechanisms by reactive species

2.6.1 OH radicals

The attack of OH radicals is the initial step of organic compound degradation. OH radicals tend to react and destroy organic pollutants through four pathways: (i) radical addition; (ii) hydrogen abstraction; (iii) electron transfer and (iv) radical combination [92]. The degradation of aromatic compounds by OH radicals should be initiated by the hydroxylation (radical addition) of benzene rings in both gas [93] and liquid phase discharges. Tezuka [93] suggested that the hydroxyl group (-OH) on the aromatic ring results in the hydroxylation to a *para* or *ortho* position.

Phenol is generally chosen as the model compound [94] to study the oxidation processes due to it being one of the main intermediate products during aromatic organic compound degradation, and its decomposition mechanism displays the degradation of an aromatic ring [64, 71, 90]. Joshi [64] used the HPLC method and concluded that the primary step products of phenol degradation are catechol resorcinol and hydroquinone, which agrees with the hydroxylation process suggested in Tezuka's research [93]. The secondary step is the further hydroxylation reaction that leads to the production of pyrogallol, 1,2,4-trihydroxybenzene, p-quinone and 2-hydroxy-1,4-benzoquinone. After that, the cleavage of the aromatic ring occurs and the further oxidation leads to the final products of CO_2 and water.

Grabowski [95] investigated phenol removal by positive pulsed corona, and found that the removal yields reached 46 g/kWh. Replacing the static liquid cathode with a flowing liquid cathode, with a rate of 0.3 L/min, leads to a higher phenol removal yield. This result may be due to the reactive species being transferred more easily into the water than in static conditions. The additions of iron lead to a Fenton-like reaction, which decomposes H_2O_2 into OH radicals, therefore, increase the ROS oxidative strength [96].

Various organic dyes such as methylene blue, azo group, etc., have been proven to be degraded effectively in electrical discharges [97, 98]. The two-nitrogen double bond (-N=N-) in azo and carbon nitrogen double bond (-C=N-) in the methylene functional group has been proven to be very sensitive to OH radicals [99]. The major mechanism of dye degradation is the cleavage of old bonds with different bond dissociation energies and the formation of new bonds. The high-energy electron and reactive species generated in discharges lead to the cleavage of organic bonds, and the discolouration of dye. Lin [100] investigated dielectric

barrier discharges in water to investigate Alizarin red degradation and found that the dye degradation rate increased with a higher energy input but then declined with further increase of the energy; Lin considered this could be due to the higher energy consuming the $O^{\cdot}$ radical to form NO_x products. Ikoma [80] investigated the degradation of methylene blue in pulsed discharges above water, and found that the degradation rate increased with increasing O_2 content in the feed gas. In this research, the degradation of methylene blue was investigated in O_2 plasma treatments, which is discussed in Chapter 9.

2.6.2 Ozone

During the oxidation process, O_3 produced above water can diffuse into the water to degrade target pollutants. In comparison to high degradation efficiency by OH radicals, the effectiveness of O_3 is relatively weaker [101]. Ognier [102] found the reaction rate constant of O_3 reaction with phenol is around four orders of magnitude lower than OH reactions at $k_2 = 10^6 \mathrm{M}^{-1}\mathrm{s}^{-1}$and the O_3 reaction can only keep a high rate constant in unsaturated organic compound solutions. Sano [103] found that organic compounds can be degraded in O_3 treatment easily; however, the total organic compound (TOC) cannot be degraded effectively. He also found that increased O_2 concentration enhanced O_3 production; however, this decreased the OH production by the consumption of O radicals, leading to a decreasing of the degradation rate of organic pollutants. This phenomenon shows that O_3 may not be the main contributor to organic compound degradation. Hoeben [90] found that the phenol degradation processes in argon and air discharges with or without additional O_3 are quite different; this also indicates that the organic decomposition mechanisms of O_3 differ from that of OH radical treatment. Hoeben concluded that O_3 treatment leads to organic compound degradation by producing molozonides and ozonides as the primary step, leading to the cleavage of aromatic rings.

2.7 Conclusion

Various models of electrical discharges involving water have been reported and proven to be effective for the production of reactive species. For the plasma generated with a pin-water electrode structure, the discharge types change with increasing applied voltage. The reactions between high energy electrons and gas molecules in different pathways have been introduced.

The electrical discharges in the gas phase above water consume much less energy compared to those required in discharges in liquid [1]. The reactive species such as OH radicals, O_3, and H_2O_2 were proven to be generated at the plasma-water interface; the generation and decomposition pathways of these species have been introduced. The reaction between energetic positive ions and water were considered as the main source for OH radical formation in gas phase discharges. The attack pathways of various reactive species to organic compounds were discussed.

Discharges in the liquid phase have been proven to produce various reactive species *in situ* and the reactive species production increases with increasing input energy [107]. In addition, Sunka [56] found that the H_2O_2 and O_3 produced in water increased with time, reaching a saturation level. In the liquid phase discharge, the degradation rate of organic compound increases with gas bubbling rate, which indicates the increasing production of reactive species. Discharges in O_2 can produce much higher levels of ROS in liquid than in air, due to the absence of oxy-nitride. However, large amounts of energy were consumed to heat up water to generate water vapour bubbles.

The main factors that impact the oxidative species production can be concluded as: (i) input power; (ii) contact area and time of plasma-water interface; (iii) plasma volumes and densities; the oxidants generally increase with increasing amounts of these three factors. Other factors such as: (iv) solution pH; (v) solution conductivity; and (vi) chemical productions such as oxy-nitride species and free radicals; all have a critical effect on oxidant production, thus a wide range of studies still need to be undertaken to optimize the processes for oxidant production. The factors were investigated in the course of the research reported in this thesis and will be discussed under several types of discharges include: impulsive current discharges, DC glow discharges and dielectric barrier discharges. Although a series of studies into reactive species production during electrical discharges have been reported, the reaction zone and the reaction mechanisms remain unresolved, and need further investigation.

3 METHODOLOGY

3.1 Introduction

A methodology was developed to investigate the reactions occurring at the plasma-water interface. Reactors were designed to initiate the electric discharges in contact with water. The pin-to-water electrode structure was employed for impulsive current discharges and DC glow discharges. A DBD reactor with a porous PTFE plate was designed to allow the discharge to develop through the micro-pores, with a diameter of 0.1-mm, into the grounded solution.

Positive or negative DC voltage was applied to investigate the impulsive current discharges and the DC glow discharges developed above water surfaces. An AC linear high frequency power supply was used in DBD treatments. Various gases (O_2, N_2, air and helium) were employed to investigate their effect on OH radical and H_2O_2 production. The variation of solution properties, such as pH, conductivity and oxy-nitride generation, were also measured after each treatment. Fluorescence and UV spectrometry were employed to determine the concentration of OH radicals and H_2O_2. Table 3.1 lists the experimental setup for the experiments processed in each chapter.

Table 3.1 Discharge types, investigation purpose and treatment times for each Chapter

Chapter No.	*Discharge types (water types)*	*Investigation field*	*Treatment times (min)*
4	ICD (U)	EDC	0.5, 1, 2, 5, 10, 15, 20
5	ICD (U)	EDC/OH & H_2O_2 production	5, 10, 15, 20
6	Controlled ICD (T)	EDC/H_2O_2 production	15, 30, 45, 60
7	DCGD (T)	EDC/H_2O_2 production	5, 10, 15
8	DCGD with flowing cathode (T)	EDC/H_2O_2 production	5, 10, 15
9	DBD (U)	EDC/H_2O_2 production	5, 10, 15, 20
	DBD (MB solution)	MB degradation	1, 2, 3, 4, 5

ICD Impulsive current discharge

EDC Electric discharge characteristics

H_2O_2 Hydrogen peroxide

DCGD DC glow discharge

U Ultrapure water

T Tap water

MB Methylene blue

3.2 Experimental equipment

A Tektronix P6015A high-voltage probe with a bandwidth of 75 MHz was employed to measure the voltage applied to the reactor. A 50-Ω coaxial cable was connected to the reactor ground for fast current measurement. A LeCroy digital oscilloscope (Waverunner 610Zi), with a bandwidth of 1 GHz and sampling rate of 20 GS/s, was used to record and process the waveforms.

For each treatment, the solution was introduced into the reactor via a 5-ml pipette (P5000G, Gilson). A conductivity meter and a pH meter (Thermo Orion Star) were employed to measure the conductivity of the solution before and after each treatment. A spectrophotometer (Thermo Scientific, Evolution 201) was used to measure the concentration of H_2O_2 and MB dye by measuring the absorption of the Titanium (IV)-peroxide complex at the wavelength of 396 nm, and for the MB samples at the wavelength of 665 nm. A Spectro-fluorometer (Edinburgh Instruments, FS5) was used to measure the concentration of 2-hydroxyterephthalic acid (HTA)-the product of OH radical reaction with terephthalic acid (TA), to determine the OH radical production. Nitrite and nitrate test strips (QUANTOFIX, Z166421, Z166413) were used for oxy-nitride detection after each treatment.

A mass flow controller and a gas pressure controller were employed during each experiment. A pressure controller (Alicat Scientific, PC-30PSIA-D/5P) was employed when O_2, N_2 and helium was used during each experiment. It has a control valve beside the gas inlet port; the control setup can be made by pressing the control button, with the use of the line-up and line-down buttons to move the arrow and adjust to the value required. The flow controller (Alicat Scientific, MC-5SLPM-D/5M) allows gas flows of up to 5 L/min. It also contains a control valve beside the gas inlet port. To change the working gas, the ‘gas type’ option on the flow controller needs to be changed, due to the control being achieved by measuring the mass of passed gases.

Table 3.2 List of equipment employed in this research

Name	Manufacturer	Measurement range	Resolution	Accuracy
AC power source	Pacific	20-5,000 Hz	-	-
DC power supply	Glassman	0-20 kV	-	-
Ultrapure pure water	Milli-Q	-	-	-
Spectro-fluorometer	Edinburgh Instruments	Excitation 230-1000 nm Emission 230-870 nm	0.3 nm	±0.5 nm
UV-spectrometer	Thermo Fisher Scientific	200-800 nm	1 nm	0.5: ±0.0004
Oscilloscope	LeCroy	1 GHz	20 GS/s	-
High voltage probe	Tektronix P6015A	0-20 kV DC	-	-
Gas Flow controller	ALICAT (MC Series)	0-5 L/min	0.1 L/min	±0.8%
Pressure controller	ALICAT (PC Series)	0-1 bar absolute	0.001 bar	±0.25%
Needle valve	HOKE	-	-	-
Weighing	OHAUS Discovery	0.1-210 mg	0.1 mg	±0.2
Pipette	Gilson	0.1-5 ml	0.1 ml	±0.6%
Conductivity meter	Thermo Scientific Orion	0.001µS-3000mS	1 ppm	±0.5%
pH meter	Thermo Scientific Orion	-2 to 16	0.01	±0.01 pH

3.3 Sample preparation

Ultrapure water (Milli-Q, type 1 ultrapure water) with a conductivity of 0.5 µS/cm was collected from a Milli-Q purification system. Tap water with a conductivity of 65 µS/cm was collected from a tap in the REN Laboratory.

Tert butanol solution

Tert-butanol (TB) (ACS reagent ≥ 99.0%, Sigma-Aldrich) has been used as a scavenger to absorb hydroxyl radicals in solutions [7, 108] (R 3.1). this allowed the role of the

dimerization reaction (R 2.25) in the production of H_2O_2 to be determined. 20 ml tert-butanol was mixed in 1 L of ultrapure water or tap water depending on the water used in the set of experiments, to prepare a 0.2 M tert-butanol solution.

$$(CH_3)_3COH + OH^{\cdot} \rightarrow (CH_3)_2C(OH)CH_2^{\cdot} + H_2O \qquad \text{(R 3.1)}$$

Terephthalic acid solution

Fluorescence spectrometry using terephthalic acid (TA) was employed to quantify OH radical formation. 200 mg of sodium hydroxide (NaOH) (ACS reagent, ≥97.0%, pellets, Sigma-Aldrich) was weighed and dissolved in 1 L of ultrapure water to make a 5-mM NaOH solution. Due to the insolubility of TA powder in acid and neutral solutions, 332-mg TA powder (98%, Aldrich) was weighed and dissolved in the 1000 ml of 5 mM NaOH solution. After that, the solution was left to stand for two hours for complete dissolution.

Potassium titanium (IV) oxalate solution

H_2O_2 production was measured by UV spectrometry. 35.4 g of potassium titanium (IV) oxalate (Technical, ≥90%, Ti basis), $K_2TiO(C_2O_4)_2{\cdot}2H_2O$, was dissolved in 300 ml of ultrapure water. 272 ml of concentrated sulphuric acid (ACS reagent, 95.0%, Aldrich) was mixed with potassium titanium oxalate solution (cooling and care are required) and made up to 1 L with ultrapure water [109]. A heat releasing process was noticed when the high concentrated sulphuric acid was slowly poured in, and mixed with titanium (IV) solution. After the treatments, 5 ml of titanium reagent and 5 ml of treated sample were pipetted into a 25-ml volumetric flask, and made up to 25 ml with ultrapure water. The peak absorbance of H_2O_2-Ti complex appears at 396 nm, the concentration of it was measured by a VIS-UV spectrophotometer

Methylene blue solution

300 mg of high-purity methylene blue (MB) hydrate (95%, Acros organics) was weighed and dissolved in 500 ml of ultrapure water to prepare the MB dye solution with an initial concentration of 600 mg/L. The peak absorbance of methylene blue appears at 665 nm and the concentration was measured by a VIS-UV spectrophotometer.

3.4 Gas vacuum and delivery system

An Edwards E2M80 rotary-vane vacuum pump was employed to evacuate the reactor chamber before injecting the working gas (air, N_2, O_2, He). Figure 3.1 shows the schematic diagram for the vacuum system used in this research; the pressure controller was connected between the gas cylinder and gas inlet of the reactor to measure the pressure in the reactor. The gas outlet was connected to the vacuum pump through a needle valve. The needle valve was employed to control the vacuum level in the reactor to avoid excessive bubbles overflowing from the solution, especially in the cases when TB was added to the solution, which reduces the solution surface tension significantly and leads to the formation of a significant amount of tiny bubbles, this phenomenon does not affect the discharge activity.

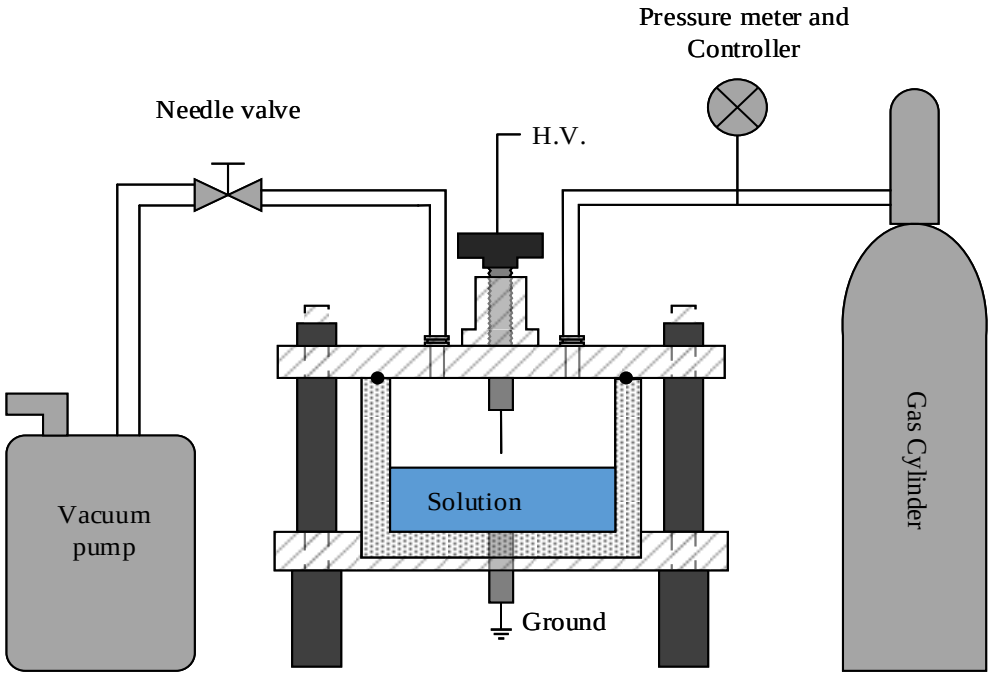

Figure 3.1 Schematic diagram for vacuum system.

The first step was to set the pressure controller to 0 Torr before vacuuming, then switch on the pump and slowly switch on the control valve to limit the vacuum level. The pressure in the reactor was reduced from atmospheric to around 10 Torr after 10 seconds. After that, the pump was switched off and the pressure meter was set to atmospheric pressure, which led to the refill of working gas. This process was repeated twice to minimize the residual air in the reactor.

3.5 OH radical, H_2O_2 and methylene blue concentration measurement

3.5.1 UV-VIS spectrophotometry

Spectrophotometry is a major technique for solution analysis and has been widely used in various fields. It measures the intensity of a beam of light that passes through sample solutions and determines properties of the samples such as concentration. A spectrophotometer (Evolution 201, Thermo Fisher Scientific), was employed to measure the absorbance of treated and control samples. To determine solution concentrations during experiments, a calibration curve which shows the relationship between absorbance and solution concentration is needed.

The Beer-Lambert law presents the attenuation of light that travels through a measured sample, in which the absorbance and measured material concentration has a linear relationship.

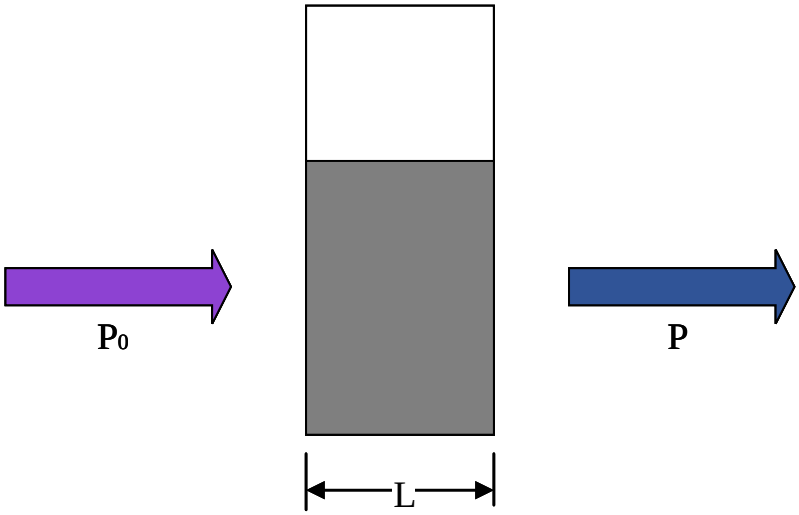

Figure 3.2 Light absorbed by sample in a cuvette.

Beer-Lambert Law:

$$ABS = \varepsilon \times l \times c \qquad \text{(Eq. 3.1)}$$

ABS Absorbance

ε Wavelength-dependent molar absorptivity coefficient with units of M^{-1} cm^{-1}

l Path length of the cuvette with units of centimetre

c Analyte concentration with units of M

The solution transmittance formula:

$$T = P/P_0 \quad \text{(Eq. 3.2)}$$

T Sample transmittance

P Radiant power output

P_0 Radiant power input

The solution transmittance can be calculated by the equation (Eq. 3.3).

$$T = 10^{-ABS} \quad \text{(Eq. 3.3)}$$

H_2O_2 concentration measurement

The molar absorptivity of the titanium (IV)-peroxide complex, prepared by adding titanium (IV) solutions into H_2O_2 solutions, was measured as ε_{396} = 905 $M^{-1}cm^{-1}$ at the peak absorbance of 396 nm. Figure 3.3 shows the calibration curve for H_2O_2 solution.

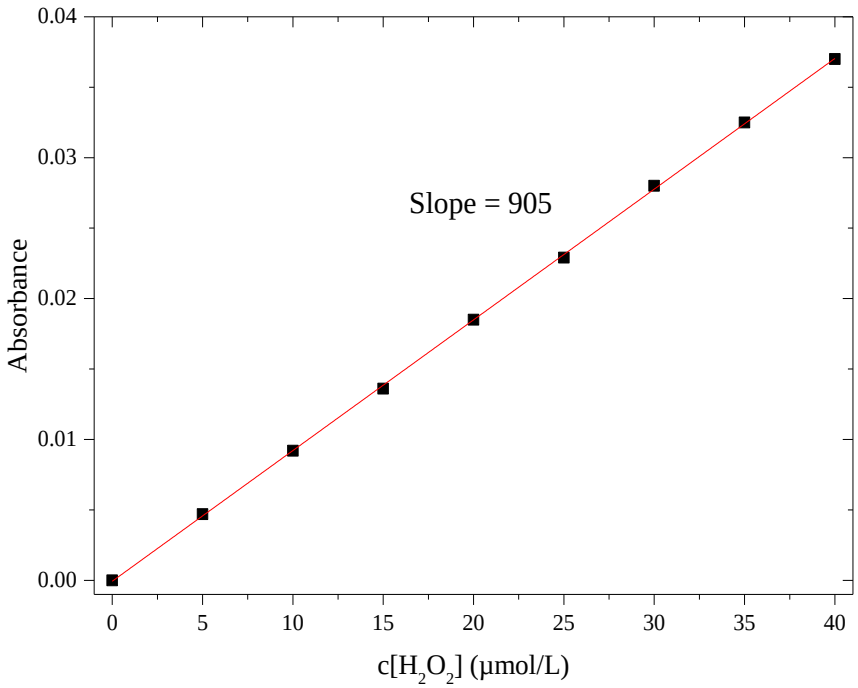

Figure 3.3 Calibration curve for H_2O_2 solution

Methylene-blue concentration measurement

The methylene blue solution was prepared by diluting methylene blue (MB) hydrate (95%, Acros organics) in ultrapure water into certain concentrations.

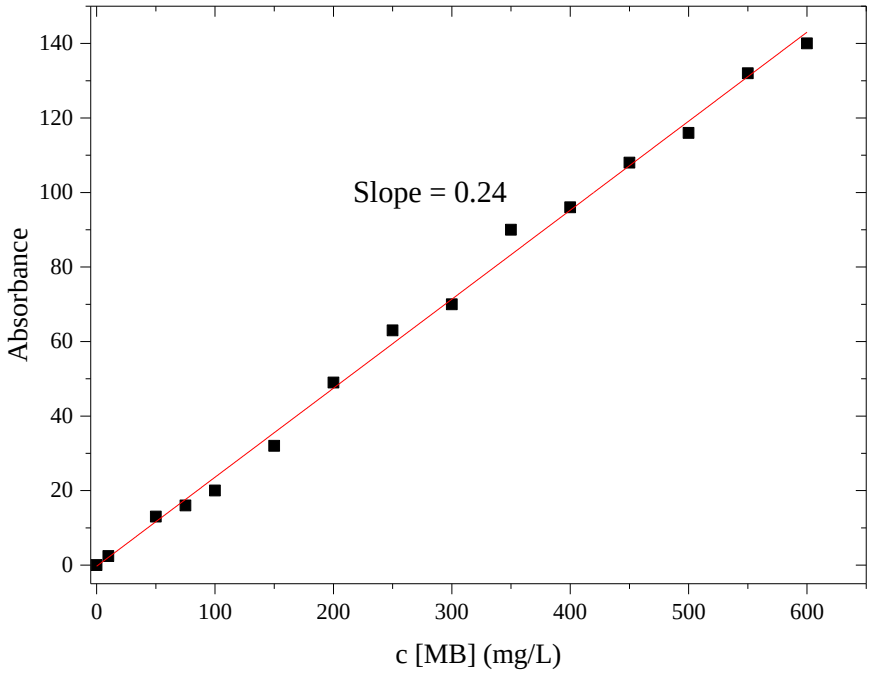

Figure 3.4 Calibration curve for methylene blue solution

The molar absorptivity coefficient (ε) of methylene-blue (molar weight of 319.5 g/mol) was calculated as 74×10^3 $M^{-1}cm^{-1}$. The degradation rate of MB dye can be determined by Equation (Eq. 3.5):

$$Degradation\ rate = \frac{ABS_0 - ABS_1}{ABS_0} \times 100\% \qquad \text{(Eq. 3.5)}$$

ABS_O Absorbance of the sample before treatment

ABS_1 Absorbance of the sample after treatment

3.5.2 Fluorescence photometry

Fluorescence spectrometry is a fast and simple method to determine the concentration of an analyte in solutions depending on its fluorescent properties. A beam with a wavelength range from 180 nm to 800 nm is passed through a cuvette with a solution, and the light emitted from the sample is measured. The intensity of the emission increases in proportion with the concentration of the analyte and a calibration curve needs to be performed before the measurement.

OH radical measurement

A calibration curve was plotted by using 2-hydroxyterephthalic acid (97%, Aldrich) (HTA), the product of terphthalic acid reacts with OH radical, to determine the amount of OH radicals. The converted OH radicals into HTA are 35%. The HTA solution was made up with 5-mM NaOH solution. When HTA molecules are irradiated with UV light with a wavelength of 310 nm, visible light of wavelength 425 nm is emitted.

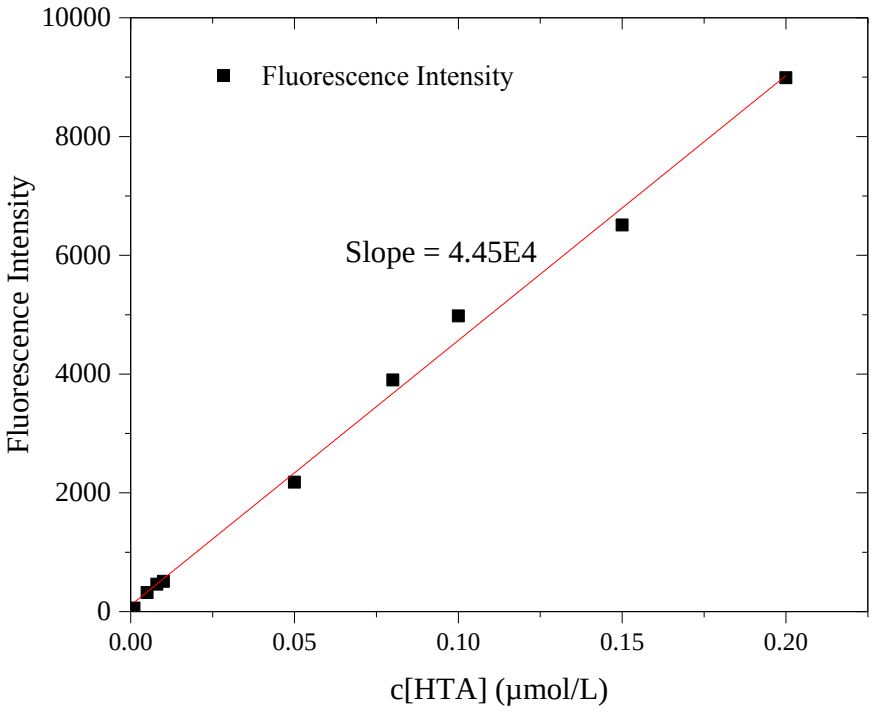

Figure 3.5 Calibration curve for HTA solution

4 DISCHARGE CHARACTERISTICS OF IMPULSIVE CURRENT DISCHARGES ABOVE WATER

4.1 Introduction

Discharges above water with a pin-to-water electrode structure have been extensively investigated. A series of studies using pulsed power with high applied voltage (several tens of kV) to initiate the inter-electrode gap breakdown have been used to investigate the breakdown mechanisms [110, 111]. The effect of solution conductivity and solution pH on reactive species production in the discharges in contact with water has also been widely investigated [3, 100]; however, their effects on the variation of discharge characteristics have rarely been discussed [27, 28]. A discharge type transition with increasing solution conductivity has been recorded in a previous study [7]; the impulsive currents were recorded at the beginning of the discharges with an inter-electrode gap of 1 mm, and tail currents occurring after the initial current impulse appeared with increasing solution conductivity; however, the mechanism of the tail currents is still not clear. Nikiforov [28] investigated discharge transition in discharges above water surfaces, and recorded similar results as those observed by Zhao [7]. Nikiforov concluded that the transition of discharge is independent of the polarity of the applied voltage, but dependent on the inter-electrode distance and the magnitude of applied voltage.

The pin-to-water electrode discharges energised using a DC power supply allows the generation of impulsive current discharges without the complexity of using a pulsed power system, thus, significantly reduces the operation cost. In addition, the investigation of discharges characteristics clarifies the fundamental of reactive species production. It is worthwhile to investigate the effect of solution conductivity on the pin-to-water electrode discharge characteristics.

In this chapter, the impulsive current discharges energized by positive or negative DC power have been investigated. The objectives of this experiment were to investigate the (i) effect of polarity on discharge characteristics; (ii) effect of solution conductivity on discharge transition and (iii) effect of applied voltage on discharge characteristics.

4.2 Reactor design and experimental set up

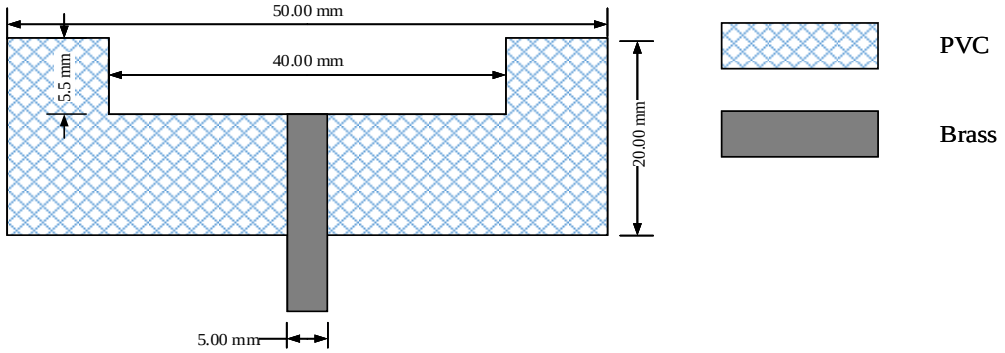

Figure 4.1 Reactor design.

An open reactor with an outer diameter of 50 mm and inner diameter of 40 mm, and an entire depth of 20 mm and inner depth of 5.5 mm was made of PVC (Figure 4.1). A brass electrode with a diameter of 5 mm and length of 25 mm was used as a grounded electrode.

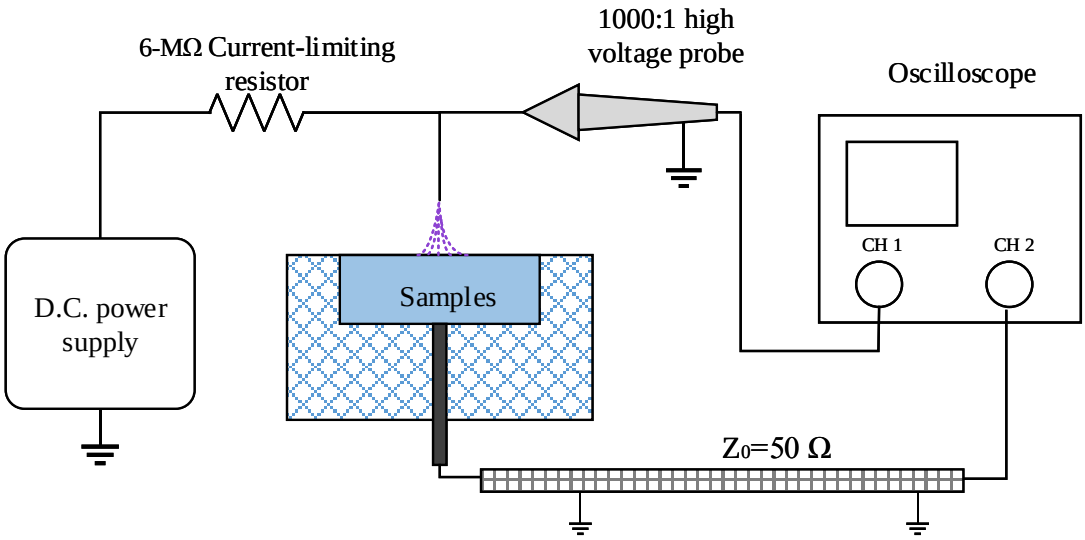

Figure 4.2 Schematic diagram for impulsive current discharge experiments in open air.

A DC power supply was employed to supply positive or negative applied voltage during experiments; a current-limiting resistor of 6-MΩ was connected in series with the reactor (Figure 4.2). A 50-Ω coaxial cable was connected to the reactor ground to investigate the variation of discharge current. A Tektronix high voltage probe was employed to measure the

pin voltage during experiments. A solution volume of 7 ml was introduced into the test cell before each treatment; the solution depth was 5.5 mm. A stainless-steel pin electrode with a tip diameter of 0.3 mm was placed 1 mm above the centre of the water surface. The inter-electrode distance (pin tip to water surface distance) was determined by a screw micro-meter. The needle electrode was not changed in this experiment.

Ultrapure water with a conductivity of 0.5 μS/cm and tap water with a conductivity of 65 μS/cm was employed in this experiment. The discharge waveforms were recorded at 0, 0.5, 1, 2, 5, 10, 15 and 20 minutes of treatment. Higher solution conductivities, being adjusted by NaOH solutions as shown in Table 4.1, were employed to investigate the variation of discharge currents; the discharge waveforms were recorded at the beginning of discharges. The variation of solution conductivity was measured after each treatment and the treated samples were removed by a pipette; the reactor was cleaned using ultrapure water and dried by N_2 jet.

Table 4.1 Solution conductivity adjusted by NaOH

Solution Conductivity	*μS/cm*			*mS/cm*				
	100	250	500	1.2	2.4	5	12	22

4.3 Gas discharge characteristics under DC positive polarity

4.3.1 Discharge above ultrapure water

The power supply was set to support 3 kV, so that the voltage does not increase after the gas gap breakdown was initialled. Figure 4.3 shows the voltage and current waveforms recorded in discharge above ultrapure water after 0 and 0.5 minutes of treatment. At the beginning of treatment, only impulsive current with short full-width-at-half-maximum (FWHM, considered as pulse width in this study) of 15 ns and amplitude of up to 40 mA was recorded (Figure 4.3 (b)); the voltage drop was less than 100 V and the pulse repetition rate was ~1×10^5 pps.

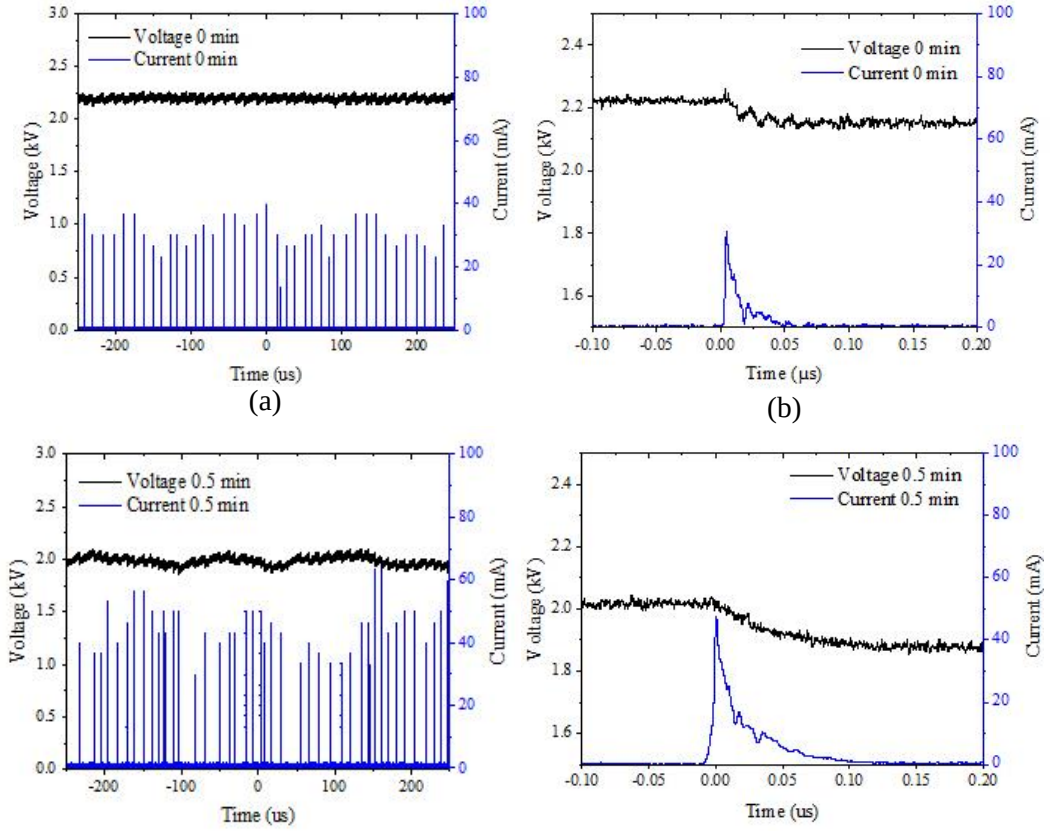

Figure 4.3 Discharge waveforms recorded in ultrapure water at 0 minutes (a) and after 0.5 minute of treatment (c); single impulse current recorded at 0 minute (b) and after 0.5 minute of treatment (d).

After 0.5 minutes of treatment (Figure 4.3 (c)), a slightly waved voltage waveform was observed, and an increase of the current amplitude up to 65 mA was recorded. The voltage drop was increased to ~150 V (Figure 4.3 (d)) and the pulse repetition rate was no longer a

constant value and varied from 0.4 to 1.43×10^5 pps. The solution conductivity slightly increased to 3.5 µS/cm after 0.5 minutes of treatment (Table 4.2).

After 1 minute of treatment (Figure 4.4 (a)), significant decreases in voltage of ~800 V were observed. A group of nanosecond current pulses with repetition rate of ~4×10^5 pps were observed corresponding with the voltage drop duration (Figure 4.4 (c)) each current pulse corresponded to a voltage drop of several tens of volts. The amplitude of pulses decreased as

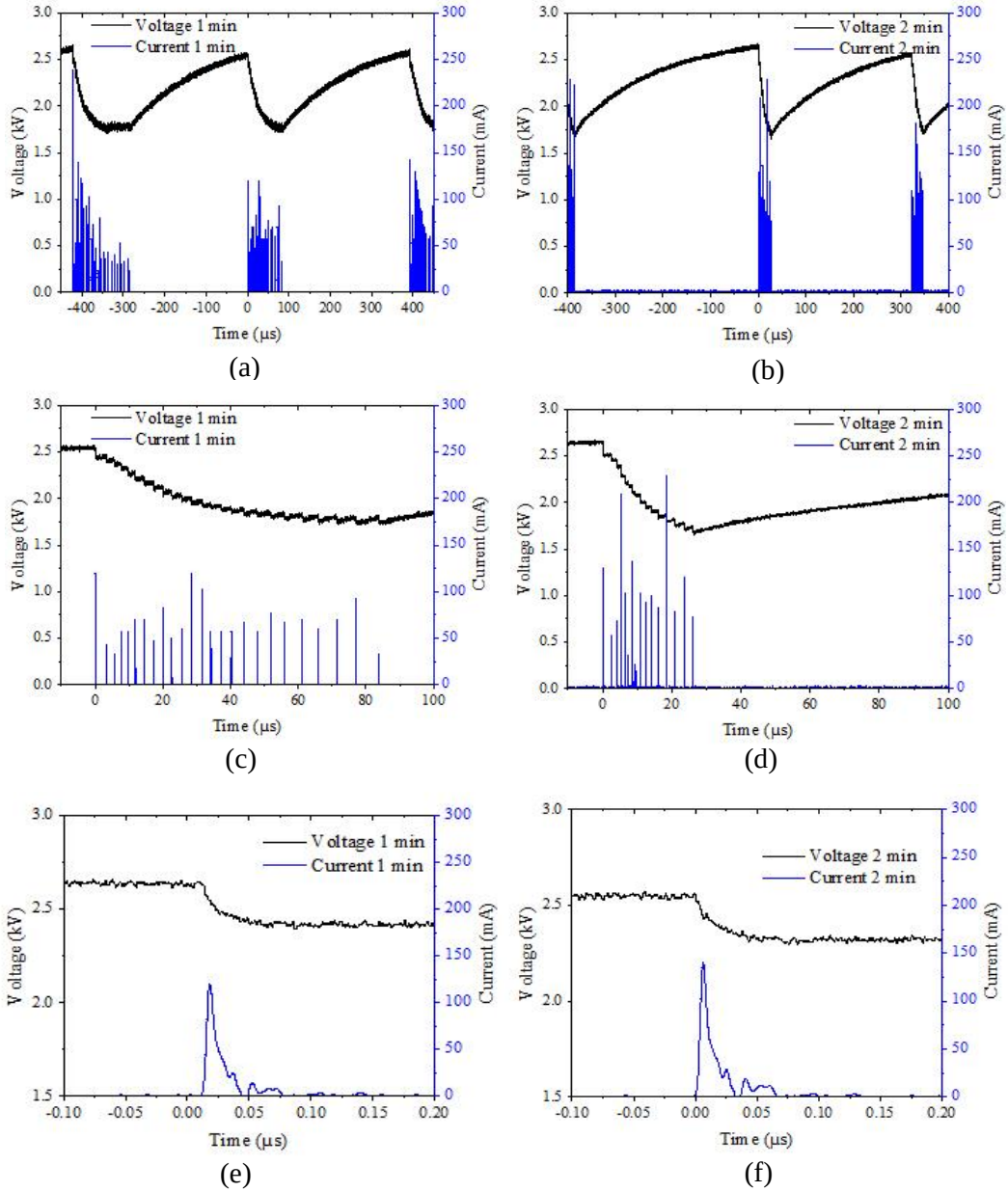

Figure 4.4 Discharge waveforms recorded in ultrapure water at 1 minute (a) and 2 minutes of treatment (b); voltage drop recorded at 1 minute (c) and 2 minutes of treatment (d); single impulse current recorded at 1 minute (e) and 2 minutes of treatment (f).

the voltage decrease during the voltage drop.

Table 4.2 Variation of solution conductivity in discharge above ultrapure water

Treatment times (min)	*0*	*0.5*	*1*	*2*	*5*	*10*	*15*	*20*
Conductivity (μS/cm)	0.5	3.5	5.5	8.4	17.5	37	54	72

After 2 minutes of treatment, voltage drops with a shorter duration (~30 μs) and a larger magnitude (~1 kV) was recorded. The repetition rate of pulses further increased to 6×10^5 pps (Figure 4.4 (d)). An increase of current amplitudes was noticed, while no variation of the current pulse width was recorded.

After 5 minutes of treatment (Figure 4.5), a further decrease of voltage drop duration (~17 μs) was recorded; the high-repetition-rate pulses were replaced by a tail current of amplitude of <3 mA and duration of ~10 μs; no corresponding voltage drop was observed associated with the tail current. High-amplitude current pulses of 200 to 300 mA and pulse width of 15 ns (Figure 4.5 (b)) only appeared at the start and end of the voltage drop. The appearance of tail currents between the impulsive currents that occurred at the beginning and the end of voltage drop indicates the start of discharge type transition.

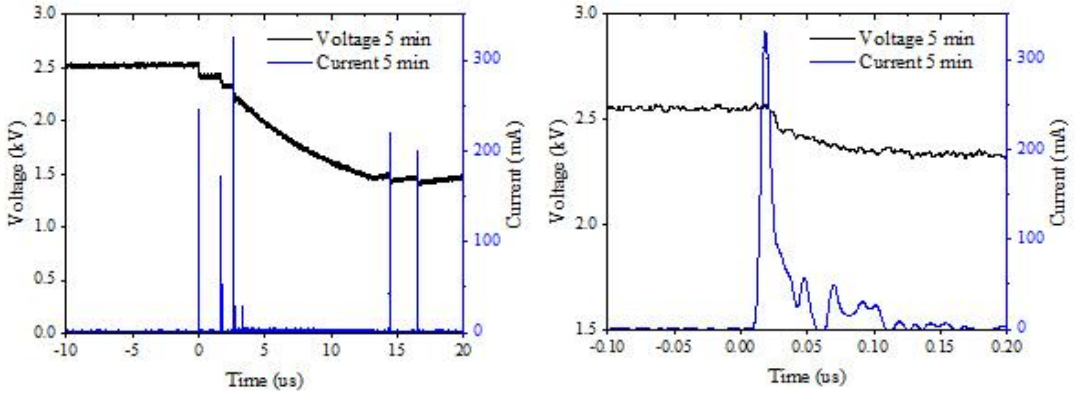

(a) (b)

Figure 4.5 Discharge waveform recorded in ultrapure water at 5 minutes of treatment (a) and single impulse current recorded at 5 minutes of treatment (b).

The discharge voltage drop increased to ~1.4 kV after 10 minutes of treatment (Figure 4.6 (a)); the high-amplitude current pulses no longer appeared at the end of the voltage drop. In addition, a current tail of amplitude of 5 mA and duration of ~7 μs was noticed following the multiple pulses with the amplitude of up to 220 mA and pulse width of 15 ns (Figure 4.6 (b)).

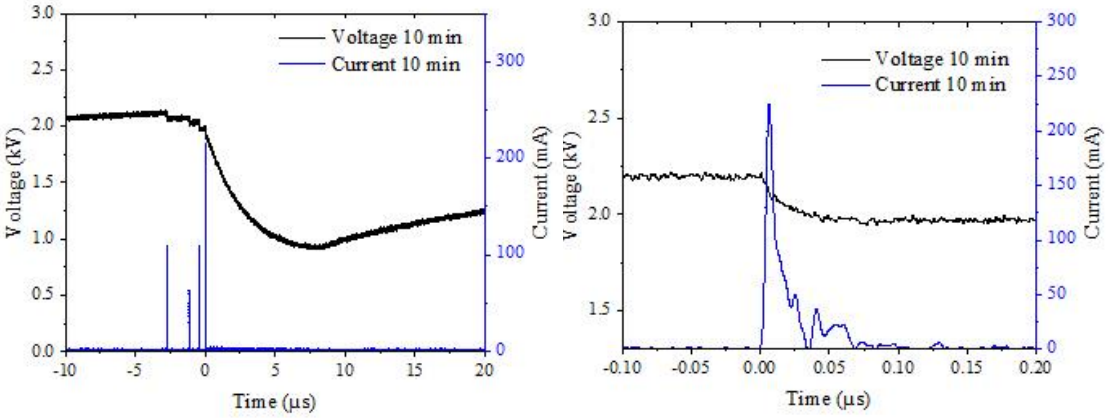

(a) (b)

Figure 4.6 Discharge waveform recorded in ultrapure water at 10 minutes of treatment (a) and single impulse current recorded at 10 minutes of treatment (b).

After 15 minutes of treatment (Figure 4.7 (a)), the reduction of the impulsive current amplitude was observed, no change of pulse width was recorded (Figure 4.7 (b)).

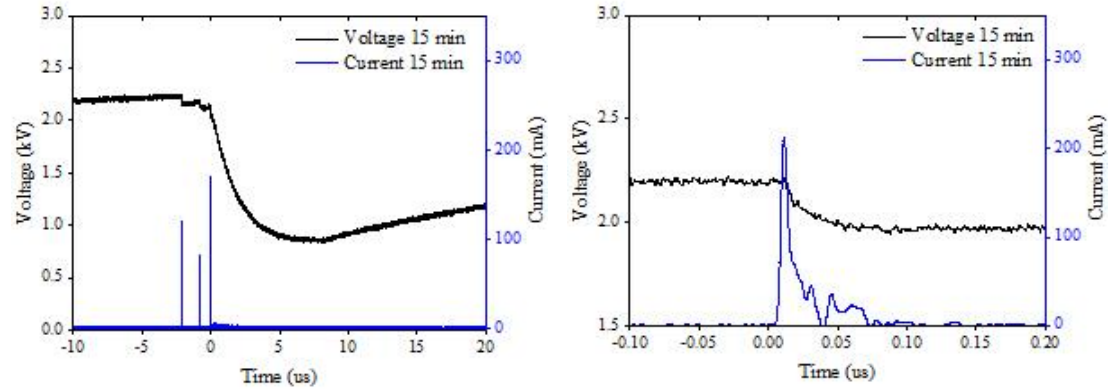

(a) (b)

Figure 4.7 Discharge waveform recorded in ultrapure water at 15 minutes of treatment (a) and single impulse current recorded at 15 minutes of treatment (b).

After 20 minutes of treatment (Figure 4.8), the amplitude of multiple current pulses further reduced to ~180 mA. The amplitude of current tail was further increased to ~10 mA while the voltage drop increased to 1.7 kV.

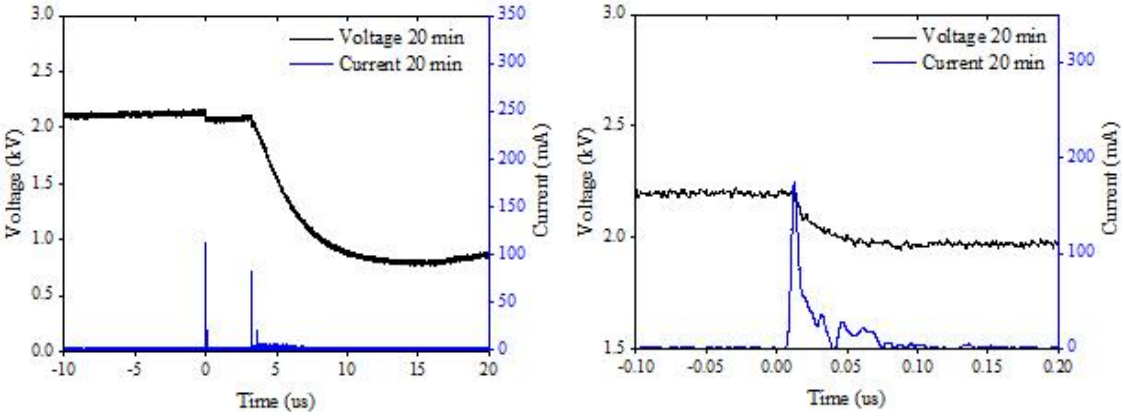

(a) (b)

Figure 4.8 Discharge waveform recorded in ultrapure water at 20 minutes of treatment (a) and single impulse current recorded at 20 minutes of treatment (b).

The discharge type transition from corona discharges to corona-diffuse discharges was observed with the increase of solution conductivity from 0.5 to 72 µS/cm.

4.3.2 Discharge above tap water

Tap water contains positive ions such as Na^+, Ca^{2+} and Mg^{2+} and inorganic negative ions such as Cl^-, CO_2^- and NO_3^-; therefore, it has a higher conductivity of 65 µS/cm compared to ultrapure water. Different applied voltage of 3 kV and 5 kV was employed to compare the discharge characteristics.

Applied voltage of 3 kV

Figure 4.9 shows the voltage and current waveforms recorded under positive discharge above tap water, with applied voltage of 3 kV. At the start of discharge, multiple current pulses with amplitude of up to 100 mA and pulse width of 15 ns (Figure 4.9 (a), (b)) were recorded, followed by a tail current with amplitude of 10 mA and duration of 15 µs. The voltage and current waveforms were almost the same as that recorded in ultrapure water when a similar solution conductivity was employed (72 µS/cm after 20 minutes of treatment

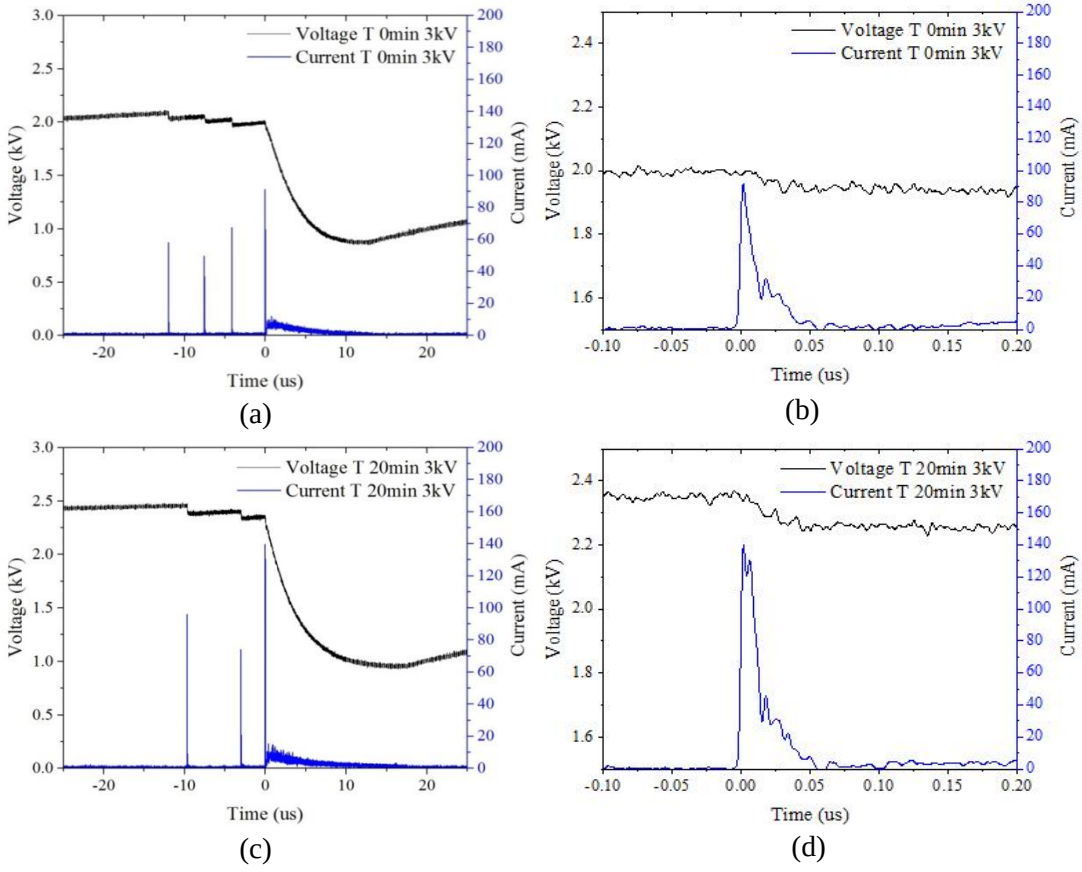

Figure 4.9 Discharge waveforms recorded in tap water under 3 kV at 0 minutes (a) and 20 minutes of treatment (c); single impulse current at 0 minutes (b) and 20 minutes of treatment (d).

with ultrapure water), indicating that the discharge characteristics are independent of the substances in solution; however, are dependent on the solution conductivity.

After 20 minutes, the solution conductivity was measured as 108 µS/cm; the amplitude of the impulsive current increased to ~140 mA (Figure 4.9 (c)), and no pulse width variation was observed (Figure 4.9 (d)); a slight increase of current tail amplitude to 17 mA was recorded.

Applied voltage of 5 kV

Fig 4.10 shows the discharge waveforms when the applied voltage was increased to 5 kV. The amplitude of impulsive and tail currents both increased with increasing treatment time; an impulsive current width of 15 ns was recorded. Increasing the applied voltage significantly shortened the recovery time of the voltage across the discharge gap, and led to the earlier appearance of the tail current after the impulsive current (Figure 4.10 (d)).

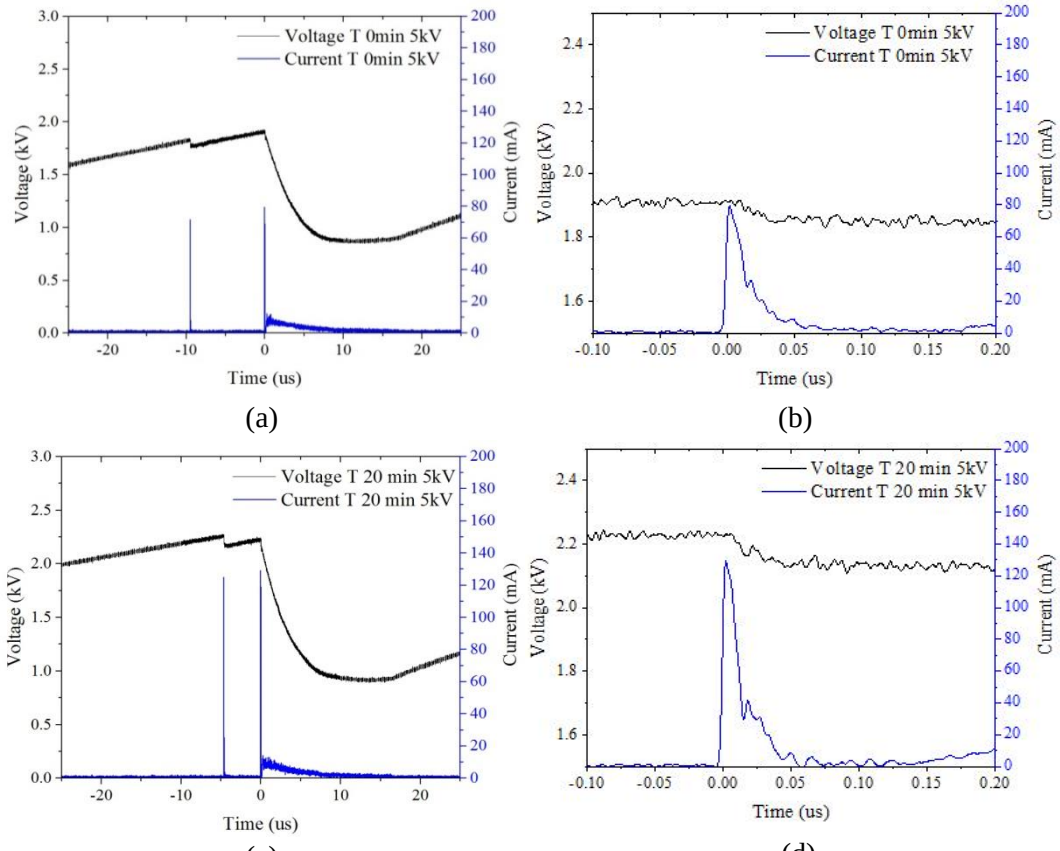

Figure 4.10 Discharge waveforms recorded in tap water under 5 kV at 0 minutes (a) and 20 minutes of treatment (c); single impulse current at 0 minutes (b) and 20 minutes of treatment (d).

Increasing the applied voltage from 3 kV to 5 kV led to the extinction of impulsive currents and the appearance of a DC component (Figure 4.11 (b)), which is similar to the results obtained in Nikiforov's research [28]. Figure 4.11 shows the variation of discharge voltage waveforms during experiments under positive applied voltage of 5 kV.

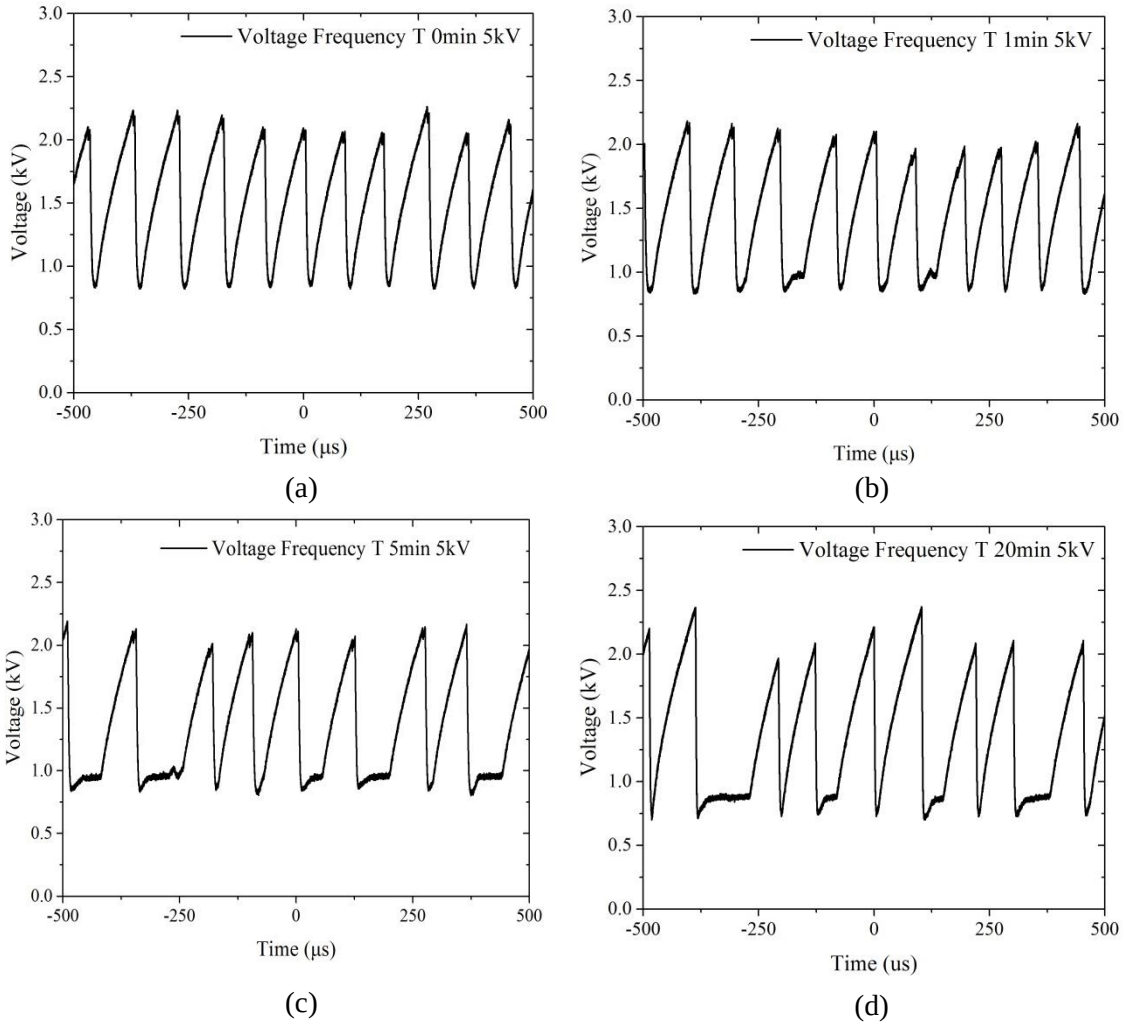

Figure 4.11 Discharge frequency recorded in tap water under 5 kV at 0 minutes (a), 1 minute (b), 5 minutes (c) and 20 minutes of (b) treatment.

After 1 minute of treatment, the discharge behaviour became irregular; with randomly occurring regions were the inter-electrode voltage did not recover. This phenomenon is likely to be due to the higher applied voltage, increasing the plasma conductivity in the discharge column, thus reducing the maintenance voltage of the plasma column. Therefore, the discharge is no longer limited by the 6-MΩ current-limiting resistor to form an impulsive current, and the transition of discharge type to a DC glow discharge randomly occurred.

Nikiforov [28] compared electrode geometries and found only spark discharge was observed with a hemispherical electrode; while with a pin electrode, a corona discharge was observed before it transited into spark discharge. Xiong [30] compared the pulsed discharges between pin-metal electrodes with an inter-electrode of 0.5 mm in various working gases and found that the voltage on the pin electrode (~4 kV) reduced to zero after each breakdown, which indicates the smaller voltage drop (~1.5 kV) in this experiment was due to the different electrode material (water in this experiment). Xiong [30] also varied the applied voltage from 4 to 9 kV and found that the breakdown voltage was not significantly changed while the repetition rate of secondary pulses was raised with increasing applied voltage.

4.3.3 Discharge above solutions with high conductivity

To investigate the discharge characteristics with various solution properties, pH values ranging from 10.9 to 13 and solution conductivity ranging from 0.1 to 22 mS/cm (Table 4.1) were applied by using different concentrations of NaOH solution. Applied voltages of 3 kV and 5 kV were employed to investigate the discharge characteristics.

Applied voltage of 3 kV

Figure 4.12 and 4.13 show the discharge characteristics under positive polarity with a V_{app} of 3 kV above NaOH solutions, with conductivities from 100 µS/cm (a similar value as that recorded after 5 minutes of discharges with tap water under the applied voltage of 3 kV) to 1.2 mS/cm.

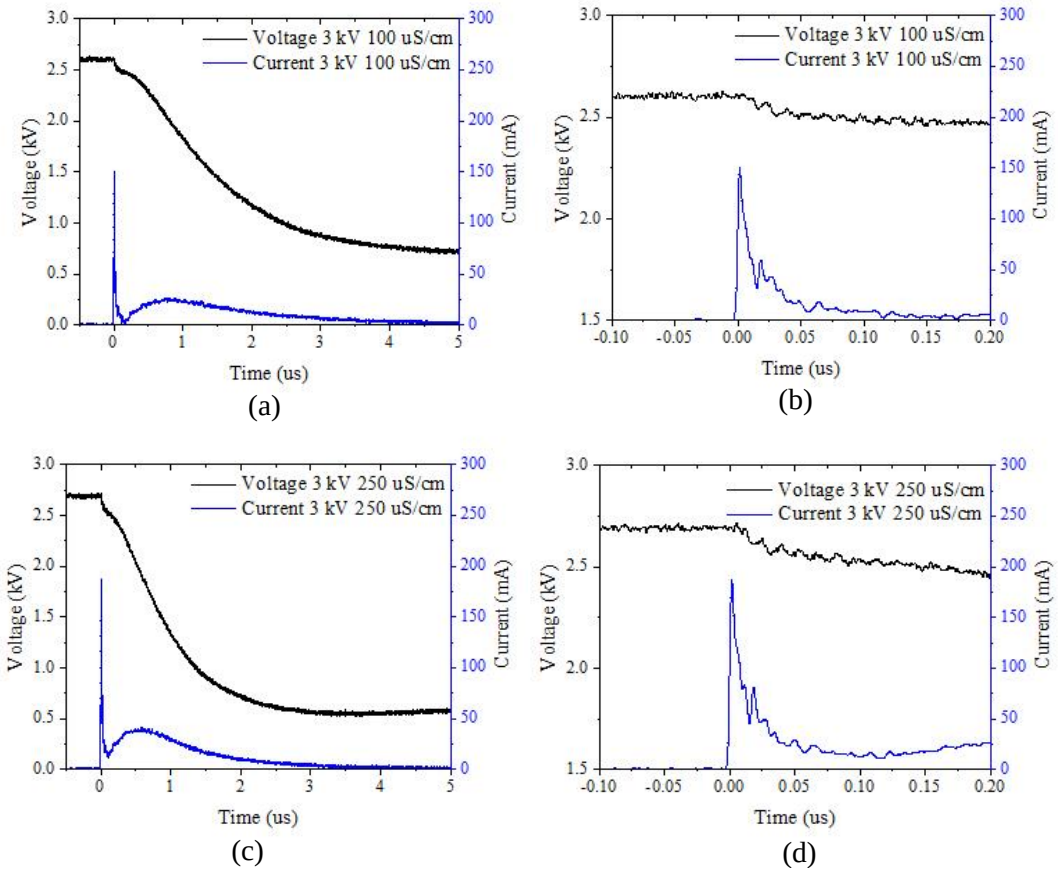

Figure 4.12 Discharge waveforms recorded under 3 kV with solution conductivity of 100 µS/cm (a) and 250 µS/cm (c); single impulse current with solution conductivity of 100 µS/cm (b) and 250 µS/cm (d).

In solutions with conductivities of 100 to 500 µS/cm, the impulsive currents amplitude of ~200 mA and pulse width of 12 ns were recorded. The tail currents were observed following the impulsive currents. The amplitude of tail currents increased from 30 to 60 mA, and the duration decreased from 4.5 to 2 µs, Figure 4.12 (a), (c) and Figure 4.13 (a), when increasing the solution conductivity from 100 to 500 µS/cm.

Increasing the solution conductivity to 1.2 mS/cm resulted in the increasing of the amplitude of impulsive currents to ~350 mA and of tail currents to ~150 mA; also, resulting in the decreasing of the tail current duration to ~1.5 µs. In addition, it was found that increased solution conductivity led to an earlier appearance of current tails, which developed at the falling edge of the impulsive currents (Figure 4.12 (d); 4.13 (b), (d)).

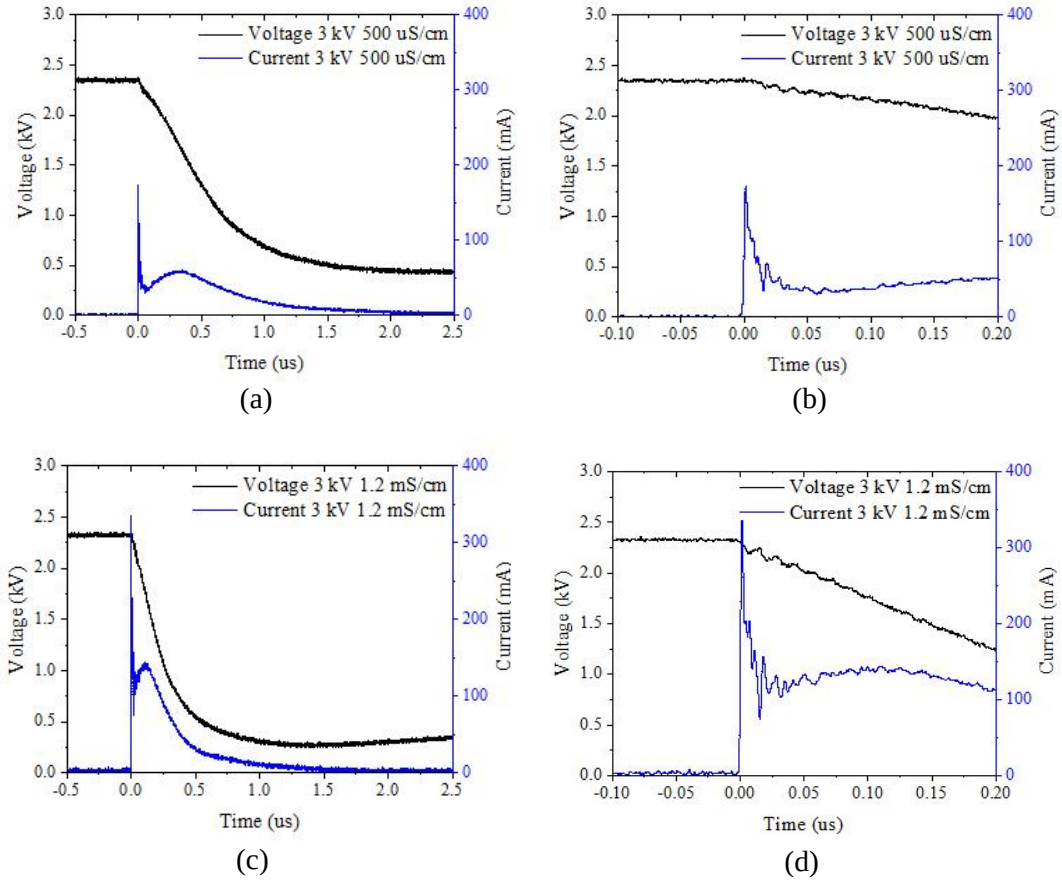

Figure 4.13 Discharge waveforms recorded under 3 kV with solution conductivity of 500 µS/cm (a) and 1.2 mS/cm (c); single impulse current with solution conductivity of 500 µS/cm (b) and 1.2 mS/cm (d)

The breakdown voltage was ~2.7 kV for 100 and 250 µS/cm solutions (Figure 4.12), which then decreased to ~2.3 kV with higher conductivity (Figure 4.13). Nikiforov [28] investigated the corona-spark transition over water and found that the breakdown voltage was independent of solution conductivity ranging from 50 to 500 µS/cm, which is different from the results obtained in this experiment.

Figure 4.14 shows the voltage and current waveforms under applied voltage of 3 kV with NaOH solutions, with conductivities from 2.4 to 22 mS/cm. As the tail current was developed closely to the impulsive current, the pulse widths cannot be determined. A significant voltage drop of ~2 kV was observed, when using the solution with a conductivity of 2.4 mS/cm (pH 12); the amplitude of impulsive currents was decreased to 140 mA, tail currents with amplitude of 250 mA and duration of 1 µs (Figure 4.14 (a)) were recorded following the impulsive currents.

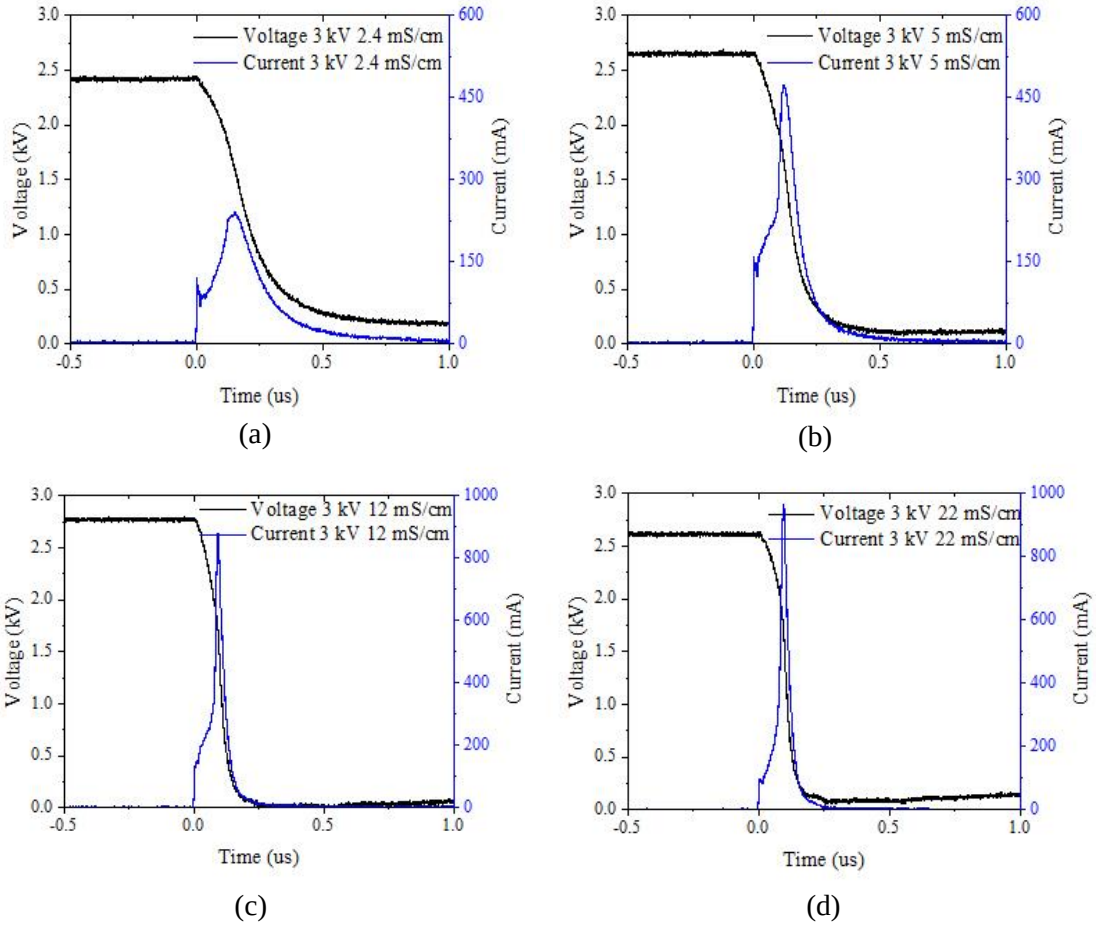

Figure 4.14 Discharge waveforms recorded under 3 kV with solution conductivity of 2.4 mS/cm (a), 5 mS/cm (b) 12 mS/cm (c) and 22 mS/cm (d).

A significant increase of the tail current amplitude and decrease of tail current duration was observed when the solution conductivity was increased to 5 and 12 mS/cm (Figure 4.14 (b), (c)); no increase of the impulsive current was observed. It was found that the increased solution conductivity led to the merging of the impulsive current and the tail current. The voltage on the anode pin reduced to almost zero, when using the solutions with conductivities of 5 to 22 mS/cm; this phenomenon indicated the solutions acted in a similar manner to a metal electrode during discharges. Therefore, spark discharges were considered to be occurring between the electrodes; the noise of each spark was noticed. The shortest tail current duration of 250 ns was observed when using the solution with the highest conductivity of 22 mS/cm.

Similar results have been observed in Shih's research [44]. Shih adjusted the solution conductivity from 150 µS/cm to 3 mS/cm and found that the current amplitude increased with increasing conductivity, however, the current duration decreased significantly.

Applied voltage of 5 kV

Figure 4.15 shows the discharge characteristics under positive applied voltage of 5 kV, with various solution conductivities from 100 to 500 µS/cm. The amplitude of the impulsive currents increased from 180 to 380 mA with increasing solution conductivity; however, no change of current pulse width (15 ns) was observed. The amplitude of impulsive currents was higher than those obtained under 3 kV. Increased applied voltage resulted in the joining of the tail current into the impulsive current, and a significant reduction of the tail current duration (Figure 4.15 (a), (c), (e)).

With a solution conductivity of 1.2 mS/cm (Figure 4.16), higher impulsive current amplitude of ~550 mA and shorter tail current duration of 1 µs were observed compared to that obtained under 3 kV. Figure 4.17 shows the discharge characteristics under positive applied voltage of 5 kV, with solutions of conductivities from 2.4 to 22 mS/cm. The decreasing of impulsive current amplitude and the increasing of tail current amplitude was observed when the solution conductivity was raised from 1.2 to 2.4 mS/cm. It can be found that increased V_{app} significantly shortened the period between impulsive and tail currents. No remarkable difference in discharge characteristics was observed between solution conductivity of 12 and 22 mS/cm; the voltage dropped to around zero and a spark discharge was occurred (Figure 4.17 (c), (d)).

Compared to the results obtained with a V_{app} of 3 kV, increased applied voltage resulted in higher amplitude of discharge currents and the early occurrence of tail currents.

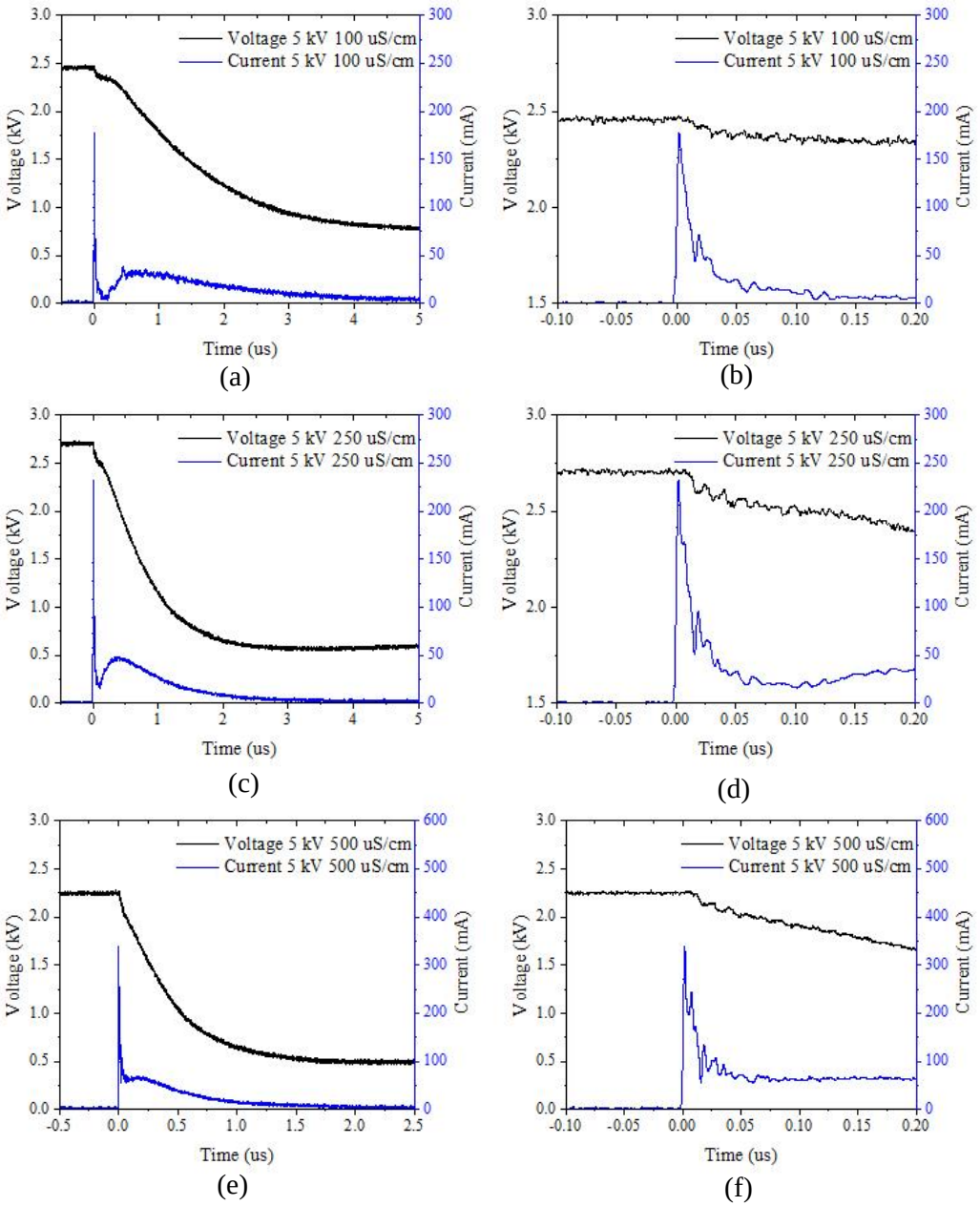

Figure 4.15 Discharge waveforms recorded under 5 kV with solution conductivity of 100 µS/cm (a), 250 µS/cm (c) and 500 µS/cm (e); single impulse current with solution conductivity of 100 µS/cm (b), 250 µS/cm (d) and 500 µS/cm (f).

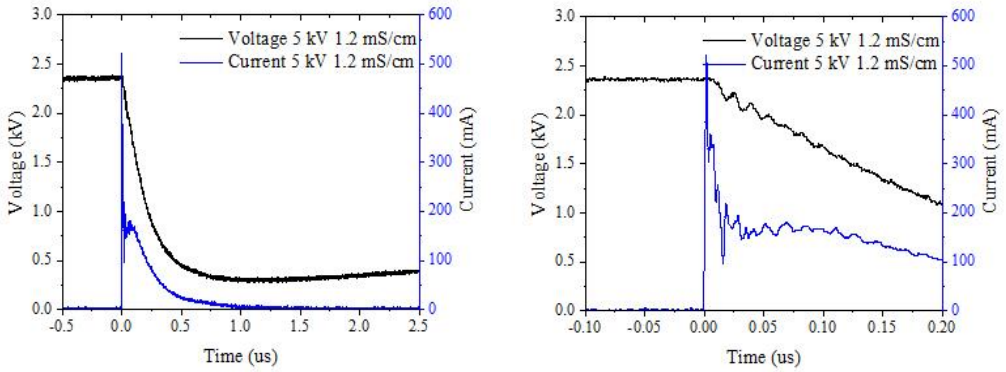

Figure 4.16 Discharge waveforms recorded under 5 kV with solution conductivity of 1.2 mS/cm (a); single impulse current (b)

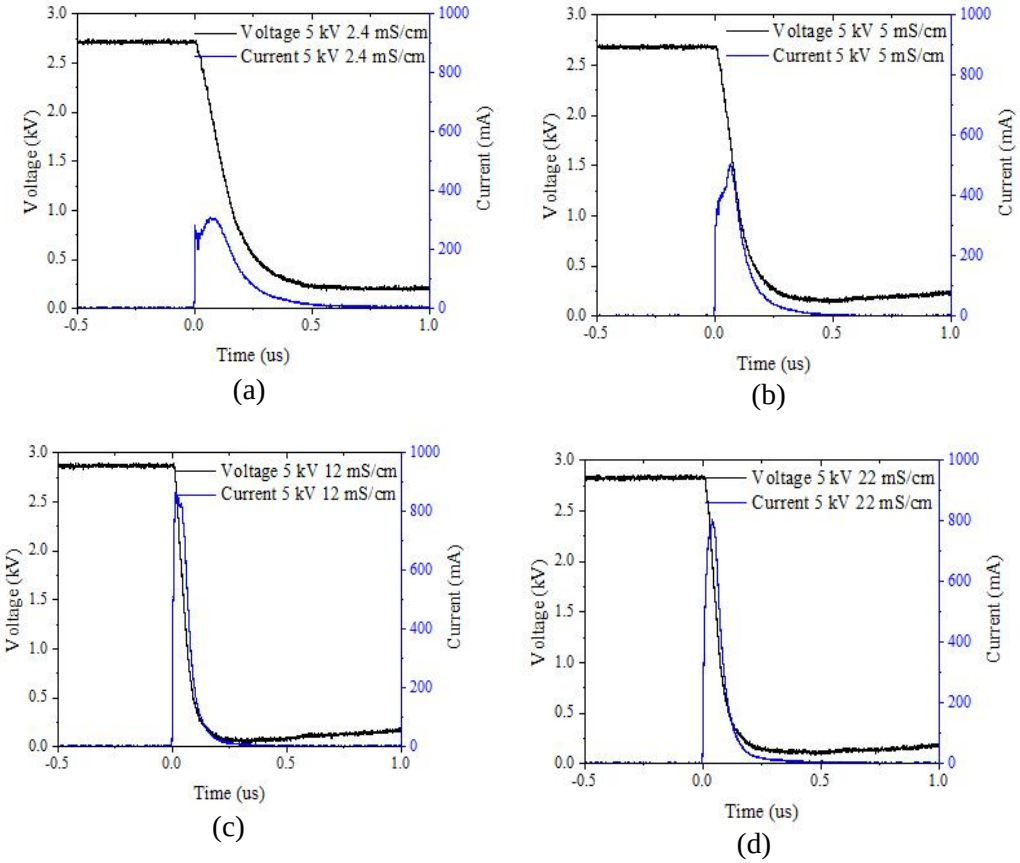

Figure 4.17 Discharge waveforms recorded under 5 kV with solution conductivity of 2.4 mS/cm (a), 5 mS/cm (b) 12 mS/cm (c) and 22 mS/cm (d).

Figure 4.18 shows the discharge voltage waveforms recorded under positive 5 kV. The occurrence of regions where the voltage did not recover was recorded, when using the solution with a conductivity of 200 µS/cm. However, when a higher solution conductivity of 2.4 mS/cm was used, this was not observed. This may be due to the discharge transition from corona-diffuse or DC glow discharges to spark discharges, when using the solution with a higher conductivity.

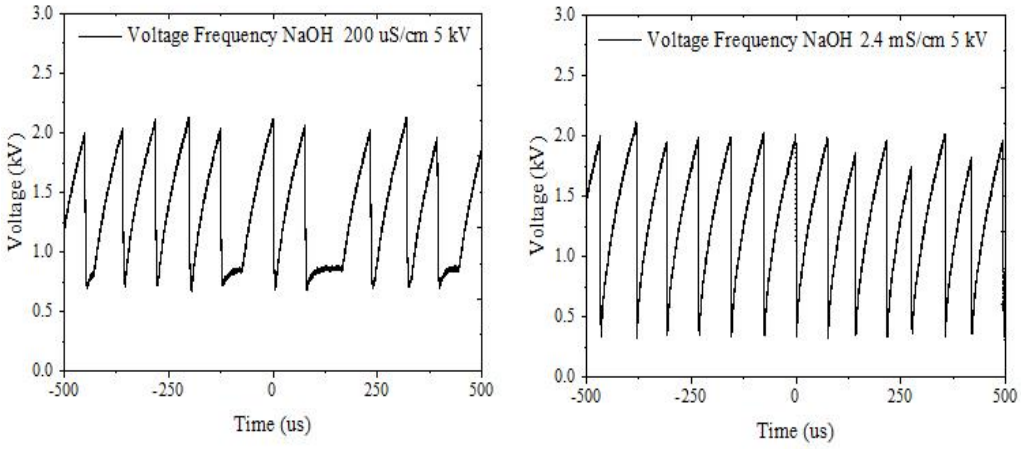

(a) (b)

Figure 4.18 Discharge frequencies recorded under 5 kV with solution conductivity of 200 µS/cm (a) and 2.4 mS/cm (b).

4.4 Gas discharge characteristics under DC negative polarity

4.4.1 Discharge above ultrapure water

The power supply was set to support -3 kV, a corona discharge (Figure 4.19) with a current of -0.25 mA and a pin voltage of -1.32 kV was recorded. The luminosity of a violet light spot was observed at the pin tip and the electron wind was noticed. After 20 minutes of treatment, a DC glow discharge was generated, obtaining a DC current of -0.34 mA and a pin voltage of -850 V. The solution conductivity measured after 20 minutes increased from 0.5 µS/cm to 45 µS/cm.

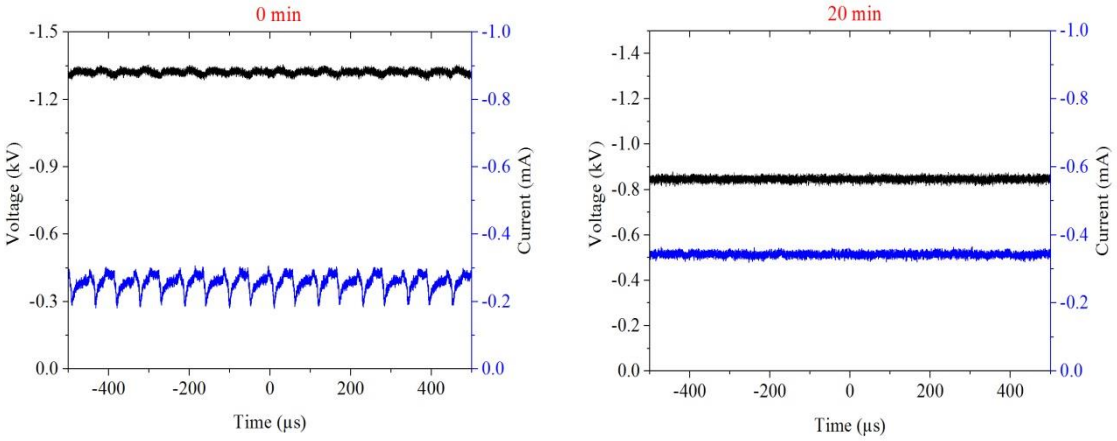

(a) (b)

Figure 4.19 Discharge waveforms recorded under negative polarity discharges with ultrapure water at 0 minute of treatment (a) and 20 minutes of treatment (b).

4.4.2 Discharge above tap water

A significant difference of discharge type was observed when tap water was employed, compared to that when ultrapure water was used; the impulsive current with amplitude of ~-300 mA and width of 10 ns was recorded (Figure 4.20), followed by a tail current with an amplitude of 18 mA and duration of 15 µs.

Compared to the discharges above tap water under positive polarity, the amplitude of impulsive current was three times higher and the pulse width was slightly shorter under negative polarity; a tail current with shorter duration of ~10 µs was observed.

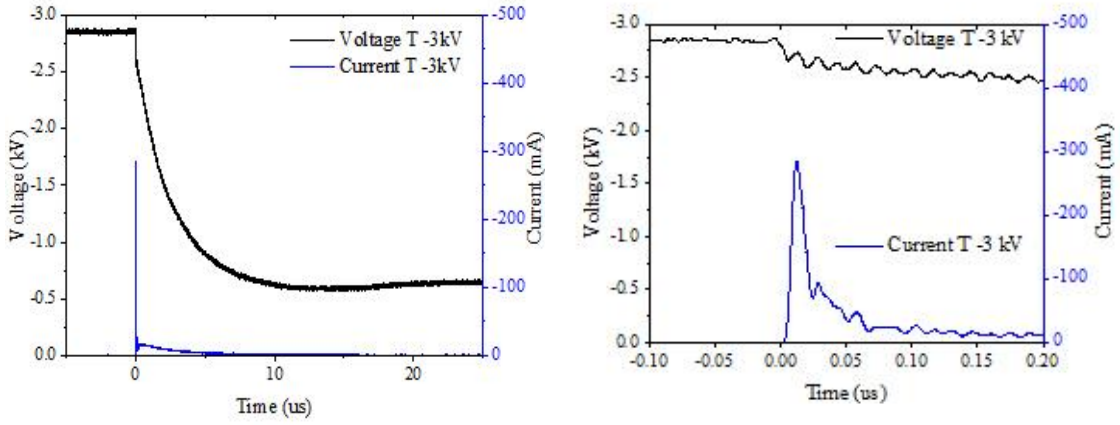

(a) (b)

Figure 4.20 Discharge waveforms recorded under negative polarity discharges with tap water at 0 minutes of treatment (a) and single impulse current recorded at 0 minutes of treatment (b).

4.4.3 Discharge above solutions with high conductivity

Figure 4.21 and 4.22 show the discharge characteristics under negative polarity with a V_{app} of -3 kV above NaOH solutions, with solution conductivities from 100 µS/cm to 1.2 mS/cm, a current pulse width of 10 ns was recorded. It was found that the amplitude of negative impulsive currents increased with increasing solution conductivity. In addition, the tail current joins the falling edge of the impulsive current, even when the solution with a conductivity of 100 µS/cm was in use (Figure 4.21 (a) (b)), which is different from the results obtained under positive polarity. The amplitude of the tail current increased with increasing treatment time (Figure 4.21).

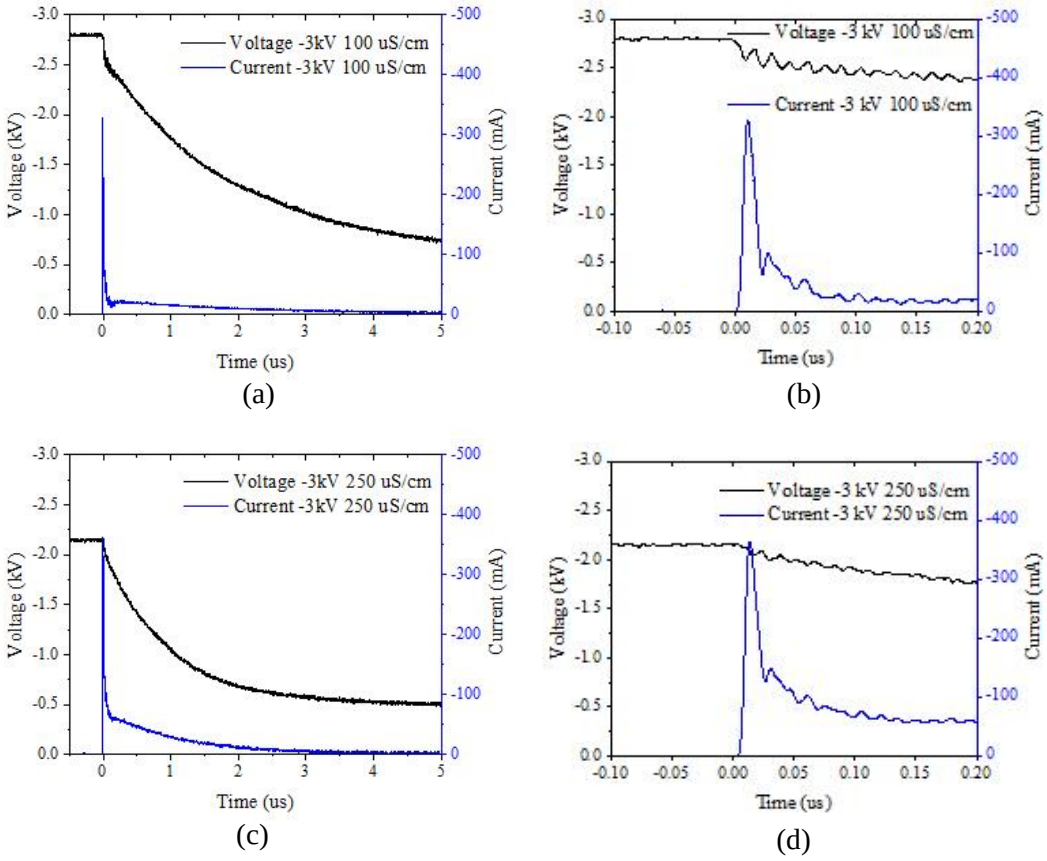

Figure 4.21 Discharge waveforms recorded under negative polarity with solution conductivity of 100 µS/cm (a) and 250 µS/cm (c); single impulse current with solution conductivity of 100 µS/cm (b) and 250 µS/cm (d).

Increasing the solution conductivity led to the joining of the the tail current into the impulsive current, resulting in a shorter duration of the discharge current. When using the solution with a conductivity of 1.2 mS/cm (Figure 4.22 (c)), no clear interval between the impulsive and the tail current was observed; a discharge current duration of ~0.5 µs was recorded. The amplitude of impulsive current reached ~-700 mA with the solution conductivity of 500 µS/cm and 1.2 mS/cm; the pin voltage dropped to around -300 V.

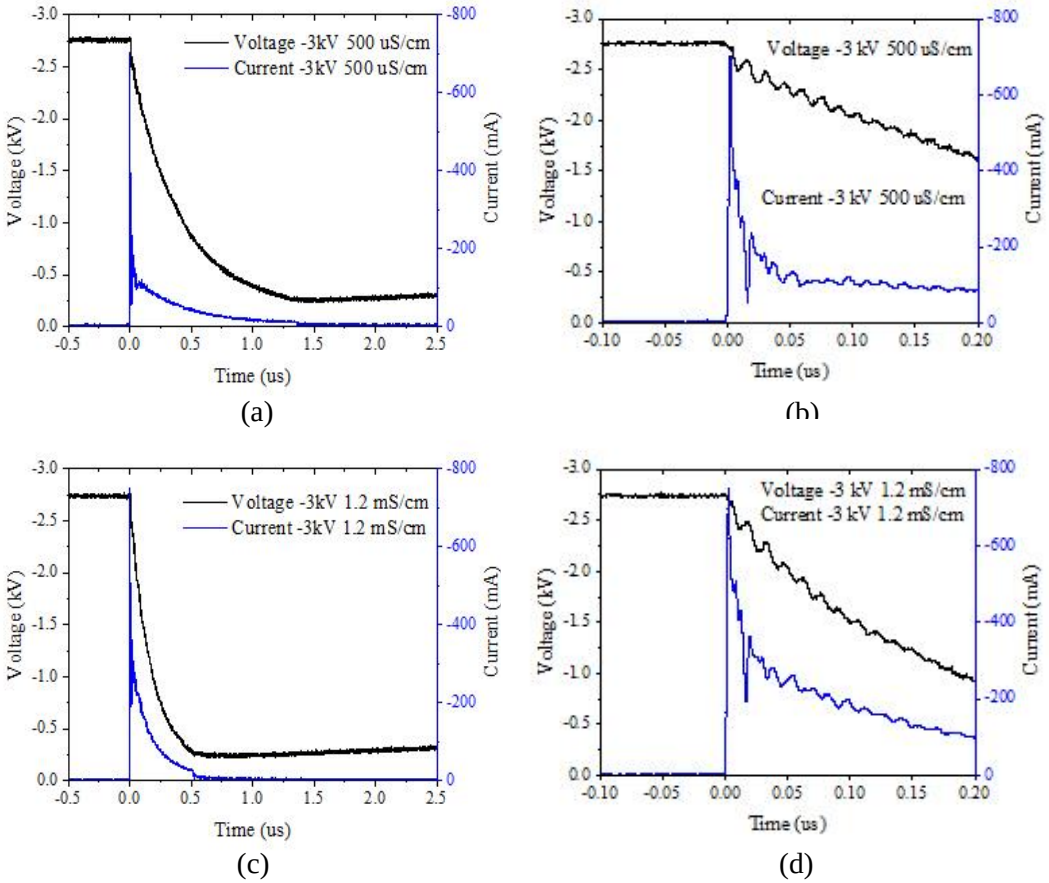

Figure 4.22 Discharge waveforms recorded under negative polarity with solution conductivity of 500 µS/cm (a) and 1.2 mS/cm (c); single impulse current with solution conductivity of 500 µS/cm (b) and 1.2 mS/cm (d).

Figure 4.23 shows the discharge characteristics under negative polarity with solution conductivities ranging from 2.4 to 22 mS/cm. The current amplitude further increased with a higher conductivity, reaching ~800 mA in solutions with conductivity of 2.4 and 5 mS/cm, and ~1500 mA in solutions with conductivity of 12 and 22 mS/cm. The duration of the tail current decreased with increasing solution conductivity, and was less than 0.25 µs when using the solution with a conductivity of 22 mS/cm.

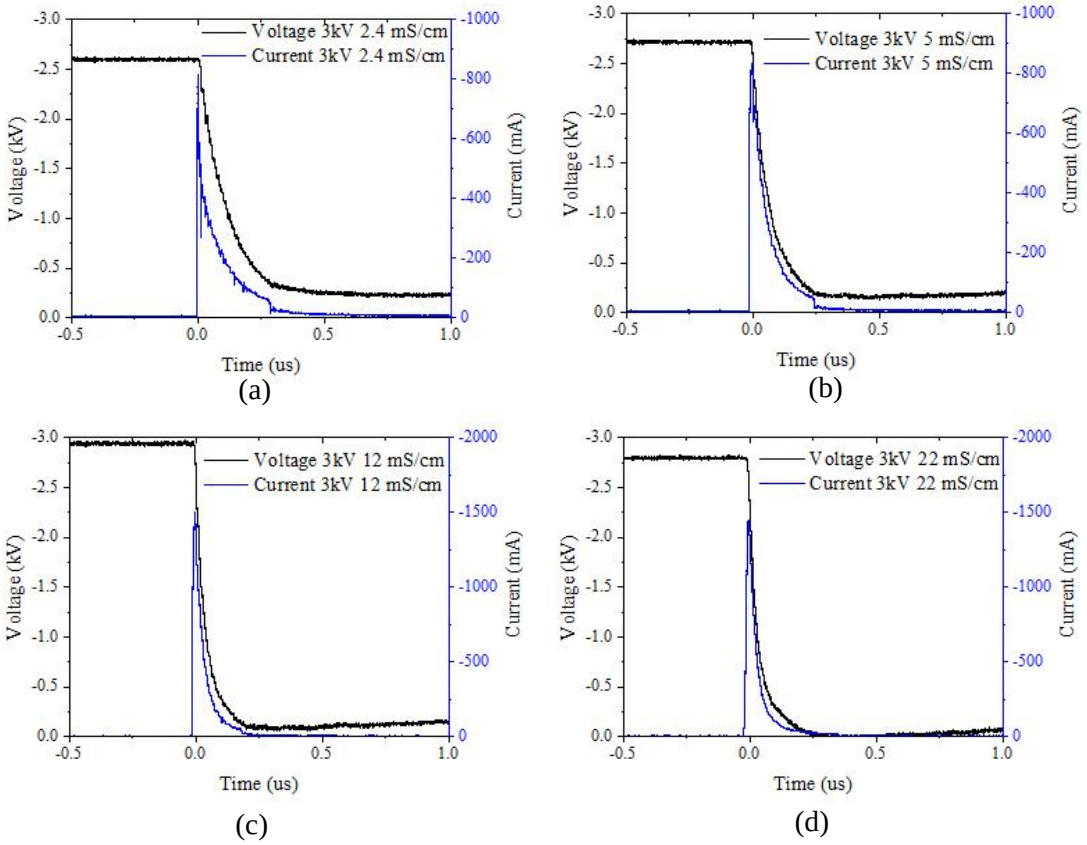

Figure 4.23 Discharge waveforms recorded under negative polarity with solution conductivity of 2.4 mS/cm (a), 5 mS/cm (b), 12 mS/cm (c) and 22 mS/cm.

The tail current completely joins into impulsive current when solution conductivity was increased to >5 mS/cm and the spark discharges occurred. Miao [35] investigated the negative glow discharge and found that the discharge was not stable at low solution conductivity until the value was increased to 37.15 µS/cm. On the other hand, Miao found that increasing the solution conductivity to 4.43 mS/cm led to the occurrence of spark discharge, which is in agreement with the results recorded in this experiment; Miao also found that further increase of conductivity resulted in unstable discharge [35].

4.5 Discussion

Ultrapure water (0.5 μS/cm) acts as a dielectric barrier at the start of discharge. Under positive polarity, the discharges were initiated when the pin voltage reached 2.25 kV; the breakdown of the inter-electrode led to the reduction of the pin voltage to 2.15 kV (Figure 4.3 (b)); the development of discharge was inhibited due to the accumulation of charges on the water surface. Therefore, only small impulsive currents with low amplitude (several tens of mA) and short pulse width (~15 ns) were recorded. It is reasonable to assume that the ultrapure water acted as dielectric barrier at the beginning of discharges, due to the very similar discharge current waveforms recorded at 0 minute compared to those seen in dielectric barrier discharges. It was found that the discharge was no longer stable when the solution conductivity was slightly increased to 3.5 μS/cm (Figure 4.3 (c)); the longer gas gap charging interval between pulses occasionally occurred and a wavy voltage waveform was recorded. Increased solution conductivity of 5.5 μS/cm led to the further increase of charging duration (~250 μs); the pin voltage was dropped to 1.7 kV before the recharging of the inter-electrode.

A further increase in solution conductivity to 8.4 μS/cm resulted in the further increase of the inter-electrode charging duration and decreasing of voltage drop duration; the discharge was not inhibited until the pin voltage was dropped to 1.65 kV. The transition of discharge type from corona to corona-diffuse was recorded after five minutes of treatment under positive polarity; the solution conductivity was increased to 17 μS/cm. A tail current with the amplitude of ~3 mA and duration of several tens of μs was observed following the impulsive current; increased solution conductivity leads to an increasing of the amplitude and a decreasing of the duration of the tail current. The increased voltage drop indicates weaker accumulation of charge on water surface with increasing solution conductivity. The higher impulsive current results in higher plasma conductivity in the discharge filaments, thus reducing the drop on the discharge filament.

It was found that the amplitude and duration of the impulsive current obtained at 0 minute of treatment with tap water was similar to that obtained with ultrapure water after 20 minutes of treatment (Figure 4.8, 4.9). This result indicated that the discharge type is dependent on the solution conductivity. Further increase in the solution conductivity by using NaOH solutions led to an increase of discharge current amplitude and decrease of the tail current duration. The tail current joins the falling edge of the impulsive current for higher solution conductivity. A higher applied voltage of 5 kV did not change the discharge current profile

but increased the current amplitude in various conductivity solutions. Compared to the results obtained with an applied voltage of 3 kV, the tail current appeared closer to the impulsive current when a higher voltage was applied.

Nikiforov [28] investigated the discharge above water with solution conductivity ranging from 50 to 500 µS/cm, and observed corona current with the amplitude of several mA at low applied voltage. Increased applied voltage resulted in the extinction of corona discharges and the generation of the impulsive currents, followed by long-duration tail currents, which are the same as obtained in this experiment. However, Nikiforov considered that the discharge type had changed to a spark discharge, while the similar phenomenon observed in this experiment is considered as a transition to corona-diffuse discharge. Nikiforov found that the 'spark discharge' was generated at the start of treatment with a half-spherical electrode while corona discharges can be generated with a pin electrode under low applied voltage; Nikiforov concluded that the type of discharge is dependent on the electrode diameter and the applied voltage. The inter-electrode capacitance using pin electrode was much lower compared to that with a half-spherical electrode; therefore, only corona discharges were generated above water at a conductivity range from 0.5 to 17.5 µS/cm. Increases in solution conductivity to the range of 17.5-500 µS/cm led to the formation of corona-diffuse discharge.

Sun [40] investigated the pin-to-metal grounded electrode discharge and observed a similar current curve as shown in Figure 4.14 (d), when extremely high solution conductivity was employed and the solution was regarded as a metal electrode. However, the streamer corona current observed in Sun's research was in the order of several amperes, which was followed by a high tail current with the amplitude of ~280 A and duration of ~2 µs. The significant amplitude difference between Sun's research and this experiment could be due to the much higher applied voltage and metal ground electrode that were used in Sun's case. Sun considered that the high-amplitude tail current was formed when the discharge channel was approaching the grounded electrode, and a spark discharge was generated. Sun also found that a streamer corona current is always generated before the spark discharge with much lower amplitude, which is also recorded in Fig 4.14, 4.17 and 4.23.

When negative polarity was applied with ultrapure water, negative corona discharges were initiated at the start of discharge, which then transited into DC glow discharge after 20 minutes of treatment. An entirely different discharge current was observed when tap water was used; an impulsive current pulse followed by a tail current was recorded, similar to the results obtained under positive polarity. It was found that the current amplitudes under

negative polarity were higher than those obtained under positive polarity at the same solution conductivity. In addition, no clear separation of the impulsive and the tail current was observed when solution conductivity was increased to 500 µS/cm; while under positive polarity the currents were not merged until the conductivity was increased to 5 mS/cm.

4.6 Conclusion

The discharges above various conductivity solutions have been investigated under positive and negative polarity. When positive polarity was employed with ultrapure water, the inhibition of discharge occurred due to the accumulation of charges on water surface. Increasing solution conductivity led to a faster relaxation of the charge distribution; reducing the inhibition effect. A significant voltage drop was observed when solution conductivity was increased to 5.5 µS/cm. The transition of impulsive current discharges to corona-diffuse discharges was observed when the solution conductivity was increased to 17.5 µS/cm. Further increase of solution conductivity led to the rise of the amplitude of discharge current and the magnitude of the voltage drop; however, this reduced the duration of the discharge current. When high solution conductivities (>12 mS/cm) were used, the liquid cathode acted as a metal ground and resulted in the occurrence of spark discharge.

Increasing the applied voltage to 5 kV resulted in the increase of current amplitude and discharge repetition rate. A DC current was occasionally observed, which indicated the inhibition of discharge sometimes did not occur. This also indicated the transition of corona-diffuse discharges to DC glow discharges.

When negative polarity was employed with ultrapure water, the transition of a DC corona discharge to a DC glow discharge was observed with increasing treatment time. The discharge waveforms obtained with tap water under negative polarity were similar to those obtained under positive polarity. Higher amplitude and shorter duration of discharge current under negative polarity was observed in solution conductivity ranging from 65 µS/cm to 22 mS/cm.

4.7 Further work

The variation of discharge type with solution conductivity was investigated in neutral and basic solutions; the effect of acid solution with various conductivities and the discharge characteristics needs to be further investigated, due to the industrial wastewater is generally acidic solution. In addition, the difference between positive and negative discharge above ultrapure water was noticed. Under positive polarity, an impulsive current discharge was developed; while under negative polarity, only DC discharge was recorded and the different phenomenon need to be further investigated.

5 OH RADICAL AND H_2O_2 PRODUCTION UNDER IMPULSIVE CURRENT DISCHARGES

5.1 Introduction

The discharge characteristics of open air discharges have been discussed in Chapter 4, and the discharge characteristics in air, N_2 and helium with a sealed reactor, are investigated in this chapter. Moreover, this chapter also focuses on the investigation of OH radicals and H_2O_2 production. A reactor with a pin-to-water electrode structure was employed in this experiment. The atmospheric plasma developed above the water surface has been proven to induce a gas flow through the transferring of momentum energy from ions to neutral particles [38, 111, 112]. This phenomenon leads to a liquid flow during plasma treatments, which results in a well-mixed solution of reactive species.

Kanazawa [113] measured OH production by using TA solution (fluorescence method), and found that OH radical production increased almost linearly with time, reaching a production of 21 nmol after 10 minutes of treatment. H_2O_2 production can be determined by using Titanium (IV) ions [109] (VIS-UV spectrophotometry), Thagard [4] used this method to investigate the H_2O_2 production in above water discharges. The TA powder needs to be dissolved in basic solution to prepare the TA solution; however, the negative effect of OH^- ions on H_2O_2 production has been proven [3, 79]. Also, the OH radical production determined by using fluorescence method is generally lower than that determined by VIS-UV method. Therefore, these two detection methods were compared in this chapter.

The main objectives of these experiments were to: (i) investigate the discharge characteristics in various gases (N_2, air, helium) with different solution pH; (ii) quantify the OH radical and H_2O_2 formation at the plasma-water interface in various gas discharges; and (iii) determine the role of the dimerization of the OH radicals into H_2O_2 by using a scavenger of OH radicals.

5.2 Reactor design and experimental set up

5.2.1 Rector design

Figure 5.1 shows the design of the reactor, which has a typical pin-to-water electrode structure. A 70-mm-high transparent solution container was made of acrylic, with an inner diameter of 40 mm, outer diameter of 50 mm and depth of 45 mm. A brass electrode with a diameter of 8 mm was inserted through the bottom of the acrylic container and acts as ground electrode. The container was placed between two nylon flanges with a diameter of 100 mm and depth of 10 mm. The gas inlet and outlet were fixed on the top nylon flange; a brass electrode of 8 mm in diameter was fixed through the centre of the top flange and a stainless-steel pin with a 0.3-mm-diameter tip was inserted in the brass electrode. A nylon handle is used to adjust the inter-electrode distance.

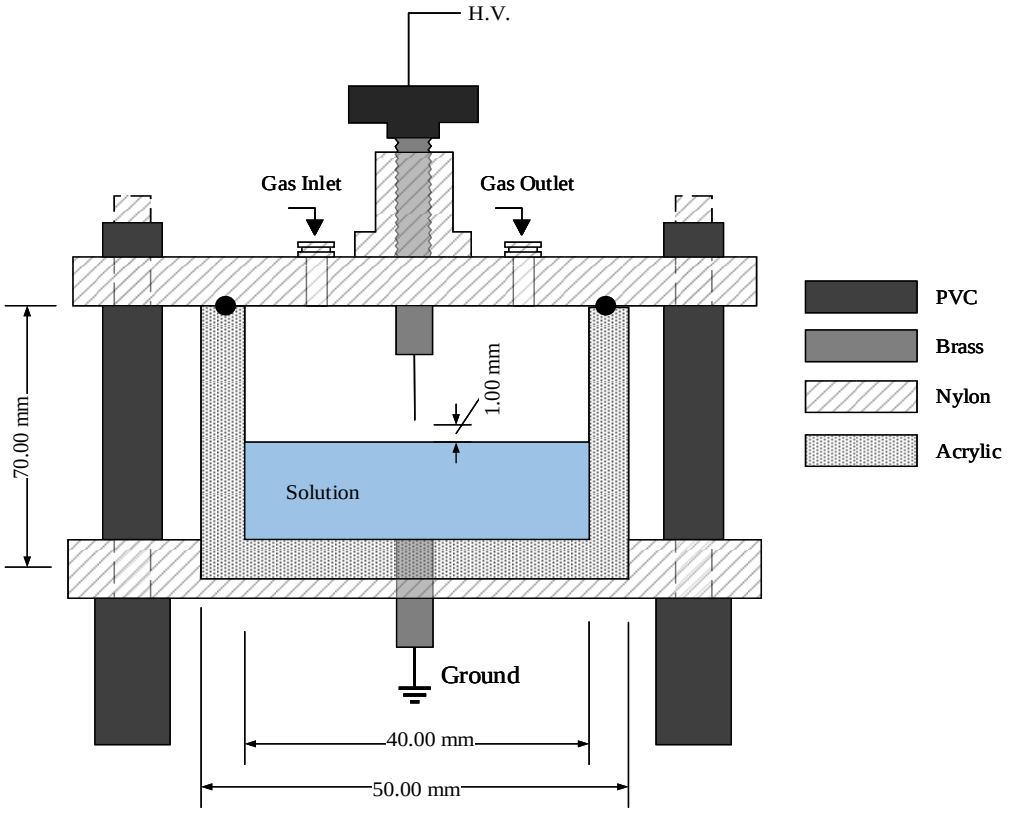

Figure 5.1 The structure of the pin-to-water electrode reactor.

An O-ring was placed between the top flange and the acyclic container to avoid gas leakage during the vacuuming process and discharge treatments. A sample volume of 10 ml was

introduced into the container before the top flange was covered and fastened. The depth of the solution was measured as 8 mm. The stainless-steel pin was adjusted in touch with the solution surface at first, and the screw electrode was turned one revolution to adjust the inter-electrode distance to 1 mm. The vacuuming process described in Chapter 3 was applied before N_2 and helium gas injection to atmosphere.

5.2.2 Experimental set up

Figure 5.2 shows the diagram for impulsive current discharge experiments; a 6-MΩ current-limiting resistor was connected in series with the reactor. The high voltage electrode was energized by a positive applied voltage of 3 kV, and a high voltage probe was used to measure the pin voltage during experiments. A 50-Ω coaxial cable was connected to the reactor ground to investigate the variation of discharge currents.

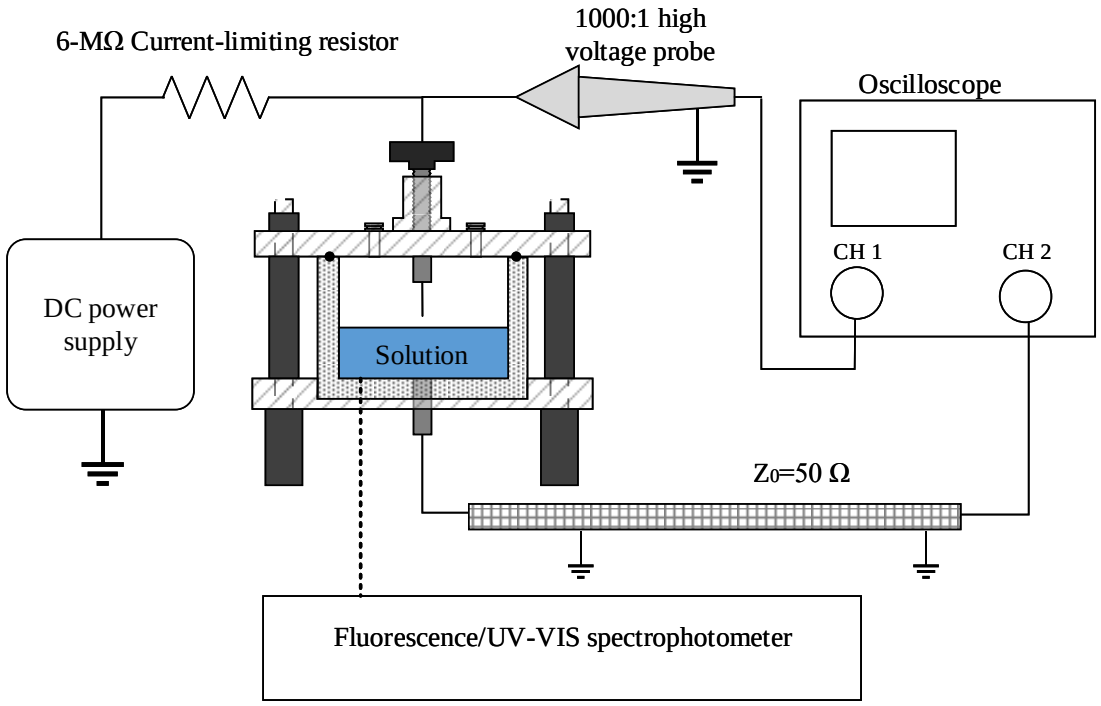

Figure 5.2 Schematic diagram for impulsive current discharge experiments.

A sample of volume 10 ml was introduced into the reactor before each treatment. Working gases of air, N_2 and He were used in this experiment to investigate the plasma-water interface reactions. The vacuuming process, described in 3.4 was applied, and then the reactor was refilled with working gas of N_2 or He to atmospheric pressure. The reactor was sealed and no gas flow was introduced during treatments. The OH radical and H_2O_2

production in air, N_2 and helium were measured after 5, 10, 15 and 20 minutes of treatments, in 5-mM NaOH solution and ultrapure water; each treatment was repeated three times.

Detection methods and radical scavenger

Fluorescence photometry was used to determine the OH radical formation by measuring the concentration of HTA, which is the product of the interaction of terephthalic acid (TA) and OH radical. As the TA powder can only dissolve in basic solution, the TA solution was adjusted to pH 11.5 by using NaOH solution; the conductivity of the TA solution was measured as 1.25 mS/cm. UV-VIS spectrophotometry was used to determine the H_2O_2 production, and the results were compared to those achieved by using the fluorescence photometry.

Various reactions lead to the formation of H_2O_2 at the plasma-water interface. A major reaction path is through the dimerization of OH radicals, as shown in reaction (R 2.25). TB was employed to terminate the dimerization of OH radicals to determine the H_2O_2 production pathway (R 3.1). A control experiment was carried out before plasma treatments; it was found that the addition of OH scavenger, tert-butanol (TB), has no effect on the solution conductivity and pH.

$$2\,OH^{\cdot} \rightarrow H_2O_2 \qquad \text{(R 2.25)}$$

$$(CH_3)_3COH + OH^{\cdot} \rightarrow (CH_3)_2C(OH)CH_2^{\cdot} + H_2O \qquad \text{(R 3.1)}$$

Discharge characteristics recorded

The discharges in various gases were investigated in a sealed reactor for the experiments being discussed in this Chapter, with no gas flow introduced during treatments; a small amount of water mist was generated at the plasma-water interface. As measured, the solution conductivity in sealed air treatments recorded in this Chapter increased faster than those recorded in Chapter 4 (operated in open air). In this case, the voltage and current waveforms in sealed air treatments with ultrapure water were recorded.

When a 5-mM NaOH (1.25 mS/cm) solution was employed, the discharge characteristics in air have no difference compared to those obtained in Chapter 4 with a similar solution conductivity (1.2 mS/cm); the voltage and current waveforms in air with NaOH solution are not shown in this chapter.

5.3 Gas discharge characteristics with ultrapure water

Figure 5.3 shows the voltage and current waveforms recorded during discharges in air with ultrapure water. An impulsive current with amplitude of 68 mA and pulse width of 15 ns was recorded at the start of treatment, the pulse repetition rate was 2×10^5 pps and the voltage drop was 150 V. After 20 minutes of treatment, a long-duration tail current with the amplitude of 5 mA, was recorded after the impulsive current.

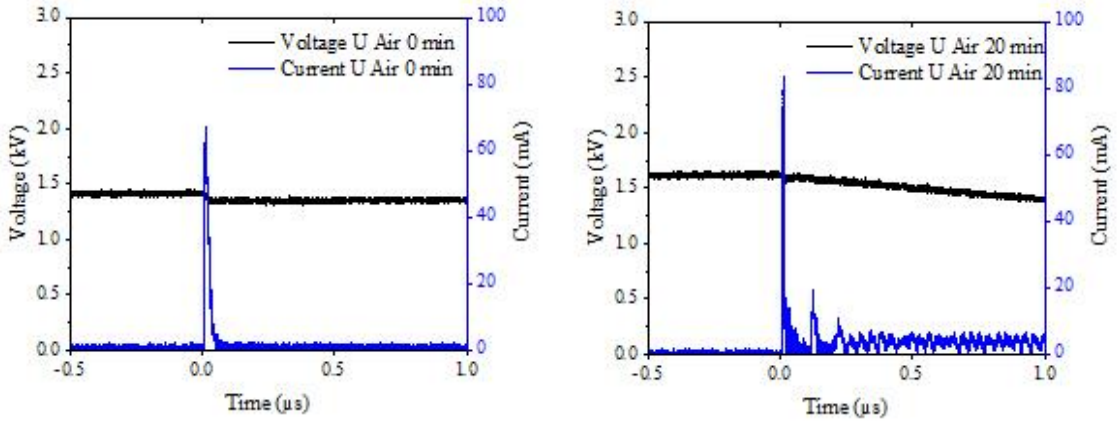

Figure 5.3 Gas discharge above ultrapure water in air, voltage and current waveforms recorded at 0 minutes (a) and 20 minutes (b).

Figure 5.4 shows the voltage and current waveforms recorded during discharges in N_2, which is similar to the results obtained in discharges in air. An impulsive current with pulse width

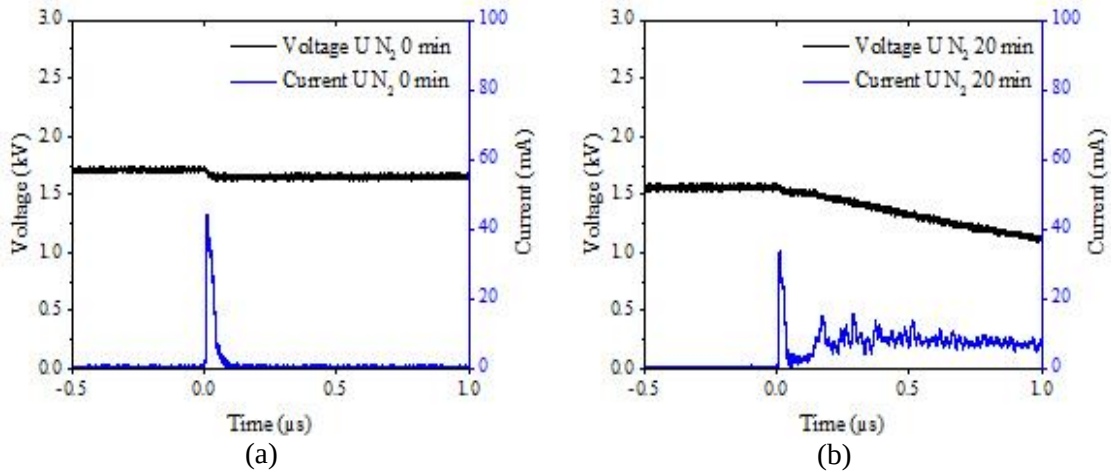

Figure 5.4 Gas discharge above ultrapure water in N_2, voltage and current waveforms recorded at 0 minutes (a) and 20 minutes (b).

of 22 ns, slightly larger than that in air, was recorded at the start of treatment; however, lower amplitude of ~45 mA and repetition rate of 1.8×10^5 pps was recorded. A micro-second tail current with an amplitude of 13 mA, was recorded after 20 minutes of treatment; the amplitude of the impulsive current decreased to ~38 mA.

Figure 5.5 shows the voltage and current waveforms recorded during discharges in He, which was significantly different from those obtained for discharges in air and N_2. An impulsive current with pulse width of 55 ns and amplitude of ~20 mA was measured superimposed on a DC charging current of 0.33 mA, the pulse repetition rate of 5×10^5 pps was recorded. The voltage drop of 90 V was recorded, which was lower than that in air and N_2. Increasing the treatment time to 20 minutes resulted in the rising of repetition rate to 1.25×10^6 pps and reduction of pulse duration to 20 ns and amplitude to 10 mA. The voltage drop for each pulse reduced to several tens of volts; the pin voltage decreased from 1200 V to 730 V.

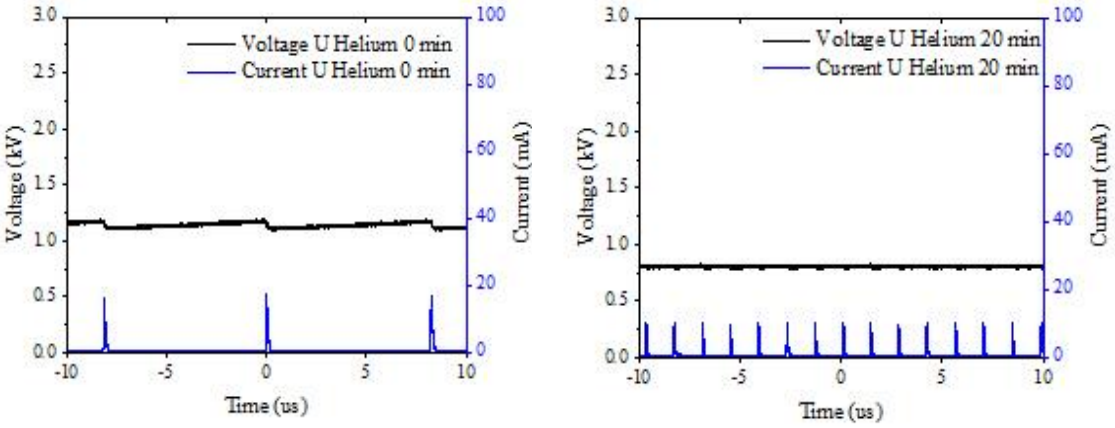

(a) (b)

Figure 5.5 Gas discharge above ultrapure water in helium, voltage and current waveforms recorded at 0 minutes (a) and 20 minutes (b).

Xiong [30] found that the discharges in He have the characteristics of single current pulses, which is similar to the results recorded in this experiment. Xiong found that the single current pulse in He discharges has a lower amplitude and longer duration compared to those in air and N_2 discharges, which is similar to the results recorded in this experiment. During the positive discharges in air and N_2, the discharge filaments developed from the pin electrode to the water surface. The spread out of filaments on water surface was observed, which is in agreement with the phenomenon observed in Bruggeman's research [115].

At the beginning of discharge, the accumulation of charges on the water surface inhibits the further development of the discharge, resulting in the impulsive currents, which are similar to the dielectric barrier discharges. The ultrapure water acted as dielectric barrier at the beginning of discharges due to its low conductivity. With higher solution conductivity, the inhibition effect is weakened and the discharge can develop more fully. The charges that arrive at the water surface in each pulse can be measured by integrating the discharge current. However, the variation of discharge current waveforms and repetition rate makes the accurate measurements of charge transfer during discharges impossible in this experiment.

5.4 Plasma-water interface reactions with ultrapure water

5.4.1 H_2O_2 production

Figure 5.6 shows the H_2O_2 production during the discharges in various gases with ultrapure water. The H_2O_2 production in He increased linearly with time, reaching 10 µmol after 20 minutes of treatment (Figure 5.6). A very slight reduction in the rate of production with time was observed in air and N_2 treatment, which led to the final production of H_2O_2 of 2.2 µmol and 5.5 µmol, respectively, after 20 minutes of treatment.

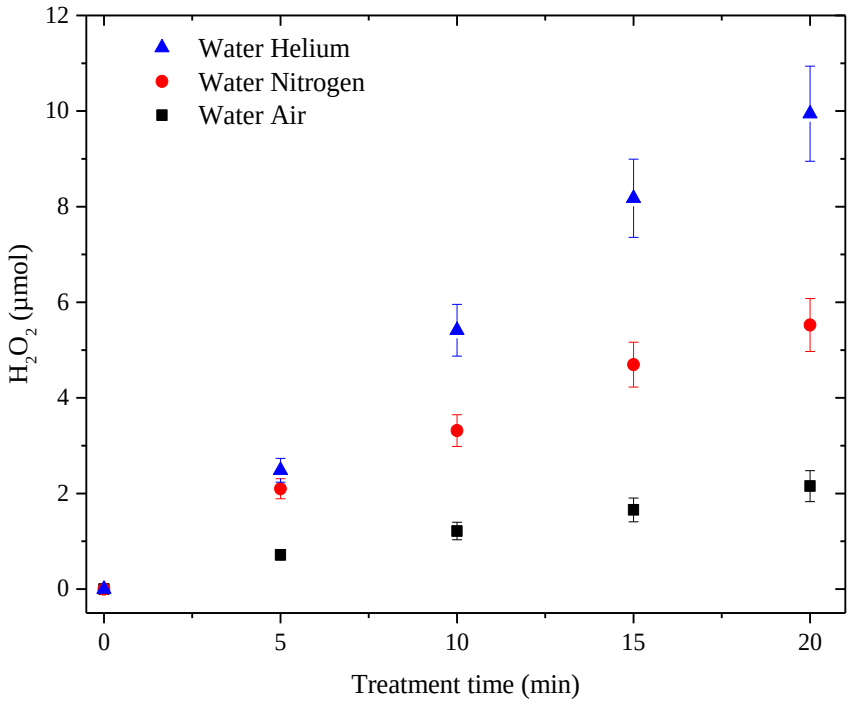

Figure 5.6 H_2O_2 production in ultrapure water in various gas treatments.

The lowest H_2O_2 production, obtained in air discharges, may be due to the lower ionization energy of O_2 of 12.06 eV compared to that of N_2 of 15.6 eV and of He of 24.6 eV. However, the discharge current and pulse repetition rate also varied among the various working gases, therefore, it is hard to establish the ionization energy effect. Another possibility is that the discharges in working gas that contains N_2 can produce a significant amount of N atoms, which lead to the production of oxy-nitride species above water by a series of reactions (Table 2.9), leading to the reduction of OH radicals and H_2O_2 in the gas phase. In addition, the oxy-nitrides generated in the gas phase can dissolve into solution, leading to the

destruction of OH radicals and H_2O_2, to generate the species with a higher valence (R 2.65, R 2.66).

Tert-butanol effect

The H_2O_2 production in N_2 and helium was significantly reduced when 0.2-M TB was added to the solution (Figure 5.7), which reached 1.2 µmol and 3 µmol in N_2 and He, respectively, after 20 minutes of treatment. Almost no effect was observed in air treatments, the H_2O_2 production reached 2 µmol after 20 minutes of treatment. It can be calculated that 7%, 78% and 70% of the H_2O_2 detected solution for discharges in air, N_2 and He, respectively, was formed from the dimerization of OH radicals. Therefore, it can be calculated that the OH radical production, resulting from discharges in air, N_2 and helium was 4 µmol, 2.4 µmol and 6 µmol (R 2.25), respectively.

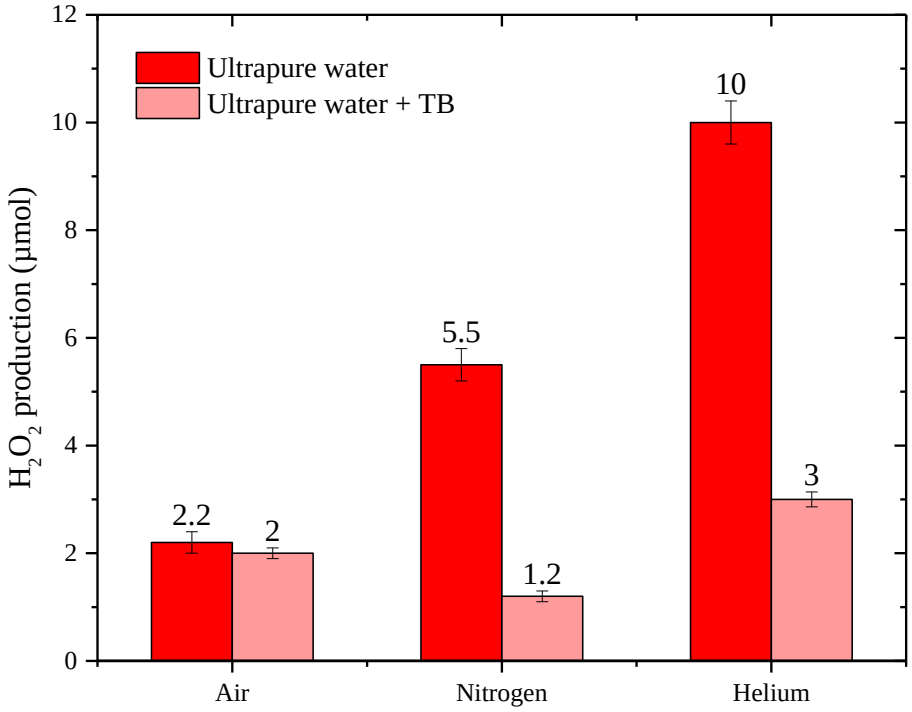

Figure 5.7 Effect of TB on H_2O_2 production in ultrapure water in various gas treatments.

The effect of TB on H_2O_2 formation was very limited in air treatment, and this could be due to the effect of O_2. One of the possibilities is the production of O_3, which cannot be scavenged by TB, at the plasma-water interface, thus dissolving into water and leading to the production of H_2O_2. However, the O_3 production in humid air is very limited; therefore, this

possibility may be less likely to occur. Another possibility is that the O_2 can react with TB to produce H_2O_2 directly in solution, which cannot be scavenged by TB. In order to investigate the O_2 effect, the discharges in O_2 were investigated in experiment Section 6.4.1.

5.4.2 Variation of solution conductivity

The water conductivity increased linearly with time in various gas discharge experiments (Figure 5.8). The highest solution conductivity of 145 µS/cm was recorded in air, after 20 minutes of treatment; in N_2 treatment, a slightly lower value of 133 µS/cm was recorded. These results suggest the production of oxy-nitride species at the plasma-water interface and then dissolved in water to form nitrite and nitrate acid. Both nitrite and nitrate ions were detected in air treated samples, while only nitrite ions were detected in N_2 treat samples. In helium-treated samples, neither nitrite nor nitrate ions were detected by using test strips; however, a solution conductivity increase of 88 µS/cm was recorded; this phenomenon needs further investigation.

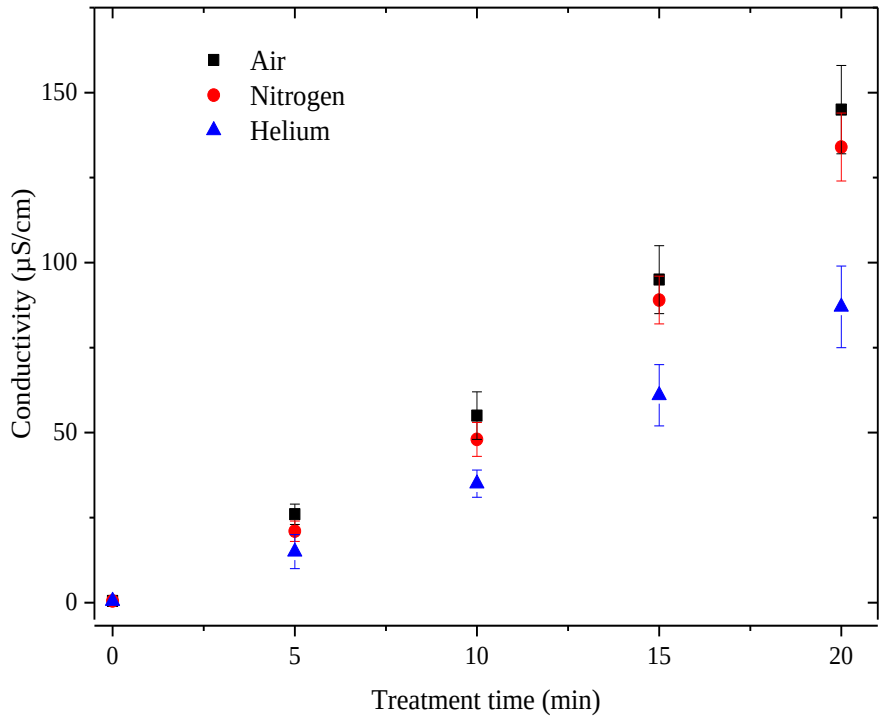

Figure 5.8 Variation of solution conductivity in ultrapure water in various gas treatments.

5.5 Gas discharge characteristics with NaOH solution

The TA solution was prepared with a 5-mM NaOH solution, with a pH of 11.5 and conductivity of 1.25 mS/cm. The discharge characteristics in air, N_2 and helium with 5-mM NaOH solution were investigated (Figure 5.9).

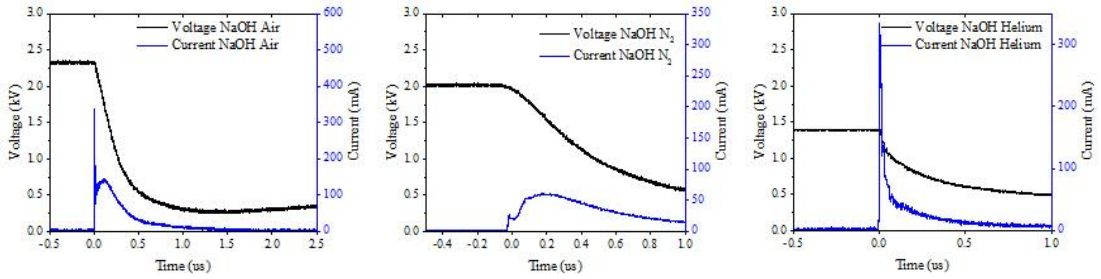

(a) (b) (c)

Figure 5.9 Gas discharge above 5-mM NaOH, voltage and current waveforms recorded in air (a) N_2 (b) and helium (c).

The discharge characteristics and repetition rate remained constant during treatments due to the very limited variation of solution conductivity (<100 µS/cm). A tail current with the amplitude of 60 mA was recorded in N_2 treatments, following the nanosecond impulsive current pulse (Figure 5.9). A voltage drop of ~800 V and tail current duration of ~1.5 µs was recorded in N_2. The discharge waveforms recorded in helium discharges have very different behaviour, in which no tail current was observed and this reduced the current duration to 0.5 µs. The highest current amplitude of ~320 mA was recorded, which was different from the results that were recorded with ultrapure water.

Sun [40] investigated the liquid phase pulsed discharges and recorded similar current waveforms. Sun found that the water conductivity plays an important role in discharge mode; the initial discharges in water are relatively weak, increased water conductivity leads to a diffuse discharge developed after the impulsive current. On the other hand, Sunka [60] found that the current amplitude increased significantly with increasing solution conductivity, which indicated denser plasma was generated in contact with water; in this experiment, a significant increase of impulsive current amplitude was recorded in helium. A significant effect of solution conductivity on helium discharge characteristics was observed (Figure 5.5 and Figure 5.9 (b)), this phenomenon needs to be further investigated.

5.6 Plasma-water interface reactions with NaOH solution

5.6.1 OH radical formation

Figure 5.10 shows that the OH radical production was significantly affected by the gas type. The OH radical formation increased in proportion with time and reached 0.03 µmol, 0.06 µmol and 0.11 µmol in air, N_2 and He, respectively, after 20 minutes of treatment. The highest production was obtained in He treatment, which was 3.7 times and 1.8 times higher than that of air and N_2. Under positive impulsive current discharges, the reactions between the energetic positive ions with water are considered as the major pathway of OH radical formation (Table 2.3).

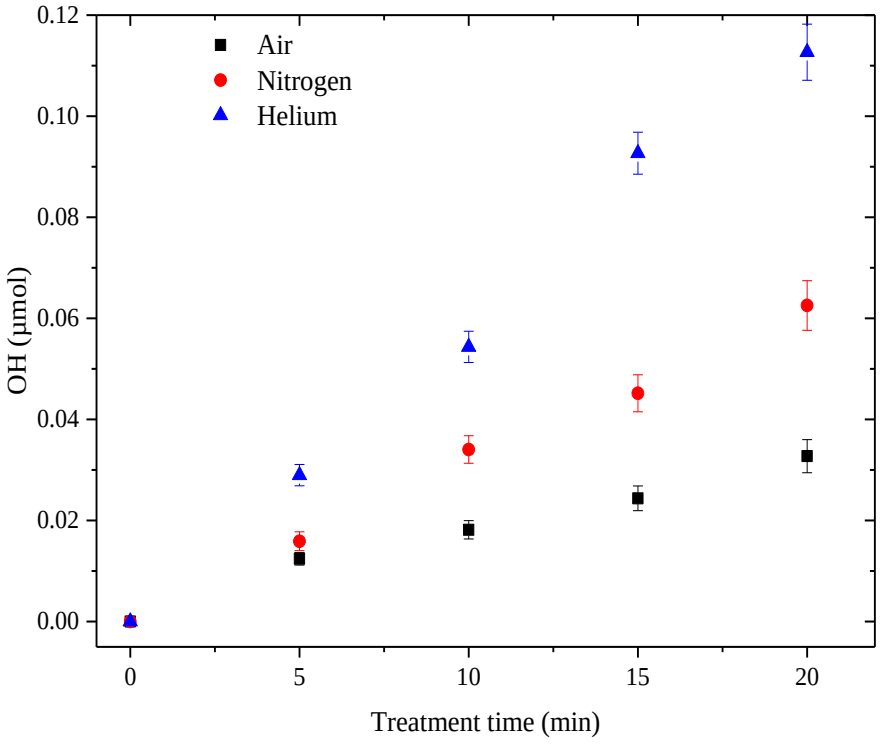

Figure 5.10 OH radical formation in TA-NaOH mixture solution in various gas treatments.

Kanazawa [113] measured the OH radical formation by a helium plasma jet above water and concluded that the OH radicals were formed in both gas and liquid phases. Kanazawa also found that although no stirring of water was performed, the HTA was diffused homogeneously from the plasma-water interface into water.

5.6.2 H_2O_2 production in 5-mM NaOH solution

A 5-mM NaOH solution was used to investigate the effect of OH^- ions on H_2O_2 production. Figure 5.11 illustrates that H_2O_2 production in a basic solution was significantly affected by OH^- ions, reaching 0.78 µmol, 2.76 µmol and 3.31 µmol in air, N_2 and He, respectively, after 20 minutes of treatment. These results are reduced by 2.8, 1.9 and 3.0 times, compared to the results recorded in the discharges above ultrapure water (Figure 5.11). The difference may be caused by the change in discharge types that occurs due to the higher conductivity of the NaOH solution. In addition, the inhibiting effect of OH^- ions on OH radical formation could occur at the interfacial reactions. One of the main possibilities however is that OH^- ions can destroy H_2O_2, leading to the formation of HO_2^-, as shown in reaction (R 2.36).

$$H_2O_2 + OH^- \rightarrow HO_2^- + H_2O \qquad \text{(R 2.36)}$$

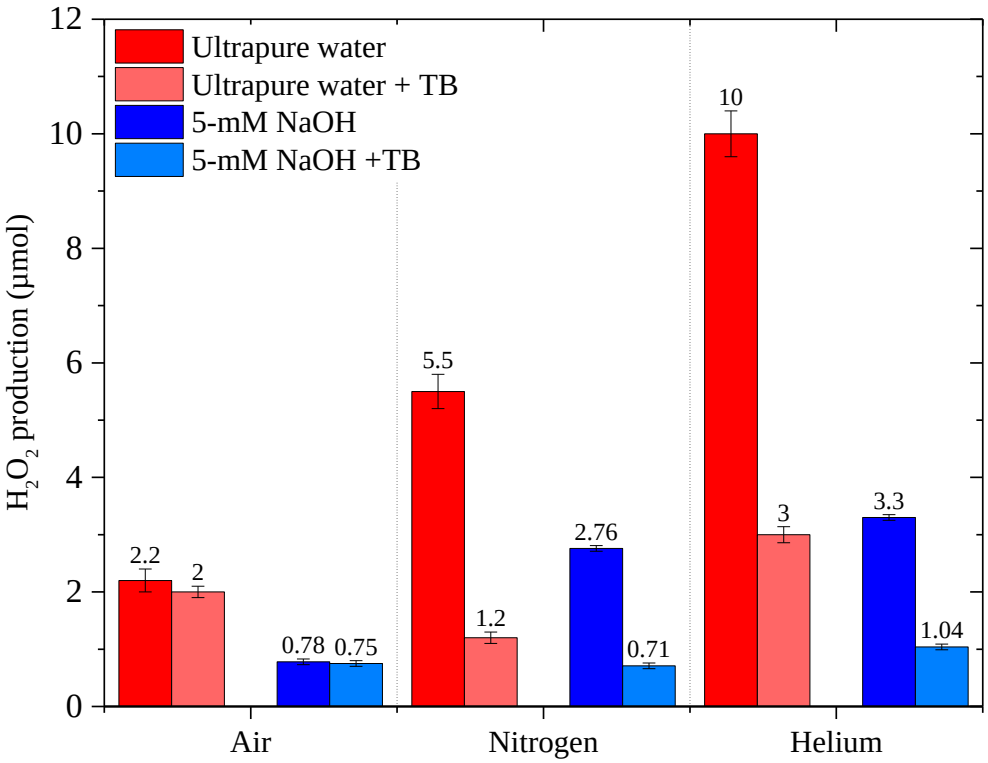

Figure 5.11 Comparison of H_2O_2 production in ultrapure water and 5-mM NaOH solution with or without TB in various gas treatments.

When TB was added to the solution, the H_2O_2 production after 20 minutes of treatment reached 0.75 µmol, 0.71 µmol and 1.04 µmol in air, N_2 and He, respectively. It can be calculated that 4%, 74% and 68% of the H_2O_2 production in air, N_2 and He, respectively, was

obtained from the dimerization of OH radicals; the corresponding amounts of OH radicals being 0.06 µmol, 4.1 µmol and 4.54 µmol.

In comparison to the OH radical detection results using the TA method (Fluorescence spectrophotometry), the results achieved by using Ti^{4+} method are 2 times, 68 times and 41 times higher in air, N_2 and He, respectively (Figure 5.12). In addition, it has been proven above that a significant inhibition of OH^- ions on H_2O_2 and OH radical production can occur in basic solutions. Therefore, the applicability of fluorescence spectrophotometry to measure H_2O_2 production using a TA solution that is prepared in a basic solution is problematic and needs to be further investigated.

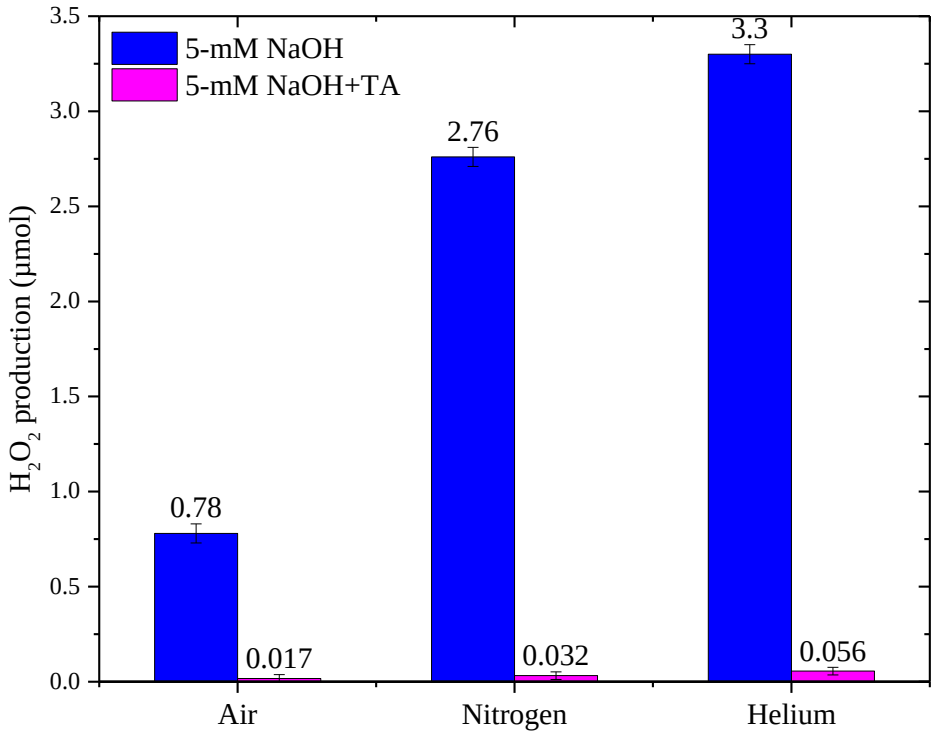

Figure 5.12 Comparison of H_2O_2 measurement by using Ti^{4+} solution and OH radical measurement by using TA solution.

5.7 Conclusion

Positive impulsive currents were recorded at the beginning of discharges above ultrapure water in air, N_2 and helium. Increased solution conductivity lead to the development of diffuse discharges in air and N_2. Compared to the results recorded in Chapter 4, the solution conductivity in air treatments increased more quickly, which could be due to the discharge being operated in a sealed reactor in this experiment. The amplitude of the tail current in N_2 was higher than that in air, which indicated that a stronger diffuse discharge was developed in the N_2 treatment. The lowest current amplitude of ~20 mA and the widest current pulse width of 55 ns was observed in helium. Increase the treatment time result in an increase of the current pulse repetition rate, from 5×10^5 pps to 12.5×10^5pps, and the reduction of pulse amplitude from 20 mA to 10 mA. A solution conductivity increase of 88 µS/cm was recorded in helium and the reason for this result is still unknown.

In the discharge above ultrapure water, the highest H_2O_2 production was obtained in helium treatments, corresponding to an OH radical production of 20 µmol; the lowest H_2O_2 production was obtained in air treatments, corresponding to an OH radical production of 4.4 µmol. The addition of TB terminates the dimerization of OH radical dimerization, which contributed to 4%, 74% and 68% of the H_2O_2 production in air, N_2 and helium, respectively.

Diffuse discharges were observed in all gases treatments, when 5-mM NaOH solutions were used. Increasing solution conductivity led to the joining of the tail current into the impulsive current. The amplitude of the impulsive current in N_2 was much lower than that of the tail current, which is different from the discharge currents recorded in air and helium. The H_2O_2 productions in all the gases used were reduced by up to 3 times in 5-mM NAOH solution, compared to those in ultrapure water. Also, the H_2O_2 productions in 5-mM NAOH solution, determined by using UV spectrometry, were up to 183 times higher than the OH radical production that was determined by using fluorescence spectrophotometry, due to the scavenging effect of OH^- ions on OH radical and H_2O_2. Therefore, the applicability of determination of OH radical production by using TA solution, which need to be dissolved in basic solution, needs further investigation.

5.8 Further work

A significant difference of discharge current in helium with ultrapure water and 5-mM NaOH solution was observed, the mechanism of this phenomenon needs to be further investigated.

A significant solution conductivity increase was observed in helium-treated samples with ultrapure water (from 0.5 µS/cm to 87 µS/cm), further investigations are required to clarify this phenomenon and the mechanism by which additional charge carriers, assumed to be ions, are being introduced into the solution.

A significant scavenging effect of OH^- ions on OH radical production was observed when a 5-mM NaOH solution was used during tests. Therefore, the applicable of the fluorescence photo-spectroscopy method to OH radical detection using TA solution, which must be prepared with 5-mM NaOH solution, needs to be further investigated.

6 H_2O_2 PRODUCTION UNDER CONTROLLED IMPULSIVE CURRENT DISCHARGES

6.1 Introduction

Kanzaki [114] found that the pin-to-water electrode structure can lead to a high charge efficiency for reactive species production. Although the impulsive current discharges in various gases have been investigated in Chapter 5, the charge transferred to water surface and the power consumed in each discharge pulse cannot be determined accurately, due to the variation of discharge characteristics with solution conductivity. In this experiment, a 1-nF high-voltage capacitor was connected in parallel with the reactor, which reduced the impact of stray capacitances, and enabled the calculation of the charge that arrived at water surface and the power consumption of each breakdown. Therefore, the charge/H_2O_2 ratio and the H_2O_2 production yield can be determined. In addition, the parallel-connected capacitor enables the generation of impulsive current discharges in O_2, N_2, air and helium under both positive and negative polarities without the requirement of a pulsed power supply.

The main objectives of this experiment were to investigate: (i) the charge transfer to water surface under controlled impulsive current discharges in various gases; (ii) the H_2O_2 production yield and charge/H_2O_2 ratio for discharges in various gases positive and negative polarities; (iii) the variation of solution conductivity and pH as a result of these discharges and (iv) the significance of the dimerization pathway for H_2O_2 formation by using a scavenger of the OH radical.

6.2 Experimental set up

Figure 6.1 shows the schematic diagram for controlled impulsive current discharge experiments. A reactor with a pin-to-water electrode structure, which has been introduced in Chapter 5, was also employed in this experiment. The samples were prepared with tap water (65 μS/cm).

As before a 0.2-M TB solution was used to terminate the dimerization of OH radical pathway to investigate the mechanism of H_2O_2 production. The electrical discharges were energized by both positive- and negative-applied voltage of 3 kV, in O_2, N_2, air and He. A sample of 10 ml was introduced into the reactor before the vacuuming process described in Chapter 3 was applied to the rest chamber.

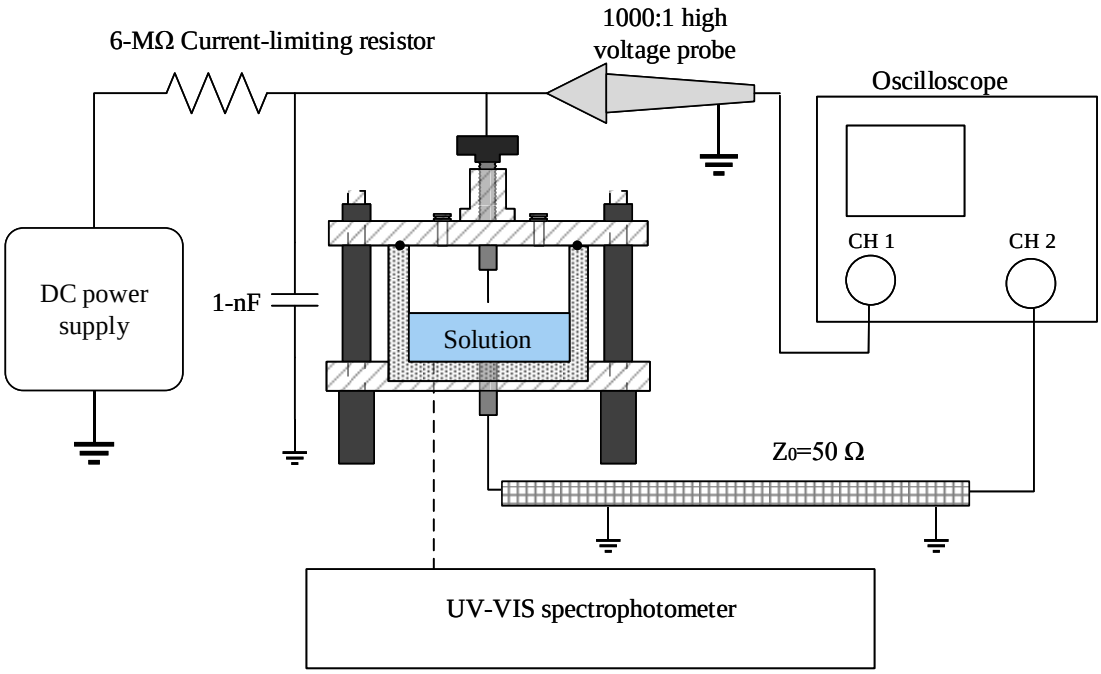

Figure 6.1 Schematic diagram for controlled impulsive current discharge experiments.

A 1-nF high-voltage capacitor was connected in parallel with the reactor to reduce the impact of stray capacitances in the circuit. The charges that arrived at the water surface in each inter-electrode breakdown can be calculated using the voltage drop and known capacitance (Eq. 6.1).

$$Q = C \cdot \Delta V \quad \text{(Eq. 6.1)}$$

C Capacitance of the high-voltage capacitor (1 nF)

ΔV Voltage drop in each discharge

The energy consumption for each discharge pulse (Eq. 6.2) and the charge/H_2O_2 ratio were calculated in this experiment.

$$P = \frac{1}{2} \cdot C \cdot (V_1^2 - V_2^2) \cdot pps \quad \text{(Eq. 6.2)}$$

P Power consumption

V_1 The voltage before discharge

V_2 The voltage after discharge

pps Pulse per second

A LeCroy Oscilloscope was used to record the discharge voltage and current waveforms in various gases. UV spectrometry was employed to measure the H_2O_2 production in the treated samples after gas discharges for 15, 30, 45 and 60 minutes. The variations of solution conductivity and pH were measured after each treatment. Each treatment was repeated three times.

6.3 Gas discharge characteristics with tap water

6.3.1 Positive polarity

Figure 6.2 and 6.3 shows the positive discharge characteristics in O_2, N_2, air and He. Tail currents due to the development of diffuse discharges were observed following the nano-second positive impulsive currents in all working gases. No significant variation of pulse repetition rate was observed in O_2, N_2 and He (~160 pps), however, in air, a lower rate of ~133 pps was recorded.

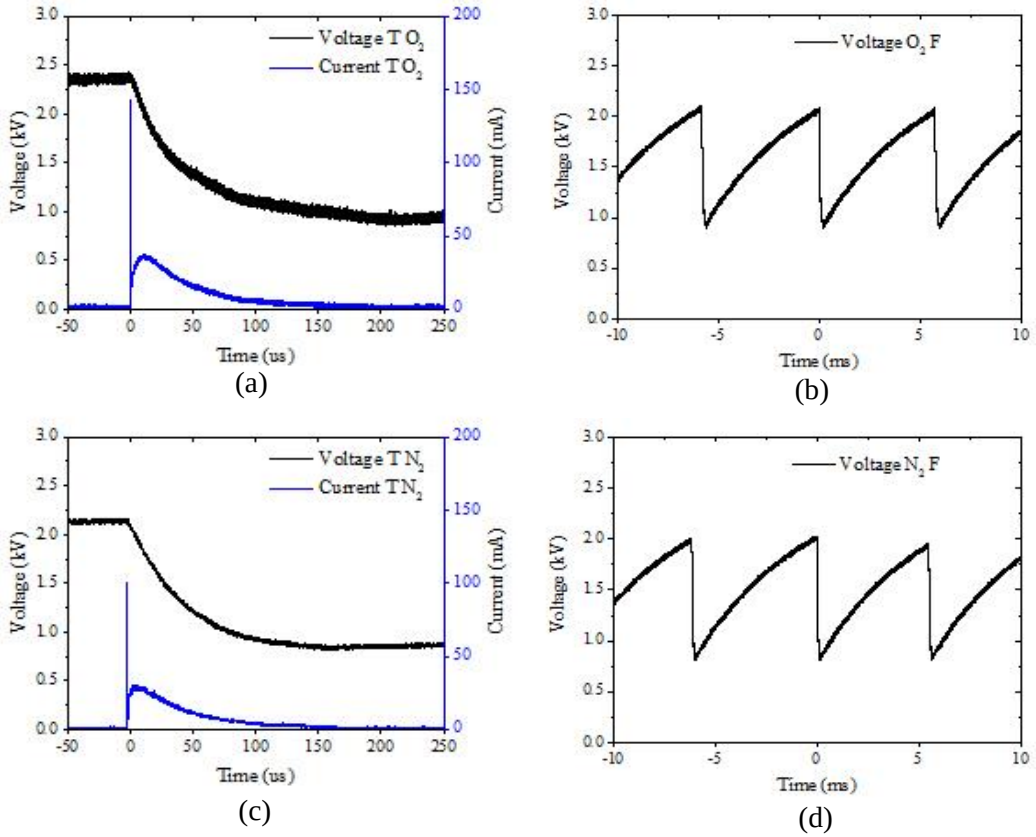

Figure 6.2 Discharge waveforms recorded under positive polarity in O_2 (a) and N_2 (c); pulse repetition rates recorded in O_2 (b) and N_2 (d).

The highest current amplitude and voltage drop were achieved in helium; amplitudes of 730 mA for impulsive currents and 90 mA for tail currents, and voltage drops of 1.7 kV were recorded (Figure 6.3 (c)). In addition, the tail current duration observed in helium (<100 μs) was the shortest.

The smallest voltage drop of 1.3 kV was obtained in N_2, slightly higher values of ~1.5 kV were recorded in O_2 and air. It was calculated by Eq. 6.1 that the charges arriving at water surface were 0.24 mCs^{-1}, 0.21 mCs^{-1}, 0.2 mCs^{-1}, and 0.27 mCs^{-1} (Table 6.1), for O_2, N_2, air and He treatments, respectively; the corresponding discharge powers were 0.37 W, 0.3 W, 0.3 W and 0.4 W. The energies for each pulse in all gas discharges were in the range of 1.9 to 2.5 mJ.

Hoeben [90] investigated the pulsed positive discharges above water and found the current amplitude in argon is higher than that in air, which is similar to the results recorded in helium and air in this experiment. Hoeben explained this phenomenon might be due to the electronegative character of O_2, which inhibits the discharge filament development in air.

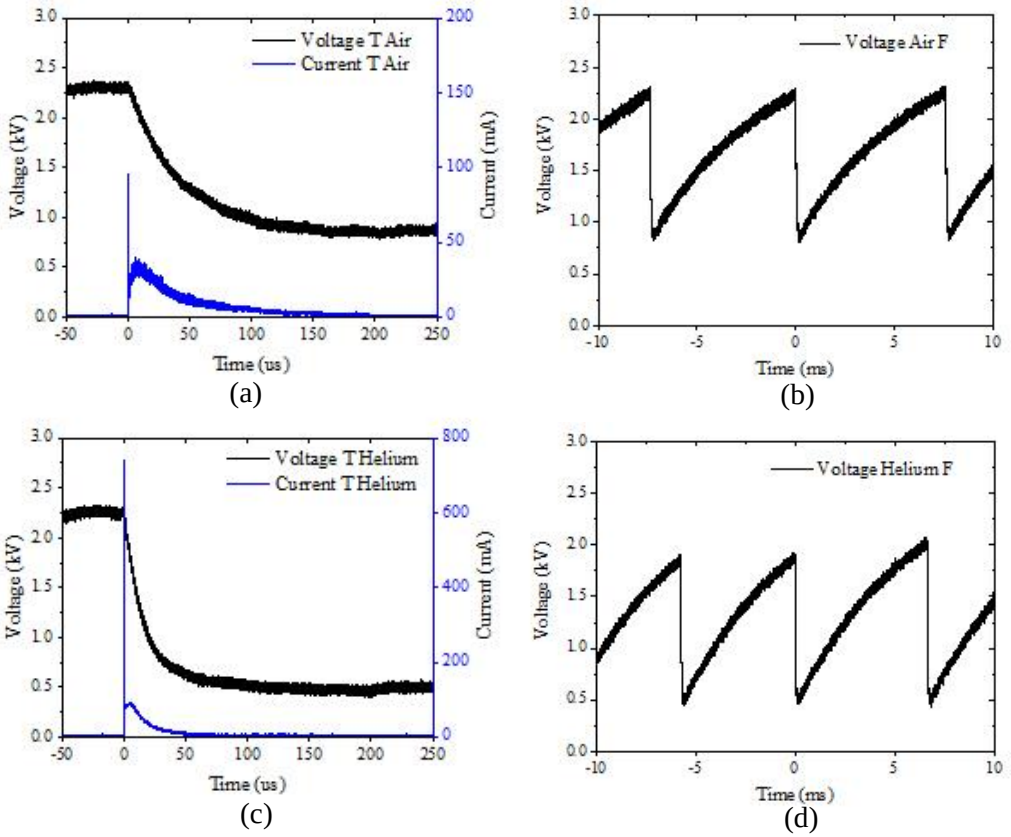

Figure 6.3 Discharge waveforms recorded under positive polarity in air (a) and helium (c); pulse repetition rates recorded in air (b) and helium (d).

6.3.2 Negative polarity

Under negative polarity, tail currents of several tens mA were recorded in all gas discharges (Figure 6.4, 6.5). In addition, higher voltage drops of ~2.1 kV was recorded in all gas discharges under negative polarity compared to those under positive polarity. The current amplitudes in He was significantly reduced from 730 mA to 210 mA for impulsive currents and from 90 mA to 60 mA for tail currents, when change the discharge polarity from positive to negative. The impulsive current amplitudes recorded in N_2, O_2 and air were higher under negative polarity, reaching ~150 mA.

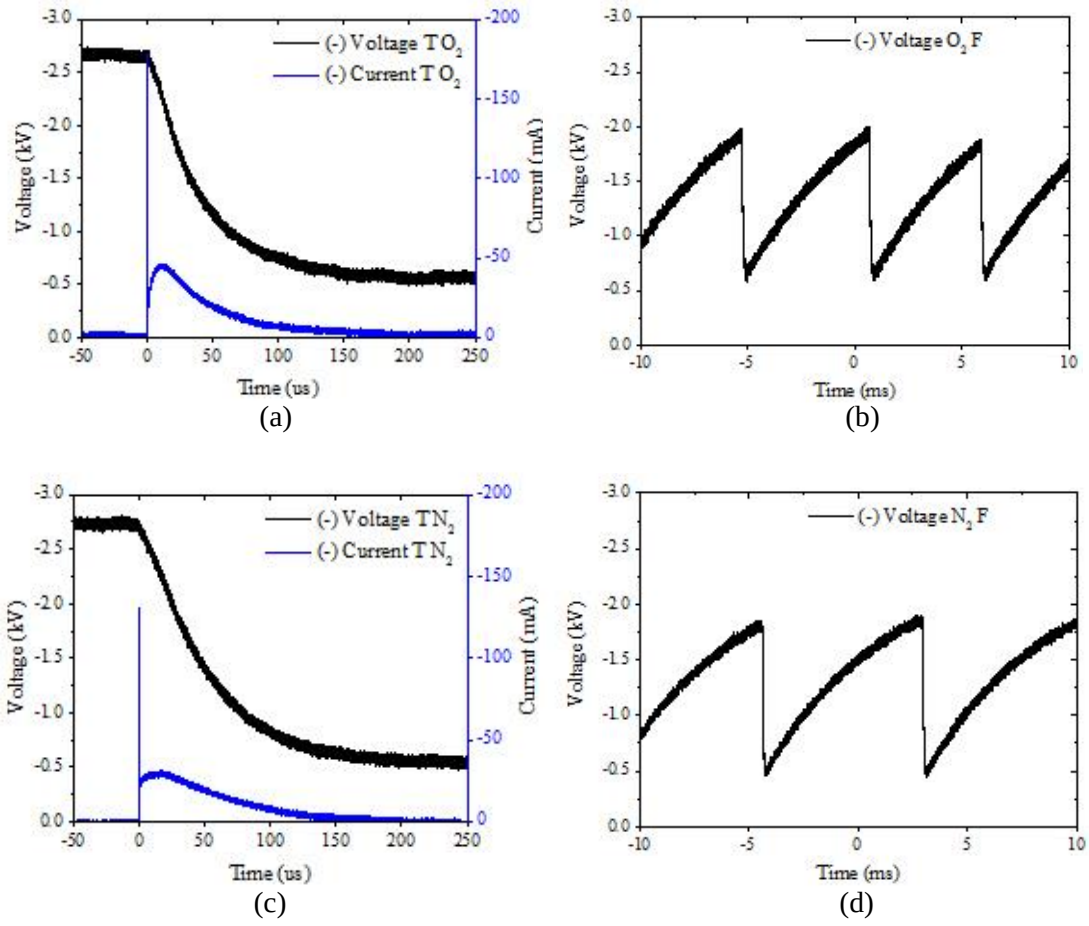

Figure 6.4 Discharge waveforms recorded under negative polarity in O_2 (a) and N_2 (c); pulse repetition rates recorded in O_2 (b) and N_2 (d).

The pulse repetition rate of 160 pps recorded in O_2 under negative polarity was the same as under positive polarity; however, lower values of 130 pps and 84 pps were recorded in N_2 and air, respectively, compared to those of 160 pps and 133 pps recorded under negative conditions; a higher value of 200 pps was recorded in He.

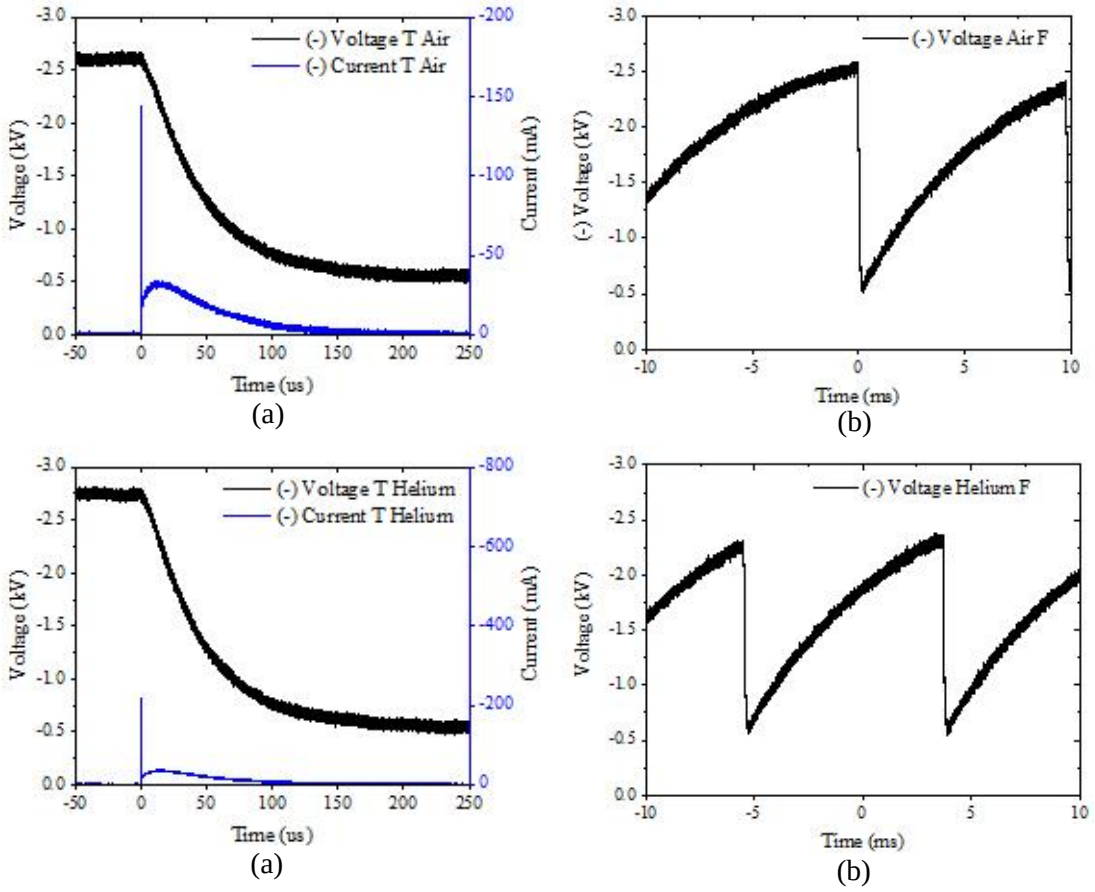

Figure 6.5 Discharge waveforms recorded under negative polarity in air (a) and helium (c); pulse repetition rates recorded in air (b) and helium (d).

Bruggeman [115] investigated the development of filaments on water surface under negative pulsed discharges and found that there is always a pre-breakdown current (several mA) formed before the development of the intensive discharge current. Bruggeman considered that was due to the deformation of the water surface. However, in this experiment, no pre-breakdown current was recorded. On the other hand, Ikoma [80] investigated the negative pulse current discharges in various gases and found that the current amplitude in O_2 is much higher than that in an N_2-O_2 mixture gas, which is different to the results recorded in this experiment.

The calculation of charges that transferred to water surface during discharges helps to investigate the H_2O_2 production pathways. In Chapter 5, the charge transfer was not able to be calculated due to the dynamics of discharge current. In this experiment, the charge transfer could be calculated and the rate of charge transfer is shown in Table 6.1 for the discharges in the gases employed.

Table 6.1 The quantity of charges that transferred to water surface per second in various gas treatments under positive and negative polarity.

Gases / *Polarity*	*Charge transfer per second (mC)*			
	O_2	*N_2*	*Air*	*Helium*
Positive	0.22	0.21	0.2	0.27
Negative	0.35	0.28	0.17	0.4

6.4 Plasma-water interface reactions under positive polarity discharges

6.4.1 H_2O_2 production

The H_2O_2 production increased almost linearly with time and reached 10.2 µmol, 9.9 µmol, 5.5 µmol and 12.5 µmol after 60 minutes of treatment in O_2, N_2, air and He, respectively. H_2O_2 production was the lowest in air and highest in helium, which is the same as for the results recorded in Chapter 5.

The charge/H_2O_2 ratios were calculated for the various experimental conditions. The lowest charge/H_2O_2 ratio of 1:0.74 was recorded in air, and the highest value of 1:1.26 was recorded in O_2 and N_2. A charge/H_2O_2 ratio of 1:1.2 was recorded in helium, slightly lower than those recorded in O_2 and N_2. If one charged particle produced within the gas is required to produce a single OH radical and the major H_2O_2 production pathway is through the dimerization of these radicals a charge/H_2O_2 ratio of 1:0.5 would be expected. It can be seen in these results that the calculated ratios are significantly higher than this suggesting that other pathways exist. Figure 6.6 shows the H_2O_2 energy efficiency in discharges with tap water.

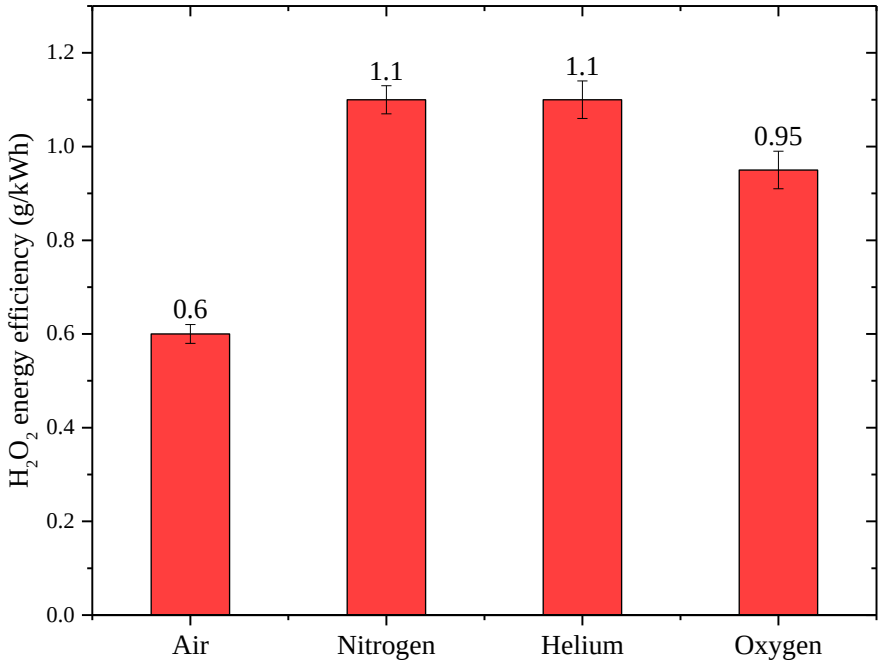

Figure 6.6 H_2O_2 energy efficiency in various gas treatments under positive polarity discharges.

A H_2O_2 production yield of 1.1 g/kWh was achieved in N_2 and helium, and a lower yield of 0.95 g/kWh was recorded in O_2. In N_2 and helium treatments the production of metastable molecules, such as N_2^* and He^*, leads to the direct formation of OH radicals by their reactions with water. The lowest production yield of H_2O_2 of 0.6 g/kWh was recorded in air, which may be due to the large amount of oxy-nitride species production at the plasma-water interface, which was detected by using test strips.

No slow-down in the trend of H_2O_2 production in air or N_2 was observed, which is different to the results recorded in Chapter 5. This may be due to the lower repetition rate of up to 160 pps under controlled positive discharges, due to the role of the capacitor, in this experiment, leading to less water vapour generation compared to that under uncontrolled positive discharges (Chapter 5), thus reducing the absorption of oxy-nitride species by water vapour.

The H_2O_2 production recorded in O_2 discharges increased in proportion with time and was almost twice the amount that was recorded in air. Similar results were achieved in Ikoma's [80] research. Ikoma found that the O_3 production in O_2 reached the maximum, leading to the highest H_2O_2 production, which can be due to reaction R 6.1. Due to the low ionization energy of O_2 gas molecules (12.06 eV for O_2 and 12.6 eV for H_2O), the production of H_2O^+ ions are less likely to occur in O_2 discharges above water. Therefore, OH radicals generated from O_3 decomposition in solution are more likely to occur [80]. Sato [55, 110] recorded a higher organic compound degradation rate in O_2 treatments than that in the air treatments, and concluded the results were due to the much higher concentration of O_3 that is generated in O_2 plasma. It should be noted that the metastable O^* generated in O_2 discharges also leads to the production of OH radicals by reaction (R 6.2).

$$H_2O + O_3 \rightarrow H_2O_2 + O_2 \quad \text{(R 6.1)}$$

$$H_2O + O^* \rightarrow 2\,OH \quad \text{(R 6.2)}$$

Another possibility for higher H_2O_2 production and charge efficiency in O_2 could be due to the electron attachment reactions that occur at the plasma-water interface, leading to the production of O_2^-, which can further react with species to produce H_2O_2 (R 6.3-6.6).

$$O_2 + e^- \rightarrow O_2^- \quad \text{(R 6.3)}$$

$$O_2^- + H^+ \rightarrow HO_2 \quad \text{(R 6.4)}$$

$$HO_2 + e^- \rightarrow HO_2^- \quad \text{(R 6.5)}$$

$$HO_2^- + H^+ \rightarrow H_2O_2 \quad \text{(R 6.6)}$$

In addition, the neutralization of H^+ ions by electrons (R 6.7), leads to the production of $H^\cdot$ radical, which can react with O_2 to form HO_2 (R 6.8), leading to the production of H_2O_2 through reaction (R 2.34).

$$H^+ + e^- \rightarrow H^\cdot \quad \text{(R 6.7)}$$

$$H^\cdot + O_2 \rightarrow HO_2 \quad \text{(R 6.8)}$$

$$HO_2^\cdot + HO_2^\cdot \rightarrow H_2O_2 + O_2 \quad \text{(R 2.34)}$$

The H_2O_2 production in N_2 was 44% higher than that in air, which is similar to the results recorded in Ikoma's research [80]. This can be due to the generation of metastable N_2 molecules by reaction (R 2.2), leading to the production of OH radicals by reaction (R 6.9).

$$N_2^* + H_2O \rightarrow OH^\cdot + N_2 + H^\cdot \quad \text{(R 6.9)}$$

Porter [116] investigated the H_2O_2 production in gliding arc discharges with water spray and concluded that the H_2O_2 production is independent of working gas (O_2, Ar, CO_2) as long as no oxy-nitride was generated during discharge to suppress H_2O_2 production. However, Porter also found that the H_2O_2 production in helium treatments was only half of that in O_2 treatments, and Porter did not explain this phenomenon. Ikoma [80] investigated dye degradation by discharges in an Ar-O_2 gas mixture and found that increase in the Ar content reduced the O_3 production; however, this did not slow down the dye degradation rate. This is in agreement with Porter's conclusion, where no significant difference of H_2O_2 production was obtained between Ar and O_2 treatments. Due to the different behaviours between helium and Ar gases on reactive species production and water treatment, it is worthwhile to investigate the effect of Ar on H_2O_2 production under impulsive current discharges.

Tert-butanol effect

When TB was applied during treatments, the H_2O_2 production after 60 minutes of treatment in air, N_2 and helium reached 5.4 µmol, 1.4 µmol, 5.3 µmol, respectively. Significant reductions of H_2O_2 production were observed in N_2 and helium treatments compared to the results when no TB was used. Almost no effect of TB on H_2O_2 production was observed in air discharges, a residual H_2O_2 content of 98% was recorded, which is the same as that recorded in Section 5.6.2.

The residual H_2O_2 content in N_2 and helium treatments was 14% and 43%, respectively (Figure 6.7). The reduction of H_2O_2 production could be due to the evaporation of TB with water, leading to the scavenging of OH radicals in the gas phase. The direct H_2O_2 formation

pathway could occur at the plasma-water interface by reaction (R 6.10), which would not be affected by TB; however, high charge energy is required in this reaction [14]. Therefore, the discharges in helium, in which the gas has a higher ionization energy compares to that in N_2, is more likely to process the reaction (R 6.10). This also explained the high residual content of H_2O_2 in helium than that in N_2.

$$H_2O + H_2O \rightarrow H_2O_2 + O_2 \qquad \text{(R 6.10)}$$

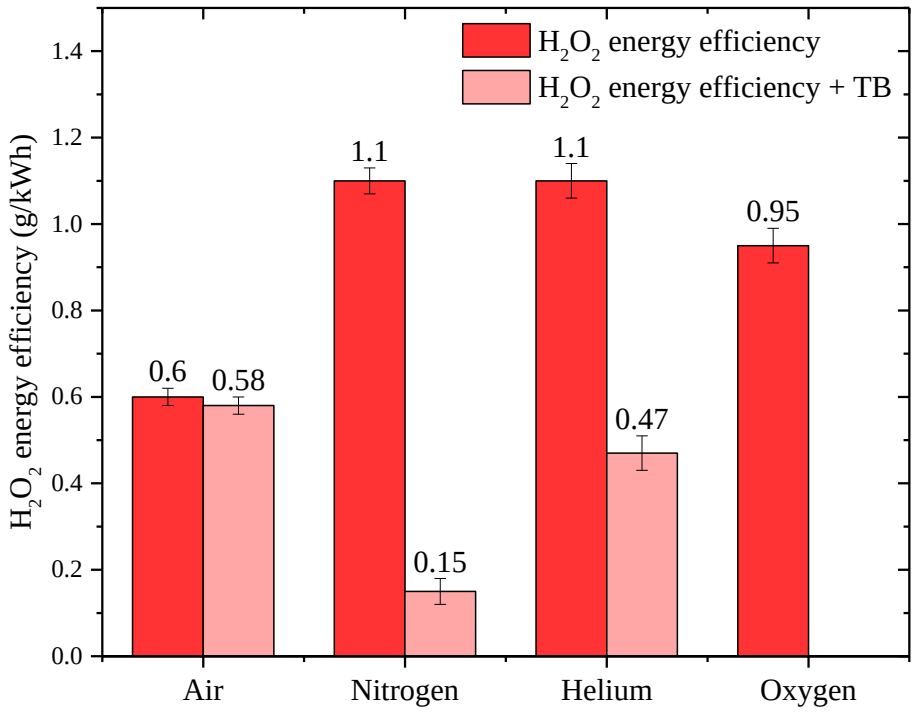

Figure 6.7 Effect of TB on H_2O_2 energy efficiency in various gas treatments under positive polarity discharges.

An increase of H_2O_2 production was observed in O_2 discharges; however, the standard deviation reached 30% among 3 samples; therefore, the results recorded in O_2 treatments are not presented here. There are a number of possible explanations for the increased but variable H_2O_2 production (i) One of the possibilities is that the generation of O_3 at the plasma-water interface, which cannot react with TB, increased the H_2O_2 production. However, if this is the case, the H_2O_2 production should remain the same as when no TB was applied. (ii) Another possibility is that the oxygen atoms and OH radicals that are generated in O_2 discharges result in the degradation of TB molecules ($(CH)_3C$-OH), leading to the cleavage of the bond between carbon atom and the hydroxyl, thus increasing the H_2O_2

production. (iii) A third possibility is that the reactions between reactive oxygen species (ROS) and TB result in a product, which can react with Titanium ions (Ti (IV)) to form an orange coloured complex; therefore, interfered with the determination of H_2O_2 production. However, the third possibility has not been extensively investigated and requires further investigation.

The low impact of TB on H_2O_2 production in air-treated samples could also be due to the existing of O_2 during treatments. The mechanisms of TB reactions with ROS need to be further investigated.

6.4.2 Variation of solution conductivity and pH

Figure 6.8 shows the solution conductivity changes during various gas treatments. The highest conductivity change was observed in air, which increased linearly with time, reaching 200 µS/cm after 60 minutes of treatment. A saturation trend was observed in N_2, the solution conductivity increased to 153 µS/cm after 60 minutes of treatment. Only nitrite acid was detected in air-treated samples and both nitrite and nitrate acids were detected in nitrogen-treated samples.

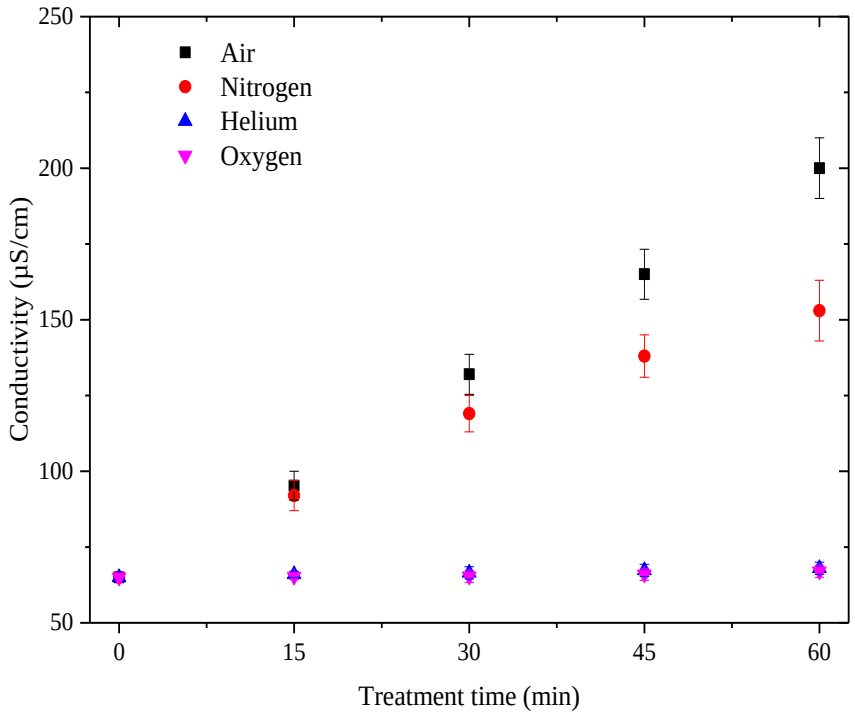

Figure 6.8 Variation of solution conductivity in various gas treatments under positive polarity.

No conductivity change was observed in helium or O_2 treatments, in which cases no N_2 was present in working gases. This result was also recorded in Ikoma's research [80]. It can be concluded that all the solution conductivity changes observed in air and N_2 treatments were due to the production of oxy-nitride species at the plasma-water interface, leading to the production of nitrite and nitrate acids in solutions, which were detected by nitrite and nitrate test strips. Similar results were recorded in Porter's research [116]. Porter investigated the electrical discharges in water spray and found that no nitrates were generated in O_2 and helium treatments; in both cases, the solution conductivity and H^+ ion production were at least one order lower than those observed in air treatments.

Although no solution conductivity change was observed in helium and O_2 treatments (Figure 6.9), the solution pH reduced from 8.5 to 6.3 and 6.05, respectively, after 60 minutes of dishcarge; corresponding to H^+ productions in the order of nmols. The solution pH reduced to 3.6 in air and 2.85 in N_2 after 60 minutes of treatments; the H^+ production in both cases was in the order of µmols (Table 6.2).

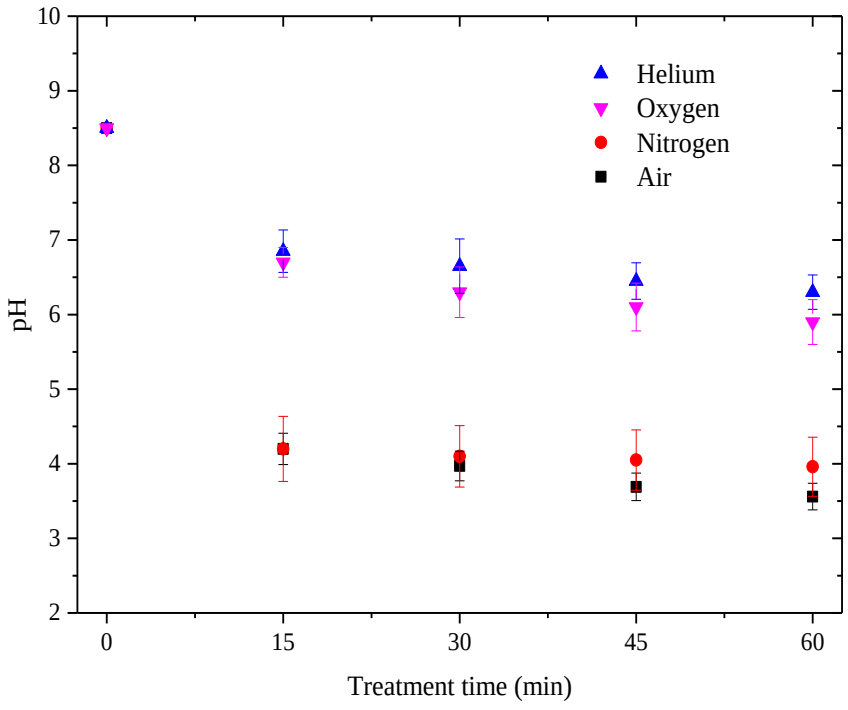

Figure 6.9 Variation of solution pH in various gas treatments under positive polarity.

Table 6.2 H^+ ions production over 15-minute intervals, under positive controlled current discharges in various gases.

Treatment period (min)	*H^+ ions production (µmol)*			
	O_2	*Air*	*N_2*	*Helium*
0-15	1.9×10^{-3}	0.6	0.4	1.4×10^{-3}
15-30	1.1×10^{-3}	0.4	0.3	0.8×10^{-3}
30-45	1.5×10^{-3}	0.9	0.1	1.3×10^{-3}
45-60	1.8×10^{-3}	0.7	0.2	1.5×10^{-3}

Tert-butanol effect

When TB was applied during various gas treatments, the solution conductivity change was reduced by 80% in N_2, compared to no-TB treatments; a final value of 82 µS/cm was recorded after 60 minutes of treatment (Figure 6.10). This could be due to the TB that vaporised together with water molecules from the liquid phase, scavenging not only OH radicals but also free radicals such as $N^{\cdot}$ and $NO^{\cdot}$, terminating the production of oxy-nitride species at the plasma-water interface.

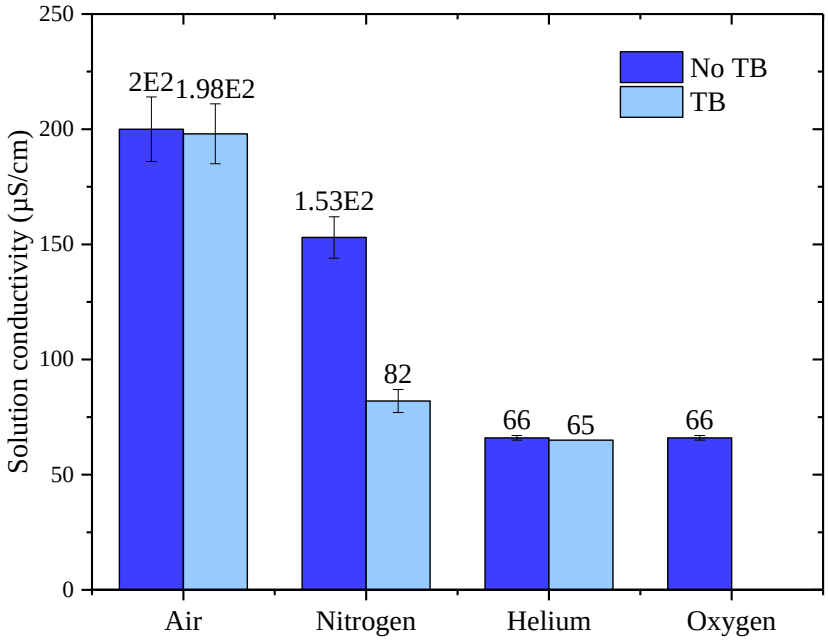

Figure 6.10 Effect of TB on solution conductivity variation in various gas treatments under positive polarity.

In air treatments, the solution conductivity of 198 µS/cm recorded after 60 minutes of treatment is similar to the value when no TB was applied. This may be due to the effect of TB reactions with O_2. However, no detailed study on the reaction between TB and O_2 has been made; therefore, the mechanism of this reaction needs to be further investigated. O_2 was not considered due to the difficulties of using with TB (has been discussed in Section 6.4.1). Almost no solution conductivity change was observed in helium treatments.

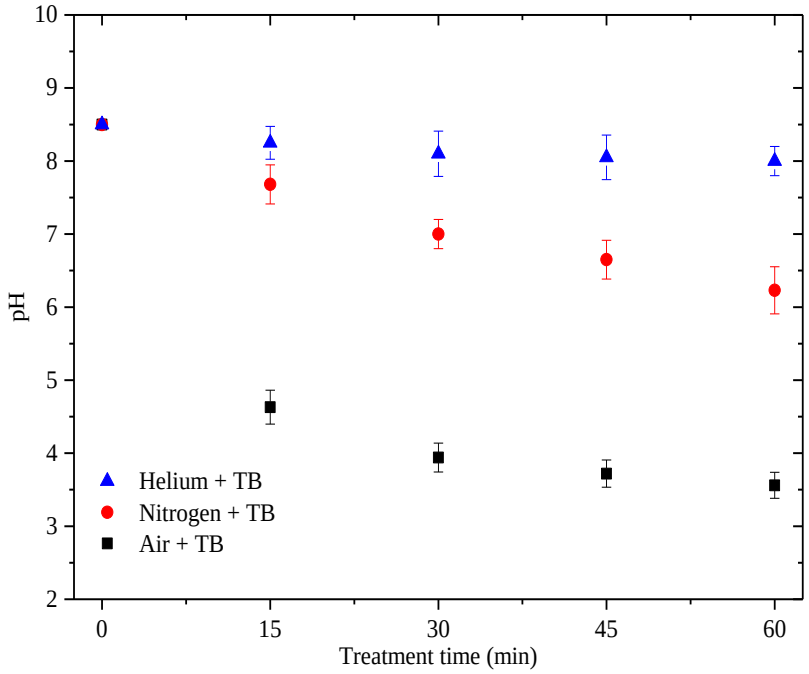

Figure 6.11 Effect of TB on solution pH variation in various gas treatments under positive polarity.

The solution pH after 60 minutes of nitrogen discharges reduced from 8.5 to 6.2 (Figure 6.11), which corresponded to the H^+ production of several nano-mols. This value is around 3 orders lower than the result recorded in N_2 treatments when no TB was applied (Table 6.2, Table 6.3). This could be due to the scavenging of $N^{\cdot}$ radicals that are generated at the plasma-water interface by the TB, thus, significantly reduced the amount of oxy-nitride species production. No significant effect of TB on air treated samples was recorded, which is the same as that recorded in H_2O_2 production and solution conductivity variation.

A slight pH change was observed in helium discharges when TB was applied, the solution pH reduced from 8.5 to 8 after 60 minutes of treatment; corresponding to the H^+ production in the order of several pico-mols (Table 6.3). In air discharges, the solution pH variation is independent of TB.

Table 6.3 Effect of tert-butanol on H^+ production over 15-minute intervals, in various gases under positive controlled current discharges

Treatment period (min)	*H^+ ions production (µmol)*		
	Air	*N_2*	*Helium*
0-15	0.2	0.2×10^{-3}	25×10^{-6}
15-30	0.6	0.8×10^{-3}	23×10^{-6}
30-45	0.8	1.3×10^{-3}	10×10^{-6}
45-60	0.9	4×10^{-3}	11×10^{-6}

6.5 Plasma-water interface reactions under negative polarity

6.5.1 H_2O_2 production

No H_2O_2 production was detected in air and N_2 treatments after 60 minutes of treatment (Figure 6.12). Visually, a very slight yellow colour was observed in helium- and O_2-treated samples; however, no absorption was measured by using UV spectrophotometer due to the concentrations of H_2O_2 in these two cases being so low. The results recorded under negative discharges strongly agree with Polyakov's research [78]. Thagard [4] compared positive and negative pulse discharges and found that the concentration of H_2O_2 detected under negative polarity in a slight basic solution of pH 9 was 95% lower than that under positive polarity.

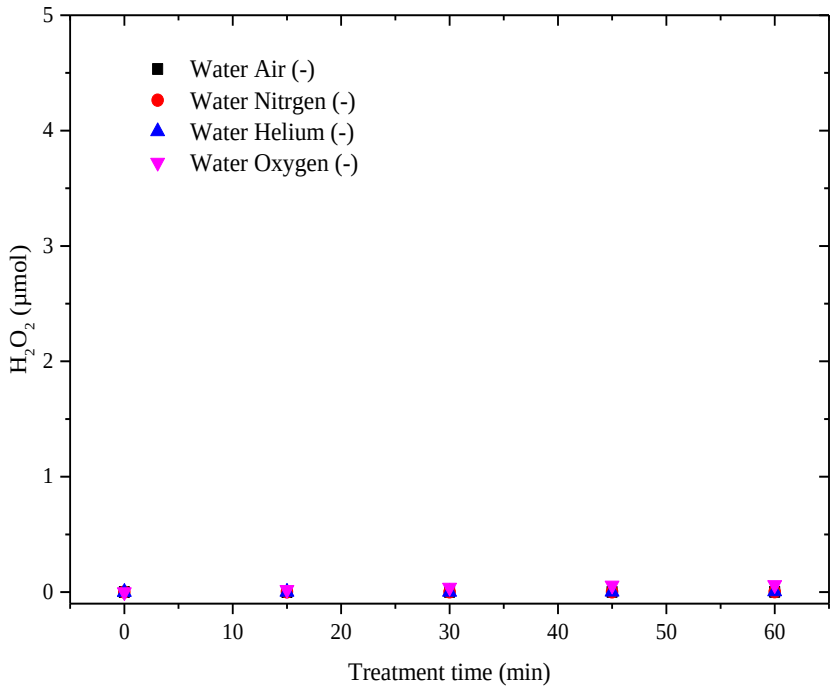

Figure 6.12 H_2O_2 production in various gas treatments under negative discharges.

Thagard [4] used silver nitrate to investigate the effect of electrons in liquid and found that significant amounts of silver ions were naturalized to elementary silver by electrons when the solution acted as an anode, indicating that a high number of electrons were generated and passed through the gas-water interface during electric discharges and react with other species in solution. Therefore, it is possible that the electrons that arrive at the water surface and then entre the water result in the attachment reactions with OH radicals (R 6.11) or H_2O_2

molecules (R 6.12), and resulting in the scavenging of OH radicals and the decomposition of H_2O_2 molecules, thus significantly reducing the H_2O_2 production.

$$OH^{\cdot} + e \rightarrow OH^{-} \quad \text{(R 6.11)}$$

$$H_2O_2 + OH^{-} \rightarrow H_2O + HO_2^{-} \quad \text{(R 2.36)}$$

Another possibility that leads to the reduction of H_2O_2 under negative discharges is that the majority of the voltage drop was located in the vicinity of the high voltage electrode rather than at the plasma-water interface. Therefore, the H_2O_2 production at the plasma water interface is significantly reduced.

Xiong [43] compared positive and negative pulsed discharges with a power of several tens Watts, and found that H_2O_2 production under negative polarity is only ~20% lower than that under positive polarity. Xiong also determined that the power, ranging from 40 to 115 W, having a limited effect on H_2O_2 production (~0.3 g/kWh). Therefore, the significant difference of H_2O_2 production under negative polarity between Xiong's and this experiment (1.9 to 2.5 mJ) may be due to the significant difference of power input, leading to a different H_2O_2 production mechanism. Under negative pulsed discharges with an energy of around 0.5 J/pulse, the direct dissociation of H_2O can occur [1]; leading to large amounts of OH radical production in water vapour. The high energy pulses also allow the spread of filaments on the water surface, enlarging the electron-water interface and resulting in higher H_2O_2 productions.

The results recorded in this experiment show that negative discharges are poor generator of H_2O_2 and therefore, commercial application should concentrate on the positive polarity impulsive current discharges for H_2O_2 production.

6.5.2 Variation of solution conductivity

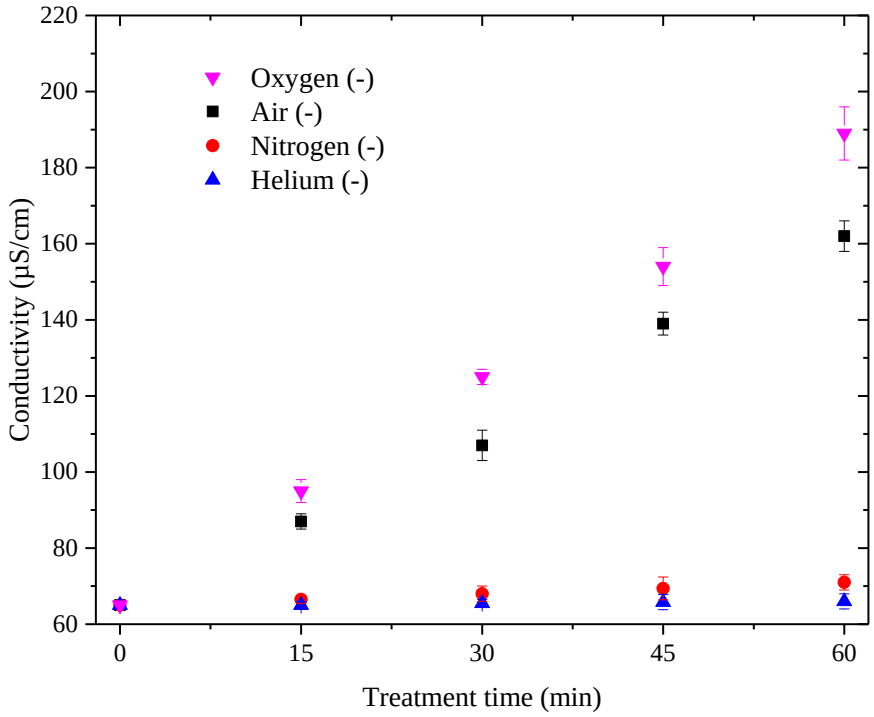

Figure 6.13 Variation of solution conductivity in various gas treatments under negative discharges.

Although no H_2O_2 production was detected under negative discharges (Figure 6.13), a significant solution conductivity increase was observed in air treatments, reaching 162 µS/cm, which was ~30% less than that under positive polarity. Both nitrite and nitrate acid were detected in air-treated solutions, by using test strips, while only nitric acid was detected under positive polarity.

The highest solution conductivity of 189 µS/cm was observed in O_2 treatments, which is significantly different from the results observed under positive polarity. This phenomenon could be caused by the electron attachment reactions, leading to the generation of negative ions in solution, significantly increase the solution conductivity (R 2.67, R 2.68).

$$O^- + H_2O \rightarrow OH^- + OH^{\cdot} \quad \text{(R 2.67)}$$

$$O_2^- + H_2O \rightarrow OH^- + HO_2^{\cdot} \quad \text{(R 2.68)}$$

A slight increase of solution conductivity (from 65 µS/cm to 73 µS/cm) was observed in N_2, which is significantly different from that recorded under positive polarity. This may be due

to the absence of OH radicals and H_2O_2 production under negative discharges, leading to no oxidation process of N atoms during N_2 treatments. As recorded under positive discharges, no solution conductivity change was obtained in helium treatments.

6.6 Conclusion

The parallel-connected high voltage capacitor controlled the charge that transferred to water surface during each pulse; the charge quantities in various gas discharges were in the range of 0.17 to 0.4 mCs^{-1}. The discharge currents recorded in various gases treatments with tap water all included micro-second tail currents, following nano-second impulsive currents.

Under positive polarity, the highest charge/H_2O_2 ratio of 1:26 was recorded in N_2 and O_2 treatments. The highest H_2O_2 production yield of 1.1 g/kWh was recorded in N_2 and helium treatments. The addition of TB suggests that 86% and 57% of H_2O_2 production in N_2 and helium treatments, respectively, is via OH dimerization. No difference of H_2O_2 production, solution conductivity and pH variation were observed in air treatment between the solutions without and with TB; the reason for this phenomenon needs further research. On the other hand, in N_2 discharges with TB, oxy-nitride species production was significantly reduced by 80%, thus reducing the solution conductivity variation. Although no solution conductivity variation was observed under positive discharges in O_2 and helium, the reductions solution pH were observed.

Under negative polarity, no H_2O_2 production was detected in various gas treatments, which is significantly different from the results recorded under positive polarity. On the other hand, a significant increase of solution conductivity was recorded in negative O_2 treatment, which is due to the electron attachment reactions. The solution conductivity variation in air and N_2 treated samples were reduced by 70% and 99%, respectively.

It was found that only positive polarity is effective for H_2O_2 production under impulsive current discharges, while no H_2O_2 production was detected under negative polarity. In addition, the controlled impulsive current discharges benefit from avoiding the expensive pulsed power system, which can reduce the operation cost.

6.7 Further work

Discharges in O_2 have been proven to increase H_2O_2 production when TB was presented during treatments. However, the mechanism of this phenomenon is still not clear; therefore, further investigations are required to clarify the reactions between TB and ROS that occurred at the plasma-water interface in O_2 treatments.

The investigations of impulse current discharges for H_2O_2 production (Chapter 5 and Chapter 6) were all investigated with an applied voltage of 3 kV and an inter-electrode distance of 1 mm, therefore, the effect of different applied voltages and inter-electrode distances can be investigated to compare the H_2O_2 production yield and charge/H_2O_2 ratio in different conditions. In addition, the effect of initial solution pH can be investigated in terms of both discharge characteristics and reactive species production. The number of pin electrodes could also be increased to observe whether the production of reactive species increased in proportion with increasing plasma columns.

7 H_2O_2 PRODUCTION UNDER DC GLOW DISCHARGES

7.1 Introduction

A series of studies have investigated DC glow discharges above water surface with a pin-to-water electrode structure [4, 117, 118]. Locke [1] found that the H_2O_2 productions in above-water discharges are mostly less than 1 g/kWh. Vasko [117] recorded a H_2O_2 production of ~0.68 g/kWh under DC discharges in helium. This chapter focuses on the H_2O_2 production under positive or negative DC glow discharges that developed above water. The effects of solution conductivity and pH on H_2O_2 production were investigated. A reactor with a pin-to-water electrode structure, which was introduced in Chapter 5, was employed in this experiment. Continuous positive or negative DC voltage of 3 kV was applied to the pin electrode to compare the polarity effect. The results obtained in this experiment were compared to those obtained in impulsive current discharges (Chapter 6) to investigate the effect of different discharge types.

A large amount of water vapour can be generated in DC discharges that occur above water [4, 38, 39]; however, the effect of water vapour on discharge characteristics and plasma-water interface reactions is not well understood. In this experiment, the effect of water vapour was investigated in various gas treatments, by introducing a gas flow during discharges. By increasing the gas flow water vapour will be driven away from the region of discharge therefore possibly reducing its effects. A scavenger of OH radicals was again employed to terminate the dimerization of OH radicals into H_2O_2, thus determining the H_2O_2 production pathway.

The main objectives of the experiment were to: (i) investigate the effect of polarity on H_2O_2 production yield and charge/H_2O_2 ratio in various gas treatments; (ii) investigate the effect of water vapour on H_2O_2 production; (iii) investigate the effect of gas flow rate on H_2O_2 production and solution conductivity variation; (iv) investigate the effect of solution pH on H_2O_2 production and (v) investigate the H_2O_2 formation pathway by using a scavenger of OH radicals.

7.2 Experimental set up

Figure 7.1 shows the schematic diagram for DC glow discharge experiments. A 200-kΩ current limiting resistor was connected in series with the reactor. The samples were prepared using tap water (65 µS/cm). The inter-electrode distance was fixed at 1 mm. Three gases: N_2, air and He were used under positive and negative discharges. O_2 was not used with DC glow discharges due to the rapid erosion of the high voltage electrode which was observed in preliminary tests. The vacuuming process described in Chapter 3 was applied before N_2 and He treatments.

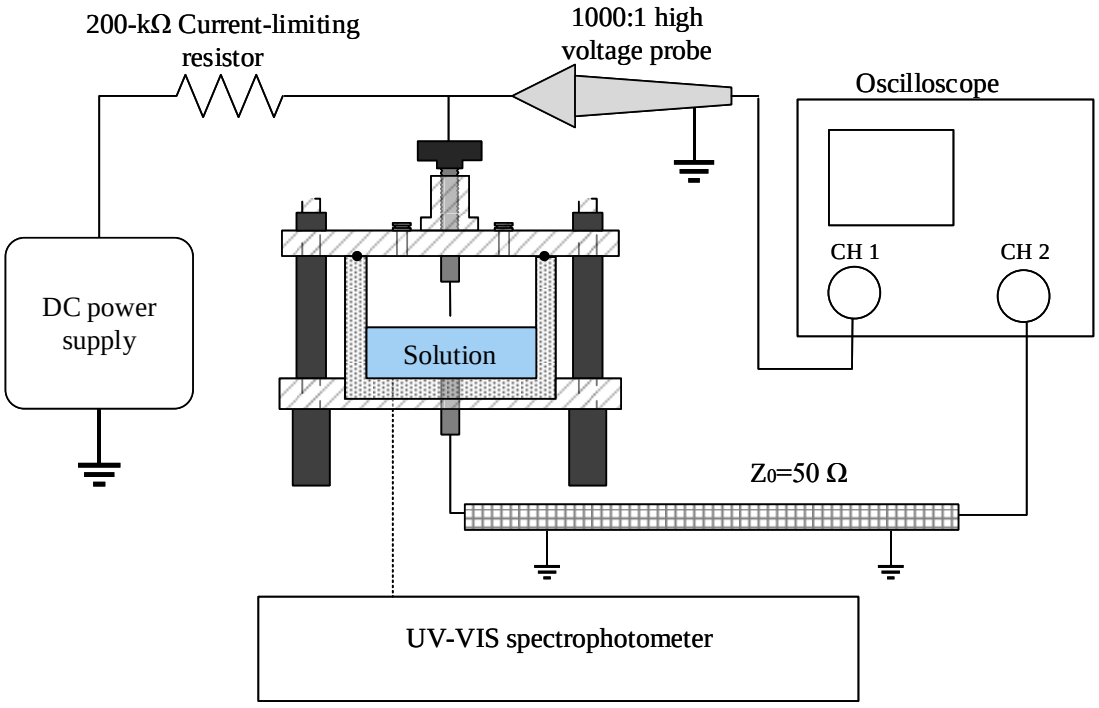

Figure 7.1 Schematic diagram for DC glow discharge experiments.

The effect of initial solution pH was investigated in air treatments, H_2SO_4 solutions of pH 3.2 and 4, and NaOH solutions of pH 11, 12 and 13 were used. The effect of water vapour on the reactions that occur at the plasma-water interface in various gas treatments (N_2, air, helium) was investigated by introducing a gas flow of 0.3 L/min. In helium treatments, to investigate the effect of different gas flow rates on H_2O_2 production and solution conductivity and pH variation, various gas flow rates of 0.06, 0.1, 0.3, 0.5 and 0.7 L/min were applied. UV spectrometry was employed to measure the H_2O_2 production after 5, 10 and 15 minutes of treatment. A 0.2-M TB was applied to terminate the dimerization of OH

radicals to investigate the H_2O_2 production pathway. The solution conductivity and pH value were measured after each treatment; every treatment was repeated three times.

7.3 Gas discharge characteristics with tap water

7.3.1 Water surface deformation before breakdown

Kawamoto [41] investigated the water surface deformation under pin-to-water electrode discharges in open air and found that the formation of a Taylor-cone on water surface can occur when the applied voltage was lower than the corona threshold (2-3 kV); this phenomenon was also observed in this experiment when using ultrapure water (0.5 µS/cm) instead of tap water. The uplift of water surface led to the connection of water to the anode pin occurring when several hundred volts were applied. This phenomenon could be due to the Coulomb force between the positive ions that assembled at the pin tip and the negative ions that gather at the water surface. Increasing the solution conductivity by using tap water (65 µS/cm) reduced the uplift effect and avoided the connection of water to the pin, although a small uplift of water was still observed. Miao [35] investigated the negative glow discharges above a solution with a conductivity of ~300 µS/cm and also observed a water surface lifting before breakdown.

Therefore in these experiments, tap water with conductivity of 65 µS/cm was used to avoid the connection of water surface to the pin.

7.3.2 Water surface depression after breakdown

Increasing the applied voltage led to the electrical breakdown of the inter-electrode gap. A depression of the water surface, leading to the appearance of a depression zone with a diameter of around 2-3 mm, was observed under positive discharges (Figure 7.2); illuminated plasma was observed to develop to the bottom of the depression region.

The movement of filaments on the water surface was observed at the beginning of discharges and became stable after 5 minutes of treatment; over this time, the diameter of the depression region was reduced to around 1 mm. This could be due to the initial solution conductivity of 65 µS/cm, being relatively low; therefore, the discharge developed more branches to transfer the charges to water surface, causing a relatively larger diameter of the depression region. Increased treatment time significantly increased solution conductivity, leading to the

gathering of the filaments into brighter colour and smaller diameter plasma filaments, which has also been recorded in Kawamoto's study [41].

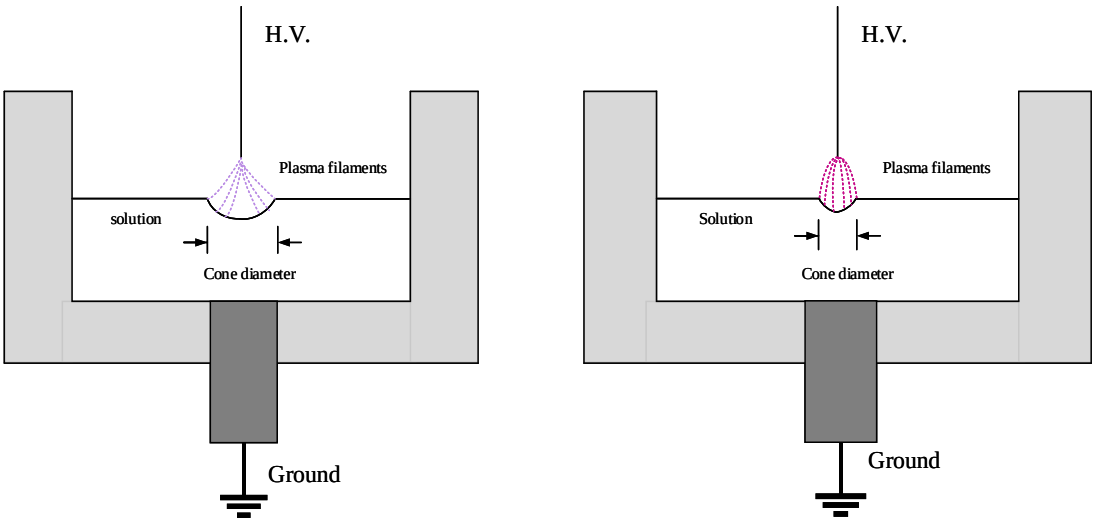

Figure 7.2 Sectional view of the water surface depression after 0 minutes (a) and 5 minutes of treatment (b).

Under negative discharges, the diameter of the depression region (~3-4 mm) on the water surface is slightly larger than that under positive discharges, which has also been recorded in Bruggeman's study [115]. Under negative air discharges, a bright purple spot was observed at the pin tip and followed by a lighter purple cone that developed to the water surface. After 1 minute of treatment the cone angle was decreased, leading to the development of a purple-red streamer column. After 10 minutes of treatment, the diameter of the depression region was reduced to <2 mm, again this is probably due to the increasing of the solution conductivity.

Lu [119] investigated the ignition phase of positive discharges above water and found that the plasma column has several contact points with the water surface; while under negative discharges, this phenomenon was not recorded. Lu explained that the multiple connecting points recorded under positive discharges were due to rippling of the water surface. The mechanisms associated with of these differences need further investigation.

7.3.3 Gas discharge voltage and current

The voltage measured at the pin electrode was 920 V, 1040 V and 690 V in air, N_2 and helium (Table 7.1), respectively, under a positive 3-kV applied voltage; the discharge current was controlled to a value of 3.4 mA by the power supply. The charge transferred to water surface was 3.06 C after 15 minutes of treatment. The lowest onset voltage was observed in helium. The discharge power of 3.13 W, 3.54 W and 2.35 W in air, N_2 and He, respectively, was calculated by equation: $P = V \times I$.

Table 7.1 Pin voltage and discharge power measured under both polarities in various gases.

Gas type	*Polarity*	*Pin voltage (V)*	*Discharge power (W)*
Air	(+)	920	3.13
N_2	(+)	1040	3.54
He	(+)	690	2.35
Air	(−)	-710	2.41
N_2	(−)	-780	2.65
He	(−)	-460	1.56

The pin voltages measured under negative discharges with applied voltage of -3 kV in air, N_2 and helium were -710 V, -780 V and -460 V, respectively; again the discharge current was limited to -3.4 mA by the power supply. The discharge power was 2.41 W, 2.65 W and 1.56 W in air, N_2 and He, respectively.

Under negative discharges, the discharge filaments were much brighter than those observed under positive discharges. The oxidation of the pin tip was observed for negative air discharges; therefore, the needle was replaced after every 3rd test in air. However, this phenomenon did not occur in N_2 and He discharges; this phenomenon may be due to the existence of O_2 in air, leading to the oxidation of metal pin tip during discharges.

7.3.4 Bubble formation

Figure 7.3 (a) shows the formation of gas bubbles, which are believed to be H_2, under positive discharges. The bubbles are of various sizes and are distributed across the bottom of the reactor. Under positive discharge, the H^+ ions at the ground electrode would be neutralized to form H radicals; the dimerization of H radicals would lead to the formation of H_2. The H_2 bubbles were initially gathered on the metal ground electrode, and then spread outwards across the bottom of the reactor.

Figure 7.3 Gas bubble formation under positive discharges (a) and negative discharges (b) after 15 minutes of treatment.

Figure 7.3 (b) shows the gas generated under negative discharges, which is considered to be O_2 in this experiment. The number of bubbles was much smaller compared to that in Figure 7.3 (a). The size of these bubbles was larger and they were observed accumulating on the anode electrode. This may be due to the lower voltage drop at the anode water, leading to less intense of discharges, thus reduced gas bubble formation. In addition, the solubility of O_2 in water is 30 times higher than that of H_2, which may have caused the lower O_2 bubbles production under negative discharges. However, this phenomenon cannot be clarified at this stage; therefore, further research is required.

7.4 Plasma-water interface reactions under positive polarity

7.4.1 Treatments without gas flow

7.4.1.1 H_2O_2 production

The reactor was sealed during treatments with no gas flow introduced. Figure 7.4 shows the H_2O_2 production in various gas treatments, which increased almost linearly with time in air and helium, reaching 9 µmol and 24.2 µmol, respectively, after 15 minutes of treatment.

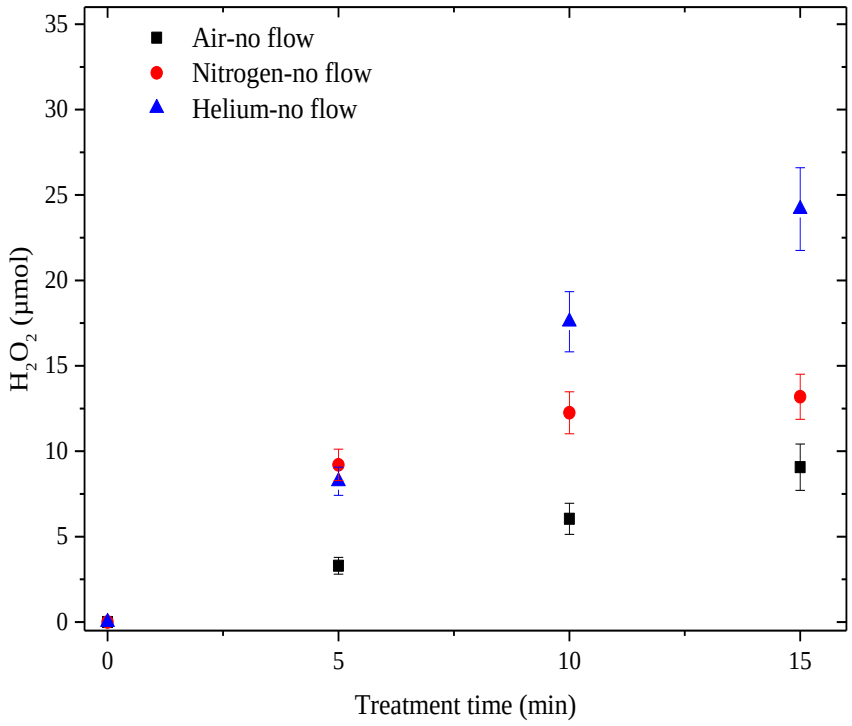

Figure 7.4 H_2O_2 production in air, N_2 and helium treatments without gas flow.

A saturation effect was observed in N_2, the H_2O_2 production reached 13.8 µmol after 15 minutes of treatment. In N_2 discharges, the oxidization of primary nitric species ($N^{\cdot}$, NO) initially occur, leading to the production of oxy-nitride species (Table 2.9). Both nitrite and nitrate acids were detected in N_2 treated samples. The nitrite acid consumed the oxidative reagents in solution, such as OH radical and H_2O_2, to form nitrate acid (R 2.65, R 2.66).

In air treatment, the oxy-nitride species were generated at the beginning of treatments, thus consuming the oxidative species and leading to a lower H_2O_2 production compared to that recorded in other working gases.

Discharges in He yielded the highest H_2O_2 production, which was 2.7 and 1.8 times that in air and N_2, after 15 minutes of treatment. The corresponding charge/H_2O_2 ratio was 1:0.29, 1:0.41 and 1:0.76 in air, N_2 and He, respectively, which is much lower compared to those obtained under positive impulsive current discharges (Chapter 6).

A large amount of water vapour was observed at the plasma-water interface under positive discharges when no gas flow was introduced during treatments (Figure 7.5). The production of water vapour can be caused by: (i) the transferring of energy from positive ions to water molecules or (ii) the resistance effect of water, leading to Joule heat production during discharges.

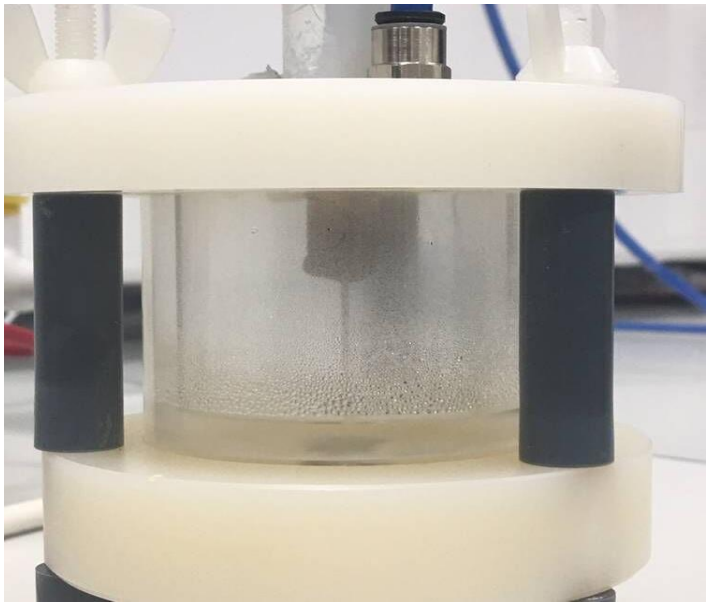

Figure 7.5 The water vapour production under positive discharges in sealed reactor after 15 minutes.

Titov [6] found that the reaction rate constant for high energy electrons depended strongly on the fraction of water molecules present in the discharge region. A significant reduction in the number of high energy electrons was observed when water vapour existed in the inter-electrode gap, and this could result in the reduction of H_2O_2 production in the gas phase. Another possibility for the low H_2O_2 production is that a large amount of oxy-nitride species could be absorbed by water vapour, leading to the consumption of OH radicals and H_2O_2 in solution (Table 2.9). The detailed mechanism of OH radical and H_2O_2 production being affected by water vapour needs further investigation.

To investigate the OH radical dimerization pathway, 0.2-M TB was added to the solution; however, the results recorded in various gases were unexpected as the standard deviation of H_2O_2 production reached up to 70% based on 3 treatments under the same experimental conditions, thus the data is not shown here. This result may be due to the effect of the vaporization of water introducing TB into the inter-electrode gap during discharges. Therefore, a gas flow was introduced to remove the water vapour from the reactor and the results are discussed in section 7.4.2.

7.4.1.2 Variation of solution conductivity and pH

Significant solution conductivity increase was observed in air treatments, reaching 1971 µS/cm after 15 minutes of treatment. This result is 46% higher than that observed in N_2 (Figure 7.6), where the solution conductivity increased to 1068 µS/cm after 15 minutes of treatment. These results could be due to the large amount of oxy-nitride species generated at the plasma-water interface during above water discharges in air and N_2 (Table 2.9).

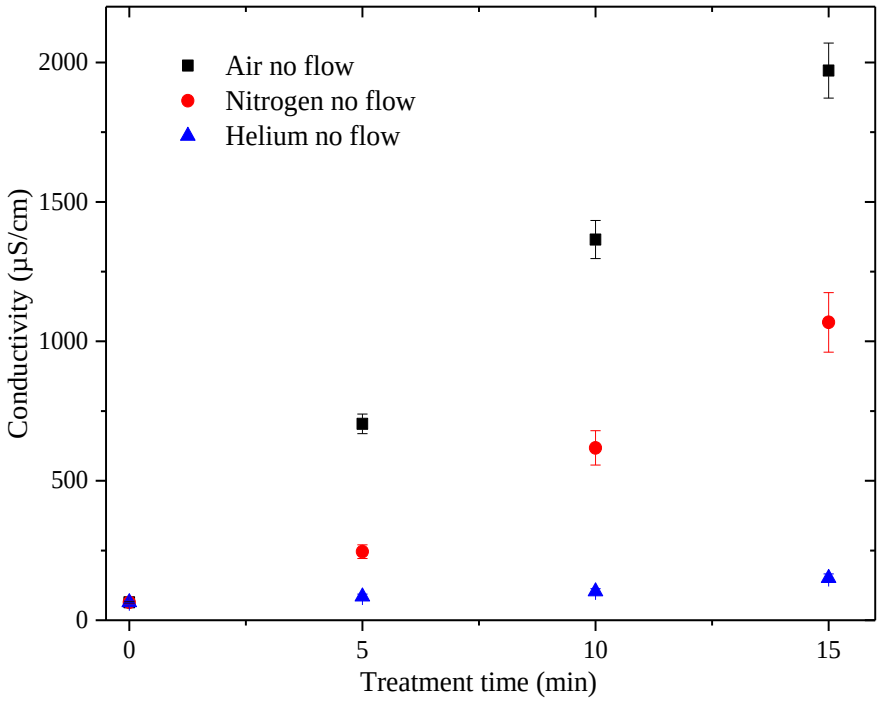

Figure 7.6 Variation of solution conductivity in air, N_2 and helium treatments without gas flow.

In N_2 discharges, a small amount of O_2 could be produced by the electrolysis of water; however, the quantity of O_2 produced would be much lower than that in air. Thus, the

solution conductivity increase in N_2 was lower than that in air. In air-treated samples, only nitrate acid was detected; however, in N_2-treated samples, both nitrite and nitrate ions were detected, this could again be due to the much less O_2 content in N_2 discharges, compared to that in air discharges. The solution conductivity increases to 152 µS/cm in helium-treated samples after 15 minutes of treatment; neither nitrite nor nitrate acid was detected.

The pH of the solutions drop from 8.5 to 2.46 in air and to 2.73 in N_2, after 15 minutes of treatment (Figure 7.7). Table 7.2 shows the H^+ ion production during the tests using the three gasses. In air discharges, a higher value of H^+ ion production occurs in the order of several tens of µmol was recorded in N_2 and helium discharges. The corresponding charge/H^+ ratio was calculated as 1:1.1 and 1:0.58 in air and N_2, respectively.

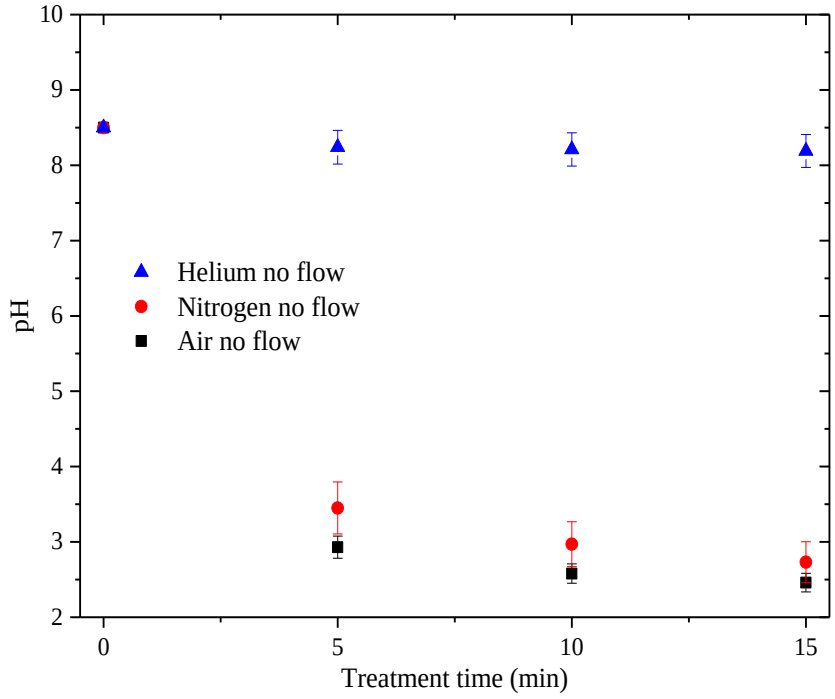

Figure 7.7 Variation of solution pH in air, N_2 and helium treatments without gas flow.

A slight pH reduction (< ±0.2) was recorded in He discharges, and this could be attributed to the weak acidic effect from H_2O_2. The large amounts of water vapour generation in the sealed reactor, when no gas flow was introduced during treatments, can absorb the oxy-nitride species that generated at the plasma-water interface, leading to the production of nitrite and nitrate acids in solutions; this explain the dramatic variation of solution conductivity and pH in air and N_2. However, due to no oxy-nitride species can be generated

in He discharges, the water vapour effect on solution conductivity change in helium is very limited.

Table 7.2 H^+ ion production over 5-minute intervals, in various gas treatments under positive discharges, with no gas flow.

Treatment period (min)	*H^+ ions production (µmol)*		
	Air	*N_2*	*Helium*
0-5	12.8	3.5	-6.5×10^{-6}
5-10	13.2	7.2	10×10^{-6}
10-15	10.9	7.9	12×10^{-6}

7.4.2 Treatments with 0.3 L/min gas flow

7.4.2.1 H_2O_2 production

A 0.3-L/min gas flow was introduced continuously through the reactor during tests with the three gases, in an attempt to remove the majority of the water vapour, and therefore minimize the effect of water vapour on the plasma and plasma-water interface reactions. Results recorded under this condition are shown in Figure 7.8, which significantly differ from those recorded under no-gas-flow treatments. One of the possibilities is that the introduced gas flow removes the majority of the water vapour that is generated at the plasma-water interface, thus reducing the water vapour effect on decreasing high energy electrons, leading to a higher H_2O_2 production. The other possibility is that the absorption of oxy-nitride species is significantly weakened when the majority of water vapour is removed, thus reducing the oxy-nitrides effect on H_2O_2 production.

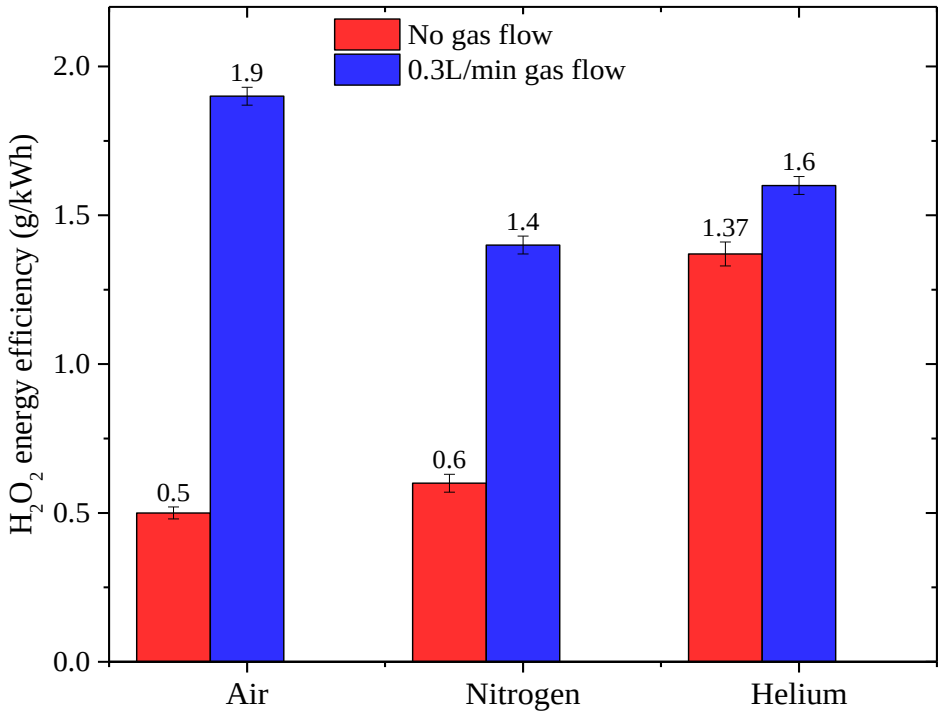

Figure 7.8 H_2O_2 production in air, N_2 and helium treatments, with a 0.3-L/min gas flow.

The highest H_2O_2 production of 34.2 µmol was recorded in air after 15 minutes of treatment, corresponding to a charge/H_2O_2 ratio of 1:1.03 and H_2O_2 production yield of 1.9 g/kWh. No slowdown in the rate of H_2O_2 production was observed in N_2, different from the results

observed under no-gas-flow condition; a H_2O_2 production of 32 µmol was recorded after 15 minutes of treatment; corresponding to a charge/H_2O_2 ratio of 1:1 and the H_2O_2 production yield of 1.4 g/kWh. The lowest H_2O_2 production of 28.2 µmol was obtained in He treatment, corresponding to the charge/H_2O_2 ratio of 1:0.89 and H_2O_2 production yield of 1.6 g/kWh. Introducing a gas flow during treatments increased the H_2O_2 production by 270%, 140% and 20% in air, N_2 and helium, respectively.

Tert-butanol effect

0.2-M TB was added to samples to investigate the H_2O_2 production pathway. The H_2O_2 produced in air discharges was observed to increase linearly with time. Figure 7.9 illustrates that the H_2O_2 production in air discharges reached 17.2 µmol after 15 minutes of treatment, approaching only 52% of the results that were recorded when no TB was used; the charge/H_2O_2 ratio was reduced to 1:0.54.

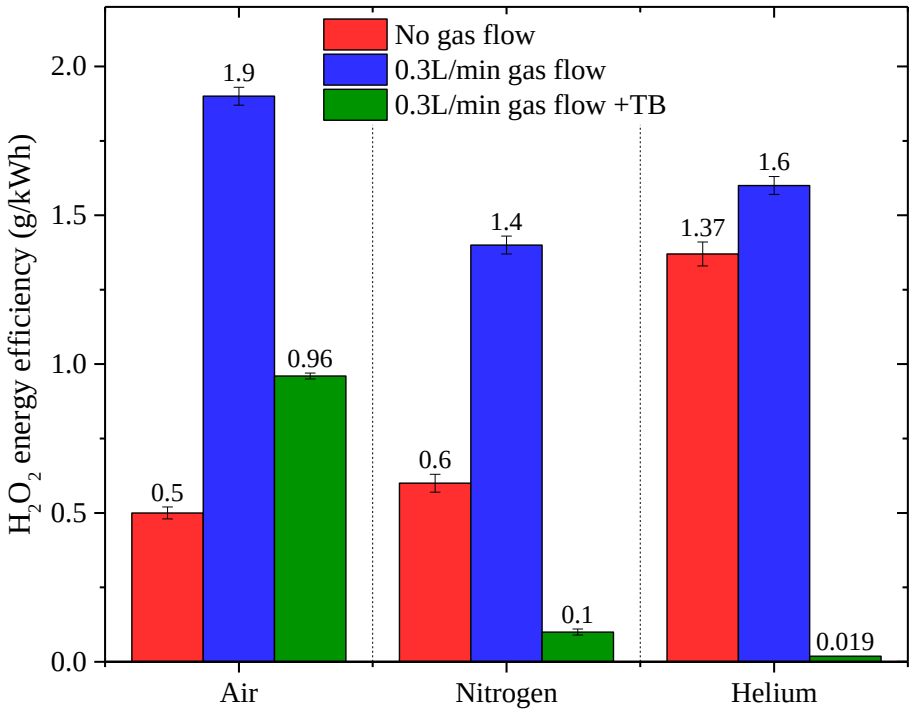

Figure 7.9 Effect of TB on H_2O_2 production in air, N_2 and helium treatments, with a 0.3-L/min gas flow.

In addition, the H_2O_2 production was significantly inhibited in N_2 and helium treatments when TB was used. 2.2 µmol and 0.2 µmol of H_2O_2, respectively, were detected after 15

minutes of treatment; corresponding to a charge/H_2O_2 ratio of 1:0.07 and 1:0. In comparison with the results without TB, it can be concluded that 48%, 93% and 99.3% of the H_2O_2 production in air, N_2 and helium, respectively, was via the dimerization of OH radicals.

7.4.2.2 Variation of solution conductivity and pH

Figure 7.10 shows the variation of solution conductivity for the three gases when a 0.3-L/min gas flow was introduced. In air and N_2 treatments, the solution conductivity increased linearly with time, reaching 800 and 292 µS/cm, respectively, after 15 minutes of treatment; this was approaching 60% and 73% lower than the results recorded under no-gas-flow condition. These results indicate that when gas flow was introduced during discharges and the majority of the water vapour was carried away, less oxy-nitride species were absorbed by water vapour at the plasma-water interface. In helium treatments, a slight conductivity variation from 65 to 71 µS/cm was recorded after 15 minutes of treatment. Sano [103] investigated the DC corona discharges above water and found that the introduction of gas flow during treatments minimized the NO_x production in the gas phase, which is in agreement with the results found in this experiment.

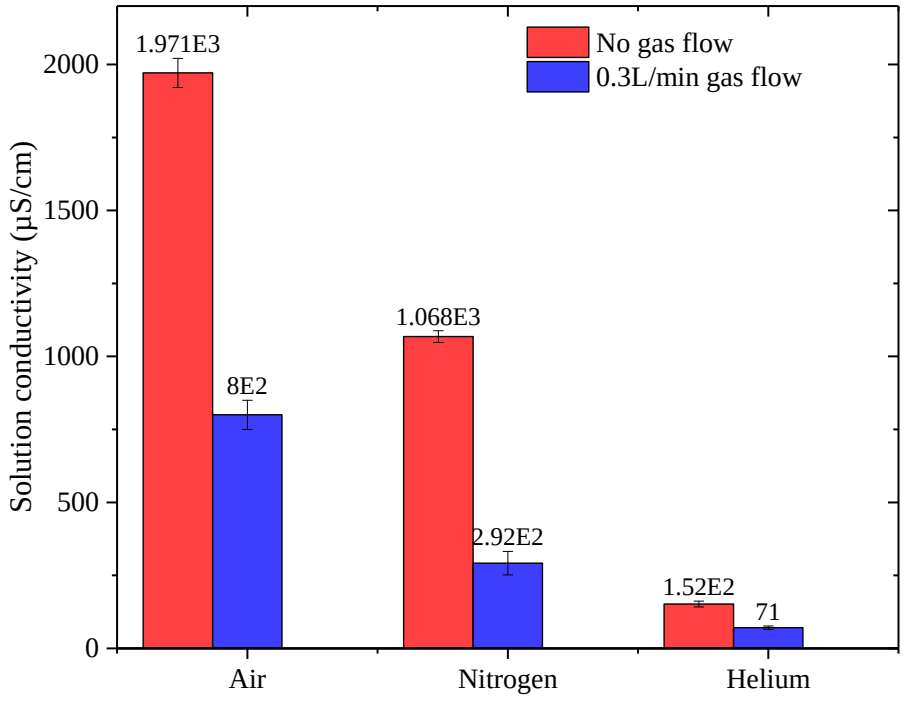

Figure 7.10 Variation of solution conductivity in air, N_2 and helium treatments, with a 0.3-L/min gas flow.

Table 7.3 shows the H^+ ions production in the tests with discharges in the three gasses, when a gas flow of 0.3 L/min was introduced during treatments. Compared to the results recorded under no-gas-flow condition, the H^+ ions production was reduced by 66% and 81% in air and N_2 discharges, respectively.

Table 7.3 H^+ ions production over 5-minute intervals, in various gas treatments under positive discharges, with a gas flow of 0.3-L/min.

Treatment period (min)	*H^+ ions production (µmol)*		
	Air	*N_2*	*Helium*
0-5	4.4	1.1	18.5×10^{-6}
5-10	4.3	1.4	6×10^{-6}
10-15	5.4	1.5	1.3×10^{-6}

Figure 7.11 shows the solution pH variation when a gas flow of 0.3 L/min was introduced during discharges. Almost no solution pH reduction was recorded in helium, while the solution pH reduced to 2.9 and 3.4 in air and N_2, respectively.

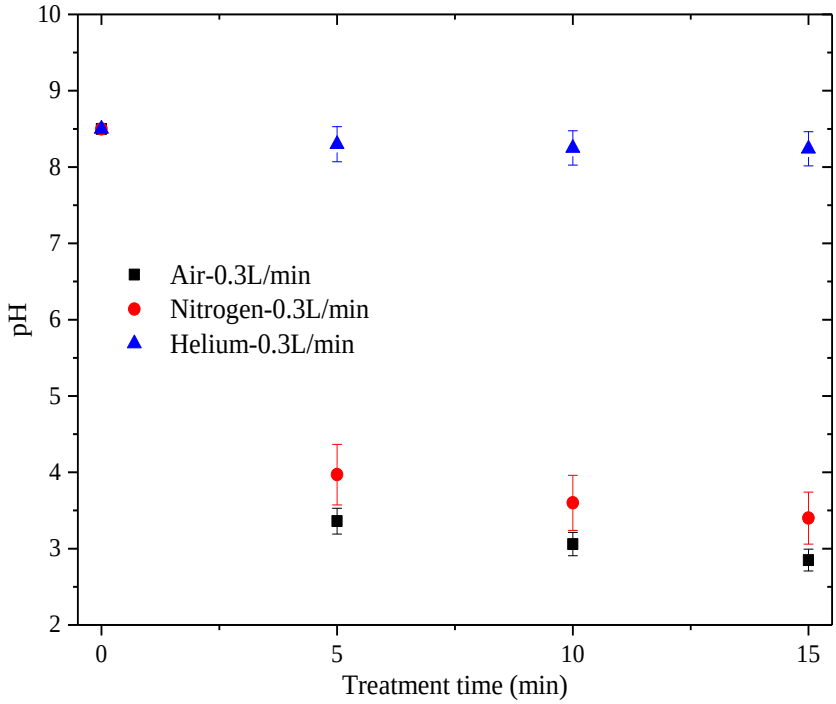

Figure 7.11 Variation of solution pH in air, N_2 and helium treatments, with a 0.3-L/min gas flow.

Tert-butanol effect

Figure 7.12 shows the variation of solution conductivity when TB was present in the water. In air tests, the change of solution conductivity was reduced by 40% compared to the results with no TB, reaching 483 µmol 15 minutes of treatment. Almost no solution conductivity variation was observed in N_2 after 15 minutes of treatment; this phenomenon was also recorded under positive controlled impulsive current discharges (Chapter 6).

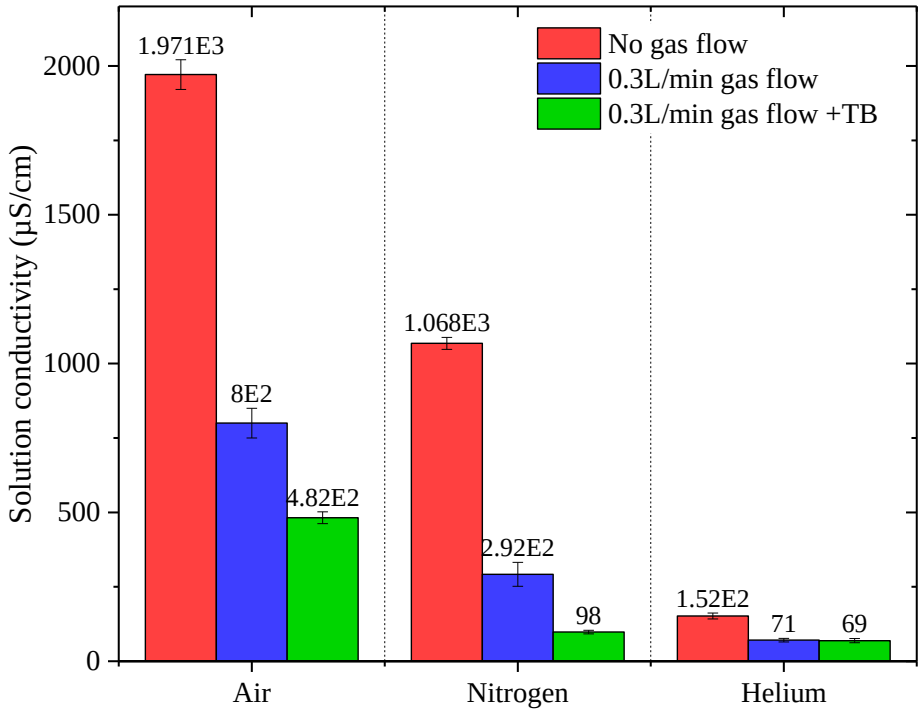

Figure 7.12 Effect of TB on solution conductivity variation in air, N_2 and helium treatments, with a 0.3-L/min gas flow.

The H^+ ions production (Table 7.4) was reduced by 4 orders of magnitude when TB was used in N_2 treatments. This result might be due to the TB vapour in the reactor chamber reducing the amount of oxide species production, thus reducing the oxy-nitride amounts that dissolved into water.

Table 7.4 Effect of TB on H^+ ions production over 5-minute intervals, in various gas treatments, with a 0.3-L/min gas flow.

Time (min)	*H^+ ions production (µmol)*		
	Air	*N_2*	*Helium*
0-5	2.6	30×10^{-6}	3.9×10^{-6}
5-10	2.9	25×10^{-6}	1.7×10^{-6}
10-15	2.4	30×10^{-6}	2.7×10^{-6}

Figure 7.13 shows the solution pH variation when a gas flow of 0.3 L/min was introduced during discharges above the solution with TB. Compared to that recorded in Figure 7.11, almost no difference is recorded in He and air; however, the solution pH reduction in N_2 is inhibited by the added TB.

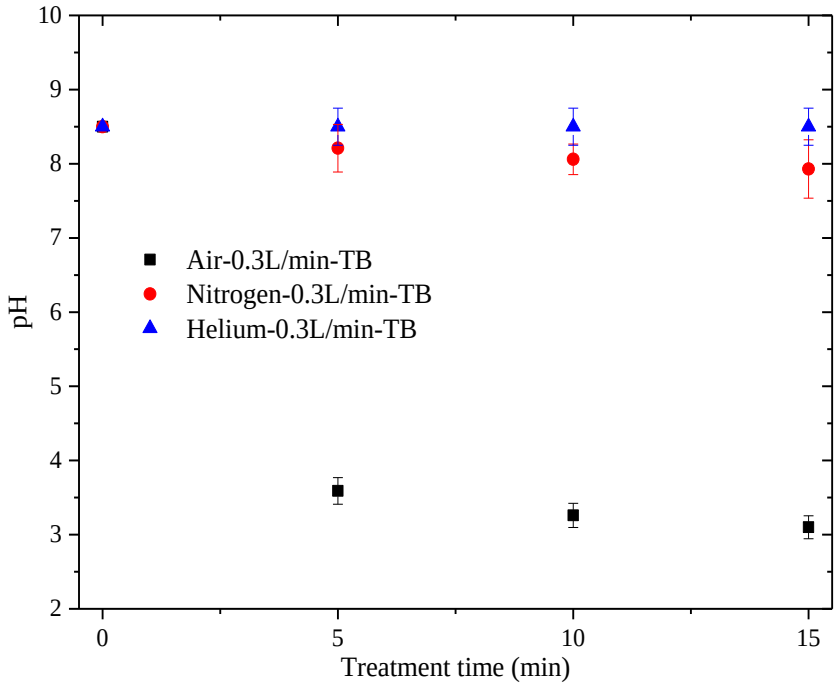

Figure 7.13 Effect of TB on solution pH variation in air, N_2 and helium treatments, with a 0.3-L/min gas flow.

7.4.3 Effect of gas flow rates in helium discharges

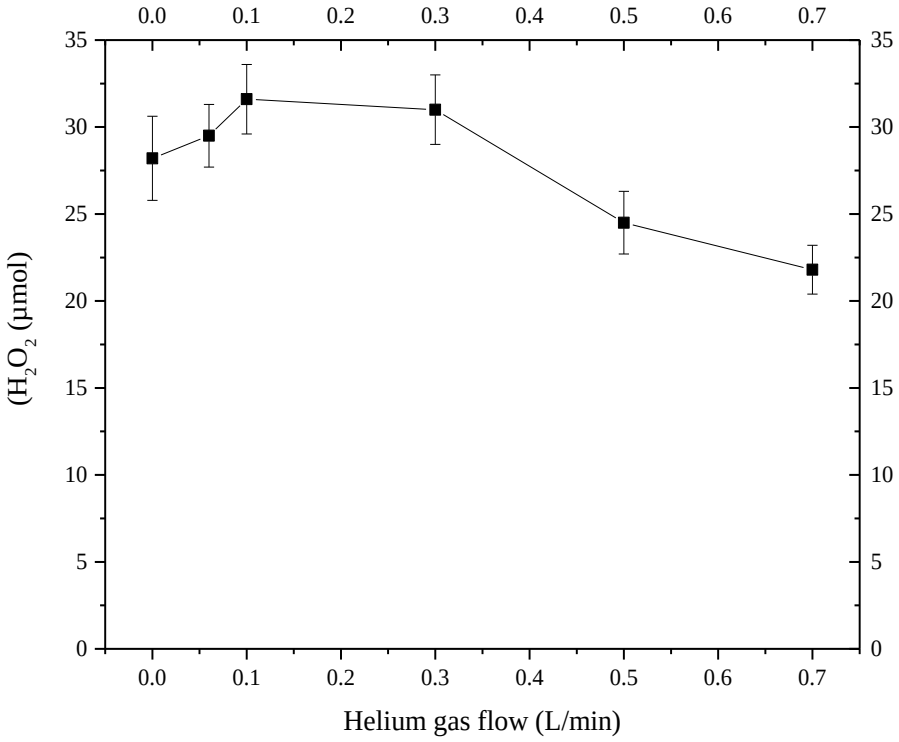

Figure 7.14 Under positive polarity, the H_2O_2 production in helium treatments, with different gas flow rates.

Different gas flow rates were introduced in helium treatments to investigate their effects on H_2O_2 production (Figure 7.14). When a gas flow rate of 0.06 L/min was introduced, a large amount of water vapour was observed in the chamber (Figure 7.15 (a)) after 15 minutes of treatment; the H_2O_2 production reached 29.5 µmol, corresponding to a charge/H_2O_2 ratio of 1:0.79.

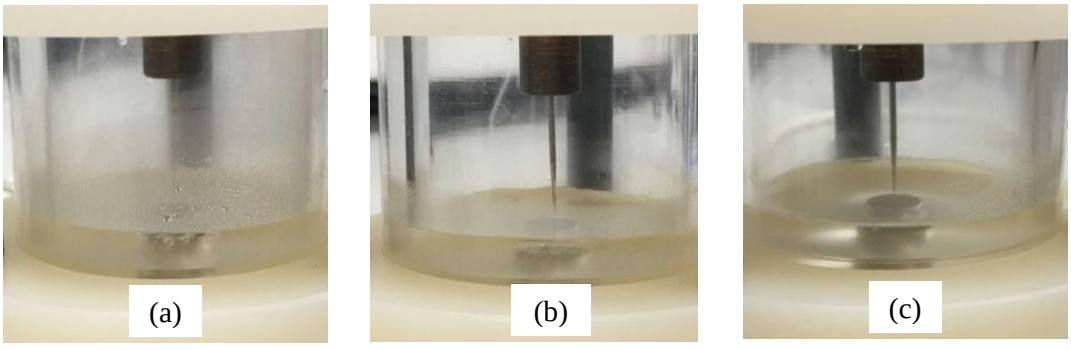

Figure 7.15 Under positive polarity, water vapour generated in the reactor chamber with gas flow rates of 0.1-L/min (a), 0.5-L/min (b) and 0.7-L/min (c), after 15 minutes of treatment.

Increasing the gas flow to 0.1 and 0.3 L/min led to an increase in H_2O_2 production of 31.6 µmol and 31 µmol after 15 minutes of treatment, corresponding to a charge/H_2O_2 ratio of and 1:0.85 and 1:0.89. Further increase of the flow rate to 0.5 L/min resulted in a reduction of water vapour in the reactor chamber (Figure 7.15 (b)); however, this reduced the H_2O_2 production to 24.5 µmol after 15 minutes of treatment, corresponding to a charge/H_2O_2 ratio of 1:0.69. When a gas flow of 0.7 L/min was introduced, almost no water vapour was observed (Figure 7.15 (c)) after 15 minutes of treatment, the H_2O_2 production reached 21.8 µmol, which corresponded to a charge/H_2O_2 ratio of 1:0.63.

It has been proven, by using tert-butanol, that the H_2O_2 production in helium discharges was generated from the dimerization of OH radicals, which may partly be formed in water vapour. The introduction of relatively higher flow rates (0.5-0.7 L/min), removing the majority of water vapour, therefore, led to the lower H_2O_2 productions compared to the ones with relatively lower flow rates (0.06-0.3 L/min). The maximum H_2O_2 production was achieved when 0.1 L/min gas flow was introduced. It is believed that the H_2O_2 production in above-water discharges is generated in both gas phase and liquid phase. To clarify the mechanisms of water vapour effect on H_2O_2 production, further investigations are required.

Tert-butanol effect

When TB was added in solution, almost no H_2O_2 was detected under the gas flow rates of 0.06 and 0.1 L/min, this may be due to the TB being vaporized with the water molecules, inhibiting the production of OH radicals in the gas phase. Increasing the gas flow rate to 0.3 and 0.5 L/min enhanced the quantity of H_2O_2, which was 0.2 and 1.3 μmol, respectively, after 15 minutes of treatment; corresponding to 0.7% and 4% of the H_2O_2 production when no TB was applied. When a gas flow of 0.7 L/min was introduced during treatments, the H_2O_2 quantity increased to 5.1 μmol, corresponding to 27% of the original value.

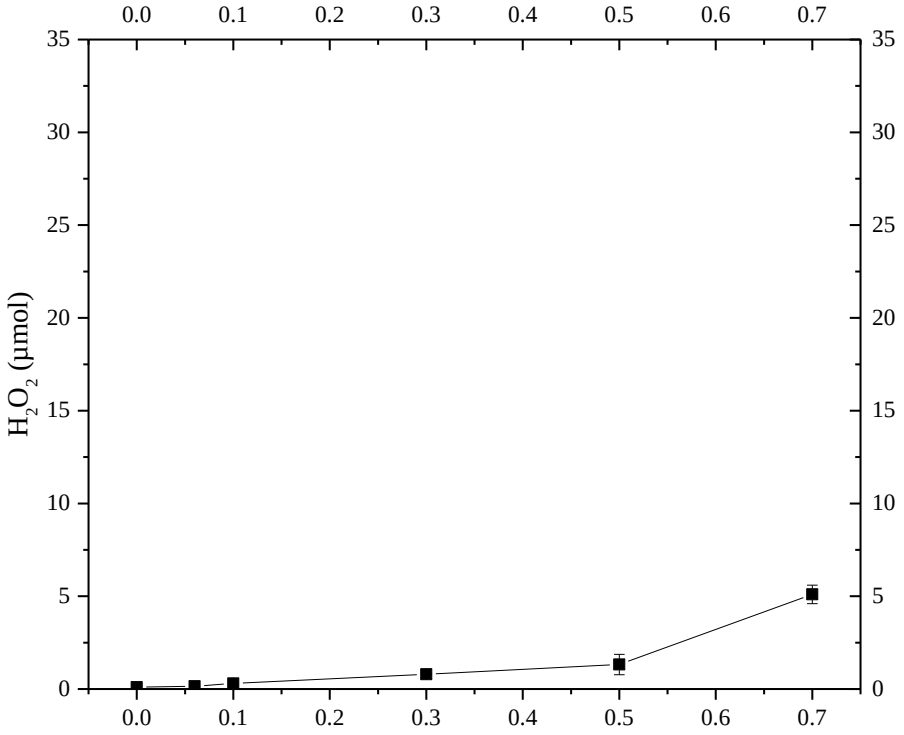

Figure 7.16 Effect of 0.2-M TB on H_2O_2 production in helium discharges with different gas flow rates.

It was found that the increased gas flow increased the H_2O_2 quantity in the solution when TB was applied. The quantity of H_2O_2 that detected in solution after treatments could be generated from the OH radicals that are generated in the gas phase. The introduced gas with higher flow rate (0.3-0.7 L/min) remove the water vapour and the vaporized tert-butanol, thus reducing the TB scavenging effect on OH radicals in the gas phase.

7.4.4 Effect of solution initial pH in air discharges

Figure 7.17 shows the effect of solution initial pH on H_2O_2 production. In acid solutions of pH 4 and 3.2, the H_2O_2 production increased linearly with time, reaching 29 µmol and 22 µmol after 15 minutes of treatment, respectively; corresponding to charge/H_2O_2 ratios of 1:0.9 and 1:0.7. These results corresponded to 11% and 32% reduction of the H_2O_2 production compared to those recorded in air treatments with tap water. Cerfalvi [118] investigated positive pin-to-water electrode discharges and found that the cathode voltage fall was almost constant at ~800 V in the solutions with pH of 4-8, and the voltage started to decrease when solutions with pH of <4 were used, which is in agreement with the results recorded in this experiment.

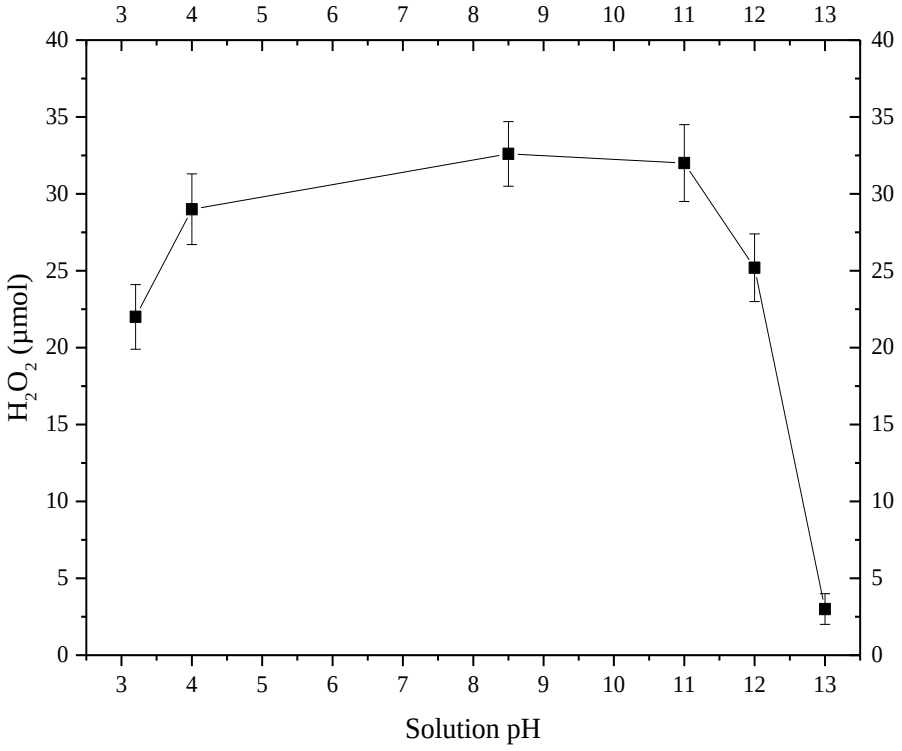

Figure 7.17 Under positive polarity, the effect of solution initial pH on H_2O_2 production in air discharges, with a 0.3 L/min gas flow.

On the other hand, almost no difference between tap water (pH 8.5) and slight basic solution of pH 11 was observed. However, the H_2O_2 production was reduced in pH 12 solutions; reaching 25 µmol after 15 minutes of treatment, corresponding to a charge/H_2O_2 ratio of 1:0.8. Further increasing the solution pH to 13 leads to a significant reduction of the H_2O_2 production; only 3.2 µmol H_2O_2 was detected after 15 minutes of treatment.

Thagard [4] investigated the discharges with H_3PO_4 and NaOH solutions and found that the H_2O_2 production in acid solutions increased with lower pH, reaching the highest rate at pH 3, which is different to the results obtained in this experiment. On the other hand, Thagard found that the H_2O_2 production in basic solutions decreased with higher solution pH, the H_2O_2 production in solution of pH 13 is only 30% of that in solution of pH 9. In this experiment, no significant change was observed when the pH was changed from 8.5 to 11 (Figure 7.17); however, the H_2O_2 production in solution of pH 13 is only 10% of that in solution of pH 8.5.

7.5 Plasma-water interface reactions under negative polarity

7.5.1 H_2O_2 production

When no gas flow was introduced during various gas treatments, the water vapour generated under negative DC voltage was much less than that recorded under positive polarity. This indicates that the water vapour generated under positive discharges could be due to the energy transfer from positive ions to water molecules.

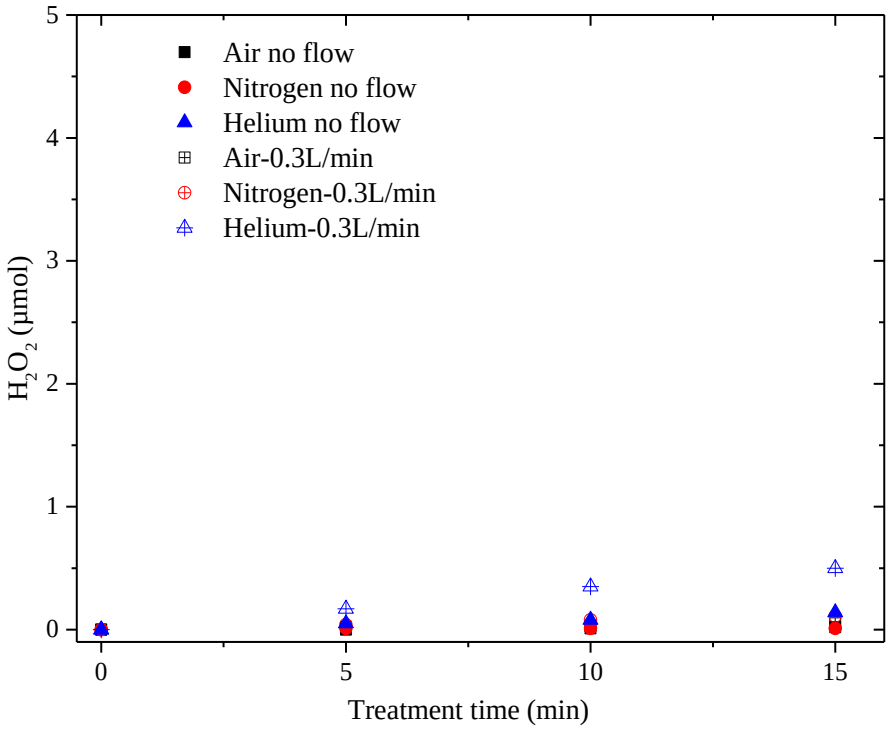

Figure 7.18 H_2O_2 production under negative discharges in air, N_2 and helium with and without gas flow.

A 0.3-L/min gas flow was introduced to blow away the majority of water vapour. No H_2O_2 production was detected under negative discharges in air and N_2 with or without gas flow (Figure 7.18). A H_2O_2 production of 0.5 µmol was measured in helium after 15 minutes of treatment. The results obtained under negative DC discharges in air are in agreement with Polyakov's research [78], where negative DC discharges were used and neither H_2O_2 nor reactive radicals were measured after treatment.

7.5.2 Variation of solution conductivity and pH

Although no H_2O_2 was detected in air and N_2 under negative discharges, significant variations of solution conductivity were recorded. The solution conductivity reached 187 and 554 µS/cm in air, 125 and 225 µS/cm in N_2 after 15 minutes of treatment, with and without the 0.3-L/min gas flow, respectively (Figure 7.19). Both nitrite and nitrate acids were detected in air-treated samples, by using test strips, which was different from the results recorded under positive discharges. The variation of solution conductivity, under negative discharges, was reduced by ~78% in air and N_2, compared to those recorded under positive discharges. No solution conductivity change was obtained in helium under negative DC glow discharges, which is the same as the results recorded in negative impulsive current discharges (Chapter 6).

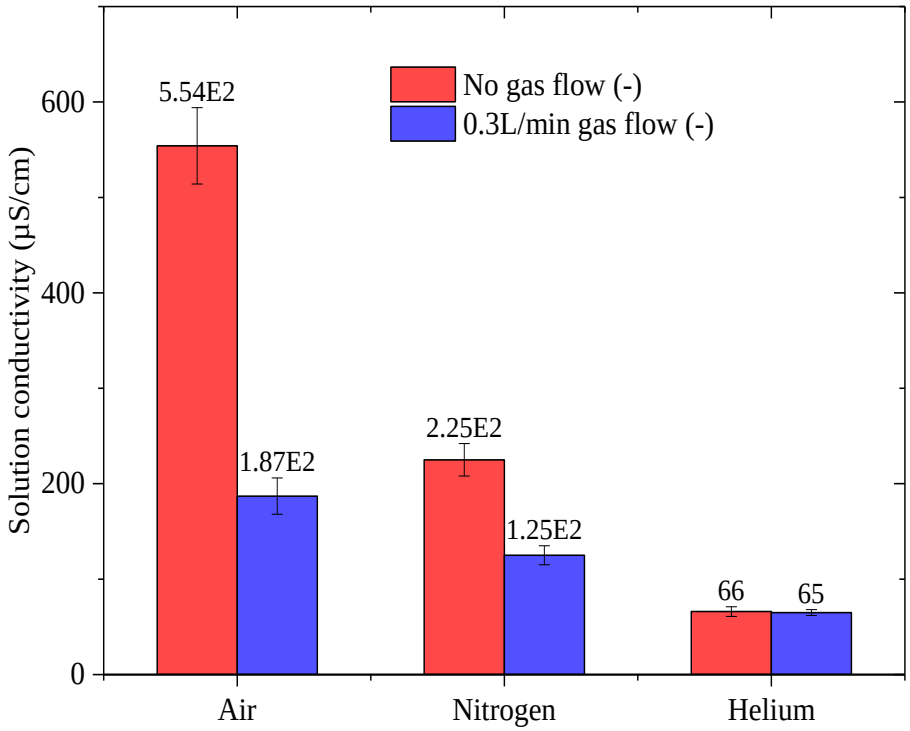

Figure 7.19 Variation of solution conductivity under negative discharges in air, N_2 and helium with and without gas flow.

Figure 7.20 shows the solution pH variation under negative discharges in various gases. Introducing a 0.3 L/min gas flow reduced the production rate of H^+ ions in the air and N_2, the solution pH decreased from 8.5 to 4.2 and 3.3 in the air; to 4.8 and 4.2 in N_2 after 15 minutes of treatment with and without gas flow, respectively. The solution pH in helium-treated samples decreased with time when no gas flow was introduced; however, increased to pH 9.5 when a gas flow of 0.3 L/min was introduced; this phenomenon needs further investigation.

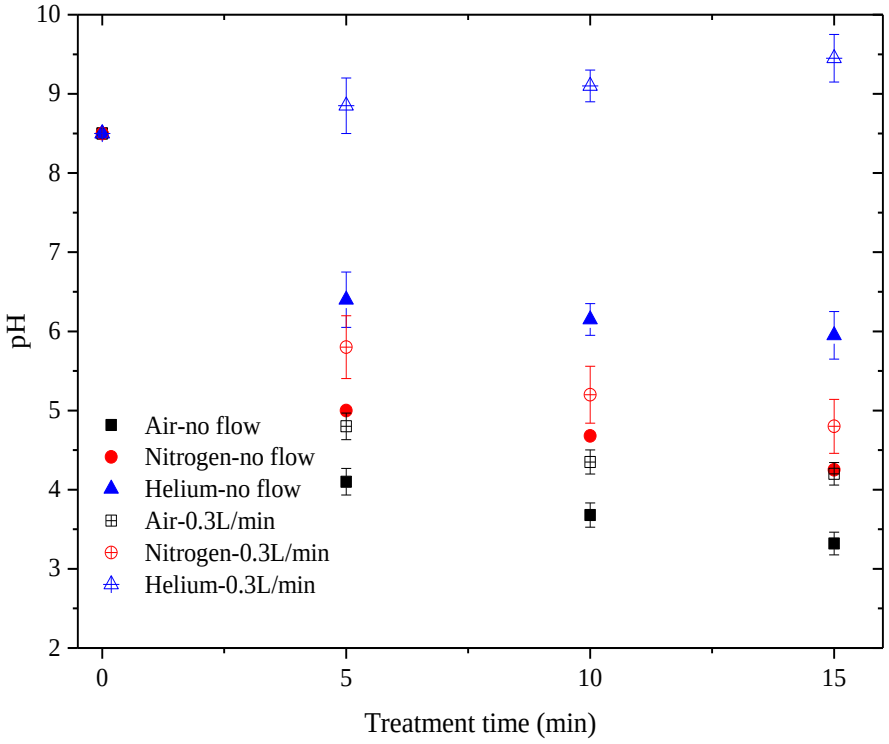

Figure 7.20 Variation of solution pH under negative discharges in air, N_2 and helium with and without gas flow.

7.6 Conclusions

The characteristics of pin-to-water DC glow discharges under different polarities and solution conductivity were investigated in this experiment. When ultrapure water was used, a Taylor cone was formed on water surface, leading to the contacting of water surface to the anode pin due to the electrostatic force; increasing the solution conductivity by using tap water solved this problem. The depression of the tap-water surface was observed under both positive and negative DC glow discharges. The constrictions of the plasma column with increasing solution conductivity were observed under both positive and negative discharges.

Under positive discharges, when no gas flow was introduced, a significant amount of water vapour was produced at the plasma-water interface, due to the energy transfer from positive ions to water molecule. Large amounts of oxy-nitride were absorbed by water vapour in this case, resulting in dramatic variations of solution conductivity and pH, leading to the consumption of OH radicals and destruction of H_2O_2 production. The introduction of a 0.3-L/min gas flow increased the H_2O_2 production yield by 270%, 40% and 20% in air, N_2 and helium, respectively, reaching 1.9, 1.4 and 1.6 g/kWh; also weakened the solution conductivity variation. The highest charge/H_2O_2 ratio of 1:1.03 and the lowest ratio of 1:0.88 were recorded in air and helium discharges, respectively. The applied TB determines that 48%, 93% and 99.3% of H_2O_2 production in air, N_2 and helium, respectively, was via OH dimerization.

Under positive helium discharges, the H_2O_2 production varied with different gas flow rates, indicating that H_2O_2 is generated in both gas and liquid phase. The highest production of 1.65 g/kWh was recorded with a gas flow of 0.1 L/min. Under positive air discharges, H_2O_2 production could be affected by initial solution pH. In acid solutions of pH 4 and 3.2, the H_2O_2 production reduced with lower solution pH. On the other hand, the concentration of OH^- ions has a critical effect on H_2O_2 production; no effect was observed in solutions of pH 11; however, almost no H_2O_2 production was detected in solutions of pH 13.

Under negative DC glow discharges, almost no H_2O_2 production was observed in various gas treatments, which was the same as the results recorded under negative impulsive current discharges. This result indicates the effect of electrons on H_2O_2 production is negligible. The variations of solution conductivity were reduced by 78% under negative air and N_2 discharges. Although no variation of solution conductivity was recorded in helium

discharges, an increase of pH was recorded when 0.3 L/min gas flow was introduced during treatment.

7.7 Further work

The ignition phase of inter-electrode breakdown need to be further investigated, image data should be provided by ICCD camera. The mechanisms of gas bubble generation should be further investigated, the gas types were assumed to be H_2 and O_2 from electrolytic principles, however, the gas types still need to be determined; also, the video of the gas bubble generation process needs to be recorded by a camera.

The effect of gas flow rates needs to be further investigated to observe the variation of H_2O_2 production in various gases. Although it has been proven that H_2O_2 is generated in both gas and liquid phase, the proportional relation is still unclear. Therefore, further research should focus on this issue. The optical spectrum of discharges in various gases above water can be measured to obtain the differing production generated at the plasma-water interface. On the other hand, the mechanism of the phenomenon of the slight increase in solution pH detected in helium-treated samples when the gas flow was introduced should be further investigated.

8 H_2O_2 PRODUCTION UNDER DC GLOW DISCHARGES WITH A FLOWING LIQUID CATHODE

8.1 Introduction

In practical water treatment systems the water itself must move, therefore, there is an interest in the effect of a flowing liquid cathode on H_2O_2 production. A series of studies have investigated the effect of a flowing liquid cathode on reactive species production and solution conductivity and pH variation [34, 120]. However, the results obtained in these studies showed with considerable discrepancy. Jamro'z [3] investigated the discharges with a flowing liquid cathode and found that the H_2O_2 production decreased with increasing liquid flow rate; Jamro'z concluded that this was due to the decreasing contact time of plasma with the same area of water surface. On the other hand, Grabowski [95] found that the O_3 dissolution into liquid was 23% faster when a liquid flow rate of 0.3 L/min was used during treatments; thus, concluding that this was due to the flowing liquid making it easier for O_3 to be transferred into liquid. Due to reactions R 2.50 and R 2.52, the dissolved O_3 in water leads to the production of OH radicals, thus increasing the H_2O_2 production. In order to clarify the effect of a flowing liquid electrode on the plasma-water interface reactions and H_2O_2 production, a reactor with flowing liquid electrode was designed; positive DC glow discharges were investigated in open air as this had been shown to be effective in generating H_2O_2 in Chapter 7.

The main objectives of the experiment were to investigate: (i) the effect of liquid flow rates on H_2O_2 production yield and charge/H_2O_2 ratio; (ii) the applied voltage effect on H_2O_2 production yield and charge/H_2O_2 ratio; (iii) the H_2O_2 formation pathway by using a scavenger of OH radicals.

8.2 Reactor design and experimental setup

8.2.1 Reactor design

A reactor with a pin-to-flowing water electrode structure (Figure 8.1) was designed in this experiment. The liquid flowing through the trough (Figure 8.2), with a length of 45 mm, width of 10 mm and depth of 15 mm, with various rates of 35, 60 and 75 ml/min. A stainless-steel electrode with a diameter of 8 mm acts as a ground electrode. The liquid was inlet and outlet through the 5-mm diameter ports on the bottom of the reactor (Figure 8.2 (a)).

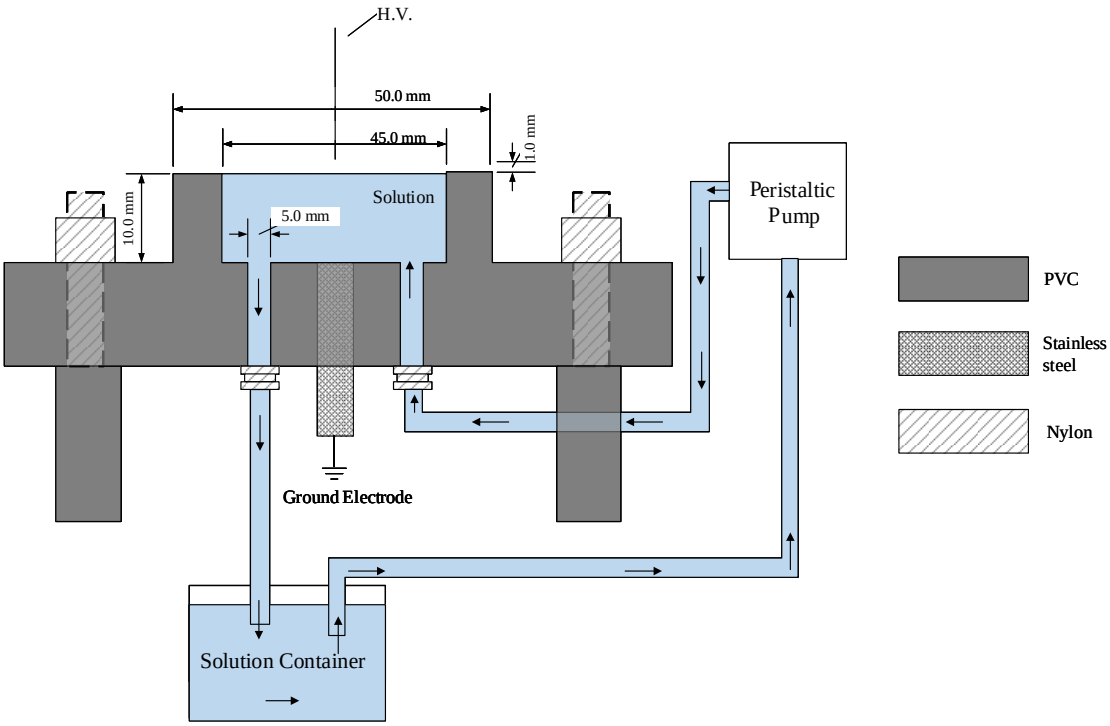

Figure 8.1 Reactor design and solution recycling system.

A peristaltic pump was employed to control the liquid flow rate, which not only reduced the local high concentration of reactive species and oxy-nitride species effect, but also prevented local heating of water, thus minimizing water evaporation [34]. A water container of 30-ml volume was placed under the reactor to collect the solution flowing out of the reactor, and enable the circulation of solutions during treatments. The solution outlet from the peristaltic pump was fixed at the same level as the reactor top surface to maintain the water surface level. A stainless-steel pin with a tip diameter of 0.3 mm was fixed 1 mm above the centre of the water surface.

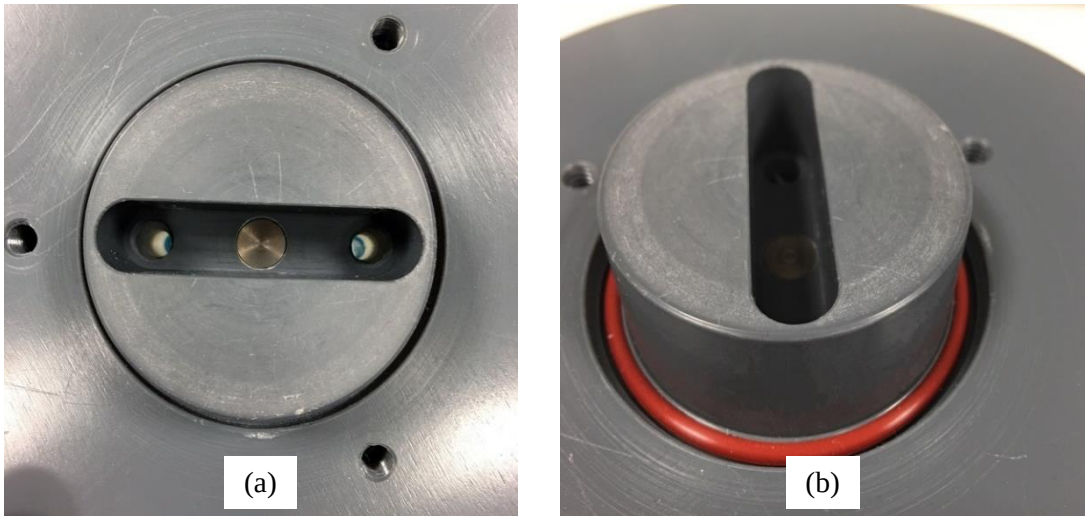

Figure 8.2 Structure of the reactor with flow liquid electrode, vertical view (a), 45 degrees vertical view (b).

8.2.2 Experimental set up

A 200-kΩ current limiting resistor was connected in series with the high voltage pin electrode (Figure 8.3); positive DC discharges were investigated in this experiment. The current output of the supply was set to two values: 3.4 mA and 5 mA in an attempt to investigate the current effect on plasma-water interface reactions; the output voltage was adjusted so that the set current flowed in circuit.

The samples were prepared from tap water with a conductivity of 65 µS/cm. A solution of 20-ml volume was used during each treatment. UV spectrometry was employed to measure the H_2O_2 production after 5, 10 and 15 minutes of treatment. TB was applied to terminate the dimerization of OH radicals to investigate the H_2O_2 production pathway. The solution conductivity and pH value were measured after each treatment; every treatment was repeated three times.

The pin voltage was measured as 920 V for the 3.4 mA current with the power supply voltage of 3 kV and 830V for the 5 mA current with the power supply voltage of 4 kV.

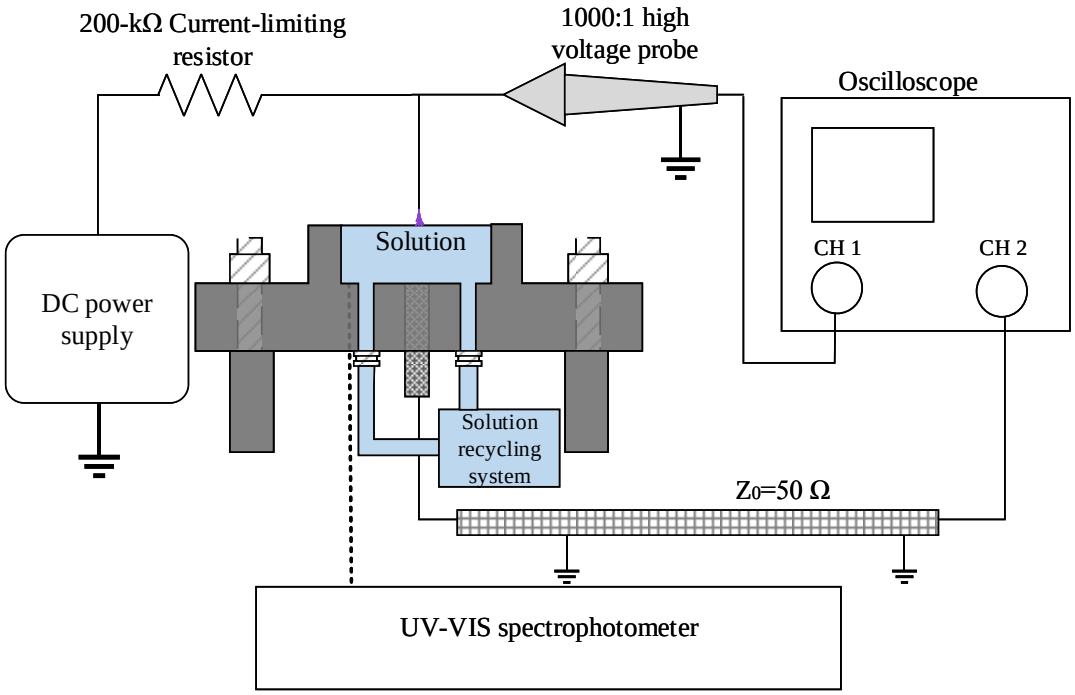

Figure 8.3 Schematic diagram for DC glow discharge experiments with a flowing liquid electrode.

8.3 Plasma-water interface reactions with flowing cathode

8.3.1 H_2O_2 production

Figure 8.4 shows the H_2O_2 production under discharge current of 3.4 mA with different liquid flow rates, which reached 14.2 µmol, 14.5 µmol and 14.8 µmol with 35, 60 and 75 ml/min of liquid flow rate, respectively, after 5 minutes of treatment; corresponding to the H_2O_2 production yield of 1.9 g/kWh, 1.92 g/kWh and 1.95 g/kWh.

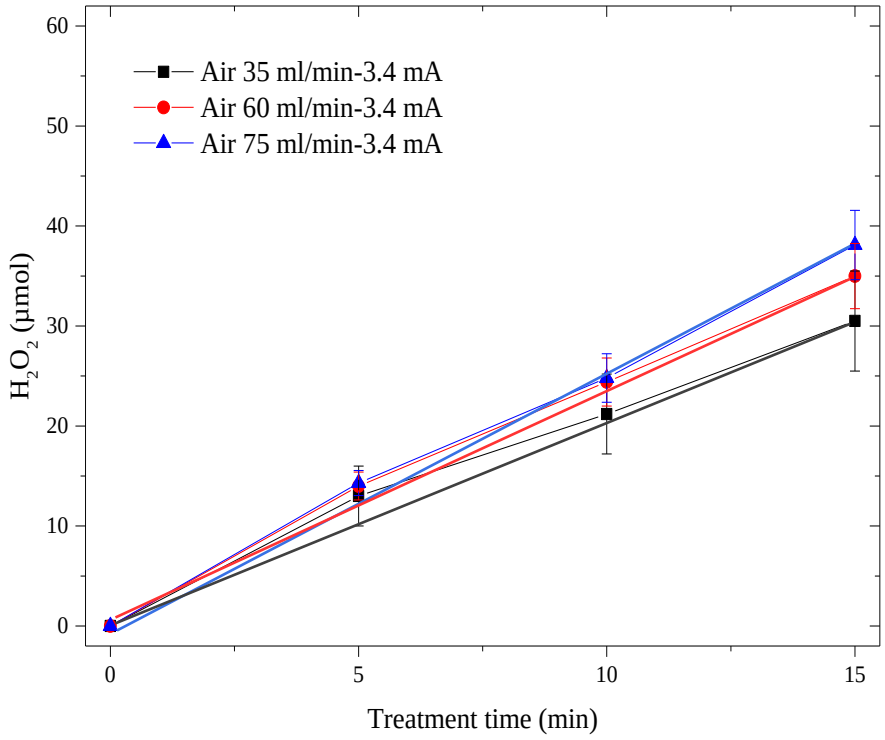

Figure 8.4 Under positive polarity, the H_2O_2 production under 3.4 mA discharge current, with different liquid flow rates.

Increasing the discharge current to 5 mA increased the H_2O_2 production by around 30%, reaching 16.4 µmol, 16.9 µmol and 17.3 µmol with 35, 60 and 75 ml/min of liquid flow rate, respectively, after 5 minutes of treatment; corresponding to yields of 1.6 g/kWh, 1.64 g/kWh and 1.68 g/kWh.

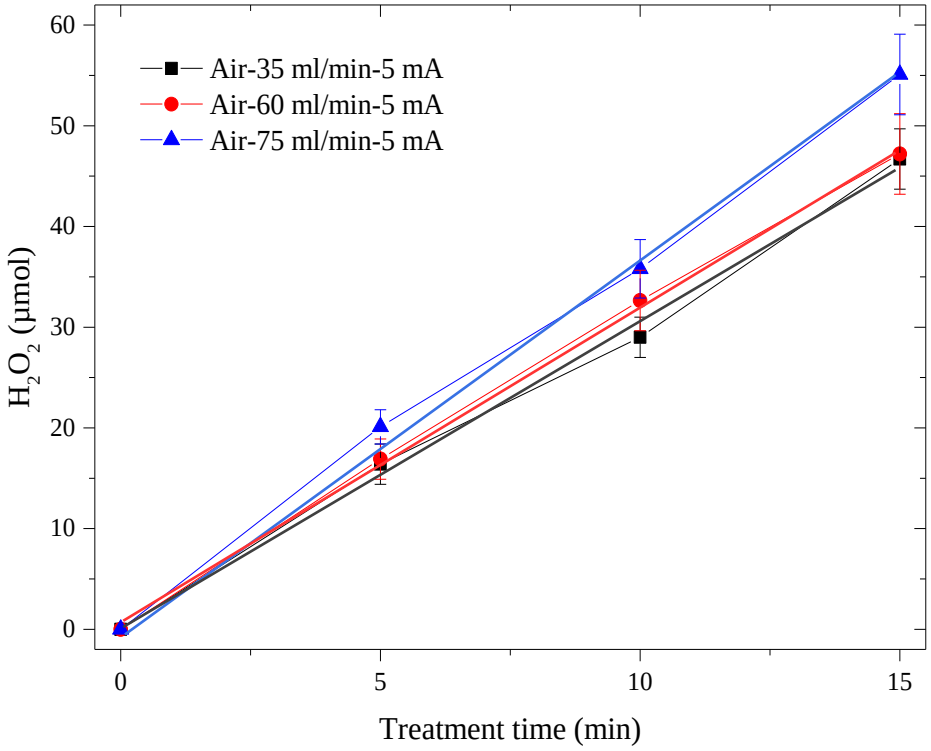

Figure 8.5 Under positive polarity, the H_2O_2 production under 5-mA discharge current, with different liquid flow rates.

The H_2O_2 yield appears to follow a linear trend with time with little evidence of any change in the rate at which H_2O_2 is produced with time, unlike the behaviour observed in the previous chapter where a static water cathode was used. The H_2O_2 production rate increased with liquid flow rate, reaching 58 nmol/s under 5 mA discharge current and 75 ml/min liquid flow rate. However, increased discharge current reduced the energy efficiency of H_2O_2 production.

Table 8.1 shows the variation of charge/H_2O_2 ratios under different discharge currents and liquid flow rates. In comparison with the results (1:1.03) recorded under static liquid cathode (Chapter 7), the ratios increased with increasing liquid flowing rates. Under a liquid flow rate of 35 ml/min, a charge/H_2O_2 ratio of 1:1.2 was recorded after 5 minutes of treatment; increased liquid flow rate to 60 ml/min led to the increase of charge/H_2O_2 ratio to 1:1.32.

Under the liquid flow rate of 75 ml/min, the charge/H_2O_2 ratio reached 1:1.35 and 1:1.29 under 3.4 mA and 5 mA discharges currents, respectively, after 5 minutes of treatment; then decreased to 1:1.2 and 1:1.18, respectively, after 15 minutes of treatment. During electrical discharges above water, the reaction interface area was limited by the size of discharge filaments, which may lead to a high regional concentration of H_2O_2 and OH radicals. The flowing cathode results in the delivery of 'fresh' solution to the plasma-water interface area and the dilution of the local concentration of H_2O_2. In this case, a higher liquid flow rate indicated faster dilution and resulted in higher H_2O_2 formation during the treatments.

Table 8.1 H_2O_2 production ratios regarding to 1 charge

	Ground electrode liquid flow rates			
	0 ml/min	*35 ml/min*	*60 ml/min*	*75 ml/min*
Current	3.4 mA			
5 min	1	1.2	1.32	1.35
10 min	1	1	1.15	1.17
15 min	1.03	0.96	1.1	1.2
Current	5 mA			
5 min	-	1.05	1.08	1.29
10 min	-	0.93	1.05	1.15
15 min	-	1	1.01	1.12

It was also noticed that the charge/H_2O_2 ratio reduced with the higher discharge current (5 mA), and this phenomenon is independent of the liquid flow rates. Increased current raised the plasma density, which led to higher gas temperatures and faster water evaporation; these two factors may have critical effects for OH radical production. As discussed in Chapter 7, higher water vapour leads to lower H_2O_2 prodcution by either decreasing the number of high energy electrons or through absorption of NO_x species leading to cscavenging of OH radicals and H_2O_2, this may explain the lower charge/H_2O_2 ratio obtaiend under higher discharge currents.

Jamro'z [3] investigated the H_2O_2 production in DC glow discharges above a flowing cathode and recorded different results compared to the ones in this experiment. Jameo'z found that the H_2O_2 production was 30% decreased when the flow rate increased from 0.5 to

3.5 ml/min. Jamro'z concluded this result was due to a higher liquid flow rate, leading to a shorter contacting time of plasma with the same area water and a lower evaporation rate of water.

Tert-butanol effect

0.2-M TB was applied to investigate the production pathways of H_2O_2 under a liquid flow rate of 60 ml/min. Figure 8.6 shows the H_2O_2 production when TB was added, which reached 17.5 µmol and 28.1 µmol under discharge current of 3.4 mA and 5 mA, respectively, after 15 minutes of treatment; this corresponds to a charge/H_2O_2 ratio of 1:0.5 and 1:0.62.

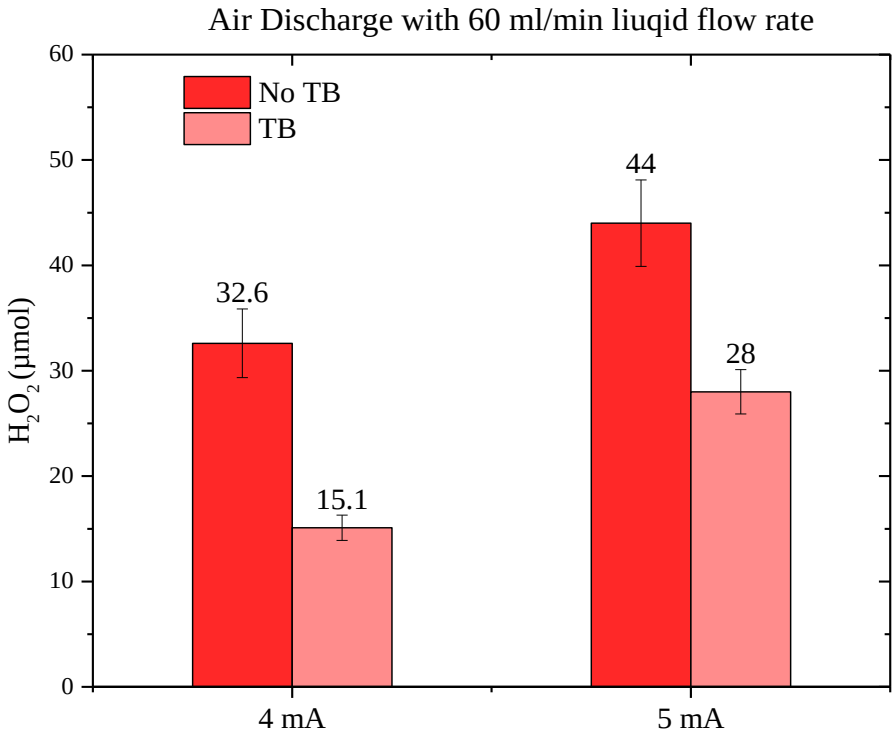

Figure 8.6 Effect of TB on H_2O_2 production in air discharges under discharge currents of 3.4 mA and 5 mA with a liquid flow of 60 ml/min.

It was calculated that under a discharge current of 3.4 mA, the H_2O_2 production via the dimerization of OH radicals was 54% for 15 minutes of treatment, which is similar to the results recorded with a static water electrode (52% in Chapter 7). While under a discharge current of 5 mA, the proportion was decreased to 36.4%.

8.3.2 Variation of solution conductivity

Figure 8.7 shows the variation of solution conductivity during treatments under a discharge current of 3.4 mA. The solution conductivity increased linearly with time, which indicated the continuous production of oxy-nitride species at the plasma-water interface, reaching 345 µS/cm, 379 µS/cm and 332 µS/cm with 35, 60 and 75 ml/min liquid flow rates, respectively, after 15 minutes of treatment.

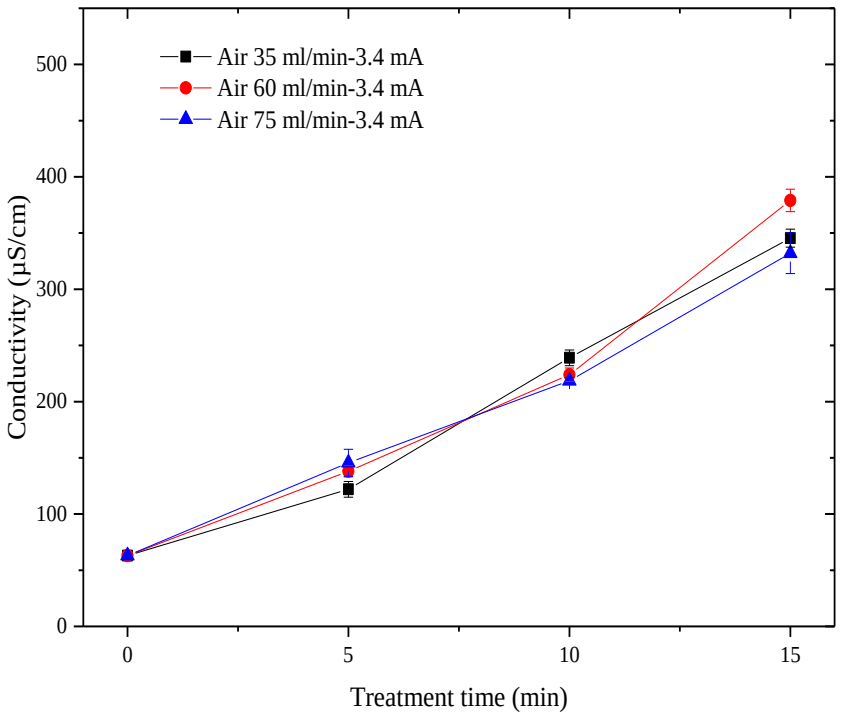

Figure 8.7 Effect of liquid flow rate on the variation of solution conductivity under a discharge current of 3.4 mA.

Increased the discharge current to 5 mA (Figure 8.8) increased the oxy-nitride species production, leading to an increase of the solution conductivity to 480 µS/cm, 461 µS/cm and 490 µS/cm with 35, 60 and 75 ml/min liquid flow rate, respectively, after 15 minutes of treatment. From figures 8.7 and 8.8 it can also be seen that the variation of solution conductivity is independent of liquid flow rate but is dependent on discharge current.

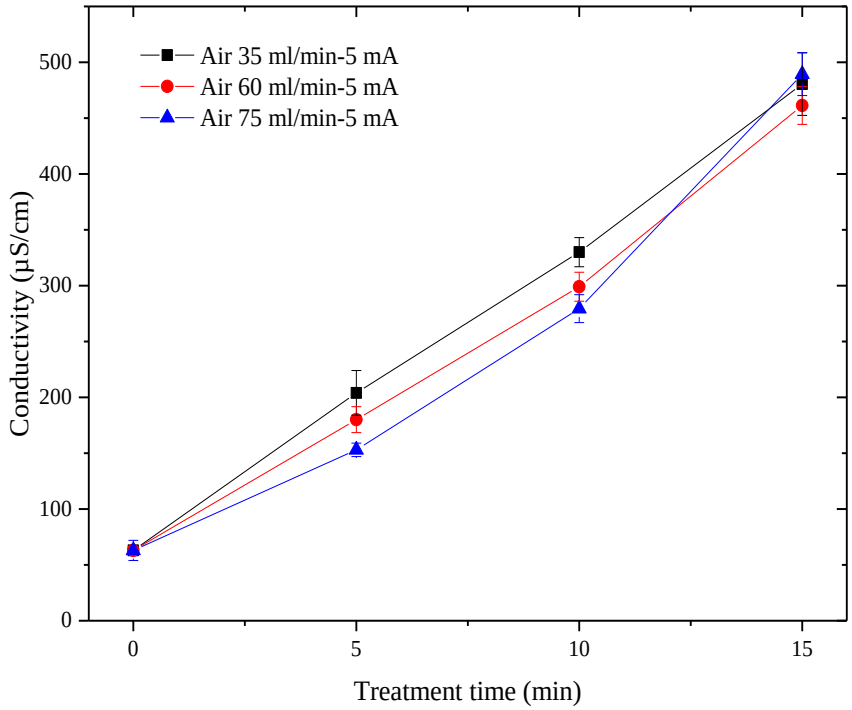

Figure 8.8 Effect of liquid flow rate on the variation of solution conductivity under a discharge current of 5 mA.

Jamro'z [3] investigated the Ar plasma jet operated in ambient gas of air and found that the concentration of NO_2^- and NO_3^- increased with increasing liquid flow rates from 60 ml/min to 300 ml/min, resulting in increasing acidity of solutions and decreasing concentration of H_2O_2; however, in this work, the concentration of H_2O_2 was observed to increase with flow rate. However, the glow rates used in this work were in general lower than those used by Jamro'z. Therefore, larger ranges of liquid flowing rate need to be further investigated.

8.4 Conclusion

A positive DC glow discharge developed above a flowing tap water electrode was investigated under two different discharge currents. The H_2O_2 production yield and charge/H_2O_2 ratio increased with increasing liquid flow rates and reached the highest value of 1.95 g/kWh and 1:1.35 under a discharge current of 3.4 mA and a liquid flow rate of 75 ml/min, after 5 minutes of treatment; these results are improved from the discharges with static liquid cathode. After 15 minutes of treatment, the ratio decreased to 1:0.96, 1:1.1 and 1:1.2 under a discharge current of 3.4 mA and a liquid flow rate of 35, 60 and 75 ml/min.

Increasing the discharge current to 5 mA induced stronger plasma-water interface reactions. The H_2O_2 production yield of 1.68 g/kWh was recorded after 5 minutes of treatment, with a liquid flow rate of 75 ml/min. No significant decrease of H_2O_2 production yield was recorded with a current of 5 mA. The variation of solution conductivity was proved to be independent on liquid flow rate, but dependent on discharge current.

The addition of TB determined that 54% and 36.4% of the H_2O_2 production under positive DC discharges above flowing liquid cathode, with discharge currents of 3.4 and 5 mA, respectively, are via the dimerization of OH radicals. Flowing cathode allows other reaction pathways to occur so the dimerization reaction is not responsible for the change in H_2O_2 as a result of changing flow rate.

The increase in H_2O_2 production observed with the flowing cathode is significant in terms of practical applications of the technology.

8.5 Further work

Due to the different discharge currents and liquid flow rates having been proven to affect the plasma-water interface reactions, a larger range of discharge current up to several tens of mA and liquid flow rates up to several L/min can be employed to investigate their effects on H_2O_2 production. The H_2O_2 production rates and charge/H_2O_2 ratios were found to increase with increasing liquid flow rates; the mechanism of this phenomenon needs to be further investigated.

9 H_2O_2 PRODUCTION AND METHYLENE BLUE DEGRADATION UNDER POROUS DIELECTRIC BARRIER DISCHARGE

9.1 Introduction

Dielectric barrier discharge (DBD) in contact with water has been investigated for its discharge characteristics, H_2O_2 production and solution conductivity and pH variation in various gases. Ognier [102] investigated the H_2O_2 production using a falling water film DBD, and recorded a H_2O_2 production yield ranging from 0.04 to 0.26 g/kWh, with the discharge power ranging from 6.3 to 18.9 W; these values are lower than those recorded in Locke's review, which could be due to the limited contact area between plasma and water.

An innovative DBD reactor involving a multi-pore PTFE layer (60 holes), which constrains the development of discharge filaments through the pores into water, was designed in this experiment. This design allows plasma to develop between the dielectric barrier and the grounded water, leading to the production of reactive species at the plasma-water interface. Both ultrapure water and 5 mM-NaOH solution were used to investigate H_2O_2 production. A scavenger of OH radicals was employed to investigate the OH radical dimerization effect and the H_2O_2 formation pathways. The H_2O_2 production recorded under DBD were compared to those under positive and negative impulsive current discharges.

Organic dyes are commonly used in industrial fields such as textile, leather and paper [121, 122]. However, these dyes have been proven to be toxic in biological systems [122, 123]. AOPs are proved to be effective for organic dye degradation due to their capability of producing OH radicals *in situ*, leading to the dissociation of organic compounds into CO_2 and H_2O. In this experiment, methylene blue (MB) dye was employed as the target pollutant to investigate its degradation by O_2 plasma.

The main objectives of the experiment were to investigate: (i) the H_2O_2 production yield and charge/H_2O_2 ratio in O_2, N_2 and air; (ii) the H_2O_2 formation pathway; (iii) methylene blue degradation by using O_2 plasma; and (iv) the contribution of OH radicals to methylene blue degradation.

9.2 Reactor design and experimental set up

9.2.1 Reactor design

Figure 9.1 shows the design of the DBD plasma-water reactor with a porous PTFE dielectric layer. The reactor was made by a PTFE cylinder, with a height of 85 mm and outer diameter of 90 mm. The test cell has a diameter of 35 mm and depth of 40 mm, which was used to contain the solution samples during treatments; a porous PTFE layer with a diameter of 50 mm and a thickness of 1 mm was placed at the bottom of the test cell. 60 micro-pores with a diameter of 0.2 mm were uniformly distributed across the PTFE layer. The micro-pores were drilled by using a stainless steel pin, with the pin tip diameter of 0.2 mm. An O-ring was used to seal the gap between the test cell and the PTFE layer. A 0.2-mm gap was fixed between the porous PTFE and the glass plate to allow the gas flow through the gap, and outlet through the pores in the PTFE layer into the water.

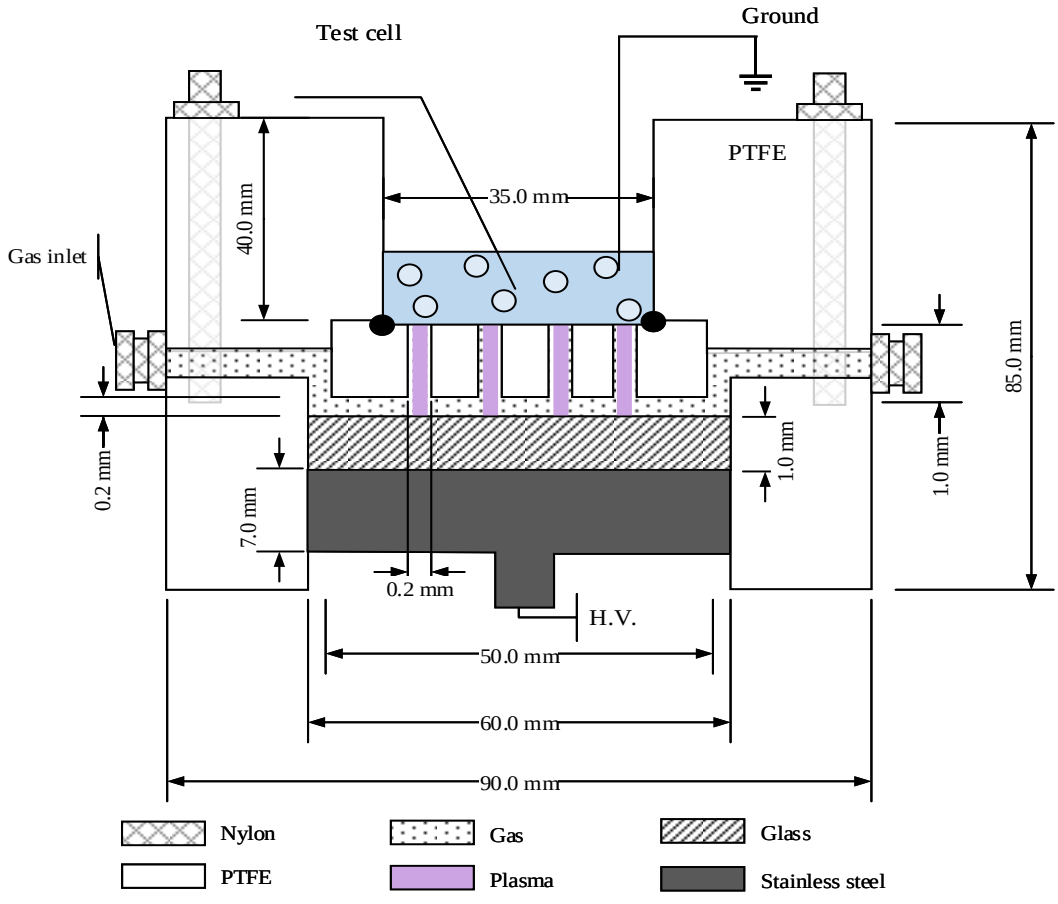

Figure 9.1 DBD configured plasma-water reactor design.

A flat stainless-steel electrode with a diameter of 45 mm was covered by a glass barrier with a diameter of 50 mm and thickness of 1 mm. The liquid samples in the test cell act as a ground electrode via a grounding stainless steel wire.

9.2.2 Experimental set up

Figure 9.2 shows the schematic diagram for DBD experiments. A linear AC power supply was employed to provide a peak to peak voltage (V_{pp}) of 20 kV of sinusoidal voltage with a frequency of 5 kHz to the reactor. A high voltage probe was used to measure the voltage applied to the reactor. The ground electrode was dipped into the solution and connected to a 50-Ω coaxial cable to measure the current waveforms. For the discharge power measurement, a capacitor of 5-nF was connected in series with the ground electrode to plot a Lissajous figure.

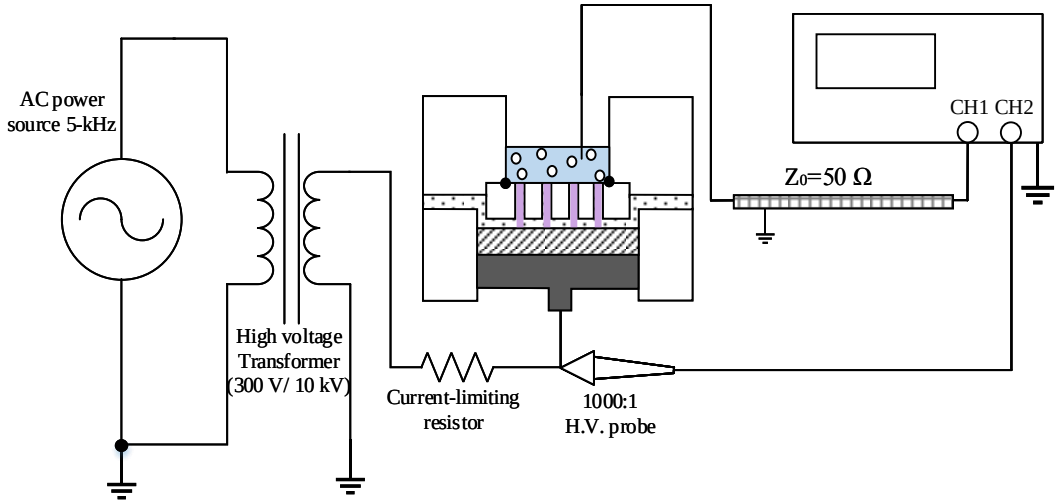

Figure 9.2 Schematic diagram for dielectric barrier discharge experiments.

The H_2O_2 production was investigated in working gases of N_2, O_2 and air, with a gas flow rate of 0.2 L/min, which was controlled by a gas flow controller. The working gas was introduced through the reactor before injecting the untreated samples, to prevent the solution entering the micro-pores. A sample of 10-ml volume was used in each treatment. In terms of H_2O_2 production investigation, the effect of solution initial pH was investigated by using ultrapure water and a 5-mM NaOH solution. In terms of MB dye degradation investigation, the MB solution with a concentration of 600 mg/L was prepared by dissolving MB powder into ultrapure water.

After each treatment, the sample was transferred to a cuvette by a 5-ml pipette. UV spectrometry was employed to measure the H_2O_2 production after 5, 10, 15 and 20 minutes of treatment, at the peak absorbance of 396 nm. The MB dye concentration was measured after 1-5 minutes of treatment, by UV spectrometry at the peak absorbance of 665 nm. TB was applied to terminate the dimerization of OH radicals to investigate the H_2O_2 production pathway, and to investigate the OH radical contribution for MB dye degradation. The solution conductivity and pH were measured after each treatment; every treatment was repeated three times.

9.3 Gas discharge characteristics in various gases

9.3.1 Discharges in oxygen

Figure 9.3 shows the voltage and current waveforms for discharges in O_2. A capacitive current was observed when the high voltage was applied; the amplitude increased to ~8 mA when the V_{pp} was increased to 20 kV.

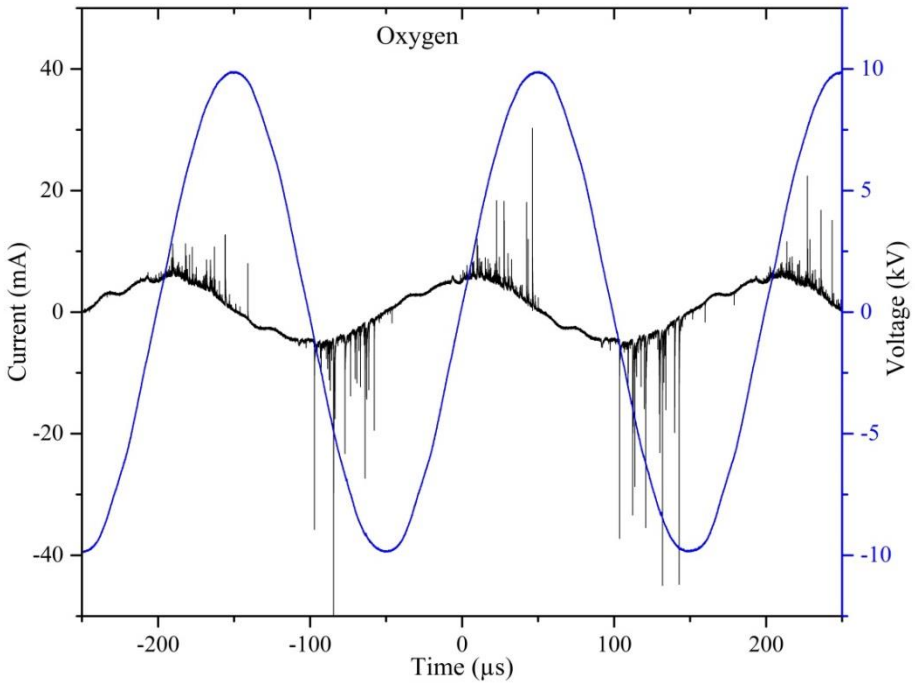

Figure 9.3 Voltage and current waveforms recorded in O_2 dielectric barrier discharges.

The electrical breakdown in the 0.2-mm gas gap was recorded when the V_{pp} was increased to 12.5 kV, negative current pulses with a mean amplitude of around -10 mA were recorded superimposed on the capacitive current. Positive filaments with a mean amplitude of <5 mA started to occur when the V_{pp} was increased to 15.5 kV. These currents with low amplitudes result from the discharges developed between the porous PTFE plate and the glass plate.

Increasing the V_{pp} to 16 kV led to a significant increase of the pulse amplitude and its duration under both positive and negative polarities. The amplitude of positive pulses increased to a mean value of ~18 mA, and that of the negative pulses increased to ~-30 mA. This result indicated the initiation of the electrical breakdown between the glass plate and the grounded water, where the filaments developed through the micro-pores on the PTFE layer. Further increasing the V_{pp} to 20 kV, the mean amplitude of the pulses increased to ~25 mA and ~-45 mA under positive and negative polarity, respectively.

9.3.2 Discharges in nitrogen

In N_2 discharge, the positive filaments with a mean amplitude of ~10 mA were initially observed under positive polarity when the V_{pp} reached 15 kV. The initial breakdown voltage recorded in N_2 was higher than that recorded in O_2.

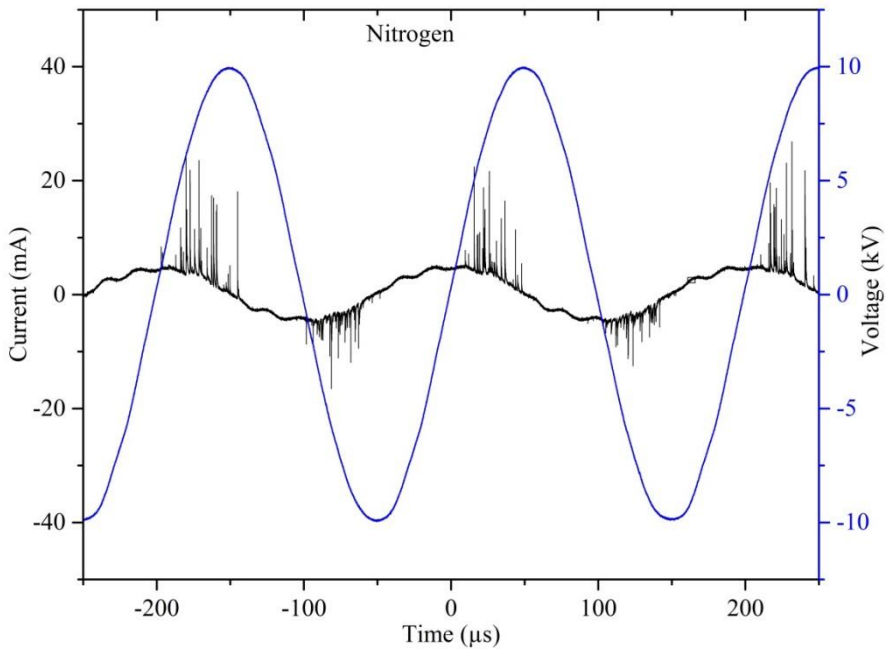

Figure 9.4 Voltage and current waveforms recorded in N_2 dielectric barrier discharges.

Increasing the V_{pp} to 16.5 kV resulted in the appearance of negative pulses with a mean amplitude of ~-5 mA. A threshold voltage of 17.5 kV was recorded in N_2 to initiate the electrical breakdown through the micro-pores, which is higher than that recorded in O_2. Increasing the V_{pp} to 20 kV increased the mean amplitude of positive pulses to ~20 mA and negative pulses to ~-10 mA (Figure 9.4). The discharges in N_2 leads to the generation of a significant amount of metastable state particles, resulting in lower current amplitudes compared to those recorded in O_2.

9.3.3 Discharges in air

In air discharges, the negative current pulses were initially observed to occur at V_{pp} of 11.5 kV, lower than those recorded in O_2 and N_2 discharges. Increasing the V_{pp} to 13.5 kV led to the occurrence of positive pulses. A threshold voltage of 15.5 kV was recorded to initiate the electrical breakdown through the micro-pores. The highest impulsive current of 48 mA was recorded under negative polarity when the V_{pp} was increased to 20 kV. Abdeaziz [124] investigated the surface DBD with N_2/O_2 mixtures and found that the positive filaments in air have a higher repetition rate than that in N_2, which has also been observed in this experiment (Figure 9.4 and Figure 9.5).

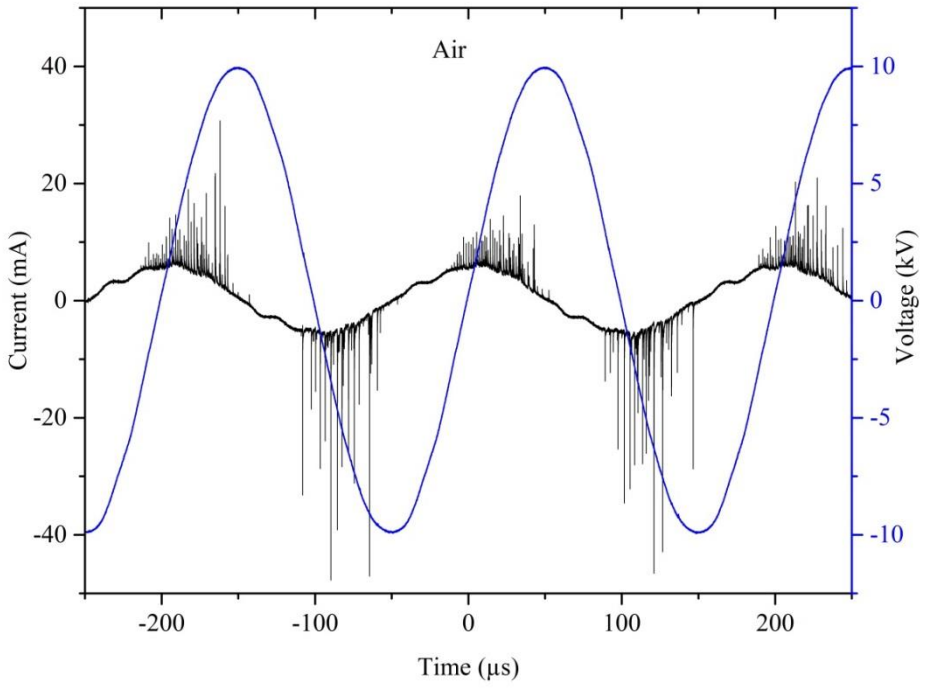

Figure 9.5 Voltage and current waveforms recorded in air dielectric barrier discharges.

9.3.4 DBD power measurement using Lissajous figure

In ultrapure water

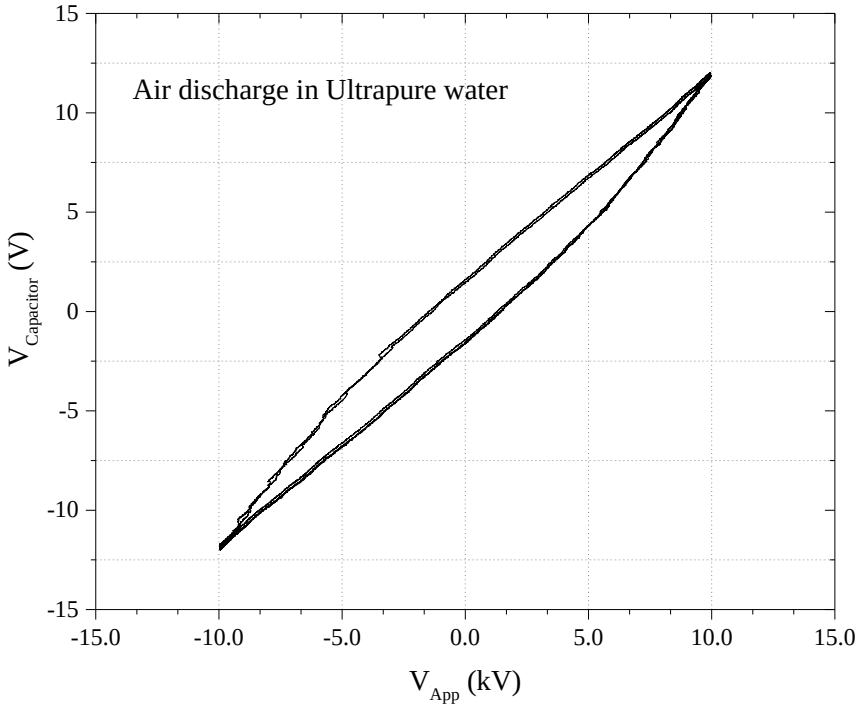

Figure 9.6 Lissajous figure recorded in air discharges with ultrapure water.

Figure 9.6 shows a Lissajous figure that was recorded using the oscilloscope under air discharges with ultrapure water. The *x*-axis shows the applied voltage that was recorded by the HV probe and the *y*-axis shows the voltage measured across the measurement capacitor C_m, which is proportional to current. The currents associated with the discharges at lower voltages occurring in the gap between the glass plate and PTFE plate did not affect the Lissajous figure, it remained as a single straight line indicating that the charge transfer in the system was dominated by a capacitive current; therefore, no plasma-water interface reactions can occur, it is expected that the reactive species produced in this case are O_3 and O atoms.

The Lissajous figures started to open up indicating the presence of a significant resistive current in the system when the applied voltage reached the threshold voltage for the electrical breakdown to develop through the micro-pores on the PTFE plate. The plasma-water interface reactions will lead to the production of reactive species, and these species were then injected into the solutions. In conventional DBD, the Lissajous figure presents a parallelogram-shape; however, in this experiment, the Lissajous figure is not an ideal

parallelogram. This could be due to the grounded material being water in this experiment, which presents both capacitance and resistance during electric discharges.

In NaOH solution

A 5-mM NaOH solution was used to investigate the effect of OH^- ions on plasma-water interface reactions and reactive species production. The discharge power can be calculated simply from the Lissajous figure when a parallelogram-shape is presented. However, the figures recorded in this experiment were of slightly oval shape; therefore, the power consumption was calculated by integrating of the area of the Lissajous figure by using MATLAB.

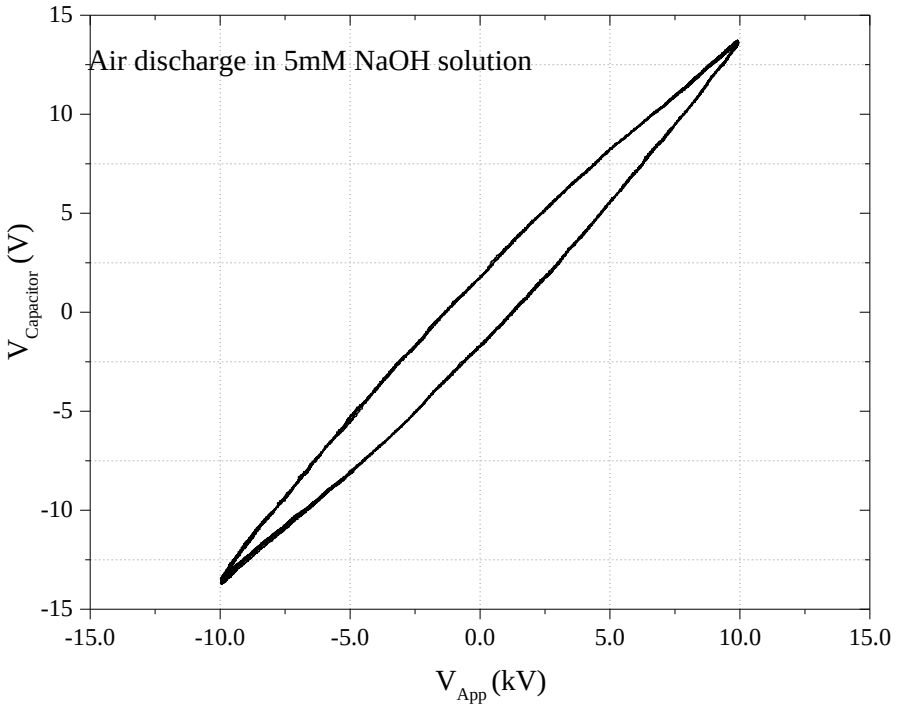

Figure 9.7 Lissajous figure recorded in air discharges with 5-mM NaOH solution.

The energy consumption for each cycle was 0.18 μJ and 0.22 μJ for the discharges with ultrapure water and 5-mM NaOH solution (Figure 9.7), respectively; this corresponds to a discharge power of 0.9 W and 1.1 W at the frequency of 5 kHz.

9.4 Plasma-water interface reactions with ultrapure water

9.4.1 H_2O_2 production

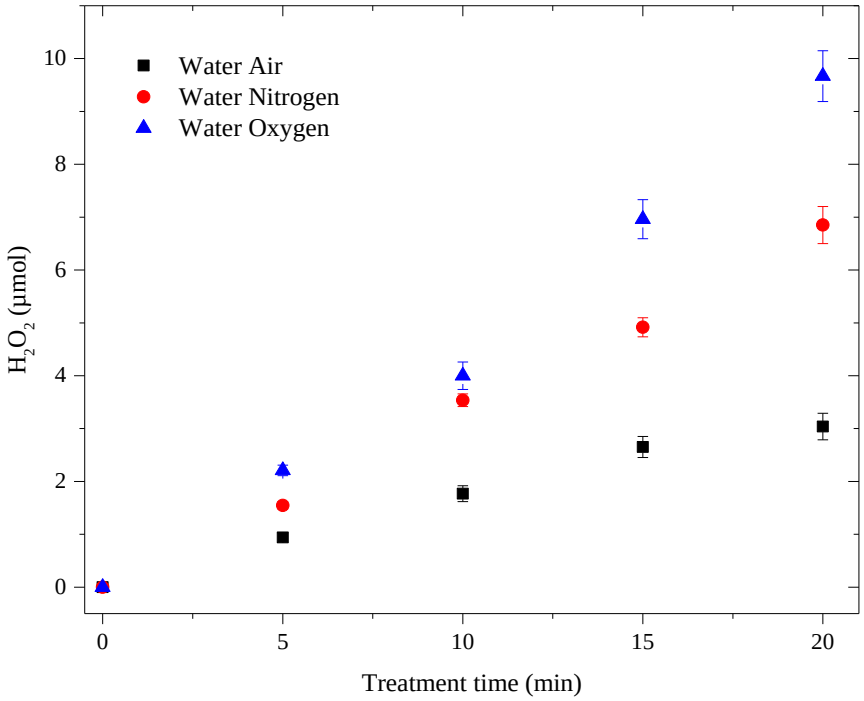

Figure 9.8 H_2O_2 production in ultrapure water under porous dielectric barrier discharges in air, N_2 and O_2

Figure 9.8 shows the H_2O_2 production in various gas discharges. The results demonstrated that the H_2O_2 production was significantly affected by the gas type, reaching 3 µmol, 6.8 µmol and 9.7 µmol in air, N_2 and O_2, respectively, after 20 minutes of treatment; corresponding to the yields of 0.1 g/kWh, 0.8 g/kWh and 1.1 g/kWh.

The highest H_2O_2 production under DBD was recorded in O_2, which was 3.2 and 1.4 times the production in air and N_2, these results are different from that recorded under impulsive current discharges (Chapter 6). This may be due to the larger amount of O atoms generated during O_2 treatments compared to that in N_2 and air treatments. The O atoms can react with water molecules, thus increasing the production of H_2O_2 through the reaction R 6.2 [122].

$$O^* + H_2O \rightarrow 2\,OH^{\cdot} \qquad \text{(R 6.2)}$$

Also, negative O_2 ions can be produced through electron attachment reactions and then react with water or HO_2 radicals to form OH radicals. However, from the previous experiments

(Chapter 6 and Chapter 7), it was found almost no H_2O_2 production was detected under negative discharges. Therefore, the negative polarity was assumed to have no significant effect on H_2O_2 production in this experiment.

O_3 was also shown to be generated in O_2 discharges. Although the water vapour that formed at the plasma-water interface can significantly terminate the O_3 formation, the H_2O_2 formed by the reactions between water and the dissolved O_3 in solution (R 6.1) should not be ignored. Zhang [125] investigated H_2O_2 production in hybrid discharges and found that the formed H_2O_2 in O_2 was at least 3 times higher than that obtained in N_2, due to the dissolving of O_3 in solution.

$$O_3 + H_2O \rightarrow H_2O_2 + O_2 \quad \text{(R 6.1)}$$

In N_2 discharges, only a small amount of O_2 can be formed by water electrolysis reactions, leading to the production of O atoms. The main pathway for OH radical production in N_2 should be through the charge transfer and the formation of water cations (H_2O^+) (R 2.9, R 2.15), leading to the production of H_3O^+ and OH radicals (R 2.17). Also, OH radicals can also be generated through the reaction between excited N_2 and water (R 6.9).

$$e^{-*} + N_2 \rightarrow N_2^+ + 2e^- \quad \text{(R 2.9)}$$

$$N_2^+ + H_2O \rightarrow N_2 + H_2O^+ \quad \text{(R 2.15)}$$

$$H_2O^+ + H_2O \rightarrow H_3O^+ + OH^{\cdot} \quad \text{(R 2.17)}$$

$$N_2^* + H_2O \rightarrow N_2 + OH^{\cdot} + H^{\cdot} \quad \text{(R 6.9)}$$

In air discharges, large amounts of oxy-nitride can be produced through the reaction of O atoms with N_2 that occurs at the plasma-water interface. This significantly reduced the quantity of O atoms and increased the solution conductivity (discussed in Section 9.4.2).

Tert-butanol effect

A TB solution was employed to terminate the dimerization of OH radicals into H_2O_2 during treatments. The H_2O_2 production reached 2.7 µmol in N_2 discharges, after 20 minutes of treatment (Figure 9.9). No TB effect was observed in air-treated samples, which is the same as that recorded in impulsive current discharges (Chapter 5 and Chapter 6). It was calculated that 6.7% and 61% of H_2O_2 production in air and N_2, respectively, was via the dimerization of OH radicals.

An increase of H_2O_2 production was observed when TB was used in O_2 treatments as with the results in Section 6.4.1 there was a very large scatter in the data so this result has been omitted from Figure 9.9. This behaviour could be due to the reactions between ROS and the TB molecule (as has been discussed in Section 6.4.1). However, this phenomenon has not been widely recorded and its mechanism is still not clear. The much lower effect of TB in air treatments may also be due to the effect of O_2.

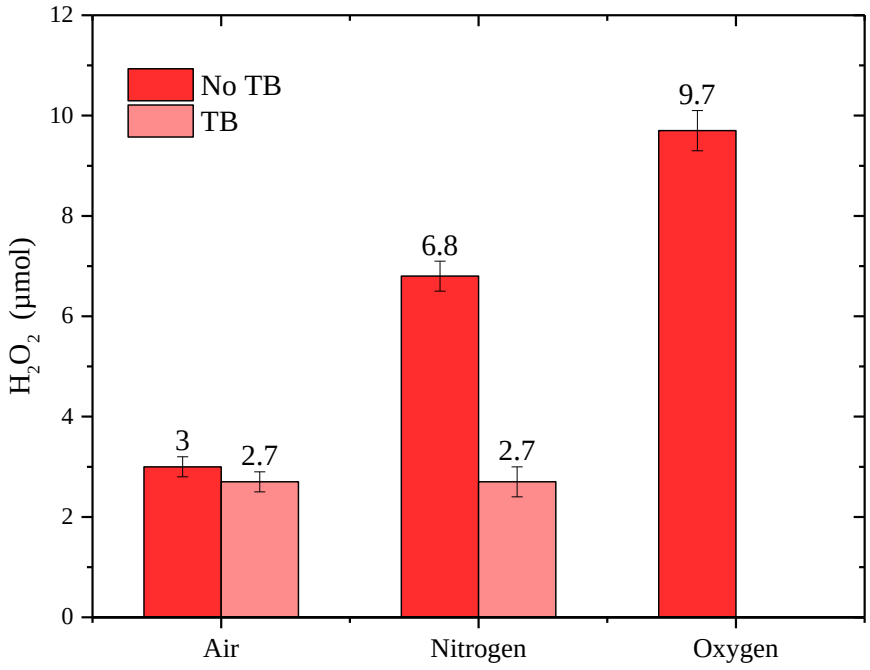

Figure 9.9 Effect of TB on H_2O_2 production under porous dielectric barrier discharges in air and N_2.

9.4.2 Variation of solution conductivity

Figure 9.10 shows the variation of solution conductivity during treatments in air, N_2 and O_2. It was found that the variation of solution conductivity is dependent on working gases, and achieved 1257 µS/cm, 448 µS/cm and 675 µS/cm after 20 minutes of treatment in air, N_2 and O_2, respectively. A dramatic increase of solution conductivity was recorded in air treatments, the value was 2.8 and 1.86 times the results recorded in N_2 and O_2; this could be due to the significant amounts of oxy-nitride species that are generated at the plasma-water interface; all the substances were then injected into the solution, leading to the generation of nitrite acid. The minimum variation of solution conductivity was recorded in N_2 discharges; this may be due to the small amount of O_2 formed by electrolytic reactions occurring in N_2 discharges limited the production of oxy-nitride species.

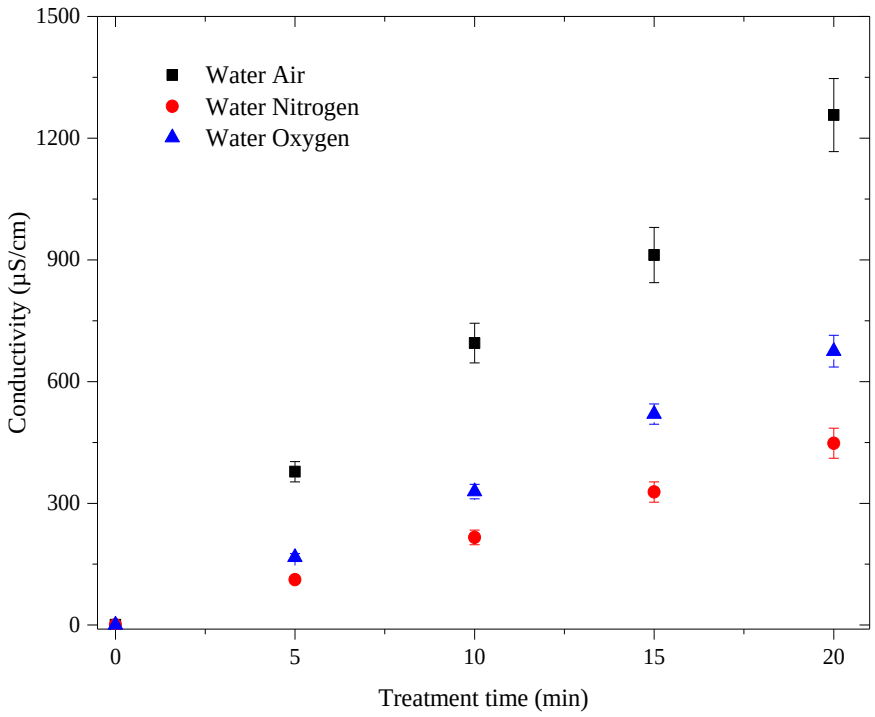

Figure 9.10 Variation of solution conductivity in ultrapure water under air, N_2 and O_2 discharges.

Neither nitrite nor nitrate acid was detected in O_2-treated samples by using test strips, however, a significant increase of solution conductivity was observed in O_2 discharges. This may be due to the occurrence of electron attachment reactions, leading to a significant production of O^- and O_2^-, which can dissolve into water and leading to the increase of

solution conductivity. A similar result was recorded in Burlica's research [45], although no oxy-nitride production was detected in O_2-treated samples, a significant increase of solution conductivity was recorded. Therefore, the mechanisms of the variation of solution conductivity in O_2 discharges need further investigation.

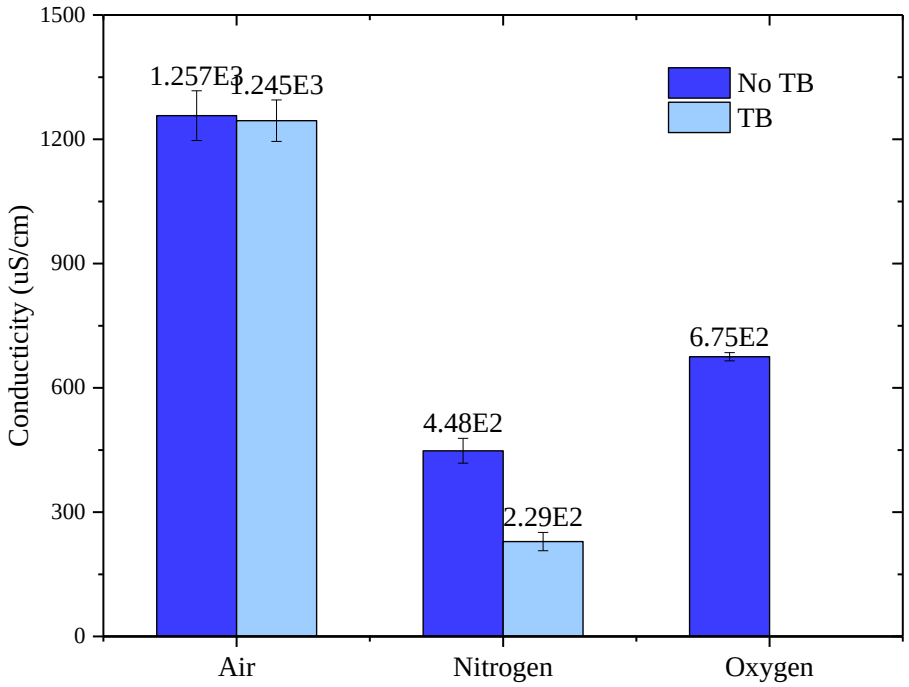

Figure 9.11 Effect of TB on the variation of solution conductivity under air and N_2 discharges.

When TB was used during treatments, the solution conductivities recorded in air discharges were the same as those recorded under no-TB condition. In N_2 discharges, the solution conductivity reached 229 µS/cm, after 20 minutes of treatment, which is 51% of the value recorded under no-TB condition (Figure 9.11). The reduced solution conductivity in N_2 may be due to the scavenging of $N^{\cdot}$ radicals by TB at the plasma-water interface and in the gas phase, thus inhibiting the oxy-nitride species production, leading to a lower variation of solution conductivity. No readings of the conductivity were made for oxygen discharges over a solution containing TB due to the large spread reported above in the H_2O_2 concentrations.

9.5 Plasma-water interface reactions with NaOH solution

A 5-mM NaOH solution with a pH of 11.5 was used to investigate the effect of OH^- ions on H_2O_2 production. A reduction of H_2O_2 production was observed in all gas treatments (Figure 9.12), compared to those recorded in treatments with ultrapure water, indicating the scavenging effect of OH^- ions on OH radical and H_2O_2 production.

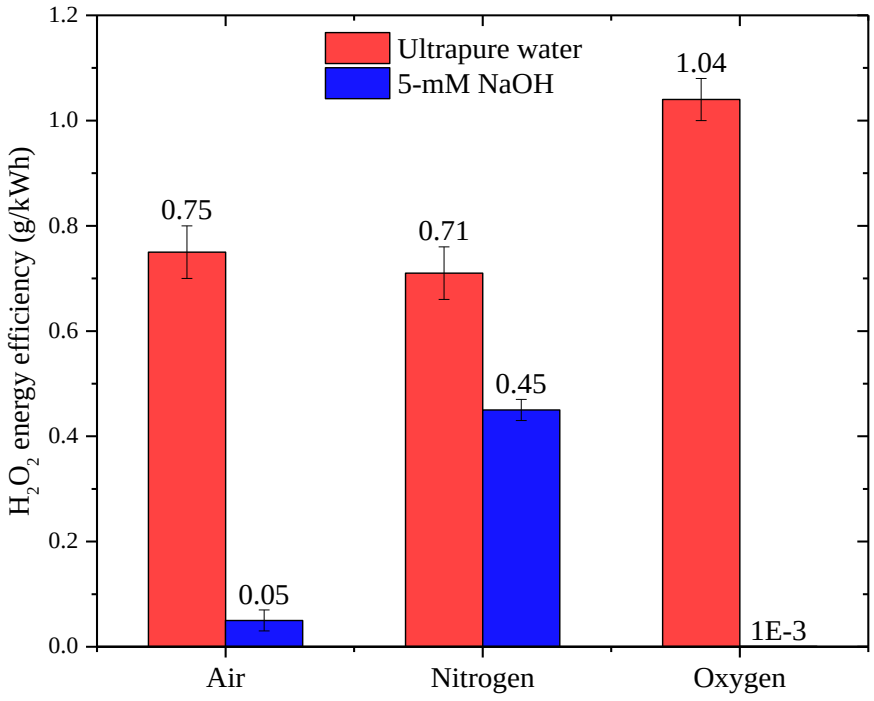

Figure 9.12 H_2O_2 production for air, N_2 and O_2 discharges with 5-mM NaOH solution.

The H_2O_2 production in basic solution under N_2 and air treatments reached 3.8 µmol and 1.6 µmol, respectively; corresponding to 45% and 47% of H_2O_2 production being inhibited by OH^- ions.

Moreover, the greatest difference appeared in O_2 discharges (Figure 9.12), in which almost no H_2O_2 production was detected in solution after 20 minutes of treatment. It can be concluded that the OH^- ions not only scavenged the OH radicals and H_2O_2 molecules, but also O atoms that are being generated at the plasma-water interface.

9.6 Oxygen plasma treatment for methylene blue degradation

9.6.1 Methylene blue degradation with various solution pH

The effect of solutions with initial pH values of 2.9, 7 and 11.5 on MB dye degradation was investigated under O_2 plasma treatments (Figure 9.13). No major differences of MB dye degradation rates were recorded among the pH solutions. After one minute of treatment, the MB concentration reduced from the initial value of 600 mg/L to 203 mg/L, 178 mg/L and 139 mg/L in solution of pH 2.9, 7 and 11.5, respectively; this corresponded to 12.4 µmol, 13.2 µmol and 14.4 µmol of MB dye being degraded. The change in MB concentration in each one minute measuring interval decreases with time. The MB dye concentrations were further reduced to 78 mg/L, 46 mg/L and 15.6 mg/L for solution pH of 2.9, 7 and 11.5, respectively, after 3 minutes of treatment. It is not clear if this is occurring partly from the change in concentration of the MB in the solution or also as a result of a multistep degradation reaction in the system. However the system does not seem to be following a first order reaction kinetic.

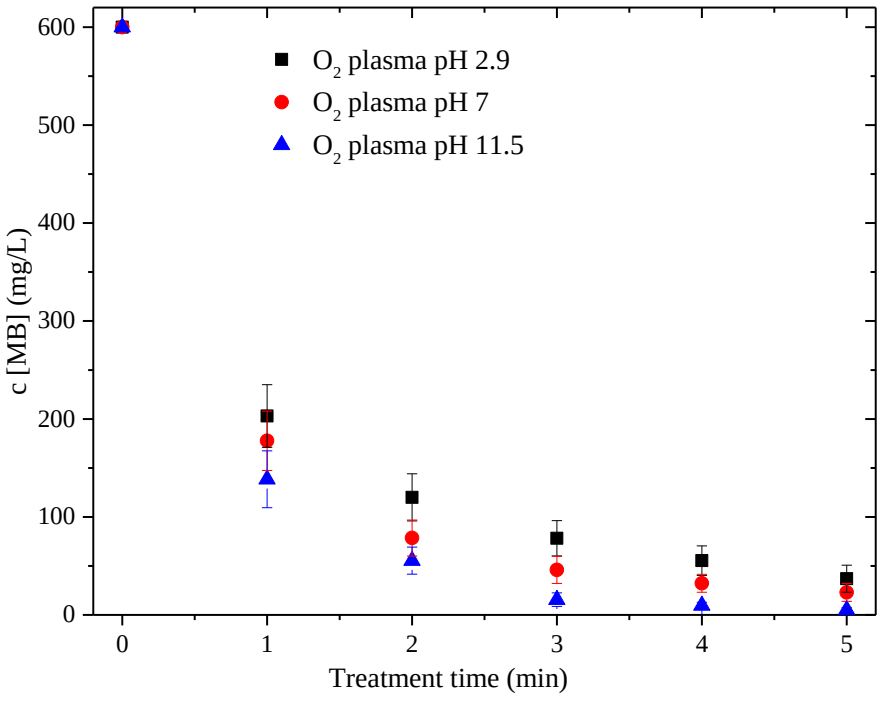

Figure 9.13 Variation of methylene blue concentration in O_2 plasma treatment, with different initial pH value.

A significant amount of dark-purple particles was observed in the samples after 1 minute of treatment. This phenomenon should be due to the first step of MB dye degradation, in which one or more methyl groups (-CH_3) were shed from the amino group (Figure 9.14) with a bond energy of 70.8 kcal/mol (Table 9.1). This reaction changes the colour functional group of MB and reduces the peak absorbance at 665 nm wavelength. In addition, the first step of degradation transits the dye molecules from methylene blue to insoluble intermediate products, which changes the colour of the samples from dark blue to dark purple.

Table 9.1 Various molecule bond energies [123]

Molecule bonds		*Bond energy (kcal/mol)*
CH_3-N(CH_3)C_6H_5	(1)	70.8
C_6H_5-S-C_6H_5	(2)	76±2
C_6H_5-NH-C_6H_5	(3)	87.4
N(CH_3)$_2$-C_6H_5	(4)	93.2±2.5
C_6H_5-NH_2		102.6±1

The second stage of dye degradation results in the breaking of complex heterocyclic structures of MB dye into single aromatic compounds, by firstly breaking the C-S^+ bond with an energy of 76±2 kcal/mol and secondary breaking the double bond between N atom and aromatic ring (C_6H_5-N-C_6H_5) with an energy of 87.4 kcal/mol [123]. The variation of sample colours from dark purple to dark green proves the formation of new intermediate products. Relatively higher energies are required to process these reactions, therefore, evidently slowing down the dye degradation rate.

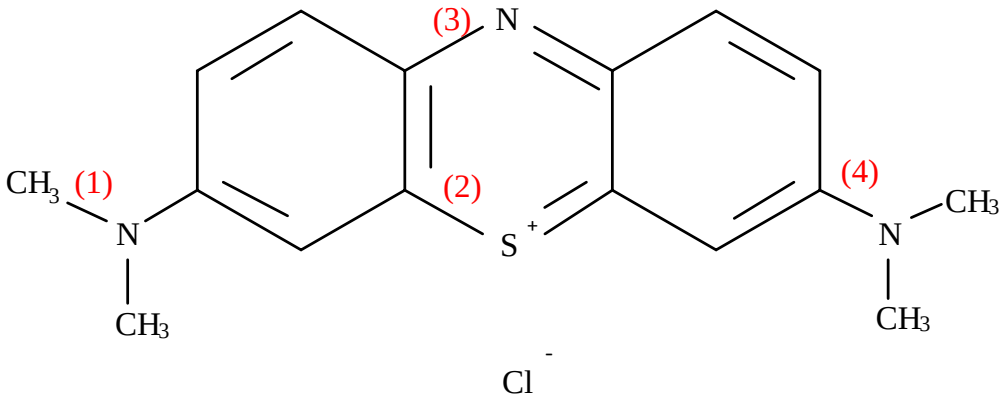

Figure 9.14 Schematic of methylene blue dye molecule.

After 5 minutes of treatment, the MB concentrations were reduced to 37 mg/L, 23 mg/L and 5.1 mg/L for pH 2.9, 7 and 11.5 solutions, respectively. The amino-groups ($-NH_2$) were formed when all methyl groups ($-CH_3$) have been removed and replaced by hydrogen. The reactive species start to attack the bond between amino-group and aromatic ring with a bond energy of 102.6±1 kcal/mol, leading to further degradation of MB molecule. A very shallow green colour was observed after 5 minutes of treatment in all pH solutions, which indicated the removal of the majority of MB dye.

In O_2 discharges in contact with water, the effect of excited oxygen atom reaction with water and the O_3 decomposition in water are considered to be responsible for the OH radical formation [24, 25]. The highest degradation rate was achieved for the initial solution pH of 11.5. The high degradation rate may be due to the large amounts of O_3 decomposition in basic solution. This result is in opposition to that recorded in previous experiments in this thesis, where the H_2O_2 production was significantly reduced in basic solutions (5-mM NaOH). One of the possibilities is that when target reactants, MB and its decomposition products exist in the solution, the OH radicals react with target reactants first rather than react with OH^- ions or process the dimerization reaction. Another option is that the OH^- ions in solution led to a higher dissolving and decomposition rate of O_3 in solution, leading to the production of a series of reactive species (Table 9.2) [126], thus increasing the MB dye degradation rate.

Table 9.2 Decomposition reactions of O_3 in basic solution [126]

Reactions	
$O_3 + OH^- \rightarrow O_2 + HO_2^-$	(R 9.1)
$O_3 + e \rightarrow O_3^-$	(R 9.2)
$HO_2^- + O_3 \rightarrow HO_2^{\cdot} + O_3^-$	(R 9.3)
$HO_2^{\cdot} + OH^- \rightarrow H_2O + O_2^-$	(R 9.4)
$O_2^- + O_3 \rightarrow O_2 + O_3^-$	(R 9.5)
$O_3^- + H_2O \rightarrow OH^{\cdot} + O_2 + OH^-$	(R 9.6)
$O_3^- + OH^{\cdot} \rightarrow O_2^- + HO_2^{\cdot}$	(R 9.7)
$O_3^- + OH^{\cdot} \rightarrow OH^- + O_3$	(R 9.8)
$OH^{\cdot} + O_3 \rightarrow HO_2^{\cdot} + O_2$	(R 9.9)

The reaction chain is initiated by O_3 reacting with OH^- ions in basic solution to form HO_2^- ions (R 9.1), which is neutralized by transferring attached electron to O_3 molecules (R 9.3). The O_3 negative ion can react with water, leading to the production of OH radicals, O_2 and hydroxide ions (R 9.6). Other reactive species such as $HO_2^{\cdot}$, O_2^-, O_3^- can also be produced during O_3 decomposition. Reactions R 9.7-9.9 show the propagation and termination reactions of OH radicals. The O_3 decomposition rate can be enhanced by increasing solution pH. With a higher solution pH, more OH radicals can be formed, thus reducing the selective manner of O_3 treatment and increasing the reaction rate. Hoigne [127] investigated O_3 decomposition in alkaline solutions and found that neutral pH solutions do not improve the dissolving and decomposition rate of O_3; the oxidation of organic compounds in high pH solutions is more efficient.

Sehested [128] investigated O_3 decomposition in acidic solutions and found that the dissociation of O_3 in solution leads to the formation of oxygen atoms (R 9.10), which can react with water to produce OH radicals (R 9.11). They concluded that the O_3 decomposition chain was initiated by O_3 reacting with OH radicals to form HO_2 radicals (R 9.12). The slow reaction rate of HO_2 radicals with O_3 leads to high stability of O_3 (R 9.13) in acidic solutions. The dissociation of HO_2 radicals in solution leads to the decomposition of O_3 (R 9.14-R 9.17).

Table 9.3 The decomposition reactions of O_3 in acidic solutions [128]

Reactions	
$O_3 \leftrightarrow O + O_2$	(R 9.10)
$O + H_2O \rightarrow 2\ OH^{\cdot}$	(R 9.11)
$OH^{\cdot} + O_3 \rightarrow HO_2^{\cdot} + O_2$	(R 9.12)
$HO_2^{\cdot} + O_3 \rightarrow OH^{\cdot} + 2O_2$	(R 9.13)
$HO_2^{\cdot} \rightarrow O_2^{-} + H^{+}$	(R 9.14)
$O_2^{-} + O_3 \rightarrow O_3^{-} + O_2$	(R 9.15)
$O_3^{-} + H^{+} \rightarrow OH^{\cdot} + O_2$	(R 9.16)
$OH^{\cdot} + HO_2^{\cdot} \rightarrow H_2O + O_2$	(R 9.17)

Tert-butanol effect

Figure 9.15 shows the effect of TB during plasma treatments with acid solution of pH 2.9. The differences of 18.5%, 14% and 11%, were recorded between the treatments without and with TB, respectively, after 1, 3 and 5 minutes of treatment; the O_3 dissociation in acid solution into OH radicals is very limited with pH 2.9 solution.

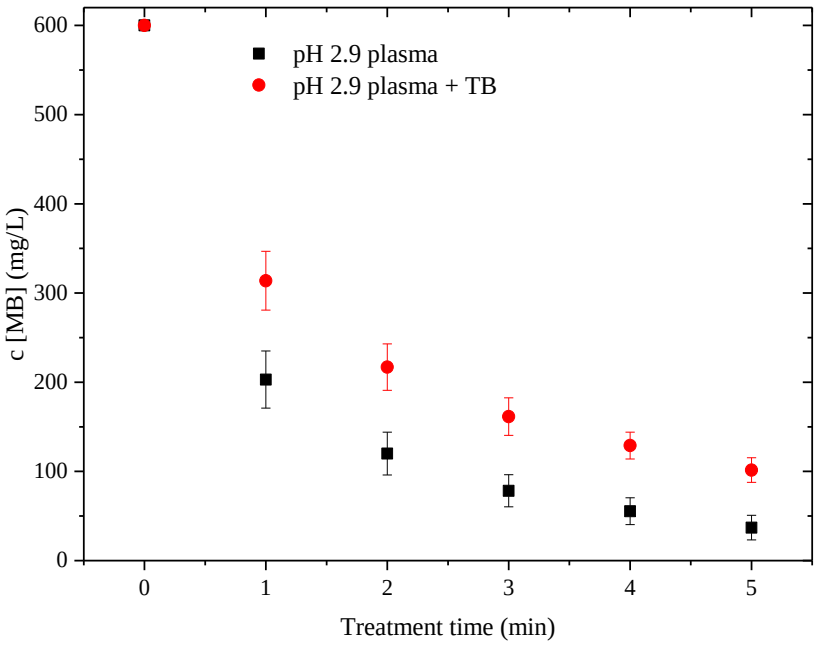

Figure 9.15 Effect of TB on MB dye degradation in pH 2.9 solution.

In solutions of pH 7 (Figure 9.16), the TB effect was increased to 20.3%, 19% and 18% after 1, 3 and 5 minutes of treatment, respectively. Larger differences of 25.6%, 28% and 22% were observed in basic solution of pH 11.5 (Figure 9.17), after 1, 3 and 5 minutes of treatment, respectively. Grabowski [95] investigated phenol removal under positive pulsed corona discharges in air and found that the addition of TB in solution decreased the degradation yield by 12.8 %.

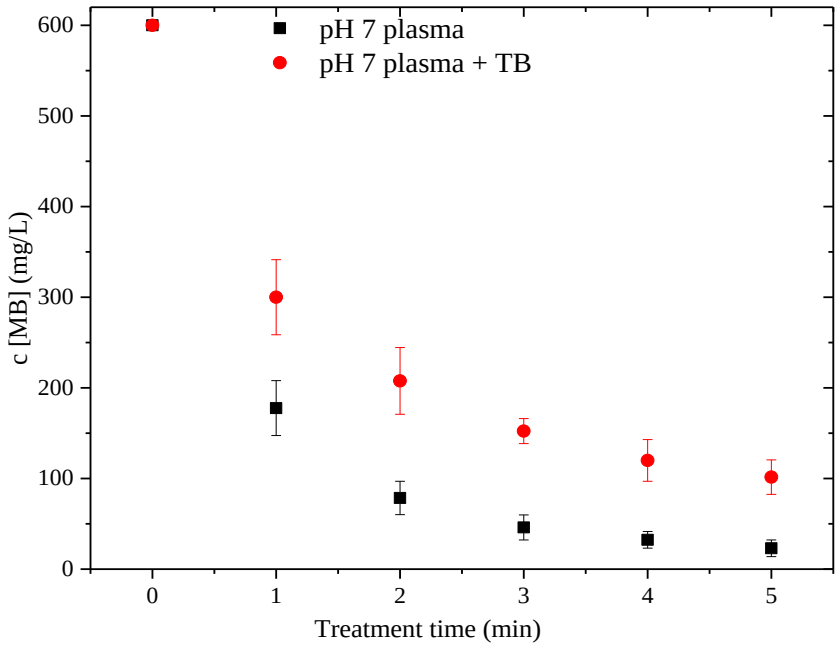

Figure 9.16 Effect of TB on MB dye degradation in pH 7 solution.

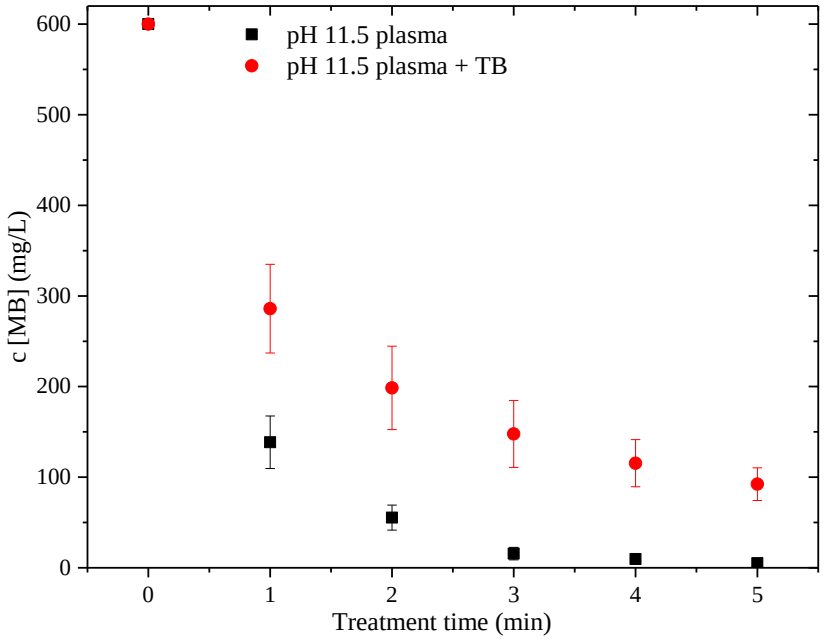

Figure 9.17 Effect of TB on MB dye degradation in pH 11.5 solution.

Smaller gas bubble sizes, due to the gas injection, were observed during the treatments when TB was used, compared to those with no TB was added; this phenomenon was also recorded in Lopez's study [108]. This could be due to the fact that TB acts as a surfactant in solution. Lopez investigated the influence of TB, with a concentration of 10^{-3} mol/L, in mass transfer during bubbling-up oxidation processes and found that the additional TB reduced the bubble size compared to that recorded in no-TB conditions. Equation 9.1 and 9.2 shows the calculation of bubble sizes without and with additional TB. Lopez found that the interfacial area was increased with increasing gas velocity; also, the addition of TB enhances the interfacial area by approximately 30%, due to the reduction of gas bubble size.

$$d_{no-TB} = 0.14U_G + 3.06 \times 10^{-3} \quad \text{(Eq. 9.1)}$$

$$d_{TB} = 0.133U_G + 1.94 \times 10^{-3} \quad \text{(Eq. 9.2)}$$

d Average of gas bubble size in the unit of mm

U_G Gas velocity in the unit of m/s

The changing size of the bubbles and the change in surface area could affect the production of H_2O_2. The influence of bubble size will be affected by the chemical reaction pathways involved in H_2O_2 production and their relative importance. There is insufficient information at present to allow the influence of this effect to be calculated.

9.6.2 Variation of MB dye solution pH

Without the addition of TB in basic solutions, the pHs were reduced from 11.5 to 4.5 after 5 minutes of treatment (Figure 9.18). However, when TB was used, the H^+ ions production was significantly inhibited; the pH after 5 minutes of treatment was recorded as 10.1. In O_2 plasma treatment for methylene blue degradation, the change in solution pH was attributed to the degradation of MB dye, leading to the production of organic and inorganic ions such as SO_4^{2-}, Cl^- and NO_3^-. The application of TB which scavenged the OH radicals, slowed down the degradation of the dye molecules, leading to a slower pH reduction rate.

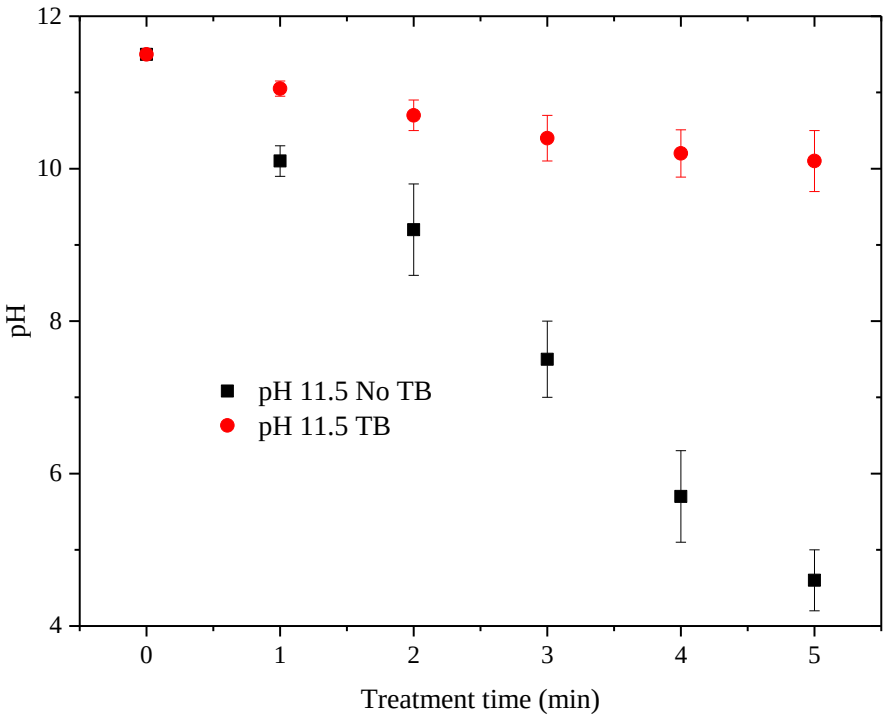

Figure 9.18 Effect of TB on the variation of solution pH in pH 11.5 MB dye solution.

With addition of TB, almost no solution pH variation (<0.1) was observed in the acid solutions of pH 2.9. The solution pH reductions were generally observed in organic dye degradation, due to the cleavage of acid elements from compound molecules to generate acid radicals (Figure 9.19-9.21) [34]. Reddy [85] investigated the methylene blue degradation by the liquid phase DBD and also observed the solution pH reduction from pH 7 to less than 2.

9.6.3 Discussion

The degradation of methylene blue leads to the final production of CO_2 and inorganic ions such SO_4^{2-}, Cl^- and NO_3^-. However, different oxidation pathways of MB degradation have been suggested for different methods of MB dye treatments.

Huang [123] investigated the MB degradation mechanism in air plasma and found that the colour of the treated samples changed with time from dark blue to dark purple and then to green, which were similar to the phenomena observed in this research. However, the variation of solution colour from blue to purple and green were not observed in all methylene blue degradation studies. For example, Tang [129] investigated MB degradation by photocatalytic reactions and observed the blue colour becoming lighter during treatments rather than transit to a different colour. This could be due to the different degradation mechanisms of MB by various treatments.

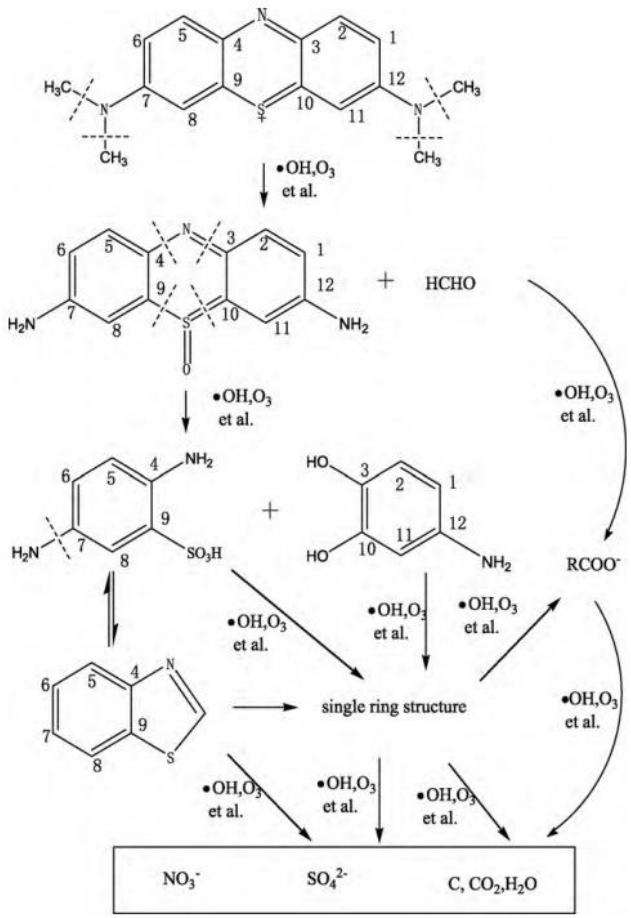

Figure 9.19 The degradation path of the methylene blue molecule [123].

Huang [123] used an emission spectrum and found that the main oxidants produced at the plasma-water interface were O_3, $OH^{\cdot}$, H_2O^+, N_2O^+. Huang also used a GC-MS to determine the intermediate products of MB degradation and concluded that the first step of MB degradation is the cleavage of bonds of methyl from amidogen (CH_3-N(CH_3)-) with a relatively low energy (Table 9.1) (Figure 9.19). The second step is the cleavage of bonds between the two aromatic rings, separating the dye molecules into two aromatic compounds. The amidogen and sulphate groups were replaced by hydroxyl radicals, reducing the molecular weight of compounds and lead to further oxidation of the aromatic ring to generate organic acid, which can result in the solution pH reduction. Finally, organic acids were further degraded into CO_2.

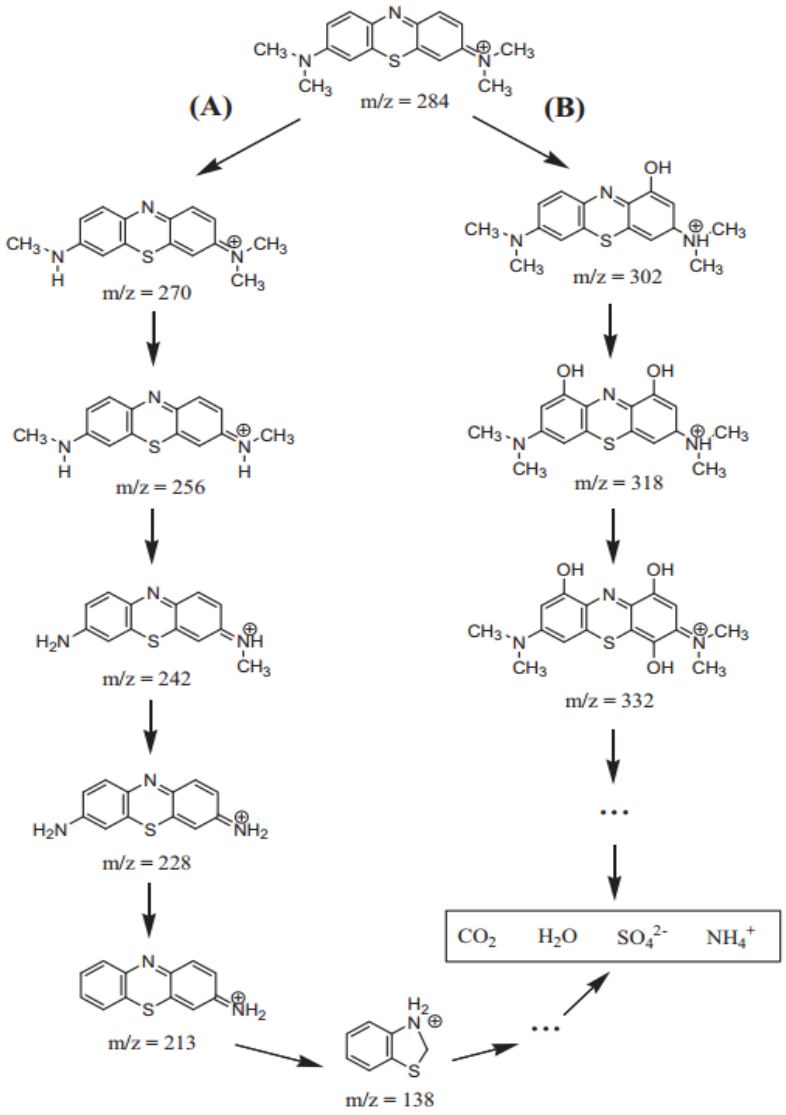

Figure 9.20 The degradation path of the methylene blue molecule [130].

Benetoli [130] investigated the MB degradation by pin-to-water electrode discharges and used pyrite as a catalyst, leading to the decomposition of generated H_2O_2 into OH radicals. Benetoli concluded the dye degradation pathways are (i) high energy electron impact reactions, leading to the removal of functional groups on aromatic rings and the separation of heterocyclic compounds into aromatic compounds; and (ii) consecutive attachment of OH radicals to the benzene ring, leading to the increase of molecular weight and the cleavage of aromatic rings (Figure 9.20). The second pathway was also reported in Oliveira's study [131]. Xue [132] investigated the hybrid DBD for Alizarin Red degradation and concluded that the first step for organic dye degradation is to remove the functional groups that are attached to the heterocyclic compounds, which is similar to the conclusion in Benetoli's study [130].

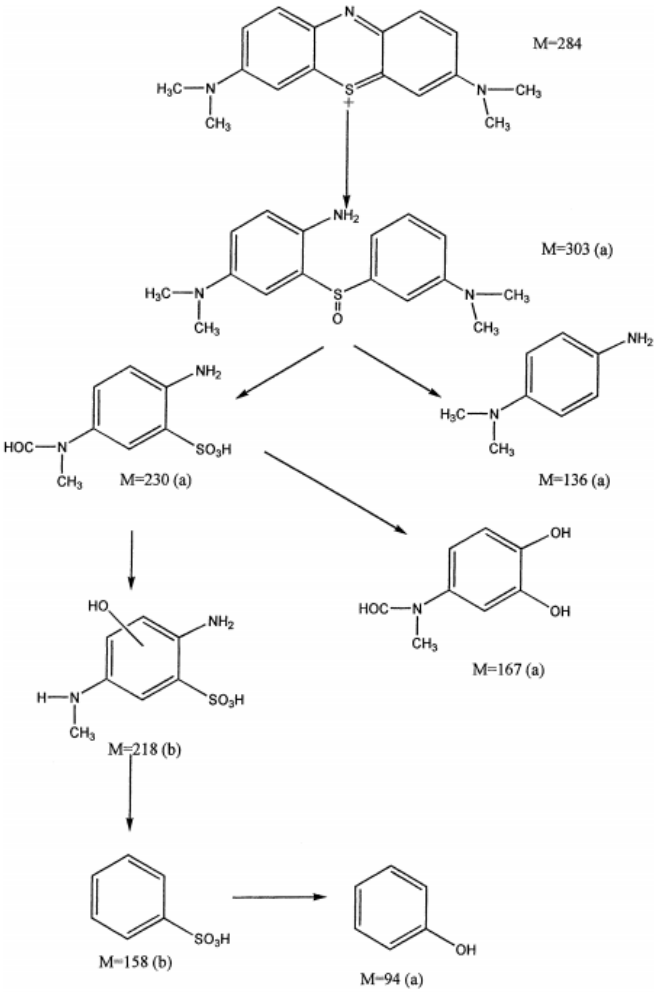

Figure 9.21 Photocatalytic degradation pathway of methylene blue; detected by GC/MS (a), detected by LC/MS (b) [133].

Houas [133] investigated the degradation pathway of methylene blue under photo-catalysis treatment and concluded that the initial degradation step was to break the C-S^+=C bonds, resulting in the formation of sulphate ions; this opinion is significantly different from the one recorded in Huang's study. Houas also employed GC-MS and LC-MS to identify the intermediates during MB degradation, and concluded that the reaction pathways are (i) cleavage of the bond between amino and aromatic ring (C_6H_5-NH-C_6H_5), (ii) reaction of C-S^+=C bonds with OH radicals (R 9.18), leading to the cleavage of the bond between sulphur and aromatic ring, separating the dye molecules into two aromatic compounds (Figure 9.21).

$$R\text{-}S^+\text{-}R' + OH^\cdot \rightarrow R\text{-}S(=O)\text{-}R' + H^+ \quad \text{(R 9.18)}$$

Reddy [85] found that the degradation of MB resulted in a significant amount of sulphate production. They investigated the effect of SO_4^{2-} ions on MB degradation and found the degradation rate was slightly (5-10%) increased when 50 mg/L of Na_2SO_4 was added to 100 mg/L MB solution. During the treatments, SO_4^{2-} ions can react with OH radicals (R 9.19) to form $SO_4^{-\cdot}$ and OH^- ions. The $SO_4^{-\cdot}$ ion has an oxidation potential of 2.6 V, which is comparable to that for OH radicals of 2.8 V.

$$SO_4^{2-} + OH^\cdot \rightarrow SO_4^{-\cdot} + OH^- \quad \text{(R 9.19)}$$

Multiple studies have recorded the effect of solution pH on the oxidation potential of reactive species. Hoigne [127] found that the oxidation potential of O_3 is 2.08 V in acid solution, however, decreased to 1.4 V in basic solution. Gao [134] determined that the oxidation potential of OH radicals reached a maximum of 2.7 V in solutions of pH 3, and dropped to 2.34 V in solutions of pH 9. Therefore, the oxidation potential of various reactive species in different pH solutions needs to be further investigated. This will provide information that will allow the feasibility of non-thermal plasma treatment to be applied to solution s with non-neutral pH. It may also be possible to tune the discharges conditions to maximize the production of reactive species with a high oxidation potential for a given pH value.

9.7 Conclusion

A DBD configured reactor with a porous PTFE plate was used in this experiment. The porous PTFE allows the development of plasma filaments through the micro-pores, leading to the production of reactive species at the plasma-water interface. Currents with small amplitudes were recorded under V_{pp} of <15.5 kV, indicating the discharges occur between the glass plate and the PTFE plate. Threshold voltages of 16 kV, 17.5 kV and 15.5 kV in O_2, N_2 and air, respectively, are required to initiate the electrical breakdown through the micro-pores to the water surface; in this case, a significant increase of the impulsive current was observed.

The highest H_2O_2 production yield of 1.1 g/kWh was obtained in O_2 treatment with ultrapure water. Due to the results that no H_2O_2 production was detected under negative impulsive current discharges in O_2 (Chapter 6), the H_2O_2 production recorded in O_2 DBD can be fully attributed to the effect of the positive impulsive currents. Although no nitrite or nitrate acid was detected in O_2-treated samples, the solution conductivity increase recorded in O_2 was higher than that in N_2, which could be due to the electron attachment reactions occurring at the plasma-water interface. In air and N_2 treatments, the added TB determined that 6.7% and 61% of H_2O_2 was generated from the dimerization of OH radicals, respectively. The effect of OH^- ions was investigated, a significant reduction of 100%, 47% and 45% of the H_2O_2 production in O_2, N_2 and air, respectively, was recorded.

In terms of O_2 plasma for MB degradation, no significant effect of initial solution pH was recorded. The highest MB dye degradation yield of 310 g/kWh was achieved within the first minutes of treatment in solutions of pH 11.5. The degradation rate of MB dye was slowed down by the production of hard-degraded intermediate matter. The required energy for bond breakage ranges from 70.8 J to 102.6$\pm$1 kcal/mol (Table 9.1). The transition of sample colours from dark blue→ dark purple→ dark green→ light green→ transparent was observed, which presented the different intermediate products of MB. After 5 minutes of O_2 plasma treatment, 94%, 96% and 99% of MB dye were discoloured in solutions of pH 2.9, 7 and 11.5, respectively.

The addition of TB indicated that OH radicals contributed to up to 28% of MB dye degradation in various pH solutions. A solution pH reduction after 5 minutes of treatment was recorded, which indicated the production of organic and inorganic acids due to the degradation of MB molecules.

9.8 Further work

The DBD characteristics in various gases need to be further investigated. Various gas flow rates can lead to different contact time of the charged particles with water; in this case, the effects of gas flow rates need to be investigated. On the other hand, the effect of the pore number on the PTFE layer on reactive species productions can be investigated in the future. The remarkable solution conductivity changes in O_2 treatment need to be investigated further.

The methylene blue degradation in plasma with various gases such as N_2 and helium needs to be investigated, in which cases neither O_3 nor excited O atoms attend but only electrons and ions take part in degrading the organic compounds; TB can be added to obtain the OH radical formation without any oxygen element effect. In addition, the intermediate products need to be investigated by either physical or chemical methods. Huang [123] employed sodium carbonate as a radical scavenger and the degradation rate of MB was observed to decrease with increasing scavenger concentration; in this case, the effect of the concentration of OH radical scavengers needs to be further investigated.

.

10 CONCLUSION

This research employed various experimental systems to investigate the (i) effect of solution conductivity on discharge current behavior; (ii) OH radical formation in different gases; (iii) difference of DC glow and impulsive current discharges; (iv) effect of flow liquid cathode; (v) effect of solution pH change and (vi) OH radical effect on methylene blue degradation. Table 10.1 shows the main factors included in the experiment for each chapter.

Table 10.1 Experimental factors for each chapter

Chapter No.	*4*	*5&6*	*7&8*	*9*
DC power	▲	▲	▲	
High frequency power				▲
Various conductivity	▲	▲	▲	
Oxygen		▲		▲
Nitrogen		▲	▲	▲
Helium		▲	▲	
Air	▲	▲	▲	▲
Tert-butanol		▲	▲	▲
Various pH	▲	▲	▲	▲
MB dye degradation				▲

10.1 Discharge characteristics

Positive impulsive current discharges in open air

The characteristics of impulsive current discharges were investigated in open air under positive and negative polarity. Various solution conductivity and different discharge current was employed to investigate the effect on discharge current. Under electrical discharges above ultrapure water, impulsive discharge currents with amplitudes of several tens of mA and pulse width of ~15 ns were recorded at the start of discharge under positive polarity. The inhibition of discharge occurred due to the accumulation of charges on the water surface. Increasing the treatment time raised the solution conductivity and the impulsive current amplitude, and decreased the charge accumulation effect. The discharge was no longer stable when the solution conductivity was increased to 3.5 µS/cm and a wavy voltage waveform occurred. A long-duration charging period started to occur when the solution conductivity was increased to 5.5 µS/cm.

The transition of discharge type from impulsive to impulsive-diffuse discharge was noticed when the solution conductivity was increased to 17.5 µS/cm, in which case most of the high-repetition-rate pulses were replaced by a tail current. Further increases in the solution conductivity raised the amplitude and reduced the duration of the discharge current. After 20 minutes of discharge above ultrapure water, the solution conductivity was increased from the original value of 0.5 µS/cm to 72 µS/cm.

A similar discharge current waveform was measured in the electric discharge above tap water (65 µS/cm). No significant difference was observed when the discharge occurred with solution conductivity from 65 to 108 µS/cm. Further increases in solution conductivity by using different concentrations of NaOH increased the amplitude of the discharge current and decreased the duration of the tail current. Moreover, increased solution conductivity reduced the interval between the impulsive current and the tail current. A spark discharge with current amplitude of ~1 A occurred when the solution conductivity was increased to >12 mS/cm.

Positive impulsive current discharges in sealed reactor with air, nitrogen and helium

Under the positive impulsive current discharges in N_2 above ultrapure water, an impulsive discharge was recorded at the beginning of treatment. As recorded in air discharges, a transit of discharge type into impulsive-diffuse discharge was noticed when the solution conductivity was increased to 133 µS/cm in N_2. The amplitude of the tail currents in N_2 discharges is higher than those recorded in air, which indicated that a stronger diffuse discharge was generated. Under the positive impulsive current discharges in helium above ultrapure water, corona discharges were recorded; however, different from those recorded in air and N_2, the discharge transition to diffuse type was not observed in helium with increased solution conductivity. In addition, the solution conductivity change in helium reached 88 µS/cm, and this phenomenon needs to be further investigated.

Under the positive impulsive current discharge above 5-mM NaOH solution, corona-diffuse discharge was observed in air, N_2 and helium. The discharge current recorded in N_2 obtained lower impulsive current amplitude, followed by a tail current with a higher amplitude. In helium discharges, no clear separation of the impulsive and the tail current can be observed. In this case, the transition of discharge type in N_2 and helium needs to be investigated in detail in the future.

Under the controlled impulsive discharges, a tail current component was observed in all gas treatments, which indicated the development of a diffuse discharge after the impulsive current discharge. Under positive polarity, the amplitude of the discharge currents in O_2 and N_2 were slightly higher (~150 mA) than those recorded under negative polarity. On the other hand, a significant reduction of current amplitude from ~800 mA to ~200 mA was recorded under negative helium discharges.

Positive DC discharges

A DC glow discharge was developed with a pin-to-water electrode structure. The lifting of the ultrapure-water (0.5 µS/cm) surface, which leads to the connection of water to the pin electrode, was noticed; the problem was solved by using tap water (65 µS/cm). A depression of the tap water surface, which formed a depression region, was observed after the inter-electrode breakdown; the diameter of the depression region decreased with increasing solution conductivity.

Negative impulsive current discharges in open air

Under negative polarity, a DC corona discharge was generated above ultrapure water, which then transited into DC glow discharge after 20 minutes of treatment, when the solution conductivity was increased to 21 µS/cm. The current waveforms observed with solution conductivity ranging from 65 µS/cm to 22 mS/cm have a similar appearance to the impulsive currents recorded under positive polarity; also, the amplitude of the impulsive current was slightly higher under negative polarity. Increasing the applied voltage raised the repetition rate and the amplitude of the discharge current, moreover reducing the interval between the impulsive and the tail current. It was found that the discharge characteristics are polarity and solution conductivity dependent.

Dielectric barrier discharge

The breakdown at the inter-electrode between the glass plate and the PTFE plate was initiated with a peak-to-peak applied voltage of <15.5 kV; low-amplitude currents were noticed (<10 mA) in this case. Threshold voltages of 16 kV, 17.5 kV and 15.5 kV in O_2, N_2 and air, respectively, are required to initiate the inter-electrode breakdown through the micro-pores, resulting in a significant increase of the impulsive current amplitude, from ~10 mA to ~48 mA, in all gas treatments. The amplitudes of the negative discharge currents observed in O_2 were higher than that obtained under positive polarity; however, a converse result was observed in N_2.

10.2 Chemical reactions

Positive impulsive current discharges

OH radical and H_2O_2 production have been investigated in air, N_2, O_2 and helium discharges above ultrapure water and 5-mM NaOH solutions. The highest H_2O_2 production was recorded in helium discharges above ultrapure water, corresponding to an OH radical yield of 20 µmol. The addition of tert-butanol terminated the dimerization of OH radicals in ultrapure water which contributed to 4%, 74% and 68% of the H_2O_2 production in air, N_2 and helium, respectively. A remarkable scavenging of OH radicals was noticed in the discharges above 5-mM NaOH solution, which led to a significant difference of up to 183 times between the fluorescence- and UV-spectrometry methods. Therefore, the applicability of fluorescence spectrometry by using TA solution to measure OH radical formation needs to be further investigated.

Under controlled positive impulsive current discharges, H_2O_2 energy yields of 1.1 g/kWh was recorded in N_2 and helium discharges, which is higher than the 0.95 g/kWh and 0.62 g/kWh that recorded in O_2 and air, respectively. The highest charge/H_2O_2 ratio of 1:26 was recorded in N_2 and O_2 and the lowest ratio of 1:0.74 was recorded in air treatment. It was determined by tert-butanol studies that 86% and 57% of H_2O_2 production in N_2 and helium treatments, respectively, is via OH dimerization.

Positive DC discharges

A significant amount of water vapour was generated under positive DC glow discharges, due to the energy transfer from positive ions to water molecules. The discharge powers were recorded ranging from 2.35 to 3.54 W in air, N_2 and helium. A dramatic solution conductivity and pH variation was recorded when no gas flow was introduced during treatments. With a gas flow of 0.3 L/min, H_2O_2 production was significantly increased, and the energy yield reached 1.9, 1.4 and 1.6 g/kWh in air, N_2 and helium, respectively. The highest H_2O_2 energy yield was achieved in air discharge, which is in opposition to results obtained under impulsive current discharges. The higher charge/H_2O_2 ratios of 1:1.03 and 1:1 were recorded in air and N_2, respectively, while a lower ratio of 1:0.88 was recorded in helium. The added OH radical scavenger determined that 48%, 93% and 100% of H_2O_2 production obtained in air, N_2 and helium with a gas flow of 0.3 L/min, respectively, was via OH dimerization. These results are different from those recorded under impulsive current

discharges, indicating the different mechanisms of reactions occur at the plasma-water interface. In helium treatments, the highest H_2O_2 energy yield of 1.65 g/kWh was achieved with a gas flow of 0.1 L/min. The water vapour amount has a critical effect on H_2O_2 production; the inhibition of H_2O_2 production occurred when a gas flow of ≤ 0.06 L/min was introduced; however, increasing the flow rate to > 0.5 L/min led to the reduction of H_2O_2 production. Therefore, the effect of various gas flow rates on plasma-water interface reactions needs to be further investigated.

It was found that the solution pH (acid and basic) have a negative effect on H_2O_2 production. Compared to the ratio of 1:1.03 recorded in tap water, the ratios in solutions of pH 4 and pH 3.2 decreased to 1:0.95 and 1:0.72, respectively. On the other hand, the ratio in the solution of pH 12 and pH 13 decreased to 1:0.82 and 1: 0.1.

Negative impulsive current discharges

Under negative impulsive current discharges, no H_2O_2 production was detected in O_2, N_2, air and helium discharges. On the other hand, a significant increase of solution conductivity being observed in O_2, which should be due to the electron attachment reaction occurred at the plasma-water interface. The solution conductivity variation under negative discharges in air and N_2 was reduced by 70% and 99%, respectively, compared to that recorded under positive discharges.

Negative DC discharges

No H_2O_2 production was observed in air, N_2 and helium treatments under negative DC glow discharges. The solution conductivity variations under negative discharges were reduced by ~78% in air and N_2. In helium treatment, the increase of solution pH was recorded under a gas flow of 0.3 L/min, and this phenomenon needs further investigation.

Dielectric barrier discharge

The highest H_2O_2 production observed in the DBD treatment occurred in O_2; a yield of 1.1 g/kWh was recorded in the discharges with ultrapure water. Due to no H_2O_2 production being detected under negative impulsive current discharges in O_2 (Chapter 6), the H_2O_2 production observed in O_2 DBD can be fully attributed to the effect of the positive impulsive currents.

Under discharges with NaOH solutions, a significant reduction of 45% and 47% of H_2O_2 production in N_2 and air, respectively, was recorded; also, no H_2O_2 production was detected in O_2-treated samples, indicating the scavenging of OH^- ions not only occurred with H_2O_2 and OH radicals, but also with O atoms.

In terms of methylene blue degradation, no significant effect of initial solution pH value was recorded in Air, N_2 and O_2 treatments. The required energy for bond breakage ranges from 70.8 J to 102.6$\pm$1 J; the highest MB dye degradation yield of 310 g/kWh was achieved within the first minutes of treatment in pH 11.5 solution. The reaction rates of MB dye in various pH solutions were all slowed by more-difficult-to-degrade compounds after the first oxidation stage. After 5 minutes of O_2 plasma treatment, 94%, 96% and 99% of MB dye were discoloured in pH 2.9, 7 and 11.5 solutions, respectively. The transition of sample colours from dark blue to light green was observed, which illustrated the different intermediate products of the MB dye. The employed TB indicated that ~28% of this dye was degraded by OH radical reactions in various pH solutions.

10.3 Conclusion

The variation of discharge behaviour with different solution conductivity, power polarity, and working gas has been clarified in this research. The variation of H_2O_2 production with different discharge type, solution pH, working gas, gas flow rates, liquid flow rates and power polarity has been investigated in this research. The highest H_2O_2 production of 1.9 g/kWh was achieved under positive DC glow discharges with an introduced gas flow of 0.3 L/min.

This thesis has achieved desired results to clarify discharge characteristics and H_2O_2 production pathways for above-water discharges. This research fills the gap of the variation of discharge current under pin-to-water electrode discharge with different solution pHs, and improves the H_2O_2 production yield compared to most previous studies.

This thesis has achieved desired results to clarify discharge characteristics and H_2O_2 production pathways for above-water discharges. This research fills the gap of the variation of discharge current under pin-to-water electrode discharge with different solution pHs, and improves the H_2O_2 production yield compared to most previous studies.

The research demonstrated a method for simple and more affordable water treatment systems by using DC power supply and high voltage capacitor, thus getting rid of the expensive pulsed power system.

This research clarified that the negative impulsive current discharges is poor generator of H_2O_2.

In addition, this research investigated a system working with a flowing water cathode and found the H_2O_2 production yield increased.

This research also found the applicable of OH radical measurement method by using terephthalic acid (TA) is doubtful due to the requirements for a basic solution which itself effects the concentration of OH radicals in the system.

11 REFERENCE

[1] B.R. Locke (2011). *Review of the Methods to Form Hydrogen Peroxide in Electrical Discharge Plasma with Liquid Water.* Plasma Sources Sci. Technol. *Vol. 20, No. 3,* 034006

[2] A. Fridman (2012). *Plasma Chemistry.* Cambridge University Press. ISBN-13: 978-1107684935

[3] P. Jamro'z (2014). *Atmospheric Pressure Glow Discharges Generated in Contact with Flowing Liquid Cathode: Production of Active Species and Application in Wastewater Purification Processes.* Plasma Chem. Plasma Process. *Vol. 34 (1),* pp. 25–37

[4] S. M. Thagard (2009). *Chemistry of the Positive and Negative Electrical Discharges Formed in Liquid Water and Above a Gas-Liquid Surface.* Plasma Chem. Plasma Process. *Vol. 29,* pp. 455-473

[5] A. F. Gaisin (2005). *Vapor-Air Discharges between Electrolytic Cathode and Metal Anode at Atmospheric Pressure.* High Temperature. *Vol. 43, No. 1,* pp. 001–007

[6] V. A. Titov (2006). *Experimental and Theoretical Studies on the Characteristics of Atmospheric Pressure Glow Discharge with Liquid Cathode.* Plasma Chem. Plasma Process *Vol. 26 (6),* pp 543–555

[7] Y. Zhao (2016). *Hydroxyl Radicals and Hydrogen Peroxide Formation at Non-thermal Plasma–Water Interface.* IEEE Transactions on Plasma Science. *Vol. 44, No. 10*

[8] R. Andreozzi (1999). *Advanced Oxidation Processes (AOP) for Water Purification and Recovery.* Catalysis Today. *Vol. 53 (1),* pp. 51–59

[9] R. Atkinson (1987). *Estimation of OH Radical Reaction Rate Constants and Atmospheric Lifetimes for Polychlorobiphenyls, Dibenzo-p-dioxins, and Dibenzofurans.* Environ. Sci. Technol. *Vol. 21 (3),* pp. 305-307

[10] J. Wang (2012). *Advanced Oxidation Processes for Wastewater Treatment: Formation of Hydroxyl Radical and Application.* Critical Reviews in Environ. Sci. and Technol. *Vol. 42 (3),* pp. 251-325

[11] R. Munter (2001). *Advanced Oxidation Processes-Current Status and Prospects.* Proc. Estonian Acad. Sci. Chem. *Vol. 50 (2),* pp. 59–80

[12] M. J. Kirkpatrick (2004). *Plasma-Catalyst Interactions in Treatment of Gas Phase Contaminants and in Electrical Discharge in Water.* Electronic Theses, Treatises and Dissertations. Paper 2884.

[13] V. Scholtz (2015). *Nonthermal plasma-A tool for Decontamination and Disinfection.* Biotechnology Advances. *Vol. 33 (6),* Part 2, pp. 1108–1119

[14] J. Meichsner (2012). *Nonthermal Plasma Chemistry and Physics.* Edited by Hans-

Erich Wagner. CRC Press. Print ISBN: 978-1-4200-5916-8

[15] T. Fujii (2008). *Characteristics of Pulse Corona Discharge over Water Surface*. Journal of Physics: Journal of Physics: Conference Series, *Vol.142, No. 1,* 012070

[16] M. H. Valsero (2013). *Removal of Priority Pollutants from Water by Means of Dielectric Barrier Discharge Atmospheric Plasma.* Journal of Hazardous Materials. *Vol. 262,* pp. 664–673

[17] B. Benstaali (1998). *Plasma Treatment of Aqueous Solutes: Some Chemical Properties of a Gliding Arc in Humid Air*. The European Physical Journal Applied Physics. *Vol. 4,* pp. 171-179.

[18] A. Hickling (1971). *Electrochemical Processes in Glow Discharge at the Gas Solution Interface.* Modern Aspects of Electrochemistry. *No. 6,* pp. 329-373

[19] X. Liao (2017). *Inactivation Mechanisms of Non-thermal Plasma on Microbes: A Review*. Food Control. *Vol. 75,* pp. 83-91

[20] T. Verreycken (2010). *Spectroscopic Study of an Atmospheric Pressure DC Glow Discharge with a Water Electrode in Atomic and Molecular Gases.* Plasma Sources Sci. Technol. *Vol. 19,* 045004

[21] K. Hensel (2015). *Effects of Air Transient Spark Discharge and Helium Plasma Jet on Water, Bacteria, Cells, and Biomolecules.* Biointerphases. *Vol. 10 (2),* 029515

[22] S. Kanazawa (2009). *Time Resolved Imaging of Pulsed Streamer Discharge at the Air/Water Interface concentration and applied voltage*. J. Plasma Fusion Res. SERIES, *Vol. 8*

[23] J.A. Robinson (1997). *A New Type of Ozone Generator Using Taylor Cones on Water Surfaces*. IEEE Industry Applications Society Annual Meeting New Orleans, Louisiana, October 5-9.

[24] S. Emile (2015). *Degradation of Organic Pollutants and Microorganisms from Wastewater using Different Dielectric Barrier Discharge Configurations-A Critical Review*. Environ. Sci. Pollut. Res. *Vol. 22 (23),* pp. 18345–18362

[25] P. Lukes (2005). *Generation of Ozone by Pulsed Corona Discharge over Water Surface in Hybrid Gas-Liquid Electrical Discharge Reactor.* J. Phys. D: Appl. Phys. *Vol. 38, No.3,* pp. 409-416

[26] S. Matejcik (1997). *Electron Attachment to Molecules and Clusters of Atmospheric Relevance: Oxygen and Ozone.* Plasma Sources Sci. Technol. *Vol. 6,* pp. 140–146

[27] E. M. V. Veldhuizen (2001). *Corona Discharges: Fundamentals and Diagnostics.* Frontiers in low temperature plasma diagnostics Conference, pp. 40-49

[28] A. Y. Nikiforov (2006). *Breakdown Process and Corona to Spark Transition between Metal and Liquid Electrodes.* Czechoslovak Journal of Physics, *Vol. 56, Supplement 2,* pp. B952–B957

[29] B. Eliasson (1991). *Nonequilibrium Volume Plasma Chemical Processing*. IEEE

Transactions on Plasma Science, *Vol. 19, No. 6*

[30] Z. Xiong (2013). *On the Electrical Characteristic of Atmospheric Pressure Air/He/O_2/N_2/Ar Plasma Needle.* IEEE Transactions on Plasma Science, *Vol. 41 (7),* pp. 1746-1750

[31] R. Ohyama (2007). *Schlieren Optical Visualization for Transient EHD Induced Flow in A Stratified Dielectric Liquid Under Gas-Phase AC Corona Discharges.* J. Phys. D: Appl. Phys. *Vol. 40, No.2,* pp. 573–578

[32] V. Karanassios (2004). *Microplasmas for Chemical Analysis: Analytical Tools or Research Toys?* Spectrochimica Acta Part B. *Vol. 59 (7),* pp. 909 – 928

[33] M. Miclea (2007). *Analytical Detectors Based on Microplasma Spectrometry*. Plasma Chem. Plasma Process. *Vol. 27 (2),* pp. 205–224

[34] P. Jamro'z (2011). *Spectroscopic Characterization of Miniaturized Atmospheric-Pressure DC Glow Discharge Generated in Contact with Flowing Small Size Liquid Cathode*. Plasma Chem. Plasma Process. *Vol. 31 (5),* pp. 681–696

[35] P. Bruggeman (2008). *DC excited glow discharges in atmospheric pressure air in pin-to-water electrode systems.* J. Phys. D: Appl. Phys. *Vol. 41, No. 21,* 215201

[36] S. Miao (2008). *Conical DC Discharge in Ambient Air Using Water as an Electrode.* IEEE Transactions on Plasma Science. *Vol. 36, No. 1,* pp. 126-129

[37] K.H. Becke (2004). *Non-Equilibrium Air Plasmas at Atmospheric Pressure.* CRC Press. ISBN-13: 978-0750309622

[38] T. Shimizu (2011). *Formation of thermal flow fields and chemical transport in air and water by atmospheric plasma.* New Journal of Physics. *Vol. 13,* 053025

[39] P Andre (2001). *Experimental study of discharge with liquid non-metallic (tap-water) electrodes in air at atmospheric pressure.* J. Phys. D: Appl. Phys. *Vol. 34,* pp. 3456-3465

[40] B. Sun (2000). *Oxidative Processes Occurring When Pulsed High Voltage Discharges Degrade Phenol in Aqueous Solution.* Environ. Sci. Technol. *Vol. 34 (3),* pp. 509-513

[41] H. Kawamoto (2005). *Electrohydrodynamic deformation of water surface in a metal pin to water plate corona discharge system.* J. Phys. D: Appl. Phys. *Vol. 38 (6),* pp. 887–894

[42] Gucker, Sarah M. N (2015). *Plasma Discharges in Gas Bubbles in Liquid Water: Breakdown Mechanisms and Resultant Chemistry*. University of Michigan, ProQuest Dissertations Publishing, 3746106.

[43] R. Xiong (2012). *Hydrogen Peroxide Generation by DC and Pulsed Underwater Discharge in Air Bubbles.* J. Adv. Oxid. Technol. Vol. 15, No. 1, pp. 197-204

[44] K. Y. Shih (2010). *Chemical and Physical Characteristics of Pulsed Electrical Discharge Within Gas Bubbles in Aqueous Solutions.* Plasma Chem. Plasma

Process. *Vol. 30 (1),* pp. 1–20

[45] R. Burlica (2010). *Formation of H_2 and H_2O_2 in a Water-Spray Gliding Arc Non-thermal Plasma Reactor*. Ind. Eng. Chem. Res. *Vol. 49,* pp. 6342-6349

[46] B. Jiang (2014). *Review on Electrical Discharge Plasma Technology for Wastewater Remediation.* Chemical Engineering Journal. *Vol. 236*, pp. 348-368

[47] A. Fridman (1999). *Gliding Arc Gas Discharge*. Prog. Energy Combust. Sci. *Vol. 25 (2),* pp. 211-231

[48] U. Kogelschatz (1997). *Dielectric-Barrier Discharges. Principle and Applications.* Principle and Applications. Journal de Physique IV Colloque, *Vol. 07 (C4),* pp.C4-47-C4-66

[49] M. P. Cal (2001). *Destruction of Benzene with Non-thermal Plasma in Dielectric Barrier Discharge Reactor.* Environ prog. *Vol. 20 (3),* pp. 151-156

[50] P. Baroch (2008). *Special Type of Plasma Dielectric Barrier Discharge Reactor for Direct Ozonisation of Water and Degradation of Organic Pollution.* Journal of Physics D: Applied Physics. *Vol. 41, No. 8,* 085207

[51] U. Kogelschatz (2003). *Dielectric-barrier Discharges: Their History, Discharge Physics, and Industrial Applications.* Plasma Chemistry and Plasma Processing. *Vol. 23(1),* pp. 1–46

[52] R. P. Joshi (2013). *Streamer-Like Electrical Discharges in Water: Part I. Fundamental Mechanisms.* Plasma Chem. Plasma Process. *Vol. 33 (1),* pp. 1–15

[53] J.F. Kolb (2008). *Streamers in Water and Other Dielectric Liquids.* J. Phys. D Appl. Phys. *Vol. 41, No. 23,* pp. 234007–234015

[54] R.P. Joshi (2009). *Aspects of Plasma in Water: Streamer Physics and Applications.* Plasma Process Polym. *Vol. 6 (11),* pp. 763–777

[55] M. Sato (1996). *Formation of Chemical Species and Their Effects on Microorganizms Using A Pulsed High-Voltage Discharge in Water*. IEEE Trans. Ind. Applicat. *Vol. 32 (1),* pp. 106–112,

[56] P. Sunka (1999). *Generation of Chemically Active Species by Electrical Discharges in Water.* Plasma Sources Sci. Technol., *Vol. 8, No. 2,* pp. 258–265

[57] B. Sun (1999). *Use of A Pulsed High-Voltage Discharge for Removal of Organic Compounds in Aqueous Solution.* J. Phys. D, Appl. Phys. *Vol. 32, No. 15,* pp. 1908–1915

[58] W. T. Shin (2000). *A Pulseless Corona Discharge Process for the Oxidation of Organic Compounds in Water*. Ind. Eng. Chem. Res. *Vol. 39, No. 11,* pp. 4408–4414

[59] M. Sato (2001). *Transient Regime of Pulsed Breakdown in Low Conductive Water Solutions.* J. Phys. D, Appl. Phys. *Vol. 34, No. 23,* pp. 3400–3406

[60] P. Sunka (2001). *Pulse Electrical Discharges in Water and Their Applications.* Phys. Plasmas. *Vol. 8, No. 5,* pp. 2587–2594

[61] P. Lukes (2001). *Water Treatment by Pulsed Streamer Corona Discharge.* Ph.D. dissertation, Prague Inst. Chem. Technol. and Inst. Plasma Phys., Acad. Sci. Czech Rep., Prague, Czech Republic

[62] T. Ohshima (1997). *Physical and Chemical Modifications of High-Voltage Pulse Sterilization.* Journal of Electrostatics. Vol. 42 (1-2), pp. 159-166

[63] A. Hickling (1964). *Contact Glow-Discharge Electrolysis.* Transactions of the Faraday Society. *Vol. 60,* pp. 783–793

[64] A. A. Joshi (1995). *Formation of Hydroxyl Radicals, Hydrogen Peroxide and Aqueous Electrons by Pulsed Streamer Corona Discharge in Aqueous Solution.* J. Hazard. Mater. *Vol. 41, No. 1,* pp. 3–30

[65] J.S. Clements (1987). *Preliminary Investigation of Prebreakdown Phenomena and Chemical Reactions Using a Pulsed High-Voltage Discharge in Water.* IEEE transactions on industry applications, *Vol. IA-23, No. 2*

[66] D.M. Willberg (1996). *Degradation of 4-Chlorophenol, 3,4-Dichloroaniline, and 2,4,6-Trinitrotoluene in an Electrohydraulic Discharge Reactor.* Environ. Sci. Technol. *Vol. 30 (8),* pp. 2526-2534

[67] J. Podliński (2008). *Bubble Flow Measurements in Pulsed Streamer Discharge in Water Using Particle Image Velocimetry.* Journal of Physics: Conference Series. *Vol. 142, No.1,* 012036

[68] M. Kurahashi (1997). *Radical Formation due to Discharge Inside Bubble in Liquid.* Journal of Electrostatics. *Vol. 42 (1-2),* pp. 93-105

[69] B.R. Locke (2006). *Electrohydraulic Discharge and Nonthermal Plasma for Water Treatment.* Industrial & Engineering Chemistry Research, *Vol. 45 (3),* pp. 882-905

[70] H. Wang (2016). *Effect of Activated Carbon Addition on H_2O_2 Formation on Dye Decoloration in A Pulsed Discharge Plasma System.* Vacuum 128 99-105

[71] D.R. Grymonpre (2001). *An experimental and theoretical analysis of phenol degradation by pulsed corona discharge.* Florida State University, Doctor thesis, USA

[72] A.T. Appleton (2002). *A Study of The Effectiveness of Different Hybrid Pulsed Corona Reactors in Degrading Aqueous Pollutants.* HAKONE 8th Int. Symposium on High Pressure, Low Temperature Plasma Chem. Proceedings. *Vol. 34 (6),* pp. 313–317.

[73] P. Lukes (2004). *Hydrogen Peroxide and Ozone Formation in Hybrid Gas–Liquid Electrical Discharge Reactors.* IEEE Transactions on Industry Applications. *Vol. 40, No. 1,* pp. 60-67

[74] D.R. Grymonpre (2004). *Hybrid Gas−Liquid Electrical Discharge Reactors for Organic Compound Degradation.* Ind. Eng. Chem. Res. *Vol. 43 (9),* pp 1975–1989

[75] H. Kusic (2002). *Gas/Liquid Hybrid Electrical Discharge Reactors for The Degradation of Organic Dyes and Phenol in Water.* The 8th Int. Conf. Advanced

Oxidation Technologies for Water and Air Remediation, pp. 17–21, Toronto, ON, Canada,

[76] Y. Deng (2015). *Advanced Oxidation Processes (AOPs) in Wastewater Treatment.* Curr Pollution Rep. *Vol. 1 (3),* pp. 167–176

[77] B. G. Kwon (2009). *Determination of Hydroxyl Radical Rate Constants in A Continuous Flow System Using Competition Kinetics.* Journal of Industrial and Engineering Chemistry. *Vol. 15 (6),* pp. 809-812

[78] O. V. Polyakov (2003). *The Yields of Radical Products in Water Decomposition under Discharges with Electrolytic Electrodes*. High Energy Chemistry. *Vol. 37, No. 5, pp. 322-327.*

[79] P. Lukes (2005). *Plasma Chemical Oxidation Processes in A Hybrid Gas–Liquid Electrical Discharge Reactor.* J. Phys. D: Appl. Phys. *Vol. 38 (22),* pp. 4074-4081

[80] S. Ikoma (2012). D*ecomposition of Methylene Blue in an Aqueous Solution Using a Pulsed-Discharge Plasma at Atmospheric pressure.* Electrical Engineering in Japan. *Vol. 179. No. 3,* pp. 1-9

[81] E. J. Benitez (1996). *Degradation of Protocatechuic Acid by Two Advanced Oxidation Processes: Ozone/UV Radiation and H_2O_2/UV Radiation*. Water Res. *Vol. 30,* pp. 1597–1604.

[82] R. Ono (2002). *Measurement of Hydroxyl Radicals iIn Pulsed Corona Discharge.* Journal of Electrostatics. *Vol. 55 (3-4),* pp. 333–342

[83] N.C. Baird (1997). *Free Radical Reactions in Aqueous Solutions: Examples from Advanced Oxidation Processes for Wastewater and from the Chemistry in Airborne Water Droplets.* J. Chem. Educ. *Vol. 74 (7),* p. 817

[84] Y. F. Yue (2016). *Measurements of Plasma Generated Hydroxyl and Hydrogen Peroxide Concentrations for Plasma Medicine Applications.* IEEE Transactions on Plasma Science. *Vol. 44 (11),* pp. 1-5

[85] P. M. K. Reddy (2013). *Degradation and Mineralization of Methylene Blue by Dielectric Barrier Discharge Non-Thermal Plasma Reactor.* Chemical Engineering Journal. *Vol. 217,* pp. 41–47

[86] S. Khuntia (2015). *Quantitative Prediction of Generation of Hydroxyl Radicals from Ozone Microbubbles.* Chemical engineering research and design. *Vol. 98,* pp. 231–239

[87] N. K. V. Leitner (2010). *Kinetic of Benzotriazole Oxidation by Ozone and Hydroxyl Radical.* Water Research. *Vol. 44 (6),* pp. 2058-2066

[88] J.Chen (2005). *Effect of Relative Humidity on Electron Distribution and Ozone Production by DC Coronas in Air.* IEEE Transactions on Plasma Science, *Vol. 33, No. 2,* pp. 808-812

[89] I. M. Piskarev (1996). *Formation of ozone and hydrogen peroxide during an electrical discharge in the solution-gas system.* Russ. J. Electrochem. *Vol. 32, No. 7,*

pp. 827–829

[90] W. Hoeben (1999). *Gas Phase Corona Discharges for Oxidation of Phenol in An Aqueous Solution.* J. Phys. D: Appl. Phys. *Vol. 32, No. 24,* L133–L137.

[91] S. Ruma (2014). *Properties Of Water Surface Discharge At Different Pulse Repetition Rates.* Journal of Applied Physics. *Vol. 116,* 123304

[92] System SE (1994). *The UV/oxidation Handbook.* Markham, Ont., Canada

[93] M. Tezuka (1999). *Liquid-Phase Reactions Induced by Gaseous Plasma-Decomposition of Benzoic Acids in Aqueous Solution.* Plasmas&Ions. Vol. 2 (1), pp. 23-26

[94] D. Hayashi (2000). *LIF Diagnostic for Pulsed-Corona-Induced Degradation of Phenol in Aqueous Solution.* J. Phys. D: Appl. Phys. *Vol. 33, No. 12,* pp. 1484–1486

[95] L. R. Grabowski. (2006). *Corona above Water Reactor for Systematic Study of Aqueous Phenol Degradation.* Plasma Chemistry and Plasma Processing, *Vol. 26 (1),* pp. 3-17

[96] P. Lukes (1999). Proc. 14th Int. Symp. Plasma Chemistry (Institute of Plasma Physics, Prague) Vol 21, pp 2703–8

[97] M. A. Malik (2002). *Synergistic Effect of Pulsed Corona Discharges and Ozonation on Decolourization of Methylene Blue in Water*. Plasma Sources Sci. Technol. *Vol 11,* pp. 236-240

[98] A. Pandey (2007). *Review-Bacterial Decolorization and Degradation of Azo Dyes.* International Biodeterioration & Biodegradation. *Vol. 59,* pp. 73-84

[99] H. Zhao (2010). *Removal of Acid Orange 7 in Simulated Wastewater using A Three-Dimensional Electrode Reactor: Removal Mechanisms and Dye Degradation Pathway.* Chemosphere. *Vol. 78 (1),* pp. 46–51

[100] Q. Lin (2014). *Degradation of Alizarin Red by Hybrid Gas-Liquid Dielectric Barrier Discharge.* Plasma Science and Technology, *Vol.16, No.11*

[101] K. Faungnawakij (2006). *Modeling of Experimental Treatment of Acetaldehyde-Laden Air and Phenol-Containing Water Using Corona Discharge Technique.* Environ Sci Technol. *Vol. 40 (5),* pp. 1622–1628

[102] S. Ognier (2009). *Analysis of Mechanisms at the Plasma–Liquid Interface in a Gas–Liquid Discharge Reactor Used for Treatment of Polluted Water*. Plasma Chem. Plasma Process. *Vol. 29 (4),* pp. 261–273

[103] N. Sano (2002). *Decomposition of Organic Compounds in Water by Direct Contact of Gas Corona Discharge: Influence of Discharge Conditions*. Ind. Eng. Chem. Res. *Vol. 41 (24),* pp. 5906-5911

[104] X. Pei (2014). *On OH Density of an Atmospheric Pressure Plasma Jet by Laser-Induced Fluorescence.* IEEE transactions on plasma science, *Vol. 42, No. 5,* PP. 1206 - 1210

[105] P. Lukes (2008). *Ultraviolet Radiation from the Pulsed Corona Discharge in Water.* Plasma Sources Sci. Technol. *Vol. 17 (2),* 024012

[106] Z. Stara (2005). *Degradation of organic dyes versus H_2O_2 generation during the dc diaphragm discharge treatment in water solutions*. Acta Physica Slovaca. *Vol. 55 No. 6,* pp. 515-519

[107] B. Sun (1997). *Optical Study of Active Species Produced by A Pulsed Streamer Corona Discharge in Water.* J. Electrost. *Vol. 39 (3),* pp. 189–202

[108] A. L. Lopez (2007). *Influence of T-Butanol and of PH on Hydrodynamic and Mass Transfer Parameters in An Ozonation Process.* Chemical Engineering and Processing. *Vol. 46,* pp. 649–655

[109] R. M. Sellers (1990). *Spectrophotometric Determination of Hydrogen Peroxide Using Potassium Titanium (IV) Oxalate.* Analyst, *Vol. 105,* pp. 950-954

[110] M. Sato (2008). *Aqueous Phenol Decomposition by Pulsed Discharges on the Water Surface.* IEEE Transactions on Industry Applications, *Vol. 44, No. 5,* pp. 1397-1402

[111] L. Loeb (1965). *Electrical Coronas: Their Basic Physical Mechanisms*. University of California, Press Berkeley

[112] J. P. Boeuf (2007). *Electrohydrodynamic Force in Dielectric Barrier Discharge Plasma Actuators.* J. Phys. D: Appl. Phys. *Vol. 40,* pp. 652-662

[113] S. Kanazawa (2002). *Measurement of OH Radicals in Aqueous Solution Produced by Atmospheric-pressure LF Plasma Jet.* Int. J. Plasma Environ. Sci. Technol. *Vol. 6 (2),* pp. 166-171

[114] Y. Kanzaki (1984). *On The Yields of Glow Discharge Electrolysis in Various Atmospheres.* J Electroanal Chem. *Vol. 167 (1-2),* pp. 297-300

[115] P. Bruggeman (2007). *Water Surface Deformation in Strong Electrical Fields and Its Influence on Electrical Breakdown in A Metal Pin–Water Electrode System.* J. Phys. D: Appl. Phys. *Vol. 40 (16),* pp. 4779–4786.

[116] D. Porter (2009). *Formation of Hydrogen Peroxide, Hydrogen, and Oxygen in Gliding Arc Electrical Discharge Reactors with Water Spray*. IEEE Transactions on Industry Applications. *Vol. 45 (2),* pp. 623- 629

[117] C. A. Vasko (2013). *Gas Phase Hydrogen Peroxide Production in Atmospheric Pressure Glow Discharges Operating in He-H_2O.* 31st Int. Con. Phenomena in Ionized Gases. July 14-19, Spain

[118] T. Cserfalvi (1996). *Operating Mechanism of The Electrolyte Cathode Atmospheric Glow Discharge.* Fresenius J Anal Chem. *Vol. 355,* pp. 813–819

[119] X. Lu (2003). *Ignition Phase and Steady-State Structures of A Non-Thermal Air Plasma.* J. Phys. D: Appl. Phys. *Vol 36,* pp. 661-665

[120] P. Jamro'z (2012). *Development of Direct-Current, Atmospheric-Pressure, Glow Discharges Generated in Contact with Flowing Electrolyte Solutions for Elemental Analysis by Optical Emission Spectrometry.* TrAC-Trends Anal Chem. *Vol. 41,* pp.

105-121

[121] B. Jiang (2013). *Degradation of organic dye by pulsed discharge non-thermal plasma technology assisted with modified activated carbon fibers*. Chemical Engineering Journal. *Vol. 215–216*, pp. 969–978

[122] Q. Tang (2009). *Degradation of Azo Dye Acid Red 88 by Gas Phase Dielectric Barrier Discharges.* Plasma Chem Plasma Process. *Vol. 29 (4),* pp. 291-305

[123] F. Huang (2010). *Analysis of the Degradation Mechanism of Methylene Blue by Atmospheric Pressure Dielectric Barrier Discharge Plasma*. Chemical Engineering Journal. *Vol. 162 (1),* 250 – 256.

[124] A. A. Abdeaziz (2014). *Influence of N_2/O_2 Mixtures on Decomposition of Naphthalene in Surface Dielectric Barrier Discharge Based Reactor*. Plasma Sources Sci. Technol. *Vol 34, pp. 1371-1385*

[125] Y. Zhang (2007). *Degradation Mechanisms of 4-Chlorophenol in A Novel Gas–Liquid Hybrid Discharge Reactor By Pulsed High Voltage System with Oxygen or Nitrogen Bubbling*. Chemosphere. *Vol. 67 (4),* pp. 702–711.

[126] F. J. Beltran (2003). *Ozone Reaction Kinetics for Water and Wastewater Systems*. CRC Press. ISBN 9781566706292

[127] J. Hoigne (1976). *The Role of Hydroxyl Radical Reactions in Ozonation Processes in Aqueous Solutions.* Water Research. *Vol. 10 (5),* pp. 376–386

[128] J. Sehested (1995). *First Direct Kinetic Study of Isotopic Enrichment of Ozone.* Journal of Geophysical Research: Atmospheres. Vol. 100 (D 10)

[129] J. Tang (2003). *Photocatalytic Degradation of Methylene Blue on $Cain_2o_4$ under Visible Light Irradiation.* Chemical Physics Letters. *Vol. 382 (1),* pp. 175–179

[130] L. O. B. Benetoli (2012). *Pyrite-Enhanced Methylene Blue Degradation in Non-Thermal Plasma Water Treatment Reactor*. Journal of Hazardous Materials. *Vol. 237–238*, pp. 55–62

[131] L.C.A. Oliveira (2007). *A New Catalyst Material Based on Niobia/Iron Oxide Composite on The Oxidation of Organic Contaminants in Water Via Heterogeneous Fenton Mechanisms.* Appl. Catal. A. *Vol. 316*, pp. 117–124

[132] J. Xue (2008). *Degradation Mechanism of Alizarin Red in Hybrid Gas–Liquid Phase Dielectric Barrier Discharge Plasmas: Experimental and Theoretical Examination.* Chemical Engineering Journal. *Vol. 138*, pp. 120–127

[133] A. Houas (2001). *Photocatalytic Degradation Pathway of Methylene Blue in Water.* Applied Catalysis B: Environmental. Vol. 31 (2), pp. 145–157

[134] J. Gao (2004). *Oxidative Degradation of Nitrophenols in Aqueous Solution Induced by Plasma with Submersed Glow Discharge Electrolysis.* Plasma Process Polym. *Vol. 1 (2),* pp. 171–176

12 LIST OF PUBLICATIONS

Y. Zhao, T. Wang, M. Wilson, S. MacGregor, Q. Ren, I.Timoshkin. "Hydrogen peroxide formation under DC glow and impulsive current discharges", Submitted.

Y. Zhao, T. Wang, M. Wilson, S. MacGregor, I. Timoshkin, Q. Ren. "Hydroxyl radicals and hydrogen peroxide formation at nonthermal plasma-water interface", IEEE Transactions on Plasma Science, Vol. 44, No. 10, pp. 2084-2091, Oct. 2016.

Y. Zhao, M. Wilson, T. Wang, I. Timoshkin, S. MacGregor. "Hydroxyl radical production in DC streamer discharge", Proceedings of the 20th IEEE International Pulsed Power Conference, Austin, 2015.

Y. Zhao, T. Wang, S. MacGregor, M. Wilson, M. Given. "Investigation of plasma-induced methylene blue degradation using dielectric barrier discharge", Proceedings of the 20th International Conference on Gas Discharges and Their Applications, Orleans, 2014.

T. Wang, **Y. Zhao**, M. MacLean, S. MacGregor, G. Huang, M. Wilson. "Investigation of water treatment using dielectric barrier discharge", Proceedings of the 19th International Conference on Gas Discharges and Their Applications, Beijing, 2012.

13 APPENDIX I: DISCHARGE CURRENT CHARACTERISTICS (CHAPTER 4)

13.1 Discharge current in tap water from 1 to 10 minutes of treatment under 3 kV applied voltage

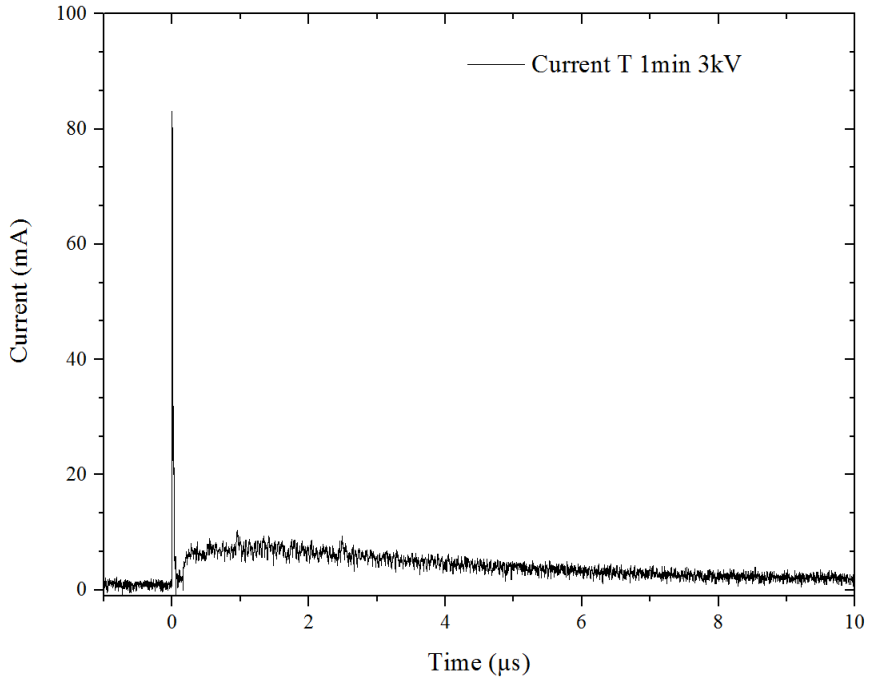

Figure I-1 Discharge current recorded under applied voltage of 3 kV, in tap water, for 1 minute of treatment.

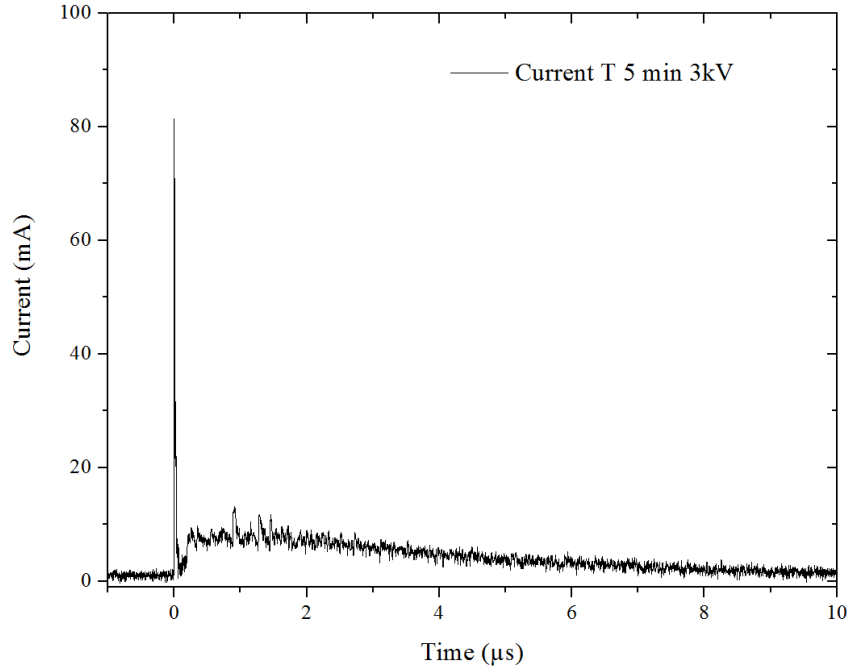

Figure I-2 Discharge current recorded under applied voltage of 3 kV, in tap water, for 5 minutes of treatment.

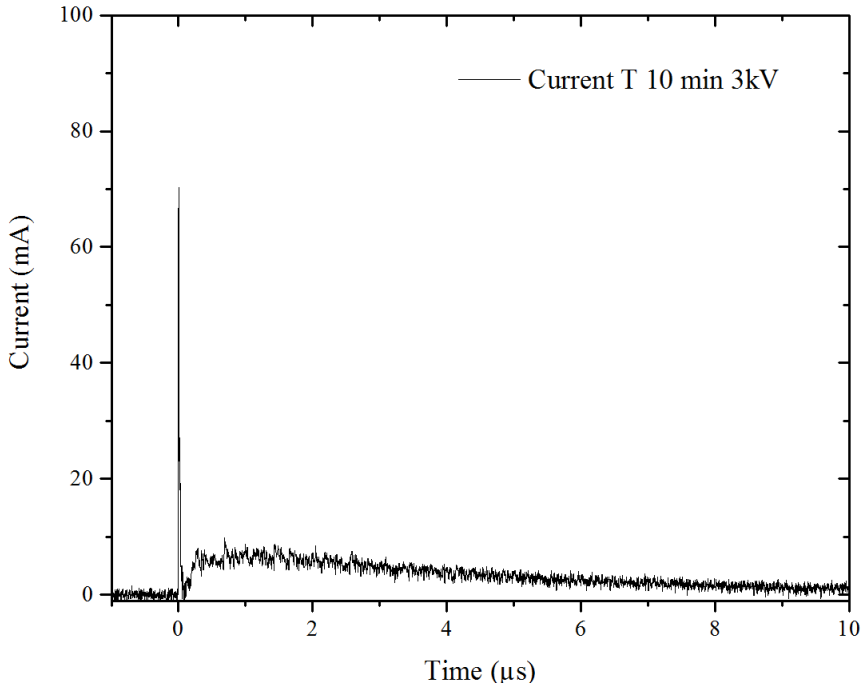

Figure I-3 Discharge current recorded under applied voltage of 3 kV, in tap water, for 10 minutes of treatment.

13.2 Discharge frequency in tap water from 0 to 10 minutes of treatment under 3-kV applied voltage

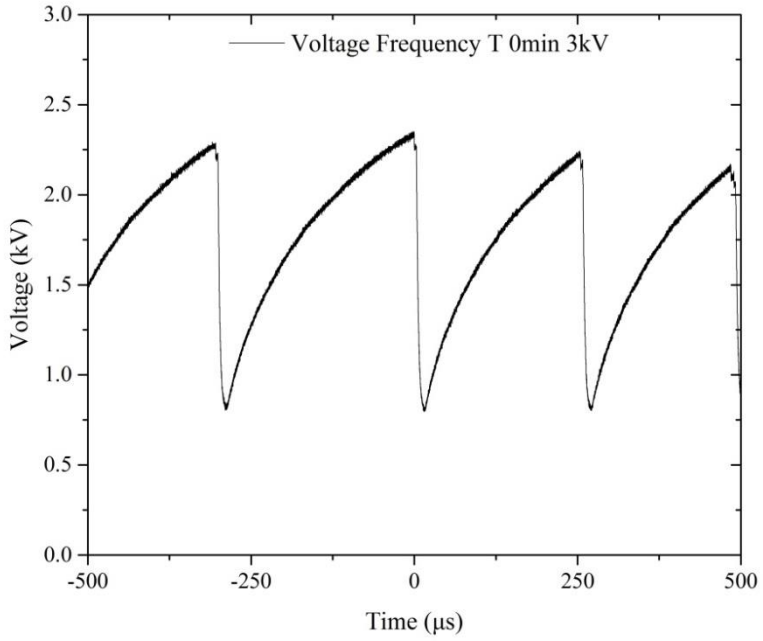

Figure I-4 Discharge frequency recorded under applied voltage of 3 kV, in tap water, for 0 minute of treatment.

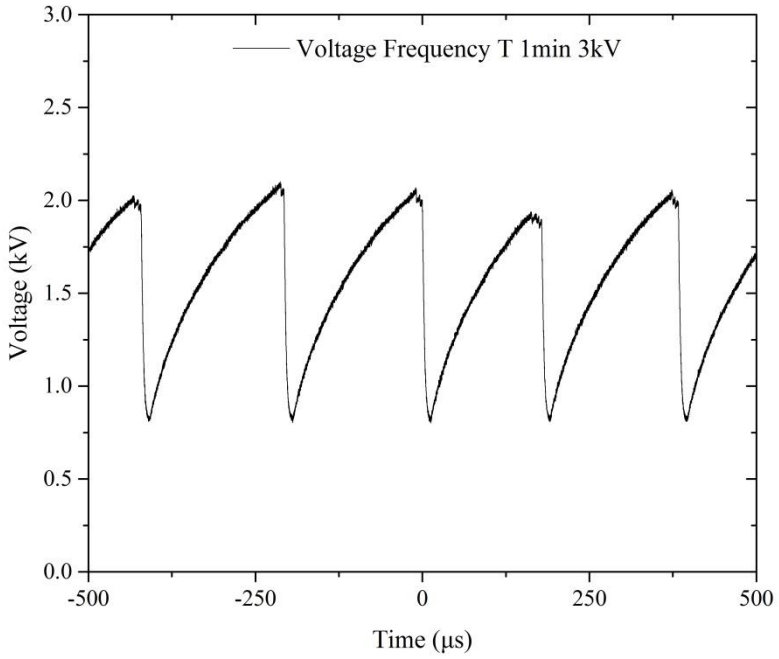

Figure I-5 Discharge frequency recorded under applied voltage of 3 kV, in tap water, for 1 minute of treatment.

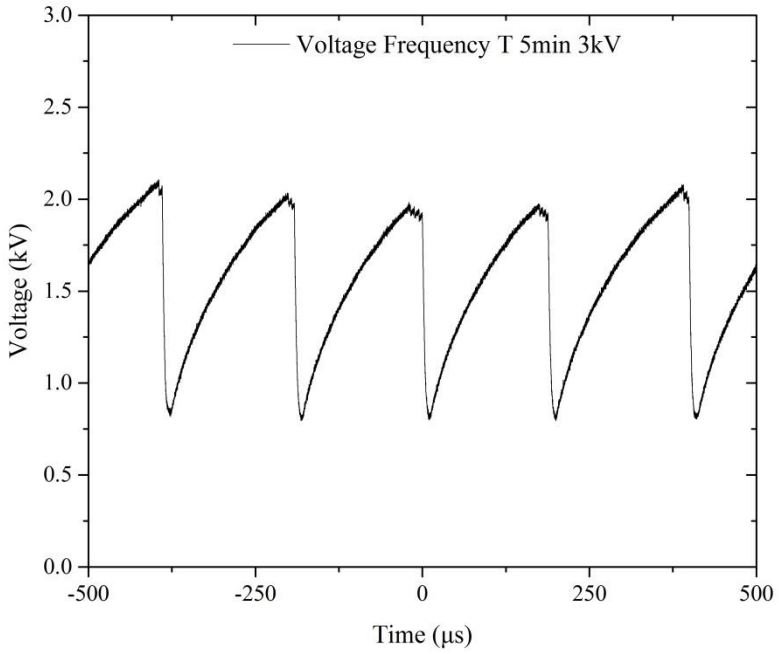

Figure I-6 Discharge frequency recorded under applied voltage of 3 kV, in tap water, for 5 minutes of treatment.

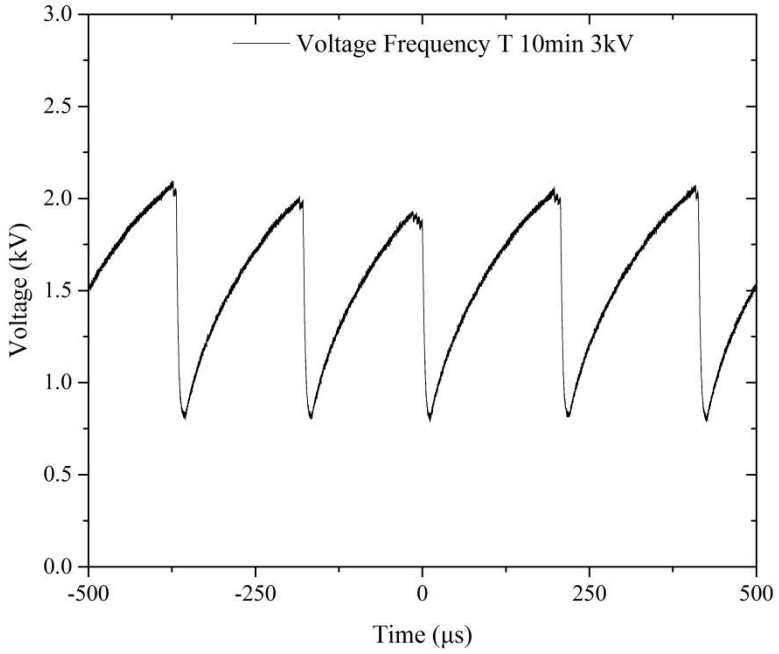

Figure I-7 Discharge frequency recorded under applied voltage of 3 kV, in tap water, for 10 minutes of treatment.

13.3 Discharge current in tap water from 1 to 10 minutes of treatment under 5-kV applied voltage

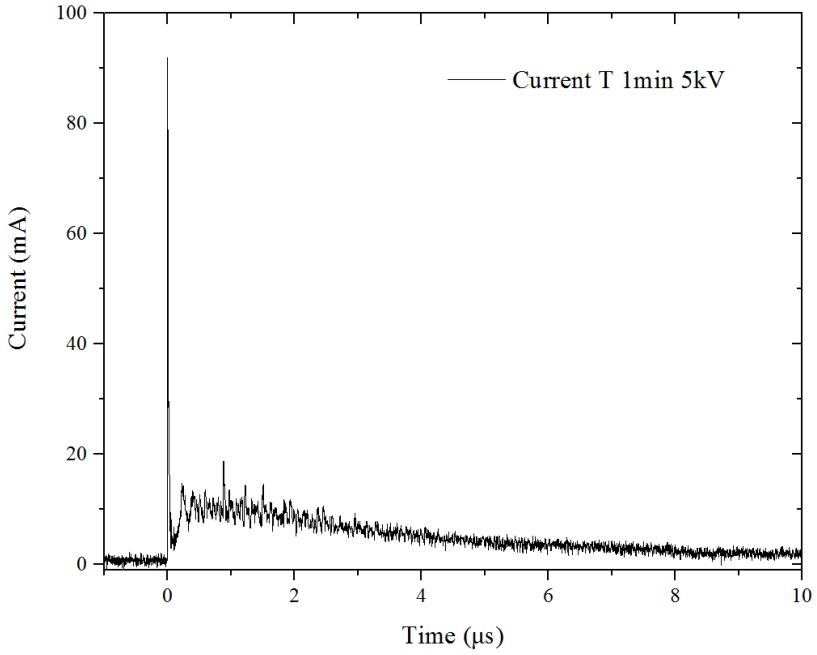

Figure I-8 Discharge current recorded under applied voltage of 3 kV, in tap water, for 1 minute of treatment.

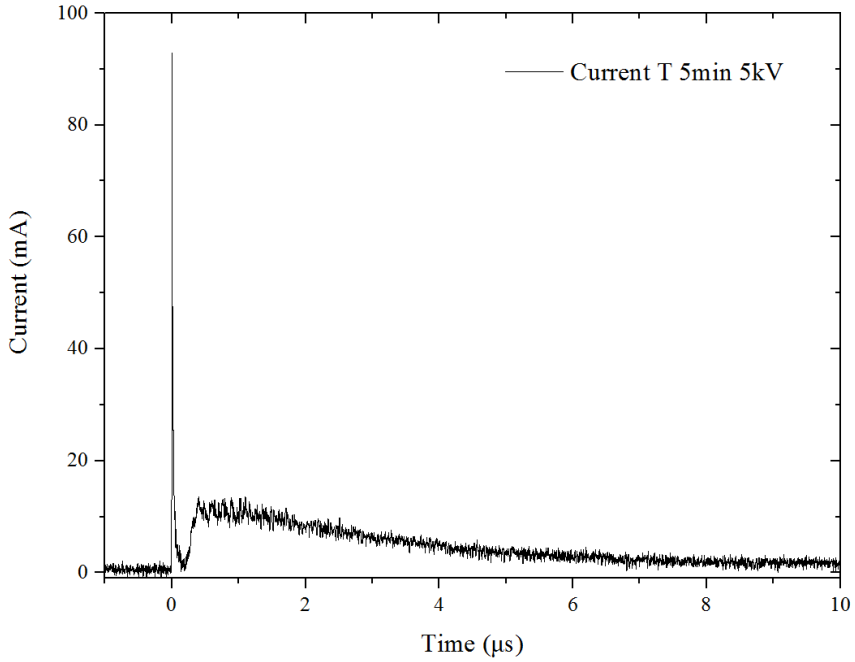

Figure 1-9 Discharge current recorded under applied voltage of 3 kV, in tap water, for 5 minutes of treatment.

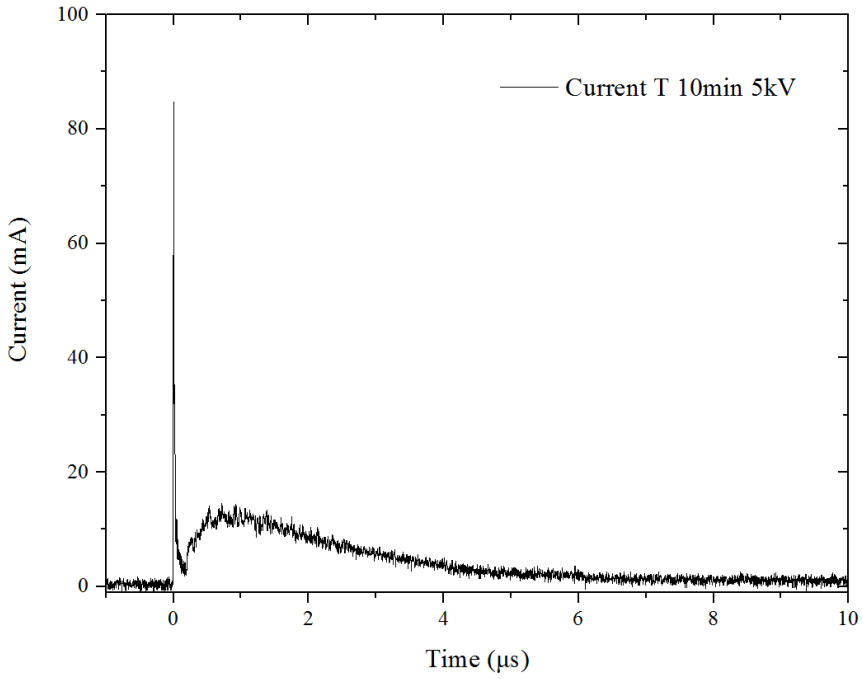

Figure I-10 Discharge current recorded under applied voltage of 3 kV, in tap water, for 10 minutes of treatment.

13.4 Discharge frequency in NaOH solution from 250 µS/cm to 22 mS/cm under 3-kV applied voltage

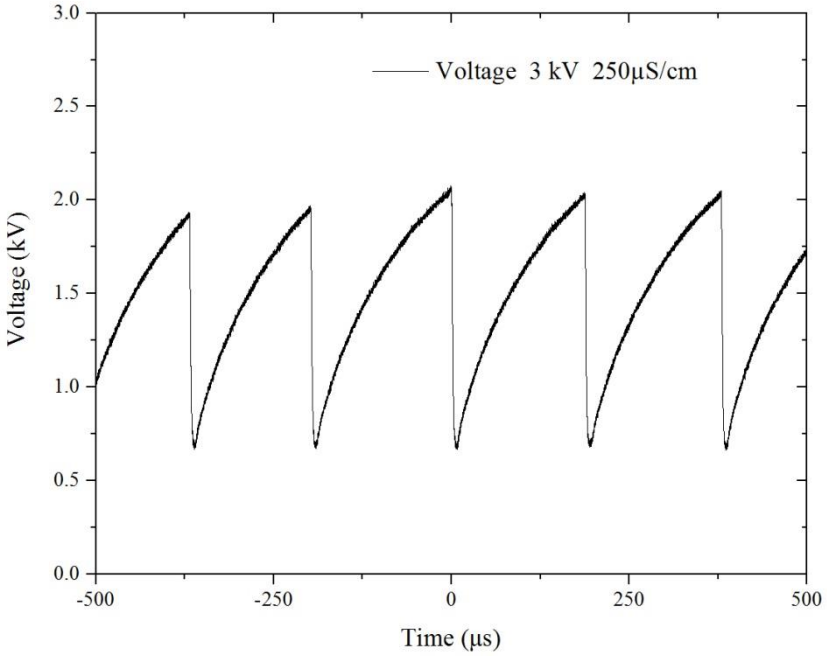

Figure I-11 Discharge frequency recorded under applied voltage of 3 kV, in 250 µS/cm solution.

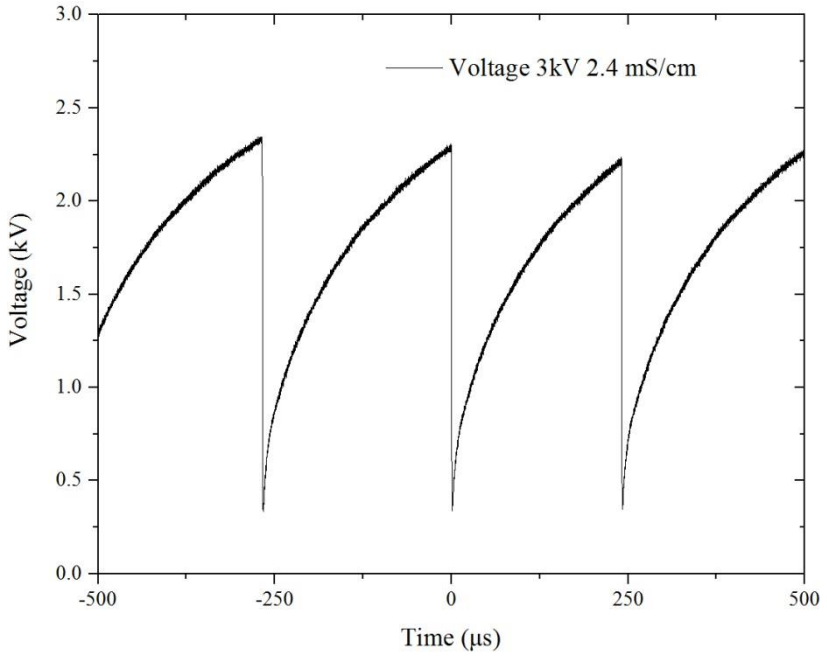

Figure I-12 Discharge frequency recorded under applied voltage of 3 kV, in 2.4 mS/cm solution.

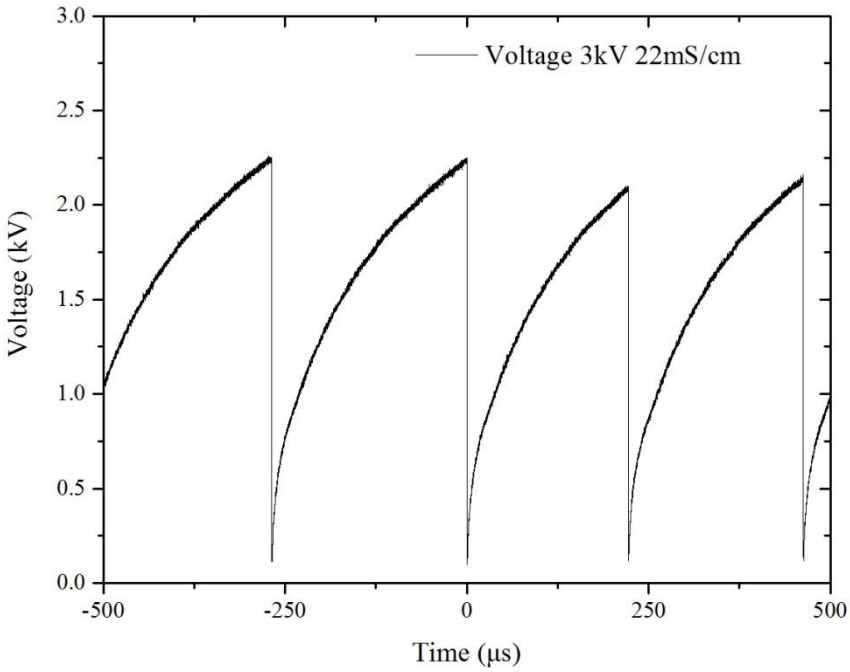

Figure I-13 Discharge frequency recorded under applied voltage of 3 kV, in 22 mS/cm solution.

14 APPENDIX II: CONTROLLED IMPULSIVE DISCHARGE CURRENT (CHAPTER 6)

14.1 Positive discharge current in tap water with air, nitrogen, oxygen and helium treatment

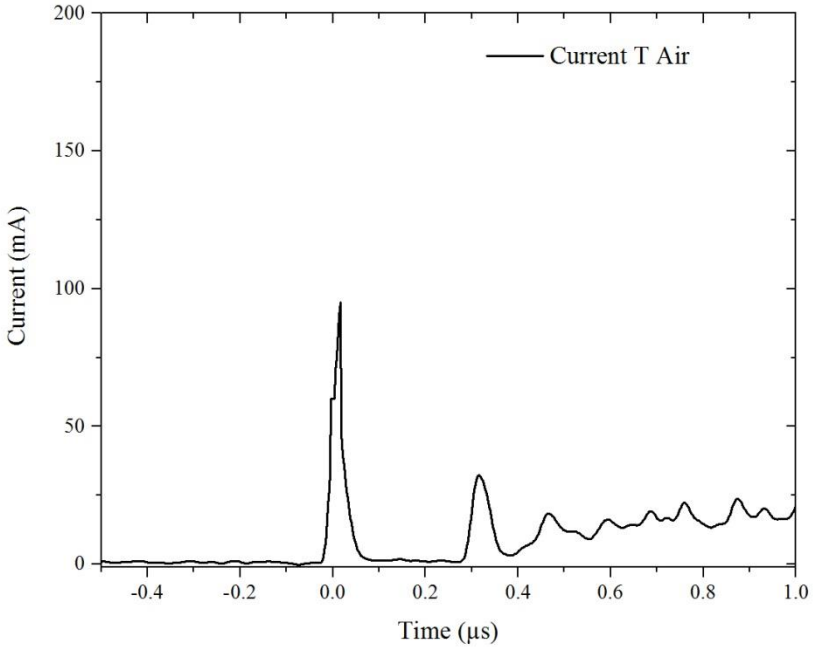

Figure II-1 The nanosecond impulsive current recorded under positive air discharges.

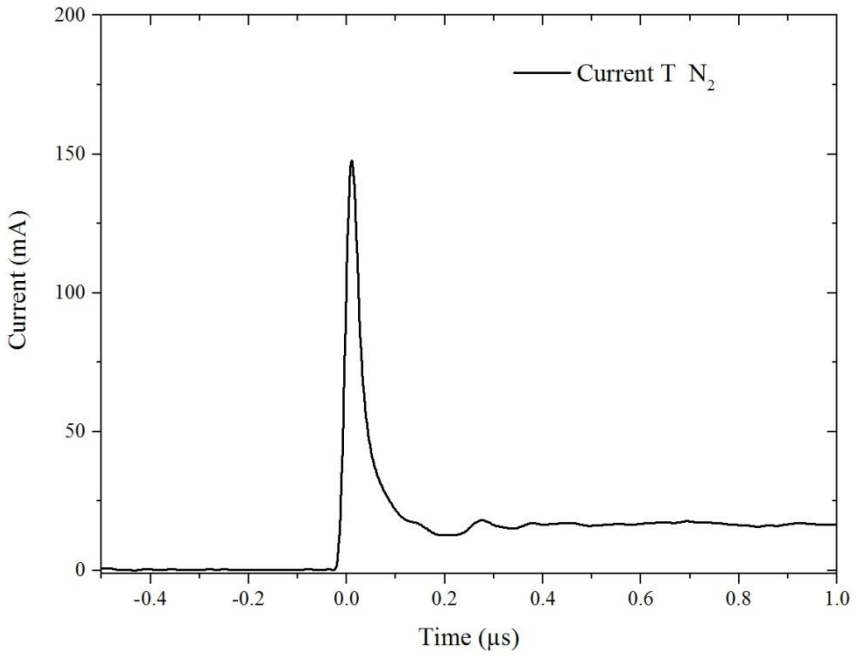

Figure II-2 The nanosecond impulsive current recorded under positive nitrogen discharges.

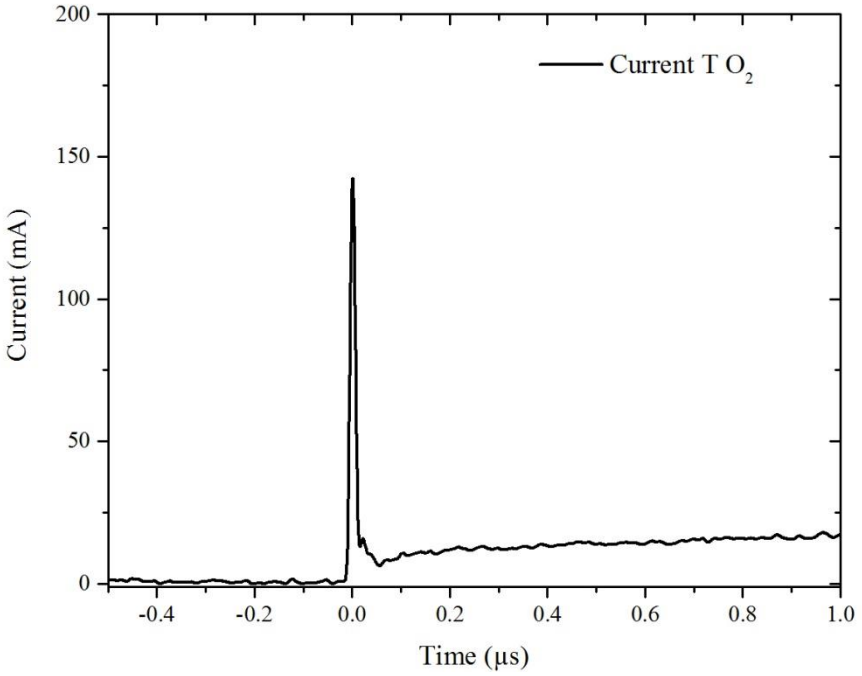

Figure II-3 The nanosecond impulsive current recorded under positive oxygen discharges.

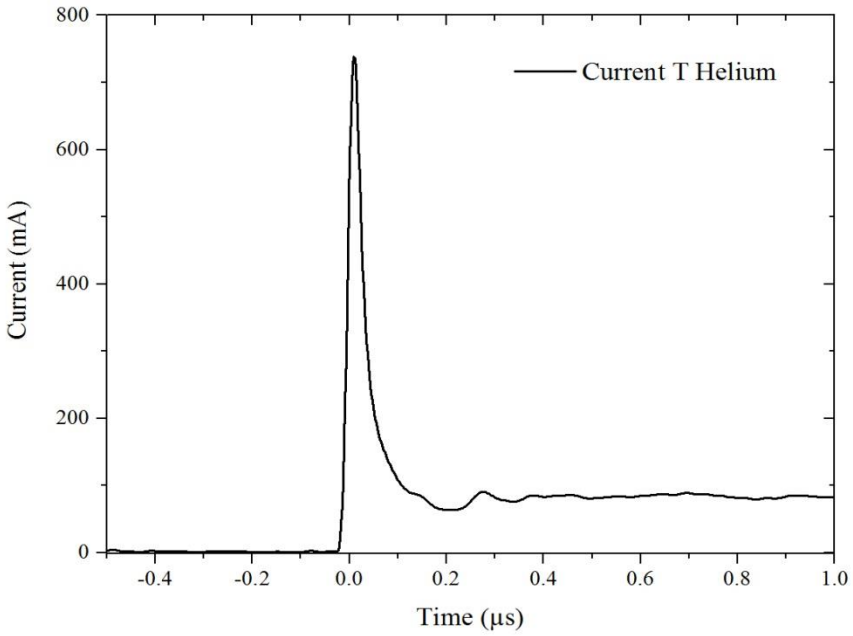

Figure II-4 The nanosecond impulsive current recorded under positive helium discharges.

14.2 Negative discharge current in tap water with air, nitrogen, oxygen and helium treatment

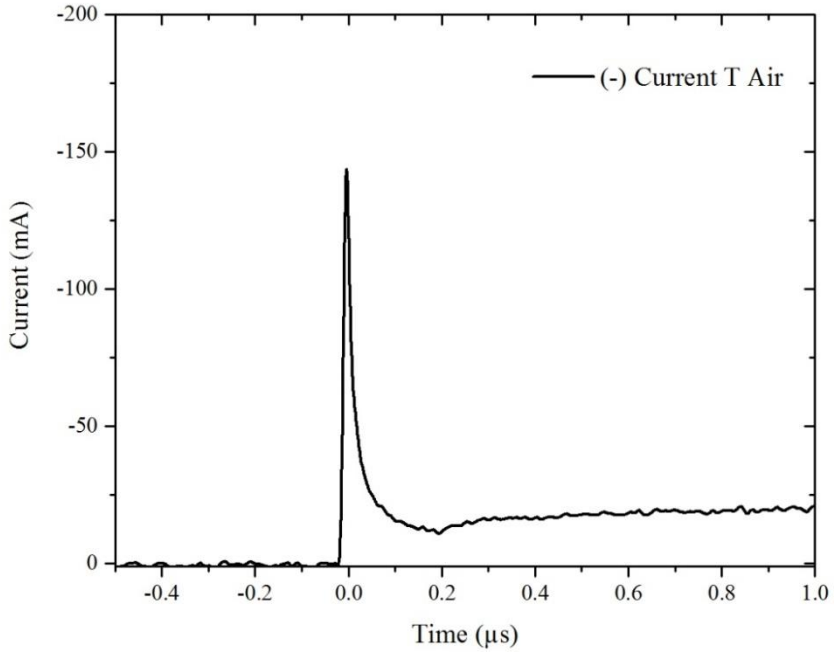

Figure II-5 The nanosecond impulsive current recorded under negative air discharges.

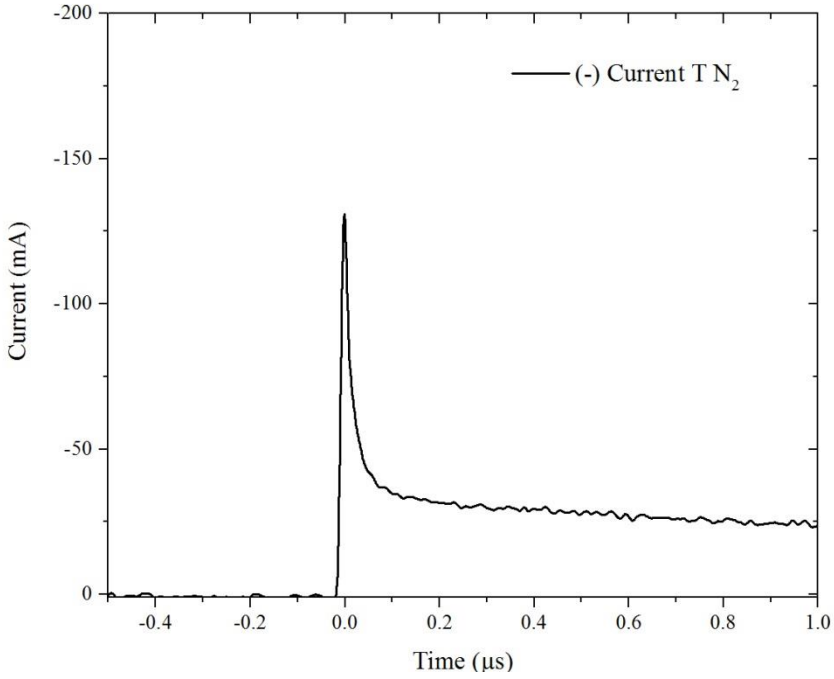

Figure II-6 The nanosecond impulsive current recorded under negative nitrogen discharges.

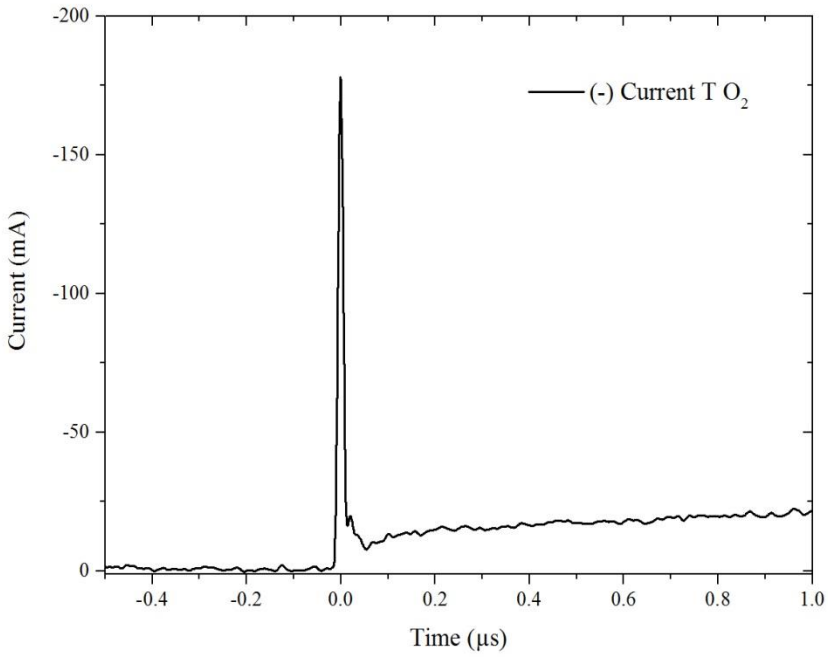

Figure II-7 The nanosecond impulsive current recorded under negative oxygen discharges.

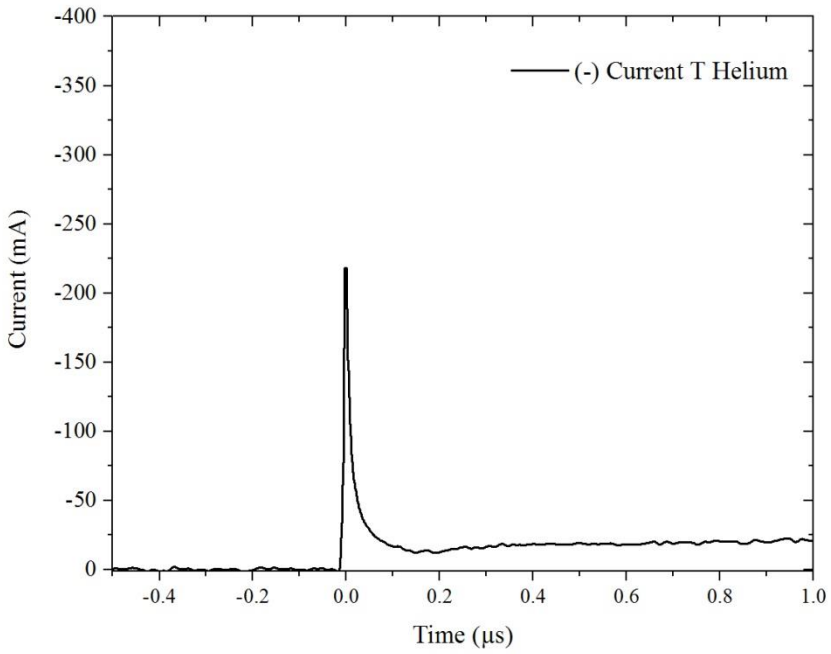

Figure II-8 The nanosecond impulsive current recorded under negative helium discharges.

15 APPENDIX III: EFFECT OF WATER ELECTRODE DEPTH AND SOLUTION INITIAL PH (CHAPTER 8)

15.1 Effect of different liquid cathode depth

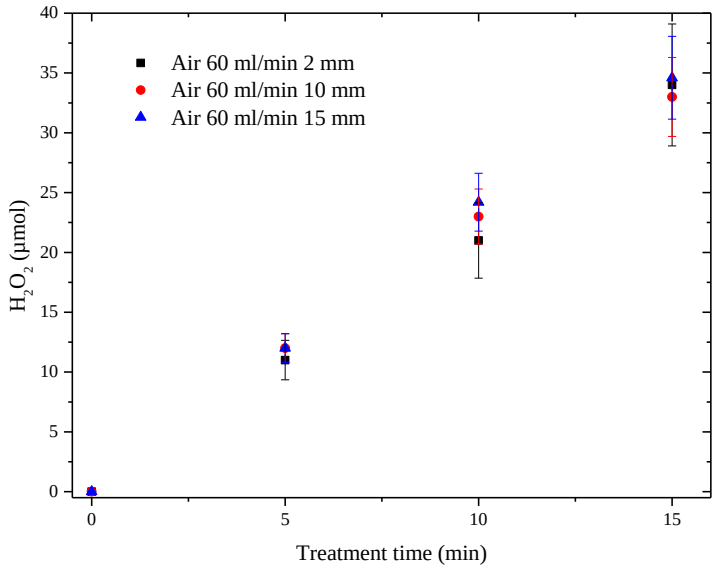

Figure III-1 Effect of different depth of water electrode on H_2O_2 production.

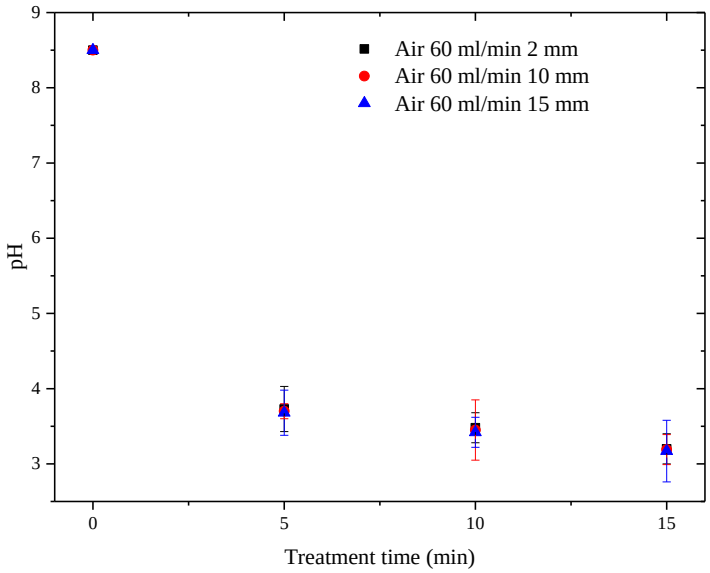

Figure III-2 Effect of different depth of water electrode on the solution pH.

15.2 The variation of solution conductivity and pH for various initial pH solutions

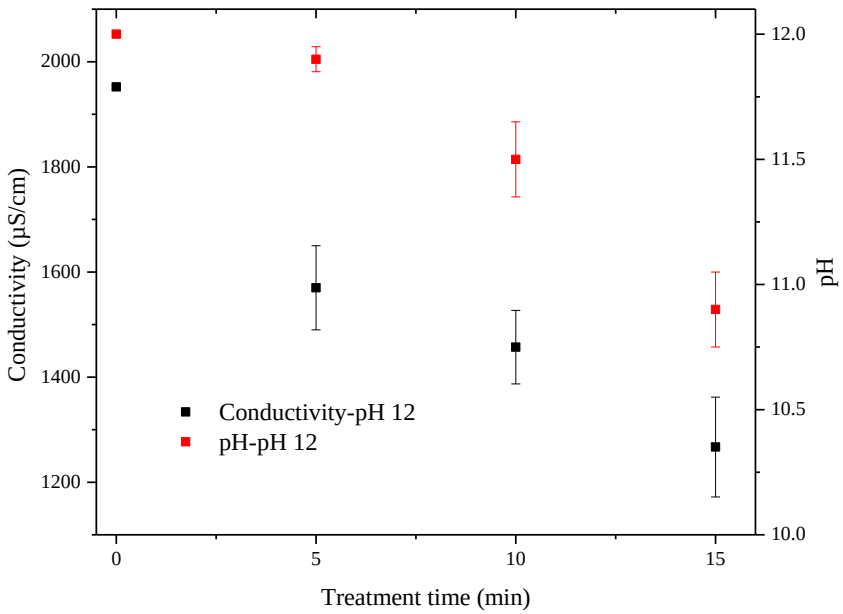

Figure III-3 Effect of different depth of water electrode on solution pH.

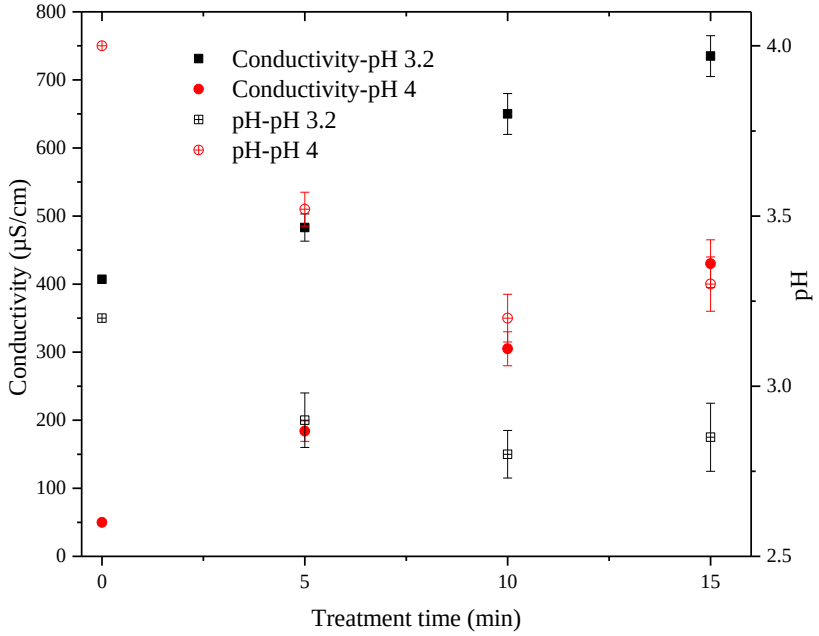

Figure III-4 Effect of different depth of water electrode on solution pH.